



City Research Online

City, University of London Institutional Repository

Citation: Tanghetti, G. (2021). Stability of Working Platforms for Tracked Plant.
(Unpublished Doctoral thesis, City, University of London)

This is the draft version of the paper.

This version of the publication may differ from the final published version.

Permanent repository link: <https://openaccess.city.ac.uk/id/eprint/27092/>

Link to published version:

Copyright: City Research Online aims to make research outputs of City, University of London available to a wider audience. Copyright and Moral Rights remain with the author(s) and/or copyright holders. URLs from City Research Online may be freely distributed and linked to.

Reuse: Copies of full items can be used for personal research or study, educational, or not-for-profit purposes without prior permission or charge. Provided that the authors, title and full bibliographic details are credited, a hyperlink and/or URL is given for the original metadata page and the content is not changed in any way.

Stability of Working Platforms for Tracked Plant

By

Greta Tanghetti

A thesis submitted for the Degree of Doctor of Philosophy

City, University of London

School of Mathematics, Computer Sciences and Engineering

Department of Civil Engineering

Multi Scale Geotechnical Engineering Research Centre

May 2021

CONTENTS

CONTENTS	ii
LIST OF TABLES	vi
LIST OF FIGURES	viii
ACKNOWLEDGEMENT	xvii
DECLARATION	xix
ABSTRACT	xx
LIST OF SYMBOLS	xxi
SUBSCRIPTS	xxv
ABBREVIATIONS	xxvi
1. INTRODUCTION	1
1.1 Background.....	1
1.2 Objectives	3
1.3 Thesis overview	3
2. FOUNDATIONS AND PLATFORMS - LITERATURE REVIEW	5
2.1 Introduction	5
2.2 Platform design methods	6
2.2.1 Bearing capacity of soils	7
2.2.2 Bearing capacity of layered soil	13
2.2.3 Specific design guidance for working platforms.....	19
2.2.4 Use of geosynthetic reinforcement.....	29
3. PLATFORM MATERIAL AND TESTING - LITERATURE REVIEW	33
3.1 Introduction	33
3.2 6F2 class material (Highways Agency, 2004).....	35
3.3 Direct shear test	37
3.3.1 Introduction	37
3.3.2 Description of the test method	37
3.3.3 Description of the testing apparatus	38
3.3.4 Determination of the appropriate displacement rate	40
3.3.5 Preparation of specimens	41

3.3.6	Data processing	42
3.4	Bearing capacity test.....	46
3.4.1	Introduction	46
3.4.2	Plate loading test	47
3.4.3	Description of the testing apparatus	48
3.4.4	Description of test procedure	50
3.4.5	Data results and calculation	51
3.4.6	Plate loading test for working platform	52
3.5	Scale effects in the tests.....	53
3.5.1	Introduction	53
3.5.2	Scale effects in direct shear tests.....	53
3.5.3	Large shear boxes for testing full scale samples with a large particle size..	65
3.5.4	Scale effects in <i>in-situ</i> plate bearing capacity tests	74
3.5.5	Scale effects in centrifuge modelling of plate bearing tests.....	75
3.6	Summary.....	78
4.	EXPERIMENTAL WORK	79
4.1	Introduction	79
4.2	Description of small scale tests	79
4.3	Small scale testing material	80
4.4	Description of full scale tests	82
4.5	Full scale testing material.....	82
5.	STANDARD SHEAR BOX TESTS.....	84
5.1	The standard shear box apparatus at City, University of London	84
5.2	Test description	85
5.3	Sample preparation.....	87
5.4	Test results.....	89
5.5	Conclusions	93
6.	PLATE LOADING TESTS USING A CENTRIFUGE MODEL.....	94
6.1	The geotechnical centrifuge at City, University of London	95
6.2	Test description	96

6.3	Sample preparation	101
6.4	Test results and back calculation of soil properties	103
6.4.1	Back calculation of soil properties	105
6.4.2	Results obtained from plate bearing tests on clay and sand overlying clay 109	
6.5	Conclusions	111
7.	LARGE SHEAR BOX TESTS	114
7.1	Apparatus design development.....	114
7.1.1	Conclusions derived from examples of large shear box apparatus	114
7.1.2	Geometry of the large shear box apparatus	115
7.1.3	Determination of the vertical and horizontal forces.....	116
7.1.4	Determination of maximum horizontal and vertical displacement	117
7.1.5	Preliminary design.....	118
7.1.6	Final design and functionality	119
7.2	Evaluation of the frictional forces	123
7.3	Apparatus and sample preparation	125
7.4	Testing programme.....	127
7.5	Test results	128
7.5.1	Test 1	130
7.5.2	Test 2	132
7.5.3	Test 3	133
7.6	Summary.....	134
8.	DISCUSSION.....	137
8.1	Introduction	137
8.2	Overview of the results obtained from large scale tests	138
8.3	Rotation of the top lid in shear box tests	139
8.4	Method for interpreting the results obtained from large scale tests	141
8.5	Comparison of the results with small scale shear tests.....	145
8.6	Comparison of the results with small plate loading tests	146
8.7	Summary.....	148

9. CONCLUSIONS.....	150
9.1 Introduction	150
9.2 Experimental procedure.....	150
9.2.1 Small scale shear box tests	150
9.2.2 Plate loading tests using centrifuge models	151
9.2.3 The large shear box apparatus.....	151
9.2.4 Large scale shear box tests	152
9.3 Conclusions and implications for working platform design.....	153
9.4 Limitations of the current work and recommendations for further research	154
APPENDIX A	156
APPENDIX B	167
APPENDIX C	170
REFERENCES.....	
TABLES.....	
FIGURES.....	

LIST OF TABLES

- Table 3. 1 Particle size distribution of 6F2 material, data obtained from Highways Agency (2004).
- Table 3. 2 Values of α and β coefficients proposed by Hamidi *et al.* (2012) for the determination of the maximum and constant volume friction angles of the base material.
- Table 3. 3 Large shear boxes in literature.
- Table 4. 1 Properties of testing samples representing scaled versions of the grading required for the 6F2 class material.
- Tables 4. 2 Theoretical and actual particle size distributions of the small-scale samples of maximum particle size equal to (a) 3.35 mm and (b) 2 mm.
- Table 4. 3 Calibration data of the sampling pipette used for the sedimentation test (according to BS 1377-2, 1990).
- Table 4. 4 Data and results of the sedimentation tests conducted on the samples with (a) maximum particle size equal to 3.35 mm and (b) maximum particle size of 2 mm.
- Table 4. 4 Data and results of the sedimentation tests conducted on the samples with (a) maximum particle size equal to 3.35 mm and (b) maximum particle size of 2 mm.
- Table 4. 5 Data and results for the determination of the specific gravity (Gs) of the two soil samples used to conduct small scale tests.
- Table 4. 6(a) Data and results of maximum index density (e_{min}) tests conducted on the sample with maximum particle size equal to 3.35 mm.
- Table 4. 6(b) Data and results of maximum index density (e_{min}) tests conducted on the sample with maximum particle size of 2 mm.
- Table 4. 7(a) Data and results of minimum index density (e_{max}) tests conducted on the sample with maximum particle size equal to 3.35 mm.

- Table 4. 7(b) Data and results of minimum index density (e_{max}) tests conducted on the sample with maximum particle size equal to 2 mm.
- Table 5. 1 Results of the standard direct shear box tests on scaled down 6F2 material (maximum particle size equal to 3.35 mm).
- Table 5. 2 Results of the standard direct shear box tests on scaled down 6F2 material (maximum particle size equal to 2 mm).
- Table 7. 1 Initial data and friction angle results obtained from the study of Fu et al. (2015) (values of friction angles scaled from the graphs presented by the author).
- Table 7. 2 Summary of the tests conducted using the large shear box apparatus.
- Table 8. 1 Mobilised angles of friction for each test conducted with the large shear apparatus and stress values used for their calculation.
- Table 8. 2 Summary of the results obtained from applying the principals of the stress dilatancy theory (Wood, 1991) to the data derived from small and large scale tests.

LIST OF FIGURES

- Figure 2. 1 Platform design method (BRE, 2004).
- Figure 2. 2 General (a), Local (b), Punching (c) shear failure mechanisms (Das, 2010).
- Figure 2. 3 Bearing capacity failure in soil under a rough rigid strip foundation (Das, 2010).
- Figure 2. 4 Types of failure at different relative depth D_f/B of foundations in sand (Vesic, 1963).
- Figure 2. 5 Bearing capacity of a strip foundation on layered soil (stronger soil underlain by weaker soil) where the depth H is relatively large compared with the foundation width (B) (Das, 2010).
- Figure 2. 6 Bearing capacity of a strip foundation on layered soil (stronger soil underlain by weaker soil) where the depth H is relatively small compared with the foundation width (B) (Das, 2010).
- Figure 2. 7 Coefficient of punching shear (K_s) expressed as function of the undrained shear strength of clay and the ratio δ/ϕ_1' . Chart showing the results for a sand top layer with $\phi_1' = 40^\circ$ (Hanna and Meyerhof, 1980).
- Figure 2. 8 Punching shear parameter (δ/ϕ_1') expressed as function of the ratio q_2/q_1 and the angle of friction of the top granular layer (ϕ_1'), Hanna and Meyerhof, 1980).
- Figure 2. 9 Plots of bearing capacity ratio against H/B from centrifuge testing reported by Okamura et al. (1997) in case of strip footings.
- Figure 2. 10 Plots of bearing capacity ratio against H/B from centrifuge testing reported by Okamura *et al.* (1997) in case of circular footings (Lees, 2019).
- Figure 2. 11 Variation of T with s_u and ϕ' for: (a) strip footing; (b) square footing (Lees, 2019).
- Figure 2. 12 General failure mechanism (TWf, 2019).
- Figure 2. 13 Local failure mechanism (TWf, 2019).
- Figure 2. 14 Punching failure mechanism (TWf, 2019).
- Figure 2. 15 Displacement of the loaded platform and subformation (TWf, 2019).
- Figure 2. 16 Load spread model in bearing capacity method (Burd and Frydman, 1997).
- Figure 2. 17 Actual pressure on formation compared with average derived from load spread method (TWf, 2019).
- Figure 2. 18 Punching shear model (BRE, 2004).

- Figure 2. 19 Punching shear model (Burd and Frydman, 1997).
- Figure 2. 20 Comparison between assumed and actual plane of failure developing in a strong soil layer underlain by weaker soil (Hanna, 1981).
- Figure 2. 21 Variation of the angle of inclination (δ) of the passive pressure (P_p) within the upper strong layer (Hanna, 1981).
- Figure 2. 22 Determination of the single forces acting on each track (Q) and loaded area on which the ground pressure is distributed (TWf, 2019).
- Figure 2. 23 Determination of the effective area of spread foundation (A') (Bond and Harris, 2008).
- Figure 2. 24 Variation of thickness of platform material (D) with design angle of shearing resistance of the platform (ϕ'_{pd}), at constant design values of undrained shear strength of fine grained subgrade (s_{ud}) and bulk unit weight of platform material (γ_{pd}).
- Figure 2. 25 Variation of thickness of platform material (D) with design undrained shear strength of fine grained subgrade (s_{ud}), at constant design values of angle of shearing resistance of the platform (ϕ'_{pd}) and bulk unit weight of platform material (γ_{pd}).
- Figure 2. 26 Variation of thickness of platform material (D) with design bulk unit weight of platform material (γ_{pd}), at constant design values of undrained shear strength of fine grained subgrade (s_{ud}) and design angle of shearing resistance of the platform (ϕ'_{pd}).
- Figure 2. 27 Reinforcement function: (a) tensile member; (b) tension member (Shukla, 2016).
- Figure 2. 28 Shear stress reduction effect of geosynthetics (Shukla, 2016).
- Figure 2. 29 Interlocking effect of geosynthetics (Shukla, 2016).
- Figure 2. 30 Slab or confinement effect of geosynthetics (Shukla, 2016).
- Figure 2. 31 Membrane effect of geosynthetics (Shukla, 2016).
- Figure 3. 1 Particle size distribution of 6F2 material, data obtained from Highways Agency (2004).
- Figure 3. 2 Typical general arrangement of shear box apparatus (BS 1377-7, 1990).
- Figure 3. 3 Displacement of the sample during shear (Powrie, 2010).

- Figure 3. 4 Definition of angle of dilation $\psi = \tan^{-1}(dy/dx)$ from the relative horizontal (dx) and vertical (dy) displacement of the shear box lid during the test (Powrie, 2010).
- Figure 3. 5 Conceptual model for: (a) compression of an initial loose sample and (b) dilation of an initial dense sample during shear (Powrie, 2010).
- Figure 3. 6 Idealised shear box results conducted under the same value of normal effective stress (σ'_v) on an initial dense and loose sample, showing (a) variation of shear stress (τ) with the sample strain (γ_s), (b) variation of volumetric strain (ε_{vol}) with strain (γ_s) and (c) variation of specific volume with strain (γ_s) (Powrie, 2010).
- Figure 3. 7 Idealised results from shear box tests, carried out at different normal effective stresses, on four samples having the same initial void ratio: (a) stress ratio τ/σ'_v vs. γ_s ; (b) specific volume v vs. γ_s ; (c) critical states (end points of tests); τ vs. σ'_v ; (d) critical states; v vs. σ'_v ; (e) critical states; v vs $\ln \sigma'_v$ (Powrie, 2010).
- Figure 3. 8 Critical state line in (σ'_v, τ, v) space with projections onto (τ, σ'_v) and (v, σ'_v) planes (Powrie, 2010).
- Figure 3. 9 Depth of influence defined by pressure bulbs generated by the Boussinesq formula (TWf, 2019).
- Figure 3. 10 Depth of influence for settlement defined by effective overburden pressure (p'_0) and increase in vertical stress (q') (TWf, 2019).
- Figure 3. 11 Grading curves for the base, scalped and parallel gradations (Hamidi *et al.*, 2012).
- Figure 3. 12 Results of critical state friction angle determination versus gravel fraction (Simoni and Houlsby, 2006).
- Figure 3. 13 Comparison of results between experiments and empirical equations for maximum friction angle of sample tested at three different relative densities and three different surcharge pressures (Hamidi *et al.*, 2012).
- Figure 3. 14 Comparison of results between experiments and empirical equations for constant volume friction angle of sample tested at three different relative densities and three different surcharge pressures (Hamidi *et al.*, 2012).
- Figure 3. 15 Major features of the concrete shear box designed and manufactured at the University of Wales, College of Cardiff (Jacobs, 1993).

- Figure 3. 16 Section through the concrete shear box designed and manufactured at the University of Wales, College of Cardiff (Jacobs, 1993).
- Figure 3. 17 Variation of the vertical stress in the direction of the nail reinforcement in case of (a) horizontal and (b) vertical shear plane alignment.
- Figure 3. 18 Variation of the normal stress along the nail in case of (a) horizontal and (b) vertical shear plane alignment.
- Figure 3. 19 Variation of the bedding planes distribution in the shear box in case of (a) horizontal and (b) vertical shear plane alignment.
- Figure 3. 20 Compression system of the Jain and Gupta (1975) shear box.
- Figure 3. 21 Shear system of the Jain and Gupta (1975) shear box.
- Figure 3. 22 Pedley (1990) shear box.
- Figure 3. 23 Palmeira (1987) shear box.
- Figure 3. 24 Krahan *et al.* (2007) shear box.
- Figure 3. 25 Santana and Estaire (2019) shear box (Etaire and Olalla, 2006).
- Figure 3. 26 Dimensionless peak loads (peak load measured during test (P_p) normalised by the unit weight of the soil (γ) and diameter of footing (B)) against plate diameter (B) (Ovesen, 1979).
- Figure 3. 27 Comparison of stress variation with depth (h) in a centrifuge model and its corresponding prototype (Taylor, 1995).
- Figure 4. 1 Grading curves representing minimum - maximum particle size values for 6F2 (solid black lines) and the particle size distribution chosen to be scaled down for the test material (dashed black line). Dashed red line indicates the effective grading curve of the sample with maximum particle size of 3.35 mm.
- Figure 4. 2 Grading curves representing minimum - maximum particle size values for 6F2 (solid black lines) and the particle size distribution chosen to be scaled down for the test material (dashed black line). Dashed red line indicates the effective grading curve of the sample with maximum particle size of 2 mm.
- Figure 4. 3 Grading curves representing minimum - maximum particle size values for 6F2 (solid black lines) and the particle size distribution chosen to be scaled down for the test material (dashed black line). Dashed red lines indicates the effective grading curve of the samples used for small scale tests having

a maximum particle size of 2 mm and 3.35 mm. In green is the grading curve of the material used for large scale shear box tests.

- Figure 5. 1 Standard direct shear box test apparatus at City, University of London.
- Figure 5. 2 Main components of the 100 x 100 mm shear box used for standard tests at City, University of London.
- Figure 5. 3 Shear box components placed in the rigid wall square and fixed by two horizontal screws.
- Figure 5. 4 Volumetric strain (ϵ_{vol}) versus shear strain (γ_s) results for standard shear box tests conducted at 100 kPa and 200 kPa vertical stress on dense samples and at 500 kPa on looser samples of limestone material with maximum particle size equal to (a) 3.35 mm and (b) 2 mm. Cross sign indicates where the values of critical state were selected for each test.
- Figure 5. 5 Shear stress (τ) versus shear strain (γ_s) results for standard shear box tests conducted at 100 kPa and 200 kPa vertical stress on dense samples and at 500 kPa on looser samples of limestone material with maximum particle size equal to (a) 3.35 mm and (b) 2 mm. d_{max} Cross sign indicates where the values of critical state were selected for each test.
- Figure 5. 6 Critical state angle of friction (ϕ'_{cr}), peak angle (ϕ'_{pk}) and angle of dilation (ψ) derived plotting the values of critical shear stress (τ_{cr}) and peak shear stress (τ_{pk}) at the variation of vertical stress (σ'_v) for all test conducted on the sample of maximum particle size equal to 3.35 mm.
- Figure 5. 7 Angle of friction (ϕ'_{cr}), peak angle (ϕ'_{pk}) and angle of dilation (ψ) derived plotting the values of critical shear stress (τ_{cr}) and peak shear stress (τ_{pk}) at the variation of vertical stress (σ'_v) for all test conducted on the sample of maximum particle size equal to 2 mm.
- Figure 5. 8 Shear box test series carried out using two sample of limestone material which were retested in two different order of normal vertical stress: 100, 200, 300 kPa (series 1) for the first sample and 300, 200, 100 kPa (series 2) for the second one.
- Figure 6. 1 Geotechnical centrifuge facility at City, University of London (Halai, 2018).

- Figure 6. 2 Centrifuge test design chart for estimating the safe normalized lateral boundary distance (L_{BD}) based on plate diameter (B) and thickness of the sand layer (H_s) (Ullah *et al.*, 2016).
- Figure 6. 3 Centrifuge modelling testing equipment and instrumentation for the plate bearing capacity tests (based upon Gorasia, 2013).
- Figure 6. 4 Centrifuge modelling testing equipment and instrumentation for the plate bearing capacity test conducted on clay and sand on clay using four plates.
- Figure 6. 5 Bearing stress (q) variation with displacement (w) obtained from testing the samples with maximum particle size (d_{max}) equal to 3.35 mm and 2 mm, tested at different plate to maximum particle size ratios (R).
- Figure 6. 6 Variation of the value of bearing stress obtained at the maximum displacement reached during the test against size of the plate (B), obtained from testing two samples with maximum particle size (d_{max}) equal to 3.35 mm (in black) and 2 mm (in red).
- Figure 6. 7 Variation of the value of bearing stress obtained at the maximum displacement reached during the test against plate diameter to maximum size ratio (R), obtained from testing two samples with maximum particle size (d_{max}) equal to 3.35 mm (in black) and 2 mm (in red).
- Figure 6. 8 Bulging of the soil in the zone adjacent to the plate typical of the general failure mechanism.
- Figure 6. 9 Variation of the angle of friction (back calculated) against plate diameter to maximum size ratio (R), obtained from testing two samples with maximum particle size (d_{max}) equal to 3.35 mm (in black) and 2 mm (in red).
- Figure 6. 10 Bearing stress (q) variation with displacement (w), obtained from the second plate bearing test conducted on clay and granular material on clay.
- Figure 6. 11 Comparison of the values of ultimate bearing capacity (q_u) obtained from centrifuge model plate loading test on sand overlying clay (d_{plate} indicates the diameter of the plate) with the values derived from the theoretical methods described by Lees (2019) and Meyerhof (BRE, 2004).
- Figure 7. 1 Variation of the angle of friction with W/d_{max} ratio at constant value of H , data obtained from the study of Fu *et al.* (2015) (values of friction angles scaled from the graphs presented by the author).

- Figure 7. 2 Variation of the angle of friction with H/d_{\max} ratio at constant value of W , data obtained from the study of Fu *et al.* (2015) (values of friction angles scaled from the graphs presented by the author).
- Figure 7. 3 Preliminary sketch of (a) the large shear box and (b) of entire apparatus.
- Figure 7. 4 Details of the large shear box apparatus design: a) 3D illustration of the apparatus; b) plan; c) section; d) elevation. All dimensions are expressed in mm.
- Figure 7.5 Large shear box apparatus (final arrangement).
- Figure 7. 6 Plate extensions having the role of preventing outflow of the material.
- Figure 7.7 Extension of the top half of the box reacting against the two horizontal load cells during shearing.
- Figure 7. 8 Load cells attached to the vertical reaction frame by the use of a steel plate connected to the frame by bolts.
- Figure 7. 9 Domed piece of steel machined to provide a rounded end for the load cells.
- Figure 7. 10 Acetal sheets on top of the three beams supporting the shear box.
- Figure 7. 11 Acetal sheets placed on the top surface of the bottom half of the box and lubricated before starting the test.
- Figure 7.12 Guides attached to the bottom of the box in order to facilitate the movement of the box during shearing.
- Figure 7. 13 Second reaction frame holding and reacting against the four 500 kN hydraulic jacks.
- Figure 7. 14 5 MN hydraulic jack attached to the horizontal beam before the latter was bolted to the vertical components of the reaction frame.
- Figure 7. 15 Platen comprising a stiffened 30 mm thick plate reinforced with crossed sections (to minimise plate deflection).
- Figure 7. 16 Stresses generated on the top plate of the large shear box apparatus under an applied load equal to approximately 450 kPa when resting on top of the sample.
- Figure 7. 17 Rigid frame holding the four vertical displacement transducers above the top of the shear box.
- Figure 7. 18 Rigid frame holding one of the horizontal displacement transducers.

- Figure 7. 19 Acetal sheet glued on top of the lower half of the shear box and put under load by the use of wooden blocks and aggregate bags.
- Figure 7. 20 Wooden platform placed around the bottom half of the shear box in order to collect the material contained in the top half.
- Figure 7. 21 Rotation of the top lid during the first large scale shear box test ($\sigma'_v = 11$ kPa).
- Figure 7. 22 Readings of the four vertical displacement transducers and derived vertical displacement V_r during the first large shear box test ($\sigma'_v = 11$ kPa).
- Figure 7. 23 Variation of the difference in vertical displacement between the two sides of the top plate during the first large shear box test ($\sigma'_v = 11$ kPa).
- Figure 7. 24 Method for determining the vertical displacement (V_r) of the soil sample in correspondence of the middle of the shearing zone.
- Figure 7. 25 Volumetric strain (ϵ_{vol}) versus shear strain (γ_s) results derived from the first large shear box test ($\sigma'_v = 11$ kPa).
- Figure 7. 26 Shear stress (τ) versus shear strain (γ_s) results derived from the first large shear box test ($\sigma'_v = 11$ kPa).
- Figure 7. 27 Rotation of the top lid during the second large scale shear box test ($\sigma'_v = 185$ kPa).
- Figure 7. 28 Variation of the difference in vertical displacement between the two sides of the top plate during the second large shear box test ($\sigma'_v = 185$ kPa).
- Figure 7. 29 Readings of the four vertical displacement transducers and derived vertical displacement V_r during the second large shear box test ($\sigma'_v = 185$ kPa).
- Figure 7. 30 Volumetric strain (ϵ_{vol}) versus shear strain (γ_s) results derived from the second large shear box test ($\sigma'_v = 185$ kPa).
- Figure 7. 31 Shear stress (τ) versus shear strain (γ_s) results derived from the second large shear box test ($\sigma'_v = 185$ kPa).
- Figure 7. 32 Variation of the difference in vertical displacement between the two sides of the top plate during the third large shear box test ($\sigma'_v = 104$ kPa).
- Figure 7. 33 Readings of the four vertical displacement transducers and derived vertical displacement V_r during the third large shear box test ($\sigma'_v = 104$ kPa).
- Figure 7. 34 Volumetric strain (ϵ_{vol}) versus shear strain (γ_s) results derived from the third large shear box test ($\sigma'_v = 104$ kPa).
- Figure 7. 35 Shear stress (τ) versus shear strain (γ_s) results derived from the third large shear box test ($\sigma'_v = 104$ kPa).

- Figure 8. 1 Method for calculating the secant angle of friction for each test conducted using the large shear apparatus.
- Figure 8. 2 Variation of the difference in vertical displacement between the two sides of the top plate during the three large shear box tests.
- Figure 8. 3 Volumetric strain (ϵ_{vol}) versus shear strain (γ_s) results derived from the three large shear box tests.
- Figure 8. 4 Shear stress (τ) versus shear strain (γ_s) results derived from the three large shear box tests.
- Figure 8. 5 Increase of the measured peak shearing resistance and reduction of the peak rate of volume due to the rotation of the top lid (Palmeira 1987).
- Figure 8. 6 Schematic of particle movements during shearing in large scale direct shear (Bareither *et al.*, 2008).
- Figure 8. 7 Direct shear box apparatus types considered by Kim *et al.* (2012).
- Figure 8. 8 Points of zero change in volume of a dense sample: at maximum compressive strain (pre-peak strength phase, point A); at constant volume and constant shear stress (post-peak strength phase, point C) (Atkinson, 2007).
- Figure 8. 9 Variation of the stress ratio (τ/σ'_v) with dilatancy of the sample (dy/dx) for standard shear box tests conducted on (a) 3.35 mm and (b) 2 mm soil samples.
- Figure 8. 10 Variation of the stress ratio (τ/σ'_v) with dilatancy of the sample (dy/dx) for the three large shear box tests.

ACKNOWLEDGEMENT

I would firstly like to express my thanks to the Temporary Works Forum. Without their financial assistance I would not have been able to pursue this PhD. I also owe a great deal of gratitude to the Research Centre for Multi-Scale Geotechnical Engineering at City, University of London who have offered me their help and support throughout the entire duration of my PhD. It was a privilege for me to be to be a member of the group during the past four years and having the opportunities to learn and grow in a very nurturing, friendly and knowledgeable environment.

My deepest thanks go to my supervisor Dr Richard Goodey, for his time and continual help, guidance and support during these years. His practical and technical knowledge was fundamental for conducting this research. Furthermore, his energy and abundant humour was always a key source for encouragement and helped me to stay positive even when facing the unexpected events or difficulties during my studies. I am also extremely grateful to my second supervisor, Dr Sam Divall for his continued support and advice during this research.

I owe my deepest gratitude to Professor Michael Davies and Professor Sarah Stallebrass for always being available to advise and discuss ideas, particularly during the writing up of the thesis. Their guidance and assistance have been invaluable and very much appreciated. Many thanks are also due to Dr Brett McKinley, Professor Neil Taylor and Dr Andrew McNamara for their assistance in developing ideas and practical solutions to this project. A special thankyou goes to the remaining members of the research centre who constantly provided support, encouragement and an atmosphere of friendship. Particularly, I am indebted to the colleagues who provided practical help during the assembling of the equipment and the hard work of shovelling the material out of the large shear box during the emptying operations. Therefore, thanks are due to Mr Eric Ritchie, Mr Ciaran Kennedy, Dr Leonardo Lalicata, Mr Hashmi Sohawon, Dr Hitesh Halai, Dr Jignasha Panchal, Dr Binh Le and Dr Sadegh Nadimi.

The experimental work which forms the key basis of this PhD would also not have been possible without the assistance and guidance from the technical staff within the School of Mathematics, Computer Sciences and Engineering Laboratory, in particular Mr Melvyn Hayes, Mr Phil Beckwith and Mr Jim Hooker. I extremely grateful for the time they were able to give me.

Finally, I would like to thank my family and friends for their love and continuous support in all my decisions. A special thank is due to my beloved brother Nicola for always filling me with faith, hope and optimism even in the most difficult moments and my friend Livia who temporarily replaced the family I was missing back home in Italy during my time in London.

DECLARATION

I grant powers of discretion to the University Librarian to allow this dissertation be copied in whole or in part without further reference to me. This permission covers only single copies made for study purposes, subject to normal conditions of acknowledgement.

ABSTRACT

The aim of this research is to improve the design of working platforms for tracked plant in order to guarantee safety but also a more economical approach to the design. The reason for this concern derives in part from incidents of overturning plant which have taken place in the past, some of them resulting in injuries and/or death of operatives, but also from the consequent use of excessively conservative and therefore uneconomical design.

Common practice for the design of working platforms is the use of bearing capacity methods normally adopted for the construction of spread foundations. The objective of this approach is the definition of an appropriate platform thickness which is back calculated from a bearing capacity equation. According to this type of design, the thickness of the platform changes based on the characteristics of the platform material and of the subgrade. Among these factors, the one having more influence on the resulting thickness is the design angle of friction of the platform material, which therefore need to be accurately established.

A common laboratory method used to measure the angle of friction of soils is the direct shear test. Difficulties in the correct interpretation of the results of this test are mainly associated with the presence of scale effects. As extensively reported by literature, scale effects can derive from testing material with a large particle size which is not suitable for testing in a standard apparatus, that would cause the shear strength of the material to be overestimated. A solution to this issue often consists of testing a scaled sample of the material using the standard apparatus. Nonetheless, even this approach can induce scale effects leading to an underestimation of the angle of friction when an important reduction in particle size is produced.

Another method used to derive the angle of friction of the platform material is the plate bearing capacity test which is normally conducted on site. In order to guarantee reliable results for the bearing capacity of the material and the derived angle of friction, an appropriate ratio between plate diameter and particle size must be used. The problem of this method is associated with the high costs of the testing apparatus which are substantially increased by the large particle size of the material requiring large plate diameters to be used during the test and consequently high reaction forces to be applied.

In order to investigate the scale effects associated with testing the material at smaller scale using the standard shear box apparatus and with using different plate diameters in case of plate loading tests, a series of small scale direct shear tests and plate loading test using a centrifuge model were conducted on two small scale samples of crushed limestone. The results of these tests were used to derive the angle of friction of the material and were compared with the ones obtained from testing the same material at full scale using a large shear box apparatus which was designed and manufactured for the purpose of this research. Comparison of the results allowed to identify the magnitude of the scale effects on the value of the angle of friction of the material. Differences in results should be taken into account in order to define an appropriate value for the design.

LIST OF SYMBOLS

$\alpha - \beta$	coefficients proposed by Hamidi <i>et al.</i> (2012) for the determination of the maximum and constant volume friction angles of the base material
A	area
A'	effective contact area of foundation subjected to eccentric load
β	load spread angle
B	breadth/diameter of the foundation or of the platform loaded area
B'	reduced breadth of the foundation or of the platform loaded area in case of eccentric load or spread load
B _g	degree of particle breakage
c'	cohesion or apparent cohesion
C _a	adhesive force
c _a '	adhesion
C _u	uniformity coefficient
C _v	coefficient of consolidation
d	drainage path length
δ	inclination of the passive force
Δ	increment
D	platform thickness
D _{Bi}	particle diameter of original grading (parallel grading method)
D _f	the depth of the foundation measured from the ground surface
D _i	particle diameter of similar grading (parallel grading method)
d _{max}	maximum particle size
D _r	relative density
dx	Incremental horizontal displacement (shear box test)
dy	Incremental vertical displacement (shear box test)
D ₅₀	sieve diameter corresponding to 50% passing material
D ₆₀	sieve diameter corresponding to 60% passing material
D ₁₀	sieve diameter corresponding to 10% passing material
ϵ_{vol}	volumetric strain
$\Delta\epsilon_{vol}$	variation in volumetric strain
e	void ratio

e_b	load eccentricity in direction of the breadth B of the loaded area
e_l	load eccentricity in direction of the length L of the loaded area
E_s	compression modulus
e_1	initial void ratio corresponding to vertical stress p_1 (oedometer test)
e_2	initial void ratio corresponding to vertical stress p_2 (oedometer test)
ϕ'	soil friction angle
ϕ_1'	angle of friction of the upper soil layer
ϕ_2'	angle of friction of the lower soil layer
F_{cc}, F_{gc}, F_{qc}	compressibility factors
F_f	friction force
F_{f1}	friction force acting on the sliding surface between the two halves of the large shear box
F_{f2}	friction force acting on the sliding surface between the bottom of the large shear box and the supporting beams
F_h	horizontal force (shear box)
F_{n1}	normal force acting on the sliding surface between the two halves of the large shear box
F_{n2}	normal force acting on the sliding surface between the bottom of the large shear box and the supporting beams
F_v	vertical force (shear box)
γ	unit weight of the soil
γ'	effective unit weight when saturated or the total unit weight when not fully saturated (bearing capacity calculation)
γ_d	dry unit weight
γ_s	shear strain
γ_1	unit weight of the upper soil layer
γ_2	unit weight of the lower soil layer
g	earth gravity
G	shear modulus of the soil
G_s	specific gravity
h	sample height
H	specimen thickness (shear box test) or thickness of the layer under the foundation

H_{cr}	critical depth
Δh	distance between the top of the tub and sample surface
h_m	height of the model (centrifuge tests)
h_p	height of the prototype (centrifuge tests)
h_l	final height of the sample (maximum index density test)
I_r	rigidity index
K_p	horizontal component of passive earth pressure coefficient
K_s	punching shear coefficient
L	length of the foundation or of the platform loaded area
L'	reduced length of the foundation or of the platform loaded area in case of eccentric load
L_{BD}	distance measured from the centre of the plate to the inner edge of the sample container (plate loading test)
m_s	dry mass of soil
μ	friction coefficient
N	vertical load or acceleration scaling factor
N_c, N_γ, N_q	bearing capacity factors
p_p	peak load measured during test (Ovesen)
P_p	passive earth pressure
P_u	footing load failure
p'_0	effective overburden pressure
$p_2 - p_1$	stress increment (oedometer test)
Q	vertical force acting on the single track of a working vehicle
q	bearing stress
q'	effective overburden pressure
q_b	bearing capacity of the lower soil layer
q_s	surface bearing capacity of clay (Lees, 2019)
q_u	ultimate bearing capacity
$q_{u(1)}$	first failure bearing capacity (local and punching failure mechanism)
ρ	density
ρ_w	water density
R	plate diameter to maximum particle size ratio (plate loading test) or scale coefficient (parallel grading method)

r	radius to any element in the soil (centrifuge test)
R_e	effective radius of model (centrifuge test)
R_t	radius to the top of the model (centrifuge test)
σ'_v	vertical effective stress
σ'_{zD}	vertical effective stress at the depth the foundation is laid
S_b, S_p	shape factors
s_u	undrained shear strength of the soil
τ	shear stress
v	specific volume
v_e	velocity
V	normalised velocity
V_1, V_2, V_3, V_4	readings of the vertical displacement transducers (large shear box test)
V_r	vertical displacement aligned with the mid-point of the shear zone (large shear box test)
V_t	volume of the soil sample
w	settlement of the plate (plate loading test)
W	width of the foundation or of the platform loaded area or specimen diameter (shear box tests)
W_e	total mass of the apparatus acting on the plate before adding the applied load, including the mass of the plate
W_{kf}	percentage retained on sieve k after testing
W_{ki}	percentage retained on sieve k before testing
x	relative lateral displacement of the shear box
ψ	angle of dilation
y	relative vertical displacement of the shear box
ω	angular rotational speed

SUBSCRIPTS

d	Design value
p	Platform property
cr	Critical value
pk	Peak value
0	Initial value
max	Maximum value
min	Minimum value
1	Upper soil layer property
2	Lower soil layer property
x	Value related to x direction
y	Value related to y direction

ABBREVIATIONS

ASTM	American Society for Testing and Materials
BRE	Building Research Establishment
BS	British Standard
CCA	Crushed Concrete Aggregate
CDW	Construction Demolition Waste
DAQ	Data Acquisition
FPS	Federation of Piling Specialists
LVDT	Linear Variable Displacement Transducer
RA	Recycled Aggregate
RCA	Recycled Concrete Aggregate
RC	Reinforced Concrete
RSA	Recycled and Secondary Aggregates

1. INTRODUCTION

The main objective of this research programme concerns the stability of working platforms. The research is sponsored by the Temporary Works Forum as part of the activities of the Centre of Excellence in Temporary Works and Construction Method Engineering of City, University of London.

1.1 Background

A working platform is a ground-supported structure consisting of granular material, used as a safe and sufficiently durable surface from which construction plant, such as piling rigs and cranes, can move around the site and operate. The material used for working platforms is generally a well-graded granular material characterised by good frictional properties and compressibility (Corke and Gannon, 2010). Working platforms can be made of crushed aggregate or construction demolition waste (CDW) which are waste material produced from the construction industry and derived from construction, reconstruction, cleaning of the work site and earth-works, demolition and collapse of buildings, maintenance and rehabilitation of existing construction (Pereira *et al.*, 2019). The largest component of CDW can be concrete, followed by brick and clay, wood and metals (Lawson *et al.*, 2001). The use of recycled resources permits reduction in costs related to extraction and transportation of granular material and limits the risk of incidents during quarrying operations and lorry movements. Further benefits derive from the reduction in environmental damage associated with the extraction of primary aggregates, transportation of materials and landfilling.

The use of recycled materials is not new since a wide range of recycled and secondary aggregates (RSA) are used in the UK construction industry. Some examples of them are: CDW (such as brick or concrete, widely used by the construction industry as a bulk fill; for example, for filling voids, foundations and as capping layers to highways), slate waste (coarse or fine, used for: road building works, ground engineering applications and low-strength concrete) or china clay waste (coarse-grained fraction is mainly used for construction fill while finer grading for low-strength concrete) (Steele, 2004). It should be noticed that considerable effort has been put into promoting the wider use of RSA through changes to specifications such as the Specification for Highway Works (Highways Agency, 2004), which defines properties of earthworks material by the use of relevant series. Among these, Series 600 (material used for earthworks) includes a description of class 6F2, a selected coarse grading fill usually made for capping. The

broad availability of recycled material accepted by this class and its coarse nature make it a good alternative to fresh aggregate for the construction of working platforms.

There are however problems relating to the use of 6F2 class material made from CDW. Firstly, it can be made from different demolition waste components (and therefore have different material properties) and secondly, despite it having to conform to certain grading requirements, this class contains a wide particle size distribution and thus its behaviour may be different dependant on the variation of these two factors.

When designing working platforms guidance is generally based on bearing capacity equations which require knowledge of the properties of the platform material (such as angle of friction and unit weight) and underling soil layer in order to determine the thickness of platform. Therefore, in order to guarantee a safe design it is necessary to obtain detailed and reliable information about the characteristics of the platform material.

In order to have a complete picture of the behaviour of 6F2 made from CDW it would therefore be necessary to test different samples with different compositions and also different particle size distributions. This presents another problem related to the study of 6F2 class material; the large size of the particles, which makes standard test apparatus unsuitable for obtaining representative results.

The proposed solution to this problem is the determination of a testing method able to allow testing of the platform material at full size. A large shear box apparatus (shear plane area equal to 2.25 m²) was designed and fabricated in order to conduct a series of full scale tests on large particles of crushed limestone material (particle size ≤ 63 mm). Results obtained from these tests were compared with the ones derived from testing the same material at small scale using a standard apparatus. Comparison of the results allowed to better understand the relationship which connects full size and scale models so that standard (small scale) tests could be validated by the introduction of corrections based on the differences in results between small and full scale tests.

1.2 Objectives

- Obtain a better understanding of the approaches adopted for the design of working platforms and investigate which factors are critical to determine its stability.
- Analyse the general characteristics of the material used for the construction of the working platform (particularly construction demolition waste) focusing on grading and components.
- Investigate the shear strength characteristics of a representative sample of platform material reduced at small scale by plate bearing capacity tests (using a centrifuge model) and standard shear box tests.
- Use the obtained results in order to inform the design of a large shear box (whose design will be defined according to examples of prototypes described in literature) and to test the same kind of material at full scale in order to investigate the presence of scale effects related to the use of downscaled sample and their influence on the results of the tests.
- Compare small and large scale test results in order to identify a correlation between them and validate the standard tests.

1.3 Thesis overview

The first part of this thesis focuses on the literature review concerning the design of working platforms and the methods used for testing the platform material. This is followed by the description of the experimental work which was conducted, the results obtained, the method used for their interpretation and discussion. Conclusions and recommendations for future work are also considered.

Chapter 2 presents a review of the methods used to evaluate the bearing capacity of shallow foundations and how these methods are generally applied for the design of working platforms. A concise description about the use of geosynthetic reinforcements is also included.

Chapter 3 gives an overview of the characteristics of platform material and in particular the class 6F2 as often used as reference for the selection of good quality platform material. Included in this chapter is the description of the testing methods which are commonly used for testing platform material: shear box and plate loading test. The chapter concludes with a description of the scale effects which can affect the two test methods. Several case studies are presented in order to identify the origins of the scale effects, the effects on the

results and possible solutions to avoid these effects or take them into account when selecting the properties of the material tested.

Chapters 4-7 present the experimental work of this research which involved conducting a series of small and large scale tests on limestone material. The small scale tests (direct shear tests using a standard apparatus and plate loading tests using a centrifuge model) are described in Chapters 4-5. These tests were carried out on downscaled samples of limestone material corresponding to a 6F2 grading which was reduced in size in accordance with two scale factors. A series of full scale tests was conducted on the same material using a large shear box apparatus in order to compare the results and identify the presence of scale effects. Description of the design and functionality of the large apparatus are described in Chapter 7 together with the test procedure and the results.

Chapter 8 presents the results obtained from the large scale tests and the description of the method used for their interpretation. A comparison of the results obtained from large and small scale tests is also included in this chapter.

Chapter 9 summarises the experimental procedure and presents the conclusions derived from the test results particularly focusing on the implications for working platform design. The chapter concludes with considerations about the limitations of the testing method adopted and recommendations for further research.

2. FOUNDATIONS AND PLATFORMS - LITERATURE REVIEW

2.1 Introduction

The expression “working platform” refers to a temporary ground-supported geotechnical structure, consisting of compacted granular fill, installed to allow construction plant and vehicles to travel and/or operate on site. The working platform is taken as including not only the platform itself but also the associated ramps and accesses (TWf, 2019; BRE, 2004).

The main aim in using a granular platform is to provide support to plant and vehicles preventing a failure event due to an excessive ground pressure. In this case the failure mechanism can be considered as a foundation failure which occurs when the shear stresses in the soil due to the vertical load on the foundation (tracks) exceeds the shear strength of the soil (Day, 2010). A suitable platform thickness would ensure spreading of the load applied at platform surface and therefore reduce the bearing pressure of the underlying soil. Although adequate thickness is the main aspect to consider when dealing with platform design, consideration should be given to the other common case of vehicle overturning due to localised weaknesses (soft/hard spots or inadequate backfilling/holes) in the platform rather than to a generally inadequate platform thickness across the site (BRE, 2004).

Working platforms are critical for plant stability and safety is a vital issue. Despite most working platforms performing well and serious incidents being relatively rare, every year piling rigs fall over and fatalities have occurred. The importance of promoting safety in the design, installation and operation of platforms cannot be underestimated (BRE, 2004).

Besides any risks associated with platform construction and function, there are also some hazards connected with the transportation and extraction of platform material, actions which can be avoided by promoting a safer, but also cheaper, method of construction. This approach to platform design relates to the use of recycled resources, especially construction demolition waste (CDW). The use of granular recycled material can reduce the costs of transportation and extraction but also the risks of incidents associated with these operations. Furthermore, replacement of the natural aggregates can sometimes improve the strength properties of the structure. This is for example the case of crushed concrete aggregate (CCA), a recycled product made out of waste concrete. As this material is crushed into smaller pieces, new surfaces of un-hydrated cement are exposed

so that with compaction and proper after-treatment the hydration reaction can start again leading to the hardening of the CCA. Self-hardening improves the compressive strength of the aggregate and the load-bearing capacity of the structure that it is in (Linden *et al.* 2019)

In order to improve and increase the use of this recycled material, it is necessary to understand its characteristics and properties so that it will be possible to develop a better design method (based on the assumption of more reliable material properties).

Most current design methods calculate the required thickness of the platform from bearing capacity formulations which (besides platform geometry) take into account the material properties of the subgrade and of the platform material. The main difficulty in ensuring a reliable design consists therefore in defining these properties. These properties might be difficult to obtain for what comprises the platform material due to the variability of components and the large particle size, which excludes the possibility of testing the material using standard laboratory apparatus. The research here presented aims therefore to investigate a test method able to be applied on the same kind of material used for the construction of working platforms so that reliable results could be obtained.

This objective will be achieved by comparing the standard testing methods which are normally used to test the material and the difficulties associated with them. Possible solutions found in the literature will be also described.

2.2 Platform design methods

The most commonly used platform design methods are based on analytical procedures which allow calculation of the thickness of the platform using bearing capacity formulations also used for foundation design. The problem is treated as two soil layers (the granular platform and the subgrade), subjected to a vertical load (representing the weight of working vehicles operating on the surface of the structure), applied on a limited surface (normally simplified as rectangular area) (Figure 2.1). From knowing the applied load (i.e. the weight of the plant) and the properties of the granular material and subgrade it is possible to derive the thickness of the platform required in order to prevent any risk of failure. Each design method takes into account the assumption of a different failure mechanism and some of these methods include in the calculation the use of geosynthetic reinforcement to increase the bearing capacity of the platform. Common to these methods is the influence of platform material properties (particularly the angle of friction) in

changing the bearing resistance of the structure and therefore the required thickness of the platform. For the purposes of this research only the case of a granular platform laying on a clay subgrade will be taken into account. The reason for this choice is to avoid the use of reinforcement solutions like geosynthetics where possible (due to the associated increase in cost) and focus on cases which would be more likely to occur in urban areas such as London where the subgrade is a relative stiff clay.

2.2.1 Bearing capacity of soils

Because all substances including soil and rock are compressible, when a load is applied on a limited area of soil (as in the case of a foundation) settlement occurs. The increasing settlement with load increment can be plotted against load per unit area giving a curve which may have any shape between those represented by the curves shown in Figure 2.2 (Das, 2010). At low load values the settlement may increase in direct proportion to the load but at higher values of load the rate of settlement usually increases. If the load becomes great enough, the increment of settlement may be excessively or uncontrollably large and the foundation is said to have broken into the ground or to have experienced a bearing capacity failure (Terzaghi *et al.*, 1996). The load per unit area of the foundation at which shear failure in the soil occurs is called the bearing capacity of the soil (Das, 2010).

The traditional analytical method for calculating the bearing capacity of soil is to use one of the many versions of the equation derived from Terzaghi's (1943) bearing capacity theory (different authors propose variations of the standard equation introducing factors to take into account more aspects affecting the bearing capacity). Terzaghi was the first to present a comprehensive theory for the evaluation of the ultimate bearing capacity of rough shallow foundations (where shallow refers to a depth of the foundation equal to three to four times their width (Das, 2010)). The analysis of a footing on soil is a contact problem of two dissimilar bodies. In making such an analysis, the soil has to be treated as an ideal material such as an elastic material, an elastoplastic material or a rigid-perfectly plastic material. If the soil were a rigid-perfectly plastic material (assumption usually made at failure when large displacements are considered), when the load reaches a certain magnitude the foundation would trap a wedge of soil (in the case of a strip foundation, cone in the case of a circular foundation) and this wedge, acted on by the footing, would push its way downward into the soil so that some regions would flow plastically (plastic zones) while other regions would show no deformation. As more load

is added, the plastic zones would increase and eventually break free to the surface. The surface between the plastic zones and the non-plastic or non-deforming zones is called a slip surface (Budhu, 2010). Based on the assumption that the soil is a semi-infinite, homogeneous, isotropic, weightless rigid-plastic material, Terzaghi suggested that for a strip foundation (the length is assumed to be large in comparison with the width of the foundation) the failure mechanism in the soil may be characterised by a slip surface similar to that shown in Figure 2.3 (Das, 2010). It is noted from this representation the presence of three different ground zones which are involved in the failure mechanism: active Rankine zone (ACD), radial Prandtl zone (ADF and CDE) and passive Rankine zone (AFH and CEG). The active zone is represented by the wedge of soil which is trapped by the footing above and acted on as the footing pushes downward into the soil. The angles CAD and ACD are assumed to be equal to an angle $\alpha = 45^\circ + \phi'/2$ (where ϕ' is the soil friction angle) (Budhu, 2010; Das, 2010). Two plastic zones can be generally distinguished: the first one is the radial zone (ADF and CDE, pushed sideways by the active zone) represented by a fan with radial slip planes defined by a logarithmic spiral slip plane, the second one is the passive zone (AFH and CEG, pushed in an upward direction), adjacent to the radial zone and consisting of slip planes orientated at angles of $45^\circ - \phi'/2$ to the horizontal plane (Budhu, 2010). The soil above the level of the bottom of the foundation is replaced by an equivalent surcharge $q = \gamma D_f$ (where γ is the unit weight of the soil and D_f the depth of the foundation) so that the shear resistance of the soil along the failure surfaces GI and HJ can be neglected. Based on these assumptions, Terzaghi derived the ultimate bearing capacity using an equilibrium analysis in the form (Budhu, 2010; Das, 2010):

$$q_u = s_u N_c + \frac{1}{2} \gamma' B N_\gamma + \sigma'_{zD} N_q \quad (2.1)$$

Where:

- $s_u N_c$ is the undrained term;
- $0.5 \gamma B N_\gamma$ is the self-weight term;
- $\sigma'_{zD} N_q$ is the surcharge term;
- s_u is the undrained shear strength of the soil ($s_u = 0$ in case of coarse grained soil);
- γ is the unit weight of the soil;
- B is the breadth of the foundation;

- σ'_{zD} is the vertical effective stress at the depth the foundation is laid ($\sigma'_{zD} = \gamma'D_f$, $\sigma'_{zD} = 0$ when the foundation lies on the surface);
- N_c , N_γ , N_q are bearing capacity factors;

Terzaghi also proposed the modified equation for square and circular footing which only differ by the coefficients used for the undrained term and the self-weight term (Das, 2010):

$$\text{Square foundation: } q_u = 1.3s_u N_c + 0.4\gamma BN_\gamma + \sigma'_{zD} N_q \quad (2.2)$$

$$\text{Circular foundation: } q_u = 1.3s_u N_c + 0.3\gamma BN_\gamma + \sigma'_{zD} N_q \quad (2.3)$$

The collapse mechanism which has just been described (Figure 2.3) is called “general shear failure mechanism” and, depending on the characteristics of the soil, is not always fully developed so that other modes of failure can be identified for shallow foundations based on stiffness and density of the soil.

Three different mechanisms were observed by Vesic (1963) who conducted several laboratory load bearing tests on circular and rectangular plates supported by sand at various relative densities. The three modes of failure were identified by Vesic (1963) correlated to different ranges of relative densities (D_r) (Das, 2010; Vesic, 1963; Vesic, 1973):

- General shear failure: foundations on relatively dense sand ($D_r > 0.70$) failed suddenly with very pronounced peaks of load per unit area when the settlement reached about 7% of the foundation width. In this failure mechanism this peak of base resistance was always reached and corresponded to the appearance of a failure surface which extended to the ground surface and to an abrupt change of rate of settlement from positive to negative (in strain-controlled conditions a visible decrease of load necessary to produce the foundation movement after failure could be observed, Figure 2.2a). This peak load per unit area of the foundation can be referred to as the ultimate bearing capacity of the foundation (q_u). A tendency toward bulging of the adjacent soil could be observed on both sides of the footing although the final soil collapse occurred only on one side.
- Local shear failure: foundations on sand of medium density ($0.35 < D_r < 0.70$) did not show a sudden failure. In this case the failure surface gradually extended outward from the foundation. As the load per unit area equalled $q_{u(1)}$ (when

settlements exceeded about 8% of the foundation width), movements of the foundation started to be characterised by sudden jerks. A considerable further movement (of about 15% of foundation width) was required at this point for the failure surface to extend to the ground surface. The load per unit area at which this happened can be considered as ultimate (q_u). In addition, first failure ($q_{u(1)}$), clearly distinguishable only in stress-controlled tests, could be noted when settlements reached magnitudes at which the general shear failure occurs in dense sand (Figure 2.2b). Terzaghi suggested the following modifications to the bearing capacity for foundation exhibiting the local shear failure mechanism (Das, 2010):

$$\text{strip foundation:} \quad q_u = \frac{2}{3} s_u N_c + \frac{1}{2} \gamma B N_\gamma + q N_q \quad (2.4)$$

$$\text{square foundation:} \quad q_u = 0.867 s_u N_c + 0.4 \gamma B N_\gamma + q N_q \quad (2.5)$$

$$\text{circular foundation:} \quad q_u = 0.867 s_u N_c + 0.3 \gamma B N_\gamma + q N_q \quad (2.6)$$

- **Punching shear failure:** foundations on relatively loose sand ($D_r < 0.35$) penetrated into the soil without any bulging of the sand surface, which means that the failure surface did not extend to the ground surface. The base resistance steadily increased as the settlement progressed. The rate of settlement increased and reached a maximum at settlements of about 15 to 20% of foundation width. The failure surface, which was vertical or slightly inclined and followed the perimeter of the base, never reached the sand surface. For punching shear failure there was no peak of base resistance (a continuous increase in vertical load was needed to maintain the foundation movement in the vertical direction), however a peak of settlement rate could be noted and the corresponding load (q_u) can be considered as ultimate load (Figure 2.2c). The soil outside the loaded area remained relatively uninvolved and there were no visible movements of the soil on the sides of the foundation.

These three characteristic types of failure were observed by Vesic (1963) at shallow depths. It can be said generally that the failure mode depends on the relative compressibility of the soil in the particular geometrical and loading conditions, a foundation on the surface of very dense sand will normally fail in general shear, while the same foundation on the surface of very loose sand will fail in punching shear. However, it is important to note that the soil state alone does not determine the mode of failure. For example (Vesic, 1973) showed that the same foundation on very dense sand can fail also in punching shear if:

- the foundation is placed at greater depth. Particularly, it was noted that as the relative depth D_f/B (where D_f is the depth of the foundation measured from the ground surface and B is the diameter/width of the foundation) increases, the limiting relative densities at which failure types change increases. The approximate limits of types of failure to be expected as relative depth D_f/B and relative density of sand D_r vary are shown in Figure 2.4. There is a critical relative depth below which only punching shear failure occurs. According to Vesic, for circular foundations on dense sand this critical relative depth seems to be around $D_f/B= 4$ and for long rectangular foundations around $D_f/B= 8$;
- the foundation is loaded by a transient, dynamic load;
- the very dense sand below is underlain by any compressible stratum (such as loose sand or soft clay)

Vesic (1973) also stated that a footing on saturated, normally consolidated clay will fail in general shear if it is loaded in the way that no volume change can take place, while it may fail in punching shear if it is loaded slowly enough so that all volume change can take place in the soil under load (Vesic, 1973).

Vesic (1973) proposed an adaptation of the bearing capacity equation in order to take into account any type of failure mechanism. This equation considers the introduction of compressibility factors (F_{cc} , $F_{\gamma c}$, F_{qc}) which can be calculated from a rigidity index (Das, 2010):

$$q_u = c'N_c F_{cc} + \frac{1}{2} \gamma B N_\gamma F_{\gamma c} + q N_q F_{qc} \quad (2.7)$$

F_{cc} , $F_{\gamma c}$, F_{qc} can be derived in accordance with the following procedure:

Step 1: calculate the rigidity index (I_r) of the soil at a depth approximately $B/2$ below the bottom of the foundation:

$$I_r = \frac{G}{c' + q' \tan \phi'} \quad (2.8)$$

Where:

- G is the shear modulus of the soil
- q' is the effective overburden pressure at a depth of $D_f + B/2$
- c' is the cohesion of the soil

Step 2: calculate the critical rigidity index ($I_{r(cr)}$):

$$I_{r(cr)} = \frac{1}{2} \left\{ \exp \left[\left(3.30 - 0.45 \frac{B}{L} \right) \cot \left(45 - \frac{\phi'}{2} \right) \right] \right\} \quad (2.9)$$

Step 3:

- If $I_r \geq I_{r(cr)}$ then: $F_{cc}, F_{gc}, F_{qc} = 1$
- If $I_r < I_{r(cr)}$ then:

$$F_{\gamma c} = F_{qc} = \exp \left\{ \left(-4.4 + 0.6 \frac{B}{L} \right) \tan \phi' + \left[\frac{(3.07 \sin \phi') (\log 2I_r)}{1 + \sin \phi'} \right] \right\} \quad (2.10)$$

If $\phi' = 0$:

$$F_{cc} = 0.32 + 0.12 \frac{B}{L} + 0.60 \log I_r \quad (2.11)$$

If $\phi' > 0$:

$$F_{cc} = F_{qc} - \frac{1 - F_{qc}}{N_q \tan \phi'} \quad (2.12)$$

It should be noted that other versions of Terzaghi's equation can be found in the literature which might consider additional coefficients relating to factors of shape/depth of the foundation or eccentricity/inclination of the load (for example Meyerhof, 1963). The application of any additional (or modified) coefficients would be similar to the process described above.

2.2.2 Bearing capacity of layered soil

The bearing capacity equations presented in the previous section consider the case in which the soil is homogeneous and extends to a considerable depth. However, many cases in real life (such as the one of a granular working platform laying on a clay subgrade) are characterised by layered soil. If the depth of the upper layer is shallow than the failure surface may extend through two or more layers.

Meyerhof (1974) developed a procedure to estimate the bearing capacity of layered soils. In the specific case of a foundation supported by a strong soil layer underlain by a weak soil (as it would be in the case of a granular platform on a clay subgrade) two different scenarios exist:

- the depth H (which represents the distance between the bottom surface of the foundation and the top of the weak layer) is relatively large compared with the foundation width (B) so that the failure surface will be completely located in the upper soil layer (Figure 2.5);
- the depth H is relatively small compared with the foundation width (B) so that a punching shear failure will occur in the upper soil layer followed by a general shear failure in the lower soil layer (Figure 2.6).

The critical depth (H_{cr}) of the upper layer representing the minimum height for which the failure surface would be confined in the upper layer is represented by (Budhu, 2010):

$$H_{cr} = \frac{B}{2 \cos\left(45^\circ + \frac{\phi'_{pk}}{2}\right)} \exp\left(A \tan \phi'_{pk}\right) \quad (2.13)$$

Where:

B = foundation width

ϕ'_{pk} = peak angle of friction of the upper layer

$A = (45^\circ - \phi'_{pk}/2)$ in radians

In the first scenario it is possible to estimate the bearing capacity using conventional bearing capacity theory based on the properties of the upper layer (Burd and Frydman,

1997). In the second case this approach may not be appropriate and therefore the ultimate bearing capacity can be calculated using the procedure proposed by Meyerhof and Hanna (Meyerhof, 1974; Meyerhof and Hanna, 1980; Hanna, 1981) for layered soils. The solution proposed considers the bearing capacity of the lower weaker layer and assumes that the upper layer serves principally to spread the load, therefore reducing its magnitude on the lower layer (Hanna, 1981). The most conservative use of this approach is to consider punching vertical shear surfaces developing in the upper soil layer rather than actual curved planes of failure (as shown in Figure 2.6). The obtained ultimate bearing capacity (q_u) of a shallow, rough, strip foundation can be expressed as follows (Das, 2010):

$$q_u = q_b + \frac{2(C_a + P_p \sin \delta)}{B} - \gamma_1 H \quad (2.14)$$

Where:

q_b = bearing capacity of the lower soil layer

C_a = adhesive force ($C_a = c_a' H$, where c_a' = unit adhesion)

P_p = passive force per unit length of faces aa' and bb' (Figure 2.6)

δ = inclination of the passive force P_p with the horizontal (since this is expected to vary within the depth of the upper soil layer, Meyerhof (1974) proposed the use of an average value of δ equal to $2\phi_1'/3$, where ϕ_1' = angle of friction of the upper soil layer)

B = breath of the foundation

γ_1 = unit weight of the upper soil layer

The equation can be expressed in the form (Das, 2010):

$$q_u = q_b + \frac{2c_a' H}{B} + \gamma_1 H^2 \left(1 + \frac{2D_f}{H} \right) \frac{K_p \tan \delta}{B} - \gamma_1 H \quad (2.15)$$

Where:

D_f = depth of foundation measured from the ground surface

K_p = horizontal component of passive earth pressure coefficient

$K_p \tan \delta = K_s \tan \phi_1'$ (K_s = punching shear coefficient)

The punching shear coefficient, K_s , is introduced in order to take into account of the strength of the lower layer. When this layer is made of relatively weak clay the punching failure of the upper layer may be accompanied by a failure surface that extends downwards into the clay. In this case the values of K_p obtained by assuming that punching failure is confined to the upper layer would be too large (Burd and Frydman, 1997). Hanna and Meyerhof (1980) conducted an experimental study of strip footings on a dense sand layer overlying a soft clay ($20 \text{ kPa} < s_u < 40 \text{ kPa}$) deposit and extended the results obtained to wide ranges of angle of internal friction of the upper granular layer and undrained shear strength of the lower clay layer. Values of K_s are presented by Hanna and Meyerhof (1980) using two charts: the first one (Figure 2.7) shows the trend of the coefficient of punching shear (K_s) based on the clay undrained shear strength (s_u) and the ratio δ/ϕ_1' (ϕ_1' is the angle of friction of the upper granular layer), whereas the second one (Figure 2.8) can be used to derive δ/ϕ_1' as a function of ϕ_1' and q_2/q_1 (where q_1 and q_2 are ultimate bearing capacities of a continuous foundation under vertical load on the surfaces of homogeneous thick beds of upper and lower soil). A drawback of this method, as stated by Lees (2019), is that the punching shear coefficient (K_s) presented by Hanna and Meyerhof in charts was derived empirically from model footing tests at 1g and the charts are presented in non-dimensional form so should be considered as appropriate only for the granular layer density and thickness used in their preparation.

The same equation can be used for rectangular and square/circular foundations by simply including shape factors (s_b and s_p) which take into account the limited extension of the foundation in the direction orthogonal to the width (B) of the foundation (Das, 2010):

$$q_u = q_b s_b + s_p \frac{2c_a' H}{B} + \gamma_1 H^2 s_p \left(1 + \frac{2D_f}{H} \right) \frac{K_p \tan \delta}{B} - \gamma_1 H \quad (2.16)$$

In the specific case of a granular strong layer overlaying a weak fine grained subgrade (as in the case of a granular platform overlaying clay) the shape factors are given by (BRE, 2004; BS EN 1997-1, 2004):

$$s_b = 1 + 0.2 B/L \text{ (in case of rectangular foundation)}$$

$$s_b = 1.2 \text{ (in case of square or circular foundation)}$$

$$s_p = 1 + B/L$$

A new design method to determine the bearing capacity of a granular layer on clay has been introduced by Lees (2019). The method was developed from considering the results obtained from a series of centrifuge model tests conducted by Okamura *et al.* (1997, 1998) on circular and strip footings on fine to medium sand overlying clay subgrades of different strengths. The tests were carried out on strip and circular footings and the thickness of the granular soil to width of the plate ratio (H/B) was also varied. The results were plotted by Lees (2019) in terms of bearing capacity ratio (bearing capacity of the granular material on clay divided by the bearing capacity of fine grained subgrade) against the ratio H/B . For tests conducted on strip footings a linear relationship was identified whose slope is indicated with T (Figure 2.9). A more linear plot was obtained for the circular footings when plotting the square root of q_u/q_s (Figure 2.10). From these results Lees (2019) identified the following equations:

$$\text{strip footing: } \frac{q_u}{q_s} = 1 + T \frac{H}{B} \quad (2.17)$$

$$\text{square or circular footing: } \frac{q_u}{q_s} = \left(1 + T \frac{H}{B} \right)^2 \quad (2.18)$$

Where:

q_u is the bearing capacity of the two soil layers

q_s is the surface bearing capacity of clay

H is the thickness of the granular layer

B is the foundation width

The factor T is calculated by knowing the angle of friction of the upper granular layer, the undrained shear strength of the underlain clay layer and the vertical effective stress at the base of the granular layer with zero foundation load:

$$T = 1.4 \left(\frac{s_u}{p'_0} \right)^A + B \quad (2.19)$$

For circular foundations, the T value should be multiplied by 1.13. According to the paper the coefficients A and B are calculated:

$$A = -0.41\phi'_{pk} - 0.18 \quad (2.20)$$

$$B = 4.2\phi'_{pk} - 3.4 \quad (2.21)$$

Where:

- ϕ'_{pk} = peak angle of friction of the upper granular layer (only appropriate where the strain level required to cause bearing capacity failure in the clay does not exceed the peak failure strain in the granular layer (like in the case of very soft subgrade). When this happens, the use of post-peak granular layer strengths is generally more appropriate)
- s_u = undrained shear strength of the lower clay layer (the author suggests to use the surface s_u value, except in cases with large foundation width and a rapid increase of s_u with depth)
- p'_0 = vertical effective stress at the base of the granular layer with zero foundation load

Equation 2.19 was derived by Lees (2019) by considering the results of three independent numerical studies: the finite-difference and FEA study conducted by Burd and Frydman (1997), the FELA study of Shiau *et al.* (2003) and the FELA study carried out by Kumar and Chakraborty (2015). By plotting the values of T obtained from Equation 2.19 against the ratio s_u/p'_0 Lees (2019) was able to identified a power-law relation between T and s_u/p'_0 (Figure 2.11) whose values would vary with the angle of friction of the granular top soil layer in accordance with Equations 2.19-2.21. Good agreement was also

identified with additional centrifuge data taken from the work of Lee *et al.* (2013) who performed circular footing penetration tests on a fine sand layer overlying clay of s_u around 17 kPa.

For B/L ratios (B= breadth of the foundation and L= length of the foundation) between 1 and 0, the bearing capacity can be interpolated linearly. The procedure consists of defining a line in a q_u vs B/L graph by connecting the values of bearing capacity calculated from the case of B/L= 0 (strip footing) and B/L= 1 (square footing) so the real bearing capacity value can be identified on this line at the point of abscissa equal to the real B/L ratio.

Furthermore, the value of q_u (bearing capacity of the granular layer on clay) obtained from these equations should be compared with the value of q_g (bearing capacity of the granular layer of infinite depth) so that:

- if $q_u \leq q_g$ then the failure mechanism involves both the granular layer and the soft subgrade. In this case the bearing capacity can be considered as equal to q_u ;
- if $q_u > q_g$ then the failure mechanism is limited to the granular layer and does not extend to the soft subgrade. In this case the bearing capacity is equal to q_g .

The value of q_g can be calculated using a standard bearing capacity equation for coarse grained soils.

The method presents the following advantages (Lees, 2019):

- it is a simple: just one design chart (or a few equations) can be used for all cases and the bearing capacity of the two layers can be derived from a few input parameters.
- it is versatile: the method is applicable to strip, square, rectangular and circular foundations with horizontal bases and vertical loading; embedded and surface; dry and saturated granular layers; a wide range of clay and granular layer strengths.
- All the relationships are dimensionless rather than derived from a narrow set of test conditions (for instance in the method of Meyerhof the punching shear coefficient is derived from model footing tests at 1g and presented in charts which are appropriate only for the granular layer density and thickness used in their preparation).

- Errors are conservative and smaller than those commonly found in existing methods (for example the method presented by Meyerhof can result in an unsafe over prediction of bearing capacity in some cases, particularly at high values of angle of friction of the granular layer and low s_u/p'_0 ratios)

2.2.3 Specific design guidance for working platforms

The fundamental mechanism of a granular platform consists of supporting piling rigs, mobile cranes and other heavy construction equipment in the same way as any other pavement structure: the platform is made with stronger material than the underlying formation with the intention of reducing the ground pressure to an acceptable level and therefore preventing a failure event from occurring and keeping settlement under acceptable limits.

Historically, the method used for the design of granular working platforms consisted of what might be described as empirical methods, largely based on previous experience of suitable material and thickness. Additionally, formal design methods have been used such as classical bearing capacity methods. Some recent publications have introduced new analytical design procedures for the design of both un-reinforced and reinforced granular platforms (for example: BRE BR470 (BRE, 2004) or Eurocode 7 (BS EN 1997-1, 2004; BS EN 1997-2, 2007)), which nowadays represent the methods expected to be used for the design of granular working platforms (TWf, 2019). One other alternative approach that has been adopted is the use of plate loading tests to prove platform capacity or geosynthetic manufacturers' design methods.

Conventional Terzaghi bearing capacity theory is based on the assumption that the soil is rigid-perfectly plastic with the strength characterised by an undrained shear strength or an angle of friction depending on the soil type. According to this theory and its development, the failure mechanism of a soil subjected to a load applied on a limited area of its surface can be described in three different ways depending on the strength and stiffness of the material (general, local or punching failure, as described in Section 2.2.1). In terms of soil settlement, the three failure mechanisms can be described in this way (TWf, 2019):

- General shear failure: occurs in relatively stiff soils of normal density. In this case the shear planes fully develop between the edges of the foundation and the ground surface with vertical settlement of the foundation and heave of the adjacent

ground. The active wedge underneath the foundation is resisted by the passive wedges on each side and connected by an intermediate radial zone (Figure 2.12). In this case failure occurs very suddenly and is usually catastrophic (failure occurs after small displacement if compared with local and punching failure).

- Local shear failure: occurs in relatively weak and compressible soils of low density. In this case the shear planes do not fully develop due to a high degree of soil compression underneath the foundation (Figure 2.13). In this case failure occurs slowly and is primarily observed as excessive settlement.
- Punching shear failure: occurs in very weak and compressible soils of very low density. In this case shear planes do not develop but vertical shearing occurs around the perimeter of the foundation with no adjacent heave (Figure 2.14). In this case failure occurs with relatively slow excessive settlement.

As described in Section 2.2.1, for each one of these failure modes it is possible to calculate the ultimate bearing capacity of the soil using different adaptations of the bearing capacity equation introduced by Terzaghi. While this approach can be successfully used for homogeneous soils, it cannot, in general, be used for cases where the soil properties vary with depth. Therefore, in the case of a layered soil this method can only be used to realistically estimate the bearing capacity of the soil when the thickness of the upper layer is large compared with the width of the foundation. If the thickness of the upper layer is comparable to the width of the applied load (such as in the case of a granular platform on which the load of a working vehicle is applied) this approach may not be appropriate (Burd and Frydman, 1997).

One of the most utilised methods successfully adopted for many years when designing for track and outrigger loads is the load spread model (or projected area method), which modifies the classical bearing capacity methods by assuming that the platform works to spread the load and thus reduces pressures on the underlying formation. The mode of failure for the granular platform is characterised by downward and outward movement of the platform and underlying formation (Figure 2.15) leading to (TWf, 2019):

- vertical deformation of the platform and subgrade beneath the load;
- upward heave of the subgrade and platform adjacent to the load;
- outward horizontal strain at the underlying formation.

The deformed shape of the subgrade is considered as indicative of an apparent angle of load spread. This method is generally used to estimate the bearing capacity of granular soil layers overlying clay, it assumes that the granular material acts to spread the load beneath the footing and that the foundation fails when the failure occurs within the subgrade. This procedure is clearly only appropriate for cases where the strength of the granular layer is substantially greater than that of the subgrade. The load spread mechanism within the granular layer may be modelled by assuming that the vertical stresses associated with the applied vertical load are confined to a zone defined by lines inclined at angle β to the vertical (Figure 2.16). The load is therefore assumed to be distributed uniformly over a width B' at the base of the granular layer, where $B' = B + (2D \tan \beta)$ (B is the width of the loaded area and D the thickness of the granular layer). The footing load failure (P_u) may then be estimated using the following expression:

$$P_u = B' s_u N_c \quad (2.22)$$

Where:

s_u = undrained shear strength of the clay

N_c = standard bearing capacity factor for undrained loading

Although the chosen value of β can have an important influence on the calculation of the bearing capacity (and therefore on the design of the granular layer), it is often not clear how its value should be selected. Burd and Frydman (1997) conducted a study of the bearing capacity of sand layers overlying clay soils for the case where the thickness of the sand layer is comparable to the width of a rigid foundation placed on the soil surface using both finite element and finite difference methods. They found that β increases with the angle of friction of the granular layer, is remarkably insensitive to the value of thickness of the granular layer and tends to reduce significantly as the ratio $s_u/\gamma D$ (where s_u is the undrained shear strength of the clay, γ the unit weight of the granular layer and D the thickness of the granular layer) is increased. For example, for a granular layer with a friction angle of 40° , Burd and Frydman (1997) found that the value of β varies from about 45° for a clay with low undrained shear strengths to zero with increasing clay strength (s_u).

The load spread model is shown to be a useful framework for understanding the mechanics of the problem, although in any practical application the method suffers from the disadvantage that it is difficult to estimate the load spread parameter in advance (Burd and Frydman, 1997). In addition there are other potential issues concerning the use of this method (TWf, 2019):

- the average pressure on the formation underestimates the pressure in the centre and overestimates pressure at the edges (as shown in Figure 2.17), which results in the formation being overstressed in the centre.
- the vertical loads cause outward pressure within the platform material which may result in shear stress on the formation at the base of the platform layer, thus reducing the bearing capacity of the subgrade by up to 50% (the load spread method does not take this into account).

The Federation of Piling Specialists (FPS), in conjunction with the Building Research Establishment (BRE), introduced in 2004 Design Guidance BRE BR470 (BRE, 2004) which provides the most widely used analytical methods for granular platforms. This guide provides an overall reference framework for the design, installation and maintenance of granular platforms and covers un-reinforced and reinforced granular platforms on both coarse grained and fine grained subgrades (TWf, 2019). The analytical method described in BRE BR470 is based on classical bearing capacity methods but uses the concept of punching shear capacity within the platform as suggested by the experimental model developed by Meyerhof (1974). Instead of assuming load spread through the granular layer, it is assumed that punching shear resistance develops within the upper layer thus partially supporting the applied load and reducing bearing pressures on the subgrade (Figure 2.18).

It is important to note that for this specific application the Meyerhof model assumes that (TWf, 2019):

- no lateral shear effects occur at formation (platform) level so that full bearing capacity can be used;
- weight of the platform and any benefit from surcharge are not included;
- unlike other analytical methods, geosynthetic reinforcement is not considered to provide lateral restraint. The bearing capacity of the geosynthetic is only taken into account in a very simplified manner by considering an additional vertical

reduction of the load on the subgrade due to the tensile membrane effect (Worbes and Moormann, 2018).

The forces on the assumed vertical punching failure surface in the granular layer can be taken as equivalent to a total passive earth pressure, P_p , inclined at an average angle δ acting upwards on the vertical plane beneath the edges of the loaded area, giving the following expression for the footing load failure (Figure 2.19):

$$P_u = BN_c s_u + 2P_p \sin \delta \quad (2.23)$$

Meyerhof suggested that the value of P_p may be obtained from the expression (Burd and Frydman, 1997):

$$P_p = \frac{1}{2} \frac{\gamma_1 D^2 K_p}{\cos \delta} \quad (2.24)$$

Where γ_1 is the unit weight of the granular layer and the value K_p (horizontal component of passive earth pressure coefficient) may be obtained from standard solutions based on the friction angle of the granular material (ϕ'). If the analysis were made using the actual curved planes of failure (Figure 2.20) the angle δ would be equal to ϕ_1' (ϕ_1' =angle of friction of the upper strong sand layer) but using the assumed vertical planes dictates that the mobilised angle δ must be less than ϕ_1' since failure does not in reality take place on the assumed vertical plane (Hanna, 1981). The average value of δ is generally in the range of about $\phi_1'/2$ to $3\phi_1'/4$ so that an approximate value of $2\phi_1'/3$, as suggested by Meyerhof (1974), seems appropriate.

Hanna (1981) studied the case of a foundation resting on a soil consisting of a strong sand layer overlaying a weak sand deposit and suggested that the value of δ decreases from about ϕ_1' near the footing edge (where actual and assumed planes correspond) to near zero (or $\lambda\phi_2'$ (ϕ_2' = angle of friction of the lower weaker layer), where λ depends on the strength of the lower soil layer and on the relative strength of the two soil layers) on the soil interface where the maximum distance to the actual failure plane increases (Figure 2.21).

The failure mechanism considered by Hanna (1981) in order to solve cases of load applied on a strong granular layer overlying a weak granular layer gives the following expression for the footing load failure:

$$P_u = 0.5\gamma_2 B^2 N_\gamma + 2P_p \sin \delta \quad (2.25)$$

Where γ_2 is the unit weight of the lower weak granular layer and N_γ is the bearing capacity factor of the same. In this case the value K_p (used to calculate P_p) can be determined from known values of angle of friction of the upper and lower layers.

Considering the model which has just been described above, an analogy can be observed with the ultimate bearing capacity equation (eq. 2.15) described in Section 2.2.2. This equation (eq. 2.15) can be modified such that no platform weight nor lateral shear effects at platform level are included (in accordance with the assumptions of the BRE method). Additionally the depth of foundation (in this case a working vehicle) measured from the ground surface (D_f) is equal to zero. Therefore:

$$q_u = q_b + \gamma_1 H^2 \frac{K_p \tan \delta'}{B} \quad (2.26)$$

Where, in the specific case of a granular platform on a fine/coarse graded subgrade:

q_b = bearing resistance of the subgrade

γ_1 = platform unit weight

H = thickness of the layer under the foundation (in this case platform thickness)

B = width of the loaded area of the platform

It should be noted that the guidance provided by BRE BR470 is not the only accepted design method and therefore design can equally be undertaken using any other approach.

Some of the known limitations of this analytical method are identified by the TWf (2019):

- Sensitivity to input parameters: the method is extremely sensitive to the values used for the platform material and subgrade strengths. In order to achieve an

economical design, the use of appropriate design parameters needs to be supported with good ground investigation and site testing of the platform;

- Limited range of fine grained subgrades: the calculations are only considered valid for undrained shear strength greater than 20kPa and less than 80kPa;
- Single strata subformation: the design method is only valid for single strata with no alternative offered for multi-layered subgrades. It is therefore assumed that the designer will adopt the worst case soil parameters;
- Geosynthetic reinforcement mechanism: the use of a geosynthetic alters the failure mechanism to one not covered by any of the previous examples making the analysis method unsuitable.

The design approach presented in BRE BR470 is based on the determination of the platform thickness as the main factor of the design.

The design procedure presented in the guidance starts by defining a radically simplified stress distribution acting on the platform surface. First of all, the magnitude of the imposed loads needs to be identified. These will include: plant weight (individual components with centre of gravity), operational loads (operating forces which can arise from: pile driving or extracting, crane lift loads, transported payloads, etc.) and wind loads. In the case of cranes or piling equipment the full range of orientation of the rig in relation to the tracks under a range of operating conditions should be taken into account and the worst of the load distribution combinations should be considered for the design. Once all of the actions acting on the working vehicle are identified, the total vertical load (N , Figure 2.22) and overturning moments (M_x and M_y , Figure 2.22) are derived from them. The effect of the total vertical load and moments shall be divided into single forces on each track (Q , Figure 2.22). Non-uniform load distribution on the defined loaded area (which means that the resultant load is affected by eccentricity in respect of the centre of the considered track loaded area) can be transformed into equivalent uniform load over a reduced loaded area using the method described by Meyerhof (1953). The study of Meyerhof includes the determination of the bearing capacity of foundations under eccentric loads considering the eccentric vertical load acting on the foundation surface as being applied at the centre of a smaller foundation. The actual foundation area is therefore reduced to an “effective contact area” (A') so that if B and L are the breadth and length of the foundation and e_b and e_l the eccentricities in the direction of B and L respectively then: $A' = (B - 2e_b) * (L - 2e_l)$ (Figure 2.23). In the specific example of Figure 2.22 the loaded

area which will be considered for design calculation would be therefore reduced to $A' = L' * B$ (Bond and Harris, 2008).

Once the loaded area and applied pressure are determined, it is possible to define the thickness of the platform by means of simple calculations. The procedure for these calculations is shown in full in Appendix A.

From the calculations in Appendix A it should be noted that the factors which can influence the value of platform thickness are: undrained shear strength of the underlying sub-formation, design angle of friction of the platform material and the bulk unit weight of the same. A sensitivity analysis of the influence of these factors on the thickness of the platform was carried out:

- the variation of platform thickness with design angle of friction of the platform was evaluated considering constant representative values of shear strength of sub-formation (equal to 50 kPa) and platform bulk unit weight (equal to 20 kN/m³). It should be noted that the range of values for the angle of friction (as shown in Figure 2.24) is quite limited. This is due to the fact that for angles of friction lower than 40° the results of the design process lead to the choice of a better quality platform material (which means higher angle of friction), while the graph which is used as reference (BS EN 1997-1, 2004) to define the values of the horizontal component of passive earth pressure coefficient (K_p) does not provide any data for angles of friction higher than 50° which is necessary for the calculation of the bearing resistance of the platform on a fine grained subgrade.
- the variation of platform thickness with shear strength of the sub-formation was evaluated considering constant representative values of platform design friction angle (equal to 45°) and platform bulk unit weight (equal to 20 kN/m³).
- the variation of platform thickness with bulk unit weight of the platform material was evaluated considering constant representative values of sub-formation shear strength (equal to 50 kPa) and platform design friction angle (equal to 45°).

The choice of these values was decided according to an appropriate range of shear strength for the subgrade and unit weight/design angle of friction for the platform material. The shear strength of the subgrade was assumed equal to 50 kPa considering

that, as the guide underlines (BRE, 2004), for a fine grained subgrade it is particularly important that the characteristic value is a cautious estimate of the field strength during the design life of the platform, since the undrained shear strength is strongly dependent on water content and near the ground surface it will be affected by climatic changes. The guide specifies that this value must be between 20 kPa and 80 kPa. Values of shear strength lower than 20 kPa would represent a very soft ground where special measures would be needed to construct a working platform and thus a more sophisticated type of design. On the other hand, for values of shear strength higher than 80 kPa, the bearing resistance of the subgrade in many cases would be adequate to support the applied load. A value of shear strength equal to 50 kPa was considered as representative for a firm subgrade quality. Furthermore, the guide indicates as typical bulk unit weight for the platform material a value of 20 kN/m³ and typical design values of angle of friction in the range between 35° and 50°. A value of angle of friction equal to 45° was assumed as average considering that gap graded materials placed with little compaction usually provide *in-situ* shear strength values in the range of 35°-40°, while well graded materials require proper compaction in layers but will provide a much higher shear strength values between 45°-50° (TWf, 2019).

The resulting values of platform thickness were plotted in three different graphs showing the variation of the thickness with shear strength of the underlying sub-formation and with design angle of friction/ bulk unit weight of the platform material (Figures 2.24-2.26). From these graphs the influence of the three factors on the thickness of the platform was evaluated separately. It is a simple matter to verify that the parameter most strongly influencing the platform thickness is the design angle of friction of the platform material: a small increase of this angle can provide a significant reduction of platform thickness. Nonetheless, it should be noted that this is true only when considering absolute changes of these parameters. If the realistic variability is taken into account then the parameter that would be subjected to larger changes is the undrained shear strength of the subgrade.

Despite the importance in determining this parameter, it seems unclear which value of angle of friction should be adopted for the design of the platform. It is well known from literature (for example: Powrie, 2010) that dense granular materials tested at low stress levels exhibit high values of strength (higher than the strength, at equal shear strain, of the same material when tested under the same vertical stress in a loose state) due to their dilatant behaviour. The initial increase of shear stress of the dense material is followed,

after the achievement of a peak value (identified by a peak angle of friction, ϕ'_{pk}), by strain softening till the achievement of a state of constant shear stress and volume well known as critical state (identified by the critical state angle of friction, ϕ'_{cr}). It is evident therefore that at low stress levels the initial density (or porosity) of a granular fill has a major effect on the magnitude of the strength parameters (among which of major interest for the purposes of this research is the angle of shearing resistance ϕ').

Therefore, the BRE guide which was taken into account (BRE, 2004) suggests that for poorly compacted granular material it is appropriate to use $\phi'_d = \phi'_{cr}$ and for heavily compacted material to use $\phi'_d = \phi'_{cr} + \Delta\phi'$, where $\Delta\phi'$ is a function of:

- normal stress level (for dense granular material under which undergo a shear strain smaller than the ones corresponding to critical state the angle of friction can achieve larger values than the critical state angle depending on the amount of compaction and applied normal stress).
- Void ratio (an increase of void ratio determines a reduction of the shear strength).
- Particle properties (such as strength, shape and roughness).

A more simple solution to adopt during the design would be the use of peak angle of friction values for fully compacted material and constant volume values if compaction is expected to be minimal (TWf, 2019).

When working platforms are constructed using material like crushed brick and/or concrete (which represent the most common constituents of the crushed demolition waste used in working platforms) with a grading similar to class 6F2, it is usual practice for the design of the platform to adopt an angle of friction of 45° or more. Consideration should however be given to the fact that the angle of friction can be particularly sensitive to the factors previously mentioned so, for optimum design, it would be useful to determine the shear strength parameters of the platform material by testing the granular fill under conditions close to those which will be experienced in the field.

One method used to validate the design of a granular platform is the plate bearing test which can be undertaken on site to verify the capacity of the platform (TWf, 2019). The results obtained need to be treated with great caution and a number of aspects must be taken into account in order to obtain reliable results:

- the plate has to be of appropriate diameter in order to be representative of the actual loaded area. For example, a test using a normal plate size (300 to 450 mm diameter) and applied to the surface of the platform will have almost no influence on the subgrade. However the use of large diameters would increase the costs associated with providing sufficient reaction to provide the bearing pressure;
- it should be possible to increase the load applied to the plate up to twice the working load;
- a sufficient number of tests should be carried out considering the geometry of the site and potential variability in the ground.

Finally, geosynthetic manufacturers' design methods are represented by alternative empirical methods of design produced by manufacturers validated by extensive past experience and appropriate experimental testing (TWf, 2019). In these specific cases the possible assumptions which can be used (and can vary according to different manufacturers) during design are:

- increase of the angle of load spread;
- increase of formation bearing capacity by elimination of the horizontal shear;
- reduction in platform thickness

It should be noted that these types of methods rely on empirical data and are therefore not as “transparent” as analytical methods (based on calculations which can be checked). These are also issues of commercial sensitivity which may limit full knowledge of a particular manufacturer's method.

2.2.4 Use of geosynthetic reinforcement

This section is dedicated to a general description of geosynthetic reinforcement and their use in working platforms. In the past three decades geosynthetics have been used successfully world-wide in several areas of civil engineering and are now a well-accepted construction material (Shukla, 2016). For a granular working platform it has to be considered that the contribution of geosynthetic to the overall platform performance varies between the different types of geosynthetic available in the market so that their use has always to be accompanied by a specific design (TWf, 2019). The aim of this research will be focusing only on the use of the granular platform as method of reinforcement for a clay subgrade so just a brief description of the geosynthetic reinforcement method will be presented in this section.

A geosynthetic is defined as a planar, polymeric (synthetic or natural) material used in contact with soil/rock and/or any other geotechnical material in civil engineering applications (Pinto, 2003). Geosynthetics can assume one or more of the following functions; reinforcement, separation, filtration, drainage, fluid barrier, protection (Shukla, 2016) and the current different fields of application can be summarised as road and railways, foundations, embankments, steep slopes and retaining walls (Pinto, 2003).

The reinforcement function of geosynthetics is provided by adding tensile properties to the soil (which is a material with good compressive characteristics) in order to obtain a composite material that has both compressive and tensile strength (Pinto, 2003). Reinforcement is therefore provided by the geosynthetic by transference of tensile stresses from the soil to the reinforcement.

Geosynthetics used in reinforcing working platforms are usually geotextiles or geogrids. The first type of geosynthetic is primarily used as a protective separation layer to reduce contamination of the platform material but also to provide a degree of reinforcement/stabilisation of the granular fill, while the second one is specifically used for reinforcement/stabilisation.

Fluet (1988) subdivided the reinforcement function into two categories:

- a *tensile member*, which support a planar load (Figure 2.27a);
- a *tension member*, which supports not only a planar load but also a normal load (Figure 2.27b).

Koerner (2005) and Jewell (1996) consider not two but three mechanisms for soil reinforcement, explaining that when the geosynthetic works as a tensile member it might be due to two different mechanisms: shear and anchorage. Therefore the reinforcement function can be distinguished in:

- *shear* (or sliding), when the geosynthetic supports a planar load due to the sliding of the soil over it;
- *anchorage* (or pullout), when the geosynthetic supports a planar load due to its pullout from the soil;
- *membrane*, when the geosynthetic supports both a planar and a normal load on a deformable soil.

Shukla (2002, 2004) describes four reinforcing mechanism based on the way the geosynthetic takes the stresses from the soil and which type of stresses (Giroud *et al.*, 1984, Shukla, 2016):

- *shear stress reduction effect*: outward movements of the granular fill (from application of vertical load) are restrained and therefore horizontal shear stresses transmitted from the platform material to the top of the underlying subgrade soil are reduced or eliminated. These stresses are transferred from the fill material to the geosynthetic, by friction, preventing these from being transmitted to the subgrade soil and therefore maintaining the full bearing capacity of the subgrade. This effect causes a change in the failure mechanism, which transforms from a local shear failure to a general failure (Figure 2.28).
- *interlocking effect*: for geogrids the reduction of lateral displacement results not only from friction development on the surface of the geogrid, but also from interlocking (anchoring effect) of the soil particles within the apertures (Figure 2.29).
- *Slab or confinement effect*: this mechanism is illustrated by Figure 2.30 which shows how the introduction of the geosynthetic at the interface of granular platform and soft subgrade produces a restraint effects and consequently limits the level of vertical displacement under load and the load transmitted to the underlying subgrade.
- *Membrane effect*: if the subgrade is relatively incompressible (e.g. saturated clay), its deformation under load causes upward heave of the subgrade and platform adjacent to the load and the geosynthetic deforms in sympathy. Therefore, the geosynthetic exhibits a wavy shape and consequently it is stretched. When a stretched flexible material has a curved shape, normal stress against its concave face is higher than normal stress against its convex face. Therefore: (i) between the load and to a lesser extent beyond the load, the normal stress applied by the geosynthetic on the subgrade is higher than the normal stress applied by the platform material on the geosynthetic; and (ii) under the load, the normal stress applied by the geosynthetic on the subgrade is smaller than the normal stress applied by the load plus the fill material on the geosynthetic (Figure 2.31). This action provides two beneficial effects: an increase in the bearing capacity of the subgrade below the loaded area and a downward loading on its surface to either side of the loaded area reducing in this way its heave potential. This is known as

the "tensioned membrane effect". The deformed geosynthetic can sustain in this way normal and shear stress and depending on the type of stresses the type of support can be classified as "normal stress membrane support" or "interfacial shear stress support".

Once a certain type of geosynthetic has been selected, some characteristics are needed for the analytical design of reinforced platforms. Some of these are (TWf, 2019):

- Tensile strength (at an acceptable level of strain, typically in the range of 2 to 5%, so that tensile strength can be mobilised but at the same time the serviceability requirements of the platform is not exceeded).
- Radial stiffness (to limit the lateral strains and thereby restricting lateral aggregate particle movement and consequently improving the bearing resistance).
- Geometric properties (together with any limitations on platform material particle size)
- Friction characteristics
- Punching resistance (particularly when using geotextiles, to minimise damage from the platform material and therefore maintain exclusion of contaminants and tensile capacity).
- Durability in service.
- Maximum spacing between layers (when more than one layer of geosynthetic is necessary or may prove beneficial). It is recommended that: they are evenly spaced, vertical spacing is less than 450 mm and more or equal to 150 mm.
- Minimum cover over geosynthetic reinforcement: it should be 300 mm but may be reduced to 150 mm where further advice is obtained from a geosynthetic manufacturer.
- Sufficient porosity (to allow drainage of the platform material).

In all cases it is recommended that the designer should refer to the relevant manufacturer's product data and/or technical support team to confirm suitability.

3. PLATFORM MATERIAL AND TESTING - LITERATURE REVIEW

3.1 Introduction

As seen in the previous chapter, the shear strength of the granular platform material is extremely important in defining the design. Due to this factor alone, the exact quantitative and qualitative nature of the platform material and its specification should be treated as being of high importance.

In general, the platform should be constructed with a durable granular material, free of any organic matter and free draining (BRE, 2004). When referring to platform material it has been common practice to use simple general descriptions such as “75 down crusher run” (TWf, 2019). However, in the interest of ensuring the use of material having a suitable strength and thereby minimising the platform thickness (and therefore the costs), design guides suggest referring to defined specifications.

One of the proposed approaches (TWf, 2019) in selecting good quality platform material is to use standard descriptions as tabulated in the Standard Specification for Highway Works (Highways Agency, 2004), especially the tables for “Series 600 earthworks” which describe the full set of requirements for classes of selected granular fill (such as 6F2 or 6F5) typically used for capping and which allow the inclusion of recycled material. Each specification includes: general description of allowed and dis-allowed materials, method of compaction, particle size distribution, strength of particles and moisture content.

Another suggested approach (TWf, 2019) is to build a specification based on previous experience and requirements. This approach defines some key items to consider:

- Nature and proportions of base material (crushed brick, concrete, stone, etc).
- Exclusion of unwanted contaminant (soil, timber, reinforcement, etc).
- Grading limits such as: limitation on proportion of fines (15% maximum); material graded/sized to engage geogrids and avoid local punching of geotextiles; uniformity coefficient C_u (defined as the ratio of D_{60} to D_{10} , less than 5 for opened graded material and greater than 10 for uniformly graded); material sized to minimise the effect of scrubbing, etc.
- Resistance of platform material to fragmentation/crushing.
- Particle shape (angular/sub-angular).

Other matters the designer should consider with regard to material specification include:

- The type of material and related construction method: gap graded materials do not require a significant compaction and provide *in-situ* shear strength values in the range $\phi' = 35^\circ\text{-}40^\circ$, so that the platform will be thicker but relatively little compaction effort will be needed. Well graded materials require proper compaction in layers but will provide much higher shear strength values ($\phi' = 45^\circ\text{-}50^\circ$) resulting in a thinner platform. It should be noted that the shear strength values provided above are purely indicative and intended by TWf (2019) as a guide to values that might be appropriate.
- Maximum particle size should be limited as follows:
 - not greater than 150 mm in all cases;
 - not greater than 2/3 the thickness of compaction layers;
 - to suit the operation to be undertaken (for example to ensure positioning of some pile types a small particle size of 75 mm may be required)

Despite these material specifications being very descriptive in defining the requirements, consideration should be given to the fact that the shear strength characteristics of the platform material can vary largely depending on the proportions of the components and the grading curve. Specific test data are therefore fundamental in defining any change in shear strength with the variation of these material parameters.

Another significant issue is guaranteeing the durability of the platform material once the structure has been constructed. Durability of working platform material can be compromised by (TWf, 2019):

- loading events: magnitude, frequency and overall number should be adequately controlled by appropriate methods of design;
- weather: strength of the platform material can be reduced by the introduction of moisture and can be controlled by considering the presence of moisture within the platform design or introducing methods able to guarantee that the platform is adequately drained;
- scrubbing and other local effects from wheels and tracks which can reduce the platform thickness and can be mitigated by use of larger aggregate sizes;
- contamination from fines and water: the introduction of a slurry into the voids of the granular fill has the effect of reducing the internal angle of friction and has the

effect of making the effective thickness of the platform considerably thinner than that established by the design, ultimately leading to failure.

- other contaminants such as: high sulfate content, asbestos, reinforcing rods, plaster, etc. (BRE, 2004).

The durability of the platform can be increased, for example, by providing a geotextile separation layer between the platform and the subgrade or a “sacrificial” layer added to the structural minimum thickness.

Considering the importance of determining the angle of friction of the granular material for the design of the platform, it is necessary to understand which testing method or methods would be the most appropriate in order to obtain the required information. Two types of test are here described and considered as the most commonly used in determining characteristic properties.

The first test is the standard direct shear test which represents the simplest standard test used to derive the angle of friction of a soil sample. The second test procedure is the plate bearing test, normally used for foundation design to derive the bearing capacity of soil *in-situ* by means of field loading tests (ASTM D1194, 1994). This last type of test can be used to validate the capacity of the platform once constructed but can also be used as method to derive the angle of friction of the platform material by carrying out back analysis using one of the standard bearing capacity formulations (this method is not ideal for current design since the test is done after the platform has been constructed but could be useful for future design in order to verify if the angle of friction considered for the previous design corresponds to the value calculated from the back analysis).

Both the tests presented here are characterised by complications in deriving reliable results on materials such as 6F2 which has large particle size. This is mostly due to scale effects associated with the ratio between the size of the testing apparatus and diameter of soil particles. Literature concerning this problem is presented in Section 3.5.

3.2 6F2 class material (Highways Agency, 2004)

In order to guarantee good performance of the platform material, it is common practice to refer to standard specifications which are used to define its main features and acceptable properties. One of these specifications is represented by the Standard Specification for Highway Works (Highways Agency, 2004) which provides

classification, definition, uses and requirements for aggregate material used for the construction of road works. The material classification is provided by series, among which the series 600 describes the requirements for earthworks material. Belonging to this series is the class 6F2 which refers to a class of selected material mainly used as a sub-base/capping for roads and buildings but also characterised by many other uses such as piling mats and general backfill.

This class is composed essentially of granular material (coarse grading) whose characteristics can largely vary depending on the origin of its components. The permitted constituents described in the Standard Specification for Highway Works includes any material, or combination of material, including recycled aggregates with not more than 50% by mass of recycled bituminous planings and granulated asphalt but excluding materials contaminated with tar and tarbitumen binders, unburnt colliery spoil and argillaceous rock (Highways Agency, 2004). Excluding the above mentioned forbidden constituents, a large variety of other materials can be included in this class: blast furnace and zinc slag, burnt colliery spoil, china clay sand and stent, foundry sand, furnace bottom ash, incinerator bottom ash, pulverized-fuel ash, reclaimed asphalt, recycled aggregate (RA), recycled concrete aggregate (RCA), recycled glass, spent oil shale and steel slag are just some examples of material of which 6F2 class can be composed.

In site roads and working platforms the use of granular material with a rounded particle shape should be avoided (at least near the surface of the road) because it may lack stability under wheel contact pressure (TWf, 2019).

As well as the physical and chemical properties, the grading requirement for the class 6F2 can largely vary. In Figure 3.1 (representing the values in Table 3.1) the lower and upper acceptable limits of particle size distribution considered as representative for this class are shown (Highways Agency, 2004) and thus the space between the two curves includes any valid particle grading.

The broad range of particle size distribution and list of allowable constituents included in this class makes it difficult to predict the material behaviour which could vary greatly with the variation in physical composition. Therefore when referring to the class 6F2 as a material for the construction of piling platforms it is of crucial importance to undertake further investigations in order to identify the actual characteristics of the material. Since

the angle of friction represents one of the main factors influencing the design of the platform, the determination of reliable values for this angle would be of vital importance.

3.3 Direct shear test

3.3.1 Introduction

As already anticipated in the description of current platform design methods (Section 2.2), effective design requires a certain degree of knowledge about the physical characteristics of the fill material (especially the angle of friction, on which the platform thickness largely depends as seen in the analysis described in Section 2.2.3). The direct shear test represents the simplest way to determine this parameter and the standard procedure is described in the following section.

3.3.2 Description of the test method

The direct shear test belongs to the class of tests in which soil strength and stiffness are investigated by loading soil samples and calculating the resulting stresses and strains. The principal loading tests are: one-dimensional compression (oedometer) tests, direct shear tests and triaxial tests. These may be drained or undrained and they may be stress controlled or strain controlled. The most important factors to record during these tests (but not in all of them) are (Atkinson, 2007):

- total stresses and pore pressures (in the case of direct shear test, pore pressure cannot be measured and therefore the test is conducted in the way to dissipate any possible pore pressure in the sample), controlled and measured separately to derive the effective stresses;
- drainage of water in the sample, in order to verify if the test is characterised by drained (change of volume with drainage of pore water from the soil) or undrained (constant volume without drainage of pore water from the soil) conditions;
- strains in the sample under application of the loads, used to verify the stiffness of the soil.

In a standard shear box (or direct shear) apparatus a soil sample of 20 to 25 mm thickness is placed inside a split metal box of internal dimensions equal to 60 mm x 60 mm or 100 mm x 100 mm on plan (BS 1377-7, 1990 after Atkinson, 2007). Once the sample is placed in the direct shear device, a normal stress is initially applied compacting or consolidating (till primary consolidation is achieved) the specimen. After this, the shear box halves that

hold the test specimen are unlocked and the sample is sheared along a mechanically induced horizontal plane by displacing one half laterally with respect to the other at a constant rate of shearing deformation while measuring the shearing force and the relative lateral and normal displacements.

Since there is no control of drainage and the procedure cannot be used for undrained tests (BS 1377-7, 1990), the shearing rate must be slow enough to allow complete dissipation of excess pore pressure in the case of fine grained soils.

By carrying out tests on a set of (minimum three) similar specimens of the same soil under different normal pressures, the relationship between measured shear stress at failure/peak and normal applied stress is obtained (BS 1377-7, 1990).

3.3.3 Description of the testing apparatus

According to the British standard (BS 1377-7, 1990) shear box apparatus can be classified in two different types based on the maximum size of the specimen that the box allows: small shear box apparatus (soil specimen of 60 mm or 100 mm square and 20 mm to 25 mm high) and large shear box apparatus (soil specimen up to 305 mm square and 150 mm high). The principle of the method is the same for both the apparatus with the difference being that the large shear box would allow a larger soil maximum particle size to be tested.

The main components of the direct shear box are represented by (Figure 3.2, BS 1377-7, 1990):

- a container for the specimen (the shear box), square in plan and divided horizontally into two halves, rigid enough to resist distortion under maximum load. Particularly in the case of a large shear box apparatus, the container should be made of steel sections rigid enough to resist distortion when supporting the specimen and when subjected to the maximum vertical and horizontal load. During sample preparation the two halves are fitted together with alignment screws (ASTM D3080, 2011);
- an outer container (the carriage) in which the box can be placed to enable the specimen to be submerged under water during test, supported by a low-friction bearing which allows movement in the longitudinal direction;
- two porous plates of negligible compressibility under load (made of silicon carbide, aluminium oxide or material not subject to corrosion (ASTM

D3080, 2011)), placed on top and bottom of the specimen to allow free drainage of water;

- a loading cap (about 0.5 mm smaller in plan than the internal dimensions of the box) to cover the top porous plate, through which vertical load is distributed uniformly across the specimen and so that it is free to move up or down as the volume of the sample changes (ASTM D3080, 2011);
- a loading system (such as a loading yoke carrying calibrated masses or another mechanical lever system);
- a motorised loading device (for example a motor-driven ram), capable of applying horizontal shear to the specimen at constant rate of displacement with less than $\pm 5\%$ deviation. In order to test a wide range of soils the apparatus should permit adjustment of the rate of displacement from 0.0025 to 1.0 mm/min (ASTM D3080, 2011);
- a calibrated force-measuring device (loading ring or load transducer) to measure the shearing resistance of the soil during the horizontal displacement (a proving ring or a load cell can be used to measure the lateral force needed to maintain the top half of the shear box stationary). The shear stress, applied at constant rate of displacement, can then be deduced dividing the lateral force by the cross-sectional area of the soil sample (ASTM D3080, 2011);
- a load cell accurate to 2.5 N (or 1% of the normal force during shear, whichever is greater) is required when using anything but dead weights to apply the normal force (ASTM D3080, 2011);
- if the normal pressure is applied hydraulically, the value should be indicated by a pressure gauge;
- a calibrated displacement transducer (or dial gauge) to measure the relative horizontal displacement of the two halves of the shear box;
- a calibrated displacement transducer (or dial gauge) to measure the vertical deformation of the specimen during the test.

The materials comprising the shear box, the outer container and all components which fit into it should be resistant to corrosion (BS 1377-7, 1990) by moisture or substance within the soil (for example: stainless steel, bronze or aluminium) (ASTM D3080, 2011).

According to the Standard ASTM D3080 (2011), the minimum specimen diameter for circular specimens, or width for square specimens, should be 50 mm or not less than ten times the maximum particle size diameter. The minimum initial specimen thickness should be 13 mm, but not less than six times the maximum particle diameter.

The weight of the lid supported by the specimen should be less than 1% of the applied normal force during shear: this will most likely require that the top plate be supported by a counter balance. The device should be able to maintain the normal force to within $\pm 1\%$ of the specified force.

During sample preparation the two halves of the box are held together by screws but before the test commences the screws are removed. The top half of the box is raised slightly so that no metal-to-metal contact will occur during shear and a gap is maintained between the two halves. Presently there is insufficient information available for precisely specifying the gap dimension based on particle size distribution but the gap between the two halves should be small enough to prevent the outflow of the soil and the test should be checked periodically to confirm that the gap persists throughout the shearing phase of the test.

The upward vertical displacement (y) of the lid of the shear box and the lateral displacement (x) of the lower half of the shear box (Figure 3.3) can be measured using dial gauges or electrical displacement transducers known as LVDTs (linearly variable differential transformers), capable of recording the changes in specimen thickness (y) with a precision of at least 0.002 mm and to measure relative lateral displacement (x) with precision of at least 0.02 mm.

3.3.4 Determination of the appropriate displacement rate

Excess pore water pressures are generated in a soil when it is subjected to an increase in load. As is well known, in a coarse grained soil water can flow relatively easily between the particles, so that the additional pore water pressures usually dissipate almost instantaneously, while in a fine grained soil these excess pressures dissipate slowly. In a standard shear box test there is no facility to measure pore water pressures within the sample in order to analyse the test in terms of effective stresses and for this reason the test must be carried out slowly enough to prevent the development of significant pore water pressures. This will ensure that the entire applied vertical load is carried by the soil skeleton as an effective stress and a test carried out under these conditions is termed as

drained test. Bolton (1991) suggests suitable shear rates aiming to conduct a drained shear box test: approximately 1 mm/min for sand, 0.01 mm/min for silt and 0.001 mm/min for clay samples. The test results should not be affected if the sample is sheared more slowly, while the results of a test which has been carried out too quickly would be meaningless.

The determination of the appropriate rate of displacement requires an estimate of the time required for pore pressure dissipation and of the amount of deformation required to reach the failure of the soil sample. These two factors depend on the type of material and its stress history and the procedure described in ASTM D3080 (2011) could be used to compute an appropriate shear rate.

3.3.5 Preparation of specimens

Specimens of either fine grained or coarse grained soil can be tested in the direct shear test apparatus and their preparation procedures depends on the type of soil. If the sample to be tested is made of coarse grained soil, the procedure depends on whether the soil is dry and can be poured, or damp and needs to be tamped, or saturated.

Dry sand can be placed or poured directly into the assembled shear box. A loose density is often achieved by rapidly pouring from certain height (small if using a small apparatus, 0.5 m when using a large shear box apparatus) and the surface levelled to give the specimen an appropriate thickness without disturbing the main body of the sample. For compacted samples, a certain amount of tamping (by a square ending tamper) or vibration (through the plate) should be applied for as long as necessary to achieve the desired density. The tamper used to compact the material should have an area in contact with the soil equal to or less than half the area of the shear box (ASTM D3080, 2011). In the case of using a large shear box apparatus, the weighted sample should be divided into three approximately equal portion. The first portion should be spread evenly in the box and compacted using a 2.5 or 4.5 kg rammer or a vibrating hammer until the layer occupies one third of the height of the final dense sample. The same operation should be repeated on two further layers. The boundaries of each layer should be positioned in the box so that they are not coincident with the shear plane defined by the two halves, unless this is the purpose for a particular test (ASTM D3080, 2011).

In order to obtain partially saturated samples of sand a quantity of soil (somewhat larger than that required for the test specimen) should be adjusted in water content to the value

required for the test specimen and the material placed in the shear box and compacted by tamping.

For saturated sand samples the shear box should be filled with water to the level corresponding to the top of the specimen. A known dry mass of sand should be placed in water and boiled for about ten minutes and allow to cool or placed under vacuum to remove air bubbles. After that, the saturated sand can be placed into the shear box and compacted by vibration to the desired density (BS 1377-7, 1990).

3.3.6 Data processing

A series of data can be obtained from the direct shear test in order to derive the shear characteristics of the sample tested (Powrie, 2010):

- the vertical effective stress (σ'_v) and the shear stress (τ), calculated with the assumption that the pore water pressure is zero, acting on the central horizontal plane of the shear box are obtained by dividing the forces N (normal load) and F (shear force) by the cross-sectional area (A):

$$\sigma'_v = \frac{N}{A} \quad (3.1)$$

$$\tau = \frac{F}{A} \quad (3.2)$$

It should be noted that the contact area of the specimen on the imposed shear plane decreases during shear and hence shear and normal stresses should be calculated accordingly.

- the shear strain (γ_s) is given by:

$$\gamma_s = \frac{x}{h_0} \quad (3.3)$$

Where:

x = relative horizontal displacement

h_0 = initial sample height

- the change in sample total volume (ΔV_t) corresponding to movement (y) of the shear box lid is equal to:

$$\Delta V_t = A y \quad (3.4)$$

the volumetric strain (ϵ_{vol}) is given by:

$$\epsilon_{vol} = \frac{\Delta V_t}{V_{t0}} = \frac{A y}{A h_0} = \frac{y}{h_0} \quad (3.5)$$

Where:

V_{t0} = initial volume of the soil sample

- the specific volume of the sample at any stage of the test is given by:

$$v = \frac{V_t G_s \rho_w}{m_s} \quad (3.6)$$

Where:

$V_t = V_{t0} + A y$

G_s = specific gravity of the sample

ρ_w = water density = 1 g/cm³

m_s = dry mass of soil

Shear box test data are conventionally plotted as graphs of shear stress (τ) or stress ratio (τ/σ'_v) against shear strain (γ_s), and volumetric strain (ϵ_{vol}) or specific volume (v) against shear strain (γ_s). During the test the lid of the shear box moves horizontally by a distance dx . If during this time it also moves vertically upward by a distance dy it means that it is travelling at an angle $\psi = \tan^{-1}(dy/dx)$ to the horizontal (as shown in Figure 3.4). This angle (ψ) is known as the angle of dilation and it is an indication of the rate at which the sample is changing in volume as it is sheared. If ψ is positive the lid is moving upward and the sample is increasing in volume (dilating), if ψ is negative the lid is moving downward and the sample is reducing its volume (compressing). More formally ψ is expressed as:

$$\psi = \tan^{-1} \left(-\frac{d\varepsilon_{vol}}{d\gamma_s} \right) \quad (3.7)$$

The reason why a sample is dilating or compressing during shear is determined by the fact that the soil is a particulate material and so its particles must take up a suitable arrangement of packing (known as critical void ratio) before continued shearing can take place. If the particles are initially more loosely packed than the critical void ratio (Figure 3.5a) then densification, corresponding to a compression of the sample, takes place. If the particles are initially densely packed (Figure 3.5b) during shearing the particles placed in the upper layer will have to climb out of the troughs resulting in dilation of the soil sample.

The achievement of a critical void ratio, at which continued shear can take place without change in volume, is illustrated by idealised results from shear box tests conducted on dense and loose samples of sand at the same value of normal effective stress (σ'_v) and shown in Figure 3.6. From these, two different cases can be visualised:

1. for the initially dense sample:
 - During the test the shear stress increases to a peak (indicated as P) before falling to a steady value (indicated with C) which is maintained as the strain is increased (Figure 3.6a).
 - The sample may undergo a small compression at the start of the shear but then begins to dilate, the curve of ε_{vol} against γ_s (Figure 3.6b) becomes steeper indicating that the rate of dilation ($-d\varepsilon_{vol}/d\gamma_s$) is increasing. The slope of the curve reaches a maximum at P but with continued strain the curve becomes less steep until at C it is horizontal ($d\varepsilon_{vol}/d\gamma_s = 0$), indicating that dilation has ceased.
 - The value of specific volume increases due to the dilation of the sample (Figure 3.6c) till achieving the critical specific volume at steady state of shear stress at C (shown in Figure 3.6a).
2. for the initially loose sample:
 - The sample displays no peak strength when sheared but eventually reaches the same critical shear stress as the initial dense sample (Figure 3.6a).
 - The sample does not dilate but gradually compresses during shear until the volumetric strain (ε_{vol}) reaches a constant value corresponding to the end of its compression (Figure 3.6b).

- This state corresponds to the achievement of the same critical specific volume for the initially dense sample (Figure 3.6c).

In both cases it can be noticed that when sheared the soil will eventually reach a critical void ratio at which continued deformation can take place without further change in volume or stress. This condition at which unlimited shear strain can be applied without further changes in specific volume (v), shear stress (τ) and normal effective stress (σ'_v), is known as critical state.

Considering now idealised results of shear box tests carried out at different normal effective stress (Figure 3.7: test 1 carried out at the lowest value of σ'_v and test 4 at higher value of σ'_v) and same initial void ratio (e_0) it can be noticed that:

- As the normal effective stress (σ'_v) is increased (from test 1 to test 4) the peak stress ratio (τ/σ'_v) is reduced while the same ratio at the critical state is unaffected (Figure 3.7a).
- The specific volume (v) at the critical state is reduced as the normal effective stress is increased (Figure 3.7b).
- Considering the different values of τ reached at the critical states for each value of normal effective stress, it can be seen that the values lie on a straight line of gradient $\tan(\phi'_{cr})$ on a graph of τ against σ'_v and the equation of this line may be written as: $\tau = \sigma'_v \tan(\phi'_{cr})$ (Figure 3.7c).
- To each value of τ and σ'_v at the critical state correspond different values of specific volume (v , as it can be seen in Figure 3.7d). As said before the values of v at the critical state decrease with the increase in σ'_v .
- Plotting the same values of v at the critical state in a graphic of v against $\ln \sigma'_v$ (Figure 3.7e), it can be found an equation having as gradient λ : $v = v_0 - \lambda \ln \sigma'_v$; where v_0 is the intersection of the line with the v -axis (i.e. the value of v on the critical state line at $\ln \sigma'_v = 0$ or $\sigma'_v = 1$ kPa) and $-\lambda$ is the slope.

From all these considerations it can be derived that the combination of specific volume (v), normal effective stress (σ'_v) and shear stress (τ) at the critical state lies on a unique line (the critical state line) when plotted on a three-dimensional graph with axes representing specific volume, normal effective stress and shear stress (Figure 3.8). In other words: if sufficient tests are carried out on a soil, so that it would be possible to

locate the critical state line (or its projections), it could be possible to predict the values of any two of the parameters at the critical states (between σ'_v , τ and v) when the third one is known.

3.4 Bearing capacity test

3.4.1 Introduction

In alternative to laboratory testing, *in-situ* tests can be used to measure the strength and settlement characteristics of soil. Plate loading tests are described by the British Standard (BS 1377-9, 1990) as suitable for the design of foundations where it is considered that the mass characteristics of the soil would significantly alter the results of laboratory tests or where more precise values of load-settlement are required (BS 1377-9, 1990).

One of the most important steps in the design of a foundation is the evaluation of the greatest pressure which can be applied to the underlying soil without causing either failure of the loaded soil or excessive settlement.

The concept of “allowable soil pressure” was firstly developed during the 1870’s in different countries, based on the general observation that under similar conditions foundations which transmit pressures of high intensity to the subsoil generally settle more than those transmitting lower pressures. Considering this principle, designers started to consider the condition of buildings supported by foundations exerting different values of pressure on soils. It was therefore considered as a satisfactory basis for design of shallow foundations to allow as maximum pressure the one not associated with structural damage. The values obtained by this procedure for each type of soil in a given locality were assembled into a table of allowable soil pressures considered appropriate for the construction of foundations in that area.

Many foundations designed on the basis of the allowable soil pressure tables performed well but other ones did not and the structure settled excessively. To avoid this problem, it became good practice to verify the allowable soil pressure with the use of load tests.

A load test consists of increasing the load on a bearing plate in small increments and measuring its corresponding settlements. There are different methods for performing the test and interpreting the results, which are usually presented as a load-settlement curve. Whatever the method may be, the test results reflect the character only of the soil located within a depth of less than about twice the width of the bearing plate. Consequently, if

the characteristics of the soil change below this depth, as often happens, the test results are certain to be misleading and the use of a larger plate would be therefore suggested (Terzaghi *et al.*, 1996).

Over the last few years it has become common practice to carry out plate loading tests to confirm the satisfactory performance of working platforms and subgrade separately. Back analysis can be used to check if the shear strength and/or deformation parameters of the installed platform correspond to the values used during the design (TWf, 2019).

Information regarding the methods used to evaluate the bearing capacity of soil and, in particular, the plate loading test procedure are described in the following sections, including an evaluation of how to determine the angle of friction from the results for the purposes of the design of working platforms.

3.4.2 Plate loading test

The plate bearing test is usually done when shallow foundations are to be used or when temporary work structures such as piling rigs or cranes are required on site. This test checks the bearing capacity of the soil near the surface of the ground and the possible settlement under a certain load. The most common Standards applicable to the test are the British Standard (BS) 1377 Part 9 (BS 1377-9, 1990) and the American Society for Testing and Materials (ASTM) D1194 (ASTM 1194, 1944).

According to the British Standard, the test can be described in the following way: *“This method covers the determination of the vertical deformation and strength characteristics of soil in-situ by assessing the force and amount of penetration with time when a rigid plate is made to penetrate the soil. Uses are to evaluate the ultimate bearing capacity, the shear strength and deformation parameters of the soil beneath the plate without entailing the effects of sample disturbance. The method may be carried out at the ground surface, in pits, trenches or adits, and at the depth in the bottom of a borehole”* (BS 1377-9, 1990).

When verifying the bearing capacity (at ultimate limit state) and deformation/settlement (at serviceability limit state) characteristic of the soil under load it is important to consider the fact that plate loading tests might not be representative of the loaded area, particularly in the case of tracks and outrigger pads and it is possible that a test using the normal plate

size (300 to 450 mm diameter) applied to the surface of a working platform will have almost no influence at all on the subgrade (TWf, 2019).

The depth of influence for spread foundations has historically been accepted as the depth at which the increase in vertical pressure diminishes to 20% of the applied bearing pressure (q) at the surface. It is normal to adopt the pressure bulbs (curves which connect all points below the ground surface at which the vertical pressure is the same) generated by the Boussinesq formula to define this depth, as shown in Figure 3.9. According to these bulbs, the depth of influence is approximately $1.5B$ for a circular pad and $3.0B$ for a strip foundation (where B is the breadth of the footing). It can be concluded from that that if a small plate is used to test the material the influence of the test will be restricted to a limited depth which might not be representative of the real depth involved by the loading of a piling rigs or crane (TWf, 2019).

However it should be noted that the depth of influence for settlement is not the same as the depth of influence defined for bearing capacity. Instead it is defined as the point at which the increase in vertical stress, due to the applied bearing pressure (q), is equal to 20% of the (existing) vertical stress from the effective overburden pressure, as shown in Figure 3.10 (TWf, 2019).

3.4.3 Description of the testing apparatus

The British Standard (BS 1377-9, 1990) and the Standard ASTM (ASTM 1194, 1944) provide a general description of the apparatus for this test, specifying that the particular form of each item is not fixed and should be determined in accordance with: job conditions, testing requirements, equipment available and degree of precision required. Following is the description of the equipment components which were considered as being the most important:

- A loading plate of rigid construction. The plate size shall be defined based on the soil fabric and take into account: the amount of reaction required, the means of mobilizing it, the magnitude of the other apparatus and the size of pit or borehole in which the test is being carried out. The British Standard (BS 1377-9, 1990) requires a plate diameter of at least 300 mm when testing fissured clay and exceeding five times the nominal size of the coarsest material when testing granular soil, while the Standard ASTM (ASTM 1194, 1944) suggests a bearing steel plate of not less than 25 mm in thickness and varying in diameter from 305

to 762 mm or, as an alternative, concrete footings of the size mentioned or larger and with a depth of not less than two thirds of their width. An important aspect to consider is that the bigger the plate size the better it mimics the actual condition of the foundation however a larger width will increase the amount of reaction load required to mobilise the plate into the soil. Any tendency for the plate to tilt should be avoided ensuring that the loading column is positioned centrally on the plate (BS 1377-9, 1990).

- Reaction loading system. The reaction load should be sufficiently far from the proposed test position in order to reduce the influence on the results. The load can be provided in different ways, such as: kentledge (water in tanks or concrete blocks), tension piles or jacking against an existing reaction such as a structure (BS 1377-9, 1990). When a hydraulic or mechanical jack assembly is meant to be used, a loading platforms or bins of sufficient size and strength should be used to supply the estimated total load required or the total load reaction (ASTM 1194, 1944).
- Calibrated force measurement system. More than one force-measuring device may be necessary to obtain the required accuracy (BS 1377-9, 1990). This can be done, for example, using a pressure gauge, electronic load cell or proving ring (ASTM 1194, 1944).
- Deformation measurement system. e.g. dial gauges or levelling system, capable of measuring settlement of the test plates, could be used as settlement-recording device (ASTM 1194, 1944).
- Test area preparation equipment. Mechanical diggers or boring equipment (including the casing) and temporary ground support are indicated by the Standard as possible solutions for preparing the test site. A flat level test area of sufficient size for the loading plate should be provided and verified by levelling equipment (BS 1377-9, 1990).

Additional apparatus are mentioned in the Standards (for example temperature gauge) and their use should be evaluated in accordance to the specific situation of the test and level of precision required.

3.4.4 Description of test procedure

As well as a description of the testing apparatus, a summary of the procedure for the plate loading test is here described. The steps which are considered as being the most relevant for the purposes of testing the bearing capacity of granular soil are:

- Primary excavation and preparation at test level. The aim of this step is to excavate the soil to a level where the plate will be placed and create a level soil surface which is as undisturbed as possible and not significantly affected by: stress relief, opening of discontinuities, wetting or climate change such as frost action (BS 1377-9, 1990). The standard ASTM (ASTM 1194, 1944) suggests that when the test is meant to verify the bearing capacity of footings the load test should be done at the elevation of the proposed foundation and under the same conditions to which the foundation will be subjected (which means that the bearing plate should be placed at the same relative depth as the actual footing). Furthermore, the Standard suggests at least three test locations at a distance not less than five times the diameter of the largest plate used in the test. The areas should be carefully levelled and cleaned so that the loads are transmitted over the entire areas on undisturbed soil.
- Preparation and erection of loading and measuring apparatus. The reaction loading, force measurement and deformation measurement system should be placed in a convenient position and made ready for immediate erection as soon as the plate is in position. The loading column should be placed centrally over the plate and made vertical so that the reaction load is applied direct to the plate without eccentricity (BS 1377-9, 1990).
- Test loading and records of measurements. The load can be applied in two different ways according to the type of soil which needs to be tested:
 - Constant rate of penetration test is suitable when the undrained loading characteristics of the soil are required. In this case the load is applied in a controlled manner so that a selected rate of penetration is maintained. The test is continued until the penetration reaches at least 15% of the plate width. Where there is no clear indication of failure prior to the 15% penetration the ultimate load is taken as equal to the load at this level of penetration.

- Incremental loada test is suitable when the drained loading characteristics of the soil are required. Load is applied in at least five increments to the tuscan be supported (BS 1377-9, 1990). According to the Standard ASTM (ASTM 1194, 1944) the load should be applied to the soil in cumulative increments of no more than 95 kPa, or of not more than one tenth of the estimated bearing capacity of the area being tested. The load should be maintained at each increment until all the primary consolidation is complete (judged according to the settlement versus log time plot) (BS 1377-9, 1990). Any selected type of time interval should be maintained for each load increment in all tests of any series (ASTM 1194, 1944).

In both cases, intermediate cycles of unloading and reloading may be made during the test at various stages to obtain an indication of the relative amounts of reversible and irreversible deformation that have occurred (BS 1377-9, 1990).

3.4.5 Data results and calculation

Results of the test are represented by applied pressure versus penetration of the plate. The maximum applied pressure (which can be considered as ultimate bearing capacity of the soil) is calculated from the following equation (BS 1377-9, 1990):

$$q = \frac{\frac{W_e 9.81}{1000} + P_u}{A} \quad (3.8)$$

Where:

q = maximum applied pressure (kPa)

W_e = total mass of the apparatus acting on the plate before adding the applied load, including the mass of the plate (kg)

P_u = applied force to cause failure. When this is not clearly defined the force causing a penetration of 15% (10% for the Standard ASTM 1194, 1944) of the plate width should be used (kN).

A = area of the base of the plate (m²)

3.4.6 Plate loading test for working platform

The plate loading test is also a good tool to determine the strength characteristics of granular working platform material and of the subgrade which supports the platform. This kind of test has become more common place over the last few years despite some difficulties related mainly to lack of specifications about its application on the granular working material.

When working vehicles operate on site the supporting platform must be stiff enough to limit deformation/settlement to acceptable limits. Wherever possible, appropriate acceptance criteria should be obtained from the vehicle supplier and/or operator which may vary depending on the exact nature and size of the vehicle and the operation being undertaken. If it is not possible to obtain clear requirements, suggested guide values for general use are (TWf, 2019):

- absolute settlement to be not greater than the lesser of $B/10$ (B = width of the loaded area) or 50 mm;
- differential settlement across tracks to be not greater than 5 mm/m (approximately 0.3°);
- differential settlement across outriggers to be not more than 10 mm/m (approximately 0.6°).

Serviceability limit state conditions can include those in which an item of plant cannot operate within accepted tolerances (e.g. driving piles) or cannot move (e.g. slewing), while ultimate limit state conditions are those which may lead to overturning of plant. In general, bearing failure occurs at deformations exceeding 20% of the width of the loaded area. It is also generally accepted that where deformations are restricted to 10%, the calculated bearing pressure can be taken to be the ultimate capacity and this is termed “tolerable settlement” (TWf, 2019).

The platform area loaded by tracks of a piling rig or crane varies from machine to machine and also depends on the particular activity which is carried out. However, considering the highest critical load condition, the load area may be typically around 2 m^2 . Considering that such large tests are impractical, over the last few years the use of small diameter plates, testing granular material and subgrade separately, became a more acceptable practice.

Plate load tests can be applied on the platform following the specifications indicated in the Standard BS 1377-9 although some difficulties may be found when testing a soil characterised by a large particle size (as for example 6F2 material). As anticipated, the British Standard (BS 1377-9,1990) suggests that when testing a granular soil the plate diameter should exceed at least five times the nominal size of the coarsest material. Due to this limitation two problems can be found: the first one is represented by the difficulty in understanding what exactly is meant by “nominal size of the coarsest material” and, second, how to apply this criterion to a large particle size like the one of 6F2. This last one represents the main issue since granular material commonly used for working platform construction are typically well graded sub-base type materials, such as MOT Type 1 or 6F2, or crushed brick, or concrete based demolition material, which generally have a similar type of grading characterised by large particle size. The large size of the particles would require a large plate diameter (equal to 375 mm for a maximum particle size of 75 mm) and hence a large load in order to satisfy the Standard BS 1377. This problem will be better described in the following section.

3.5 Scale effects in the tests

3.5.1 Introduction

The aim of this section is to provide a description of the difficulties associated with the two test procedures previously described and, in particular, the consequences of scale effects on the results of direct shear tests and *in-situ* plate loading tests. Both test types may be affected by scale effects which originate from testing material using apparatus which does not guarantee sufficiently large ratios between the size of the equipment and maximum particle size of the tested material. The section is structured in such a way that, for each type of scale effect described, a possible solution is provided in order to avoid the effect or evaluate how the results might be affected. In both cases the aim will be to provide solutions to the problem in order to obtain reliable test results such that it would be possible to use the outcomes for design purposes.

3.5.2 Scale effects in direct shear tests

As previously mentioned, the easiest way to obtain information regarding the shear resistance of soil is the use of the direct shear test. Despite the simplicity of the procedure, there are some limits in performing the test as a result of the configuration of the apparatus. Among these are the fact that the shear plane is predetermined during the test

and there is no way to measure pore pressure in the soil so that the test must be always conducted in drained conditions. Other difficulties are associated with direct shear tests carried out on material having a large particle size, since the limited size of standard apparatus would affect the sample behaviour during the test leading to misleading results which cannot be considered as representative of the real characteristics of the material.

Based on this last consideration, it is important to define, prior to testing, the appropriate geometry of the sample with respect to the maximum particle size characterising the soil. The Standard ASTM D3080 (2011) specifies the minimum sample dimensions to be adopted in standard direct shear tests:

“The minimum specimen diameter for circular specimens, or width for square specimens, shall be 2.0 in. [50 mm], or not less than ten (10) times the maximum particle size diameter, whichever is larger.”

“The minimum initial specimen thickness shall be 0.5 in. [13 mm], but not less than six (6) times the maximum particle diameter.”

While the British Standard (BS1377-7, 1990) refers only to the height of the sample:

“The size of the largest particle shall not exceed one-tenth of the height of the specimen.”

“For a very compressible soil the initial specimen thickness should be adequate to ensure that after consolidation the plane of the shear is formed near the mid-height”

Despite this guidance, studies were found in the literature suggesting the presence of geometric effects leading to different values of friction angle when testing the same material in apparatus of different sizes. Specifically, what was found is a decrease in the measured angle of friction when testing the material in a larger box rather than in a smaller one (despite both the two different sizes of the apparatus adopted conforming to the limit provided by ASTM D3080 (2011) and BS1377-7 (1990)). The ASTM Standard was mainly taken into account despite the limits imposed by this standard being less conservative than the ones proposed by the British Standard (which means that the size of the shear box required by the British Standard is larger than the one required by the ASTM Standard). The reason for this is that the ASTM Standard also provides additional sizing information compared with the BS (e.g. guidance on width). These studies are discussed in this section.

Sobol *et al.* (2015) tested a soil having a maximum particle size of 2 mm in a medium (120 x 120 mm) and in a large (250 x 250 mm) shear box. Despite the ratio between sample and maximum particle size being clearly acceptable according to the testing standards, a decrease in the peak angle of friction and of the shear stress when using the large box has been observed. The same behaviour was found by Taylor and Leps (1938) and Bishop (1948), both conducting tests on sand samples. Taylor and Leps (1938) tested dried Ottawa sand in both small (76 mm) and large (305 mm) square shear box and found a difference in angle of friction of 0.5° when using a different size of the apparatus (larger values were obtained when using the smaller apparatus) (Sobol *et al.*, 2015). Bishop (1948) used two square boxes, whose dimensions were 60 mm and 305 mm for testing dry sand and the angle that he obtained from the test in a small box was about 2° higher than the values obtained with the use of a large apparatus (Sobol *et al.*, 2015). Sobol *et al.* (2015) explained the phenomenon as an effect of the angularity and roughness of the material's particles which would cause wedging of the grains in the medium box leading to higher peak shear stress and higher peak friction angles.

Cerato and Lutenecker (2006) conducted tests on different particle size samples considering the results obtained from previous studies (Parsons, 1936; Palmeira and Milligan, 1989). Parsons (1936) tested Ottawa sand ($d_{\max} = 0.83$ mm) and crushed quartz (screened into ten samples which varied in d_{\max} from 0.74 to 4.7 mm) prepared in a loose state in three different box sizes: a small (60 x 60 mm), a medium (100 x 120 mm) and a large (120 x 200 mm) apparatus. The results identified a decrease in the critical state friction angle with the increase of the sample size. Palmeira and Milligan (1989) could not, however, find significant differences related to the critical state angle of friction values when testing samples made with Leighton Buzzard sand ($d_{\max} = 1.2$ mm) in a dense state in three different apparatus: a small (60 x 60 x 32 mm), a medium (252 x 152 x 152 mm) and a large (1000 x 1000 x 1000 mm) apparatus. Considering these results, Cerato and Lutenecker (2006) tested in three different shear box sizes (60 x 60 x 26.4 mm, 101.6 x 101.6 x 40.64 mm and 304.8 x 304.8 x 177.8 mm) four different maximum particle size soils (5 mm, 2 mm, 1.7 mm, 0.9 mm) at three different relative densities (dense, medium and loose state). A decrease in the critical state angle of friction with the use of larger samples was observed for all the specimens. They pointed out the necessity of using the largest size specimen possible for the determination of the critical state angle of friction of soil and proposed as reasonable limits the following values: H/d_{\max} (H = specimen

thickness) greater than 6 (in line with ASTM D3080 (2011), which was defined although it was unclear if adequate, suggesting the need for more testing to confirm this ratio) and W/d_{\max} (W = specimen width) greater than 50 (from Jewell and Wroth (1987) who suggested a ratio of the shear box length to average particle size in the range of 50 to 300).

Fu *et al.* (2015) provided an explanation of this phenomenon pointing out the fact that the shear strength of coarse-grained soils derives from resistance against sliding between particles and particle rolling. When shearing coarse-grained soil specimens along a specified shear band (as happens in a direct shear apparatus) the sliding between particles and particle rolling depends upon specimen size and gap dimension. If the diameter (or length) and height of the specimen or the gap between the shear box halves (or combination of both) are too small, a portion of particles within the specified shear band will tend to crush and fracture during shearing. The occurrence of such failures would be the cause (according to Fu *et al.*, 2015) of overestimations of actual shear resistance of the coarse-grained soil. In order to investigate the correct sample size a modified apparatus, able to adjust its height, diameter and gap between the two halves, was built and used to test two uniformly coarse graded soil samples (one having a maximum particle size equal to 5 mm and the other one equal to 10 mm). The two halves of the shear box were assembled from a series of steel structures capable of superimposition and nesting to enable variation of specimen size in diameter and height. Each layer was 25 mm thick and a maximum layer number of four was allowed for each half. The height of the apparatus could therefore be equal to 50, 100, 150 or 200 mm while possible diameters corresponded to 61.8, 100, 150, or 200 mm. In order to prevent leakage of specimen particles via the gap during shearing, a piece of annular foam was placed between the two shear box halves so that no influence on results might occur due to outflow of sample material from the shear box. Considering the results obtained from these tests, the range of gap size (able to maintain shear stress and angle of friction values relatively constant when testing the same sample at different gap sizes) was found for both the samples:

- $0.86d_{\max} < \text{gap size} < 1.28d_{\max}$ for the first sample (maximum particle size of 5 mm).
- $1d_{\max} < \text{gap size} < 1.3d_{\max}$ for the second sample (maximum particle size of 10 mm).

Considering this, the author decided to adopt as reasonable gap sizes the following values: 5.3 mm for the first sample and 12 mm for the second one (i.e. just over the maximum particle size of the sample).

Using these gap sizes, reasonable limits were found for both samples on the minimum diameter (W) and minimum height (H), over which the angle of friction remains relatively constant:

- $W/d_{\max} > 15$ (angle of friction relatively constant assuming adequate height of sample).
- $H/d_{\max} > 10$ (angle of friction relatively constant assuming adequate diameter of sample).

It should be noted that these values are more restrictive than the ones provided by ASTM D3080 (2011) and could represent a good method to evaluate the size of a sample made of angular and coarse-grained soil when tested in direct shear box apparatus. During the tests conducted by Fu *et al.* (2015) each specimen was sheared until a long stable tail appeared after the peak condition or until lateral displacement reached approximately 10% relative to the specimen diameter. The values of angle of friction were then determined by the author by considering the maximum shear stress or the shear stress corresponding to 10% relative lateral displacement in the absence of peak behaviour. It must be noted that no outflow of specimen particles via the gap was allowed during shearing due to the use of a piece of annular foam placed between the two shear box halves. Therefore, effects on shear strength deriving from changes in gap size cannot be associated with the loss of particles.

Conclusions derived from this last study seem to suggest that not just the size of the sample (height and length/width) has an effect on the shear resistance parameters but also the gap between the two halves of the shearbox. Other research conducted on the effect of the gap size on the shear behaviour of granular material in a direct shear test was produced by Kim *et al.* (2012), who conducted tests using a direct shear box having a diameter of 60 mm and a height of 20 mm. Seven different types of material (having a maximum particle size ranging between 0.21 mm and 2.14 mm) were tested at constant vertical stress. The tests were conducted in two different conditions: first allowing the outflow of particles during shearing without applying any supplementary means to the gap of the two box halves and secondly using a Teflon sheet which prevented this

phenomenon. From the first series of tests it was observed that the peak shear stress and the dilatancy for all soil samples were affected by the opening size. If outflow of sample from the opening occurred, reasonable shear behaviour could not be measured due to the variation of the condition of the sample during shearing. These results were used to derive a guideline for opening size according to the mean particle size of the sample. Through the application of Teflon sheet, similar shear behaviour for all the samples were obtained regardless of the opening size. Thus, by eliminating the outflow of sample through the application of some supplementary means, the shear behaviour can be obtained regardless of the opening size. What was found by Kim *et al.* (2012) appears therefore to be in contrast with what was concluded by Fu *et al.* (2015), whose results seemed to be affected by the change in gap size regardless of whether the outflow of particles was prevented during test. On the other hand, no clear explanation of the phenomenon is provided by Fu *et al.* (2015), thus it appears that preventing outflow of particles from the shear apparatus would be advisable to avoid effects on the results of the test.

As anticipated, when the particles of a sample are very large it is not always possible to test the material in a standard apparatus which typically has a width (or diameter) of 64-73 mm (Bareither *et al.* 2008). The particle size which could normally be accommodated whilst respecting ASTM Standards (D3080, 2011) is approximately 5 mm and, depending on the testing device, rarely exceeds 10 mm with standard apparatus (Simoni and Houlsby, 2006). Therefore, excluding the use of a larger shear box for economic reasons (the costs will often not be justifiable by the importance of the work), another solution needs to be adopted. It is common practice that when granular backfill materials contain gravel (i.e. particle size over 2 mm) the gravel-sized particles are removed using one of several methods for preparing laboratory specimens. Among these methods, the most commonly used are the parallel grading technique and the scalping method. In both methods a fraction of the representative grading will be ignored (Figure 3.11).

The parallel technique provides the use of a scaled sample of the original material whose grading curve maintains the shape of the grain size distribution. The sample grading is obtained by a parallel shift of grading distribution curve such that the maximum particle size is in line with the size of testing device. The grading distribution curve is drawn by considering the following (Kim and Ha, 2014):

$$D_i = \frac{D_{Bi}}{R} \quad (3.9)$$

Where:

D_i = particle diameter of similar grading (mm)

D_{Bi} = particle diameter of original grading (mm)

R = similarity ratio (or scale coefficient, defined as the ratio between the maximum particle size of the original graded soil and the maximum permissible particle size of the test)

Through this method, the particle size distribution curves of the sample and original graded soil are exactly parallel. The sample obtained from the use of this technique will have a similar geometric arrangement and same uniformity/curvature coefficient of the original grading. The uniformity coefficient is represented by the D_{60}/D_{10} ratio and is related to the general shape and slope of the particle size distribution curve. The higher the uniformity coefficient, the larger is the range of particle size. Granular material with a uniformity coefficient of less than 10 may be regarded as uniformly graded while the ones with a uniformity coefficient of more than 10 may be regarded as well-graded. The coefficient of curvature is equal to $D_{30}^2/D_{60}D_{10}$ and a well-graded soil generally has a coefficient of curvature in the range 1-3 (Powrie, 2010). Therefore in the parallel grading, both gravel content and gravel size will be reduced compared with the base soil (Hamidi *et al.*, 2012).

The proportion of oversize in the sample should not be more than 15 % by dry mass (BS1377-7, 1990). In the scalping method all particles considered oversize are removed (scalped) from the original material and the test is performed on a finer fraction of the soil. In this case the grading is prepared by changing the base grading between a certain size range. Indeed, in this method the gravel content as the main and controlling part of the grading remains constant, only the maximum gravel size differs from the base material (Hamidi *et al.*, 2012).

Considering the use of one of these two methods, the question is if testing a sample whose maximum particle size is smaller than the original material will give the same results

compared with those that would be obtained by testing the soil at full size in a larger box. Several examples presented in literature have investigated this issue.

The first considered is the study presented by Simoni and Houlsby (2006). They added two different kinds of medium-rounded to subangular gravels (one poorly graded and the other one well graded) to Leighton Buzzard sand in different proportions (from 10% to 60% by weight) and tested the material (the mixtures plus the samples of only sand and only gravel separately) in a large box (254 mm x 152 mm in plan and 150 mm in depth). The test results showed that the addition of gravel (by as little as 10-20% by weight) to the sand sample resulted in an increase in the critical state friction angle, maximum angle of dilation and peak angle of friction in comparison with a pure sand sample tested at the same relative density. Despite that, they reported similar friction angles for pure sand and gravel mixtures with up to 20% gravel and a significant increase in peak strength friction angle only for sand and gravel mixtures with gravel $\geq 30\%$ (reported by Bareither *et al.*, 2008). The maxima of the increases were observed up to gravel fractions of 60%, for percentages of gravel higher than 60% the authors suppose a decrease of the angle of friction of sand-gravel mixtures. This last conjecture is based on the fact that the angles of friction found for the pure sand samples were lower than the one found for 60% gravel mixtures (Figure 3.12).

The same result (increase of the angle of friction with gravel content) was found by Moulay Smaïne *et al.* (2014) who tested two kinds of material: a crushed gravel (maximum particle of 5 mm and gravel content equal to 50%) and a tuff material whose maximum particle size was reduced using a scalping method. Three different maximum diameters were considered for the tuff (10 mm, 5 mm, 2 mm) so that the percentage of gravel obtained in the three samples was respectively equal to 80%, 27% and 0%. Shear box tests were conducted in a 60 mm square box and from the results of the tests an increase of the critical state angle and reduction of apparent cohesion (intercept with the y-axis) with increasing maximum particle size of the sample was observed. In addition higher values of shear strength were found for the crushed gravel sample (gravel content equal to 50%) than the tuff material (gravel content equal to 27%) at equal maximum particle size, suggesting that the factor mainly influencing the shear behaviour of the material is its gravel content rather than the maximum size of its particles. The same behaviour (reduction of shear strength with reduction in particle size) was confirmed by Kim and Ha (2014) testing a coarse grained soil in a 300 mm square box and adopting a

parallel method to reduce the maximum particle size of the soil (25 mm) to 4.75 mm, 7.9 mm and 15.9 mm.

Bareither *et al.* (2008) carried out shear box tests on thirty sandy backfill materials using two boxes of different size: a large box (305 mm square), accommodating a maximum particle size of 25.4 mm, and a small box (64 mm square) allowing a maximum particle size equal to 4.75 mm (both the maximum particle sizes were in accordance with the width of the box to maximum particle size ratio provided by ASTM D3080 (2011)). The thirty base materials had gravel contents ranging from 0% to 30%, so that twelve of them required different amounts of scalping to meet the maximum particle size criteria of the small box. The results of the tests showed no significant differences suggesting that the peak angle of friction for clean sand backfill with gravel content up to 30% can be measured with similar accuracy using any of the two methods (with the use of a large box testing the base material or in a small box accommodating a scalped sample of the same).

Nakao and Fityus (2008) investigated the effect of three different factors on the angle of friction of the tested sample: shearing rate, retesting on the sample and scale of the box. The soil was tested in two different size boxes: a large box (300 mm square and 190 mm height), accommodating a maximum particle size of 19 mm, and a small box (60 mm square and 50 mm height) allowing a maximum particle size equal to 4.75 mm (maximum size allowed in accordance with the Australian Standard Q181C (1994; 2002) and obtained using a scalping method to remove from the sample all the particles exceeding this size). It was found that the shearing rate proposed by Q181C (1994; 2002), which uses the data recorded during the consolidation phase as an indicator of the relative rate of pore pressure dissipation, seems to be a good basis for shearing rate selection even if it is not clear from the standard how to select a shearing rate when the sample is made of permeable material and therefore would not undergo a consolidation process. Significant decrease in shear strength was found for samples that are tested a second time: peak angle of friction was found to decrease from 33.4° to 28° and critical state angle of friction from 32.4° to 28°. The reason for the measured reduction in shear strength was explained by the author as a consequence of particle crushing. This was demonstrated by comparing the particle size distributions before and after the tests from which is possible to verify how almost all the particles greater than 10 mm were eliminated and the proportion of particles larger than 1mm was reduced from around 50% to around 8%.

The most interesting aspect of these tests was related to the effect of test scale. The authors underlined the fact that when a scaling method is adopted (scalping in this case) two factors must be separately considered: different maximum particle size of the sample (assuming that mechanical interaction of large particles could affect measured soil strength) and different size of the testing apparatus (assuming that geometric effects could cause differences in the developed shear zones). The first factor was investigated by testing both the base material (a silty sandy gravel composed of 50% gravel and having a maximum particle size of 19 mm) and the scaled down sample (silty gravelly sand composed of 20% gravel and with a maximum size of 4.75 mm) in the large box. It was found that a significant reduction of angle of friction occurs when the gravel content in the mixture was reduced from 50% to 20% by weight (the peak and critical friction angles were reduced from 37.1° and 34.2° to 32.8° and 31.6° respectively for the two samples), indicating that the addition of 30% gravel in the sample causes a considerable increase of the effective shear strength values (as already found by Simoni and Houlsby 2006). The second factor was investigated by testing the scaled sample in both the large and the small box. Considering the size of the particles and the sizes of the two boxes, both were satisfying the limit defined by the ASTM D3080 (2011) ($D/d_{max} > 10$) and in fact despite small differences in peak friction angle values the results obtained from the two apparatus were very similar.

Considering the information obtained from all of these tests, it seems possible to confirm that when the content of oversized particles (i.e. exceeding the size limit defined in ASTM D3080 (2011)) in the testing material exceeds 30% by weight the sample must be tested in a larger apparatus in order to prevent an underestimation of the angle of friction of the soil. On the other hand, when the use of a scaling method is allowed (when the scaling technique would result in a reduction of gravel such that in the scaled material it does not exceed 30% of the weight) attention should be paid to the choice of the scaling method. As mentioned before, the most commonly used methods are represented by the parallel and scalping technique, but the question remains of which one is the best to use and what differences on the results obtained are produced by each method.

Bagherzadeh-Khalkhali and Mirghasemi (2009) carried out numerical simulations and experimental tests on both base material (having a maximum particle size of 38 mm) and four downsized samples of the same (downsized to a maximum particle size of 25.4 mm and 4.76 mm and obtained using two different scaling methods: scalping and parallel techniques). In order to test the soil two different sizes of shear box were used: a 60 mm

square and 20 mm high small box (for testing sample with 4.76 mm maximum particle size) and 300 mm square and 150 mm high large box (for testing maximum particle size equal to 25.4 mm). For the numerical simulations, the program ELLIPSE was adopted and modified in order to simulate the direct shear test. The numerical simulations were carried out in three stages. In the first stage, the generated loose assembly was compacted hydrostatically, vertical stress was then applied on the assembly in the next stage and finally the assembly was sheared in the direct shear box under constant vertical stress. For both numerical and experimental tests, a reduction of shear stress and angle of friction (both at peak and critical state) with the reduction of maximum particle size of the sample was observed. This reduction was larger when the parallel method was used concluding that the scalping technique for preparing the specimen in a direct shear test leads to more representative behaviour for coarse grained soil.

Hamidi *et al.* (2012) performed large scale direct shear tests (using a 300 mm square box with 170 mm height) on a sandy gravel base soil (with a maximum particle size of 25.4 mm) and on two equivalent scalped and parallel gradings (maximum particle size was reduced to 12.5 mm). The tests were performed at three different relative densities (35%, 60% and 85%) and under a surcharge pressure (σ'_v) of 100, 200 and 300 kPa. In this case the results of the experiments showed how the scalped grading is a better approximate grading -compared to the parallel one- for the determination of the peak and critical shear strength of coarse grained soils. According to the authors, this was related to the important and controlling effect of gravel content which was maintained constant for the base and scalped grading. It was also concluded that increasing the normal stress would increase the differences in shear strength results between base/scalped samples and parallel scaled samples, while this difference would decrease when the relative density is increased. From the results obtained the authors concluded that, although shear strength characteristics of well graded coarse grained soils can be determined using the scalping method with an allowable tolerance, a set of equations were proposed to define the maximum (peak) and constant volume (critical) friction angles of the material. This angle can be determined by testing a finer fraction of grading (obtained by the use of parallel or scalping method), reducing difficulties in experiments on well graded coarse grained soils and limitations in the size of experimental specimens. The solution provided by the authors is represented by the following equations:

$$\phi'_{max} = 0.4\psi_{max} + \alpha \quad (3.10)$$

$$\phi'_{cv} = 0.4\psi_{max} + \beta \quad (3.11)$$

Where:

ϕ'_{max} = maximum friction angle of the soil (peak friction angle)

ϕ'_{cv} = constant volume friction angle of the soil (critical state friction angle)

Ψ_{max} = maximum angle of dilation of the sample (at peak)

Values of α and β coefficients were proposed by the authors in Table 3.2.

Comparison between calculated and experimental values of ϕ'_{max} and ϕ'_{cv} for different gradings show how all values obtained from these equations have maximum error equal to $\pm 1.5^\circ$ for ϕ'_{max} and $+1.5$ to -3.0 for ϕ'_{cv} (Figures 3.13-3.14). This suggests the applicability of these equations at the same range of relative density and surcharge pressure considered for this study.

Considering all the information derived from literature with regard to scale effects in the direct shear test it was possible to derive the following conclusions:

- The series of tests conducted during these studies generally, but not always, follow the limits suggested by modern standards (ASTM D3080, 2011 and/or BS1377-7, 1990);
- When testing material with a large particle size the use of full scale samples in a standard apparatus is allowed only whilst maintaining certain limits of width (or diameter) and height of the box to maximum particle size of the soil sample. Proper limits for these ratios can be taken from the study conducted by Fu *et al.* (2015) as more restrictive (a larger height and width of the shear box would be required) if compared with the limits provided by the Standard ASTM D3080 (2011) and equal to the British Standard (BS1377-7, 1990) for what concerns the limit imposed on the height of the sample. Considering this the width (or diameter) of the shear box to maximum particle size ratio should exceed the value of fifteen and the height to maximum particle size ratio should be larger than ten.

- Whenever the test material includes particles with a large size the use of standard apparatus would be possible if the sample is reduced to a smaller size by the use of a scaling method (parallel or scalping). This operation is allowed only if the reduction of gravel content in the sample does not exceed 30% of the total mass.
- Considering the case of samples with a maximum particle size of about 100 mm, it is evident that the scaling operation would not be possible without effects on the results since the quantity of gravel would be large and definitely exceed 30% of the total mass of the sample. In this case the only solution to obtain reliable results would be testing the material at full scale by the use of a large unconventional shear box apparatus.

3.5.3 Large shear boxes for testing full scale samples with a large particle size

As explained in the previous section, the most appropriate way to avoid scaling problems when using the direct shear test on material with a large particle size would be the use of a large apparatus (taking into account the previous discussion on geometry). Despite their use not being widespread, there are several examples of large shear boxes in the literature which were considered in this research as reference for the design of the apparatus later described (Section 7.1) and used to conduct large scale tests. In this section, a brief description of these large shear apparatus is presented, while a summary of their main characteristics can be found in Table 3.3.

Barr *et al.* (1991), Jacobs (1993) and Davies and Le Masurier (1997) shear boxes

Among the shear boxes here considered, the largest one is described by Davies and Le Masurier (1997). The structure consisted of a large box (internal dimension equal to 3 m x 1.5 m x 1.5 m, 2.25 m² shear plane) designed and manufactured at the University of Wales, College of Cardiff, with the aim of studying the performance of 2.8 m long soil nail reinforcement (hence the need for a 3 m length box).

The apparatus was initially designed as a box made of concrete slabs (Figures 3.15 and 3.16), bolted together at the corners and held in position by angle sections (Barr *et al.*, 1991). The system was later modified by Davies and Le Masurier (1997), who decided to build the box with steel panels bolted together at the corners. In both cases, the sides were connected (by the use of angle sections in the case of concrete shear box, welded in place where the box was made of steel panels) to two steel plates (2 m x 2 m x 20 mm thick) placed at the top and bottom part of the box creating the confinement of the sample. The

base of the box was designed with the aim of fixing one of the two halves of the box and, at the same time, allowing the displacement of the other one. This system consisted of three joist sections, firmly attached to a strong floor in the laboratory, on top of which are welded other components: on one side, three similar joists (used to carry and restrain the fixed container) and on the other, two channel sections with the aim of creating runways in which six machine skates could slide and allow the movement of the other half of the shear box. One roller (a central steel tube surrounded by stiff rubber material) was located at the gap between the two halves and used to prevent the outflow of the soil.

The shear force was applied to the sample through a 500 kN capacity hydraulic jack, which pushed one of the two halves of the box in the horizontal direction creating a vertical shear plane. Reaction for the jacking force was provided by a rigid frame tied to the strong floor and the fixed base. The compression load was applied by four steel plates (located on each side of each container) and four air bags (situated in the gap between the steel plates and the side). The system worked in the way that the lateral stress was applied to the sample by increasing the air pressure in the air bags (to a maximum allowed value of 400 kPa). In this configuration the lateral stress was the major principal stress, whose direction coincides with the direction of shear. A rigid beam across the top of the rear of each container (not shown in Figures 3.15-3.16) prevented outward movement of the two halves of the box when surcharge was applied through the airbags.

The presence of the steel plates inside the box was provided for several reasons:

- application of a uniform pressure:

Without the presence of the plates the airbags would have tent to bulge concentrating pressure at the centre and thus providing a less uniform compression on the sample.

- dilation of the sample:

While the shearing occurred a dilation effect was expected, therefore during the filling of the box with soil the airbags were partially inflated to accommodate this. Without plates the filling of the box would have been difficult since the air within the bags would have been squeezed from the bottom as the filling progresses.

- protection:

The plates protected the air bags from accidental damage.

- dilation measurements:

The plates were able to move on some smooth steel pins, which were welded at each corner of the side wall of the box and passed through holes situated in the plate corners. The displacements of the plates could be measured by four linear variable differential transducers (LVDT), which were fixed in a steel sleeve welded to the plate around the hole through which the supporting pin passed. Once the displacements of the steel plates were recorded it was possible to relate them to sample volume change (from the average of the four LVDT readings).

Another important characteristic of this apparatus was represented by a 90° rotated shear plane (if compared with common shear boxes whose plane is normally horizontal). This fact guarantees some advantages to the system from different technical points:

- static earth pressure:

Due to the large size of the shear box (3 m long) the horizontal shear plane arrangement would dictate that a constant value of vertical stress due to the self weight of the soil was not possible and there would be a variation of nearly 30 kPa (for a soil unit weight of 20 kN/m³) from the top of the box to the shear plane level and consequently the same amount of change for the lateral earth pressure along the length of the nail. Using a container arranged side by side provided instead a uniform static pressure (due to the self-weight of the soil) along the length of the nails when tested (Figure 3.17).

- vertical stress:

In a conventional shear box vertical stress is usually applied at the top through rigid loading platens and because of small scale any losses in stress over the depth of the shear box can be generally ignored. For a shear box 3 m tall with this loading system a decrease in applied vertical loads of the order of 80% would have occurred from the top of the shear box to the bottom. For any nails then placed vertically across the shear plane the normal stress against the nail would have also

varied by 80% which would have had a detrimental effect upon the behaviour of the nail (Figure 3.18).

- bedding planes:

Generally in shear boxes of large scale, soil is placed in layers. This is likely to lead to thin bands of low density soil throughout the sample. If these bands coincide with the shear plane then a weaker response from the soil may occur. With the chosen configuration any bedding planes were normal to the shear plane, thereby reducing any possible weakening effects upon the shear strength (Figure 3.19). Although, as underlined by other authors (Arthur and Menzies, 1972), shearing soil in a direction normal to the bedding planes could increase the measured angle of friction by as much as 5°.

Other practical considerations derive from this type of configuration (Jacobs, 1993):

- increased shear deflection:

Considering the size of the apparatus and therefore the higher weight when compared to standard shear box apparatus, the fact of keeping the two halves parallel to each other (instead of having one on top of the other one) allowed to increase the amount of deflection which could be obtained safely at such a large scale.

- Filling and emptying of the box:

With the volume of the shear box being approximately 6.5 m³, filling and emptying operation were made more efficient having the containers side by side.

- Laboratory space restriction:

Having the containers side by side also required less headroom within the laboratory (practical when a crane was used for filling of the shear box).

The tests were conducted placing the nail reinforcement in a medium dense sand and in a compacted clay fill. The differences between the stiffer sand and the less stiff clay were as would be expected from established soil/nail interaction mechanism and the tests gave consistent results allowing a greater understanding of the development of forces in soil nails and providing a basis for the prediction of displacements which occur in soil nailed structures (Davies and Le Masurier, 1997). Despite the use of this apparatus was limited to the study of the behaviour of soil nails, the magnitude of the direct shear box makes it

ideal for the testing of other forms of soil reinforcement, such as geogrids, using representative samples of prototype soil or for studying the mechanical properties of materials which cannot be successfully tested using smaller scale apparatus (Barr *et al.*, 1991).

Jain and Gupta (1975) shear box

The shear box developed by Jain and Gupta (1975) was designed with the aim of testing the shear strength of compacted layers of river bed material and processing plant waste (both material being part of a dam fill). The samples tested by this apparatus were therefore represented by: a well graded sand, gravel and cobble mixture normally containing particles of maximum size up to 900 mm and processing plant rejects generally containing cobbles of size 38 mm-340 mm (hence the need to use a large apparatus of internal size equal to 1.2 m x 1.2 m x 1.2 m, corresponding to 1.44 m² shear plane). The tests on this box were conducted on materials containing particles of maximum sizes up to 200 mm.

The box was composed of two concrete halves. The upper half, able to move horizontally, sited on pipe rollers resting on the lower half (which was fixed).

The vertical stress (Figure 3.20) was provided by two 50 tonne hydraulic jacks, which applied the normal load to the sample through a reinforced concrete bed plate, placed on the test material with the aim of uniformly distributing the force. During the displacements of the upper half the jacks were maintained in vertical position by mild steel rollers, placed between the jacks and the thick mild steel plate. The jacks were rested against a top girder assembly consisting of two rolled steel joists, which were well connected to each other at mid-span and at the end by thick mild steel plates. The top girder assembly was supported by vertical steel bars encased in concrete columns. The steel bars connected the top girder to two rolled steel joists centrally placed below the lower half of the box.

The shear stress (Figure 3.21) was applied by the use of one 100 tonne hydraulic jack, placed against a RC wall (3.5 m long) which was constructed parallel to the girder assembly.

The apparatus was successfully used to derive the shear strength of the material containing maximum particle size up to 200 mm by carrying out three tests at different

normal stresses on different grades of the processing plant waste and river bed material placed at the same density. The normal load at shearing plane was calculated by summing up the loads applied by the hydraulic jack, self load of the jack, bed plate and of the test material over the shearing plane. After stabilisation of normal settlement under the normal force, the horizontal forces were applied in small increments, until loads very near to failure were reached. The results obtained from testing the material containing cobbles of maximum particle size up to 200 mm were compared with the ones obtained from testing cobbles having a particle size between 50-100 mm. The results showed the same stress strain relationship indicating that the no scale effect was affecting the test outcome even when the ratio between size of the box and maximum particle size was equal to six. However the additional precaution of keeping a particular spacing between the two halves of the box was considered essential by the author who explained how the parts of the box should be further apart than the diameter of the largest particle to prevent the top half from riding upon a grain which gets between the edges. Because the tests were conducted on the material permitting maximum particle sizes ranging between 75 mm to 200 mm, the spacing between the two halves of the box was kept as 160 mm (Jain and Gupta, 1975).

Pedley (1990) shear box

The apparatus of Pedley (1990), shown in Figure 3.22, was a modified version of the Oxford University large direct shear apparatus originally reported by Palmeira (1987). The large shear box was designed with the aim of testing the performance of soil reinforcement, which was placed inclined to the central plane of the shear box by a tensioned steel wire suspended over the top of the shear box so that it was possible to hold it in position during pouring of the soil sample inside the box.

The structure consisted of a cube of internal side 1 m (1 m² shear plane) and split at mid-height in the horizontal direction. The box was made of 25 mm thick mild steel sides supported by a steel grid structure, one of the sides is a 25 mm thick Perspex wall allowing the use of markers, displaced at the boundary of the sample to check the movements of the soil. The box was separated into two halves by four screw jacks and the top half of the box was free to move relative to the lower half generating a horizontal shear plane. Some track roller bearings separated the two halves of the box minimising friction in the system and a single roller was also used, between one half and the piston of the compression loading jack, to allow relative horizontal displacements (number 13 in

Figure 3.22). The box was completed by a 40 mm thick mild steel plate at the top (bolted to the steel sides of the box) and a concrete slab at the bottom.

The load system was provided by five hydraulic jacks: four 80 kN jacks (at each corner of the cube, displaced symmetrically about the shear plane to not induce a moment on the sample; number 7 in Figure 3.22) applied the compression load pulling the upper and lower halves together; while one 600 kN hydraulic jack (number 8 in Figure 3.22) pressurised by an electric pump applied the shear load at the level of the shear plane through a shear force boss (number 17 in Figure 3.22). The rate of displacement between the two halves of the shearbox was controlled by varying the applied shear load by means of flow control and dump valves.

The original design (Figure 3.23) reported by Palmeira (1987) mainly differed from this apparatus in the way of applying the normal vertical pressure to the sample. In Palmeira's (1987) large apparatus the normal pressure was applied by a rubber bag filled with water which was adopted with the aim of avoiding non uniform stress distributions on top of the sample (which would occur with a rigid fixed plate) and more complex/costly design involving a jack on top. The rubber bag was clamped to the mild steel plates of the box and connected to the hydraulic system able to control the pressure and keep it constant during the test (Palmeira, 1987). Problems associated with the original design led to rotation of the soil sample within the shearbox, resulting in a non uniform stress distribution across the central plane, and to difficulties in measuring the dilation from the top boundaries. The arrangement used for applying the vertical load also prevented installation of reinforcement after application of this force. The performance of the Large Direct Shear Apparatus was enhanced by making the upper and lower boundaries symmetrical by fixing the top platen to the upper half of the shearbox and by changing the method of applying the vertical load. The modifications led to reduced rotation of the upper half of the shearbox, an improvement in the measurement of sample dilation at the boundaries, and a more uniform shear strain distribution across the central plane (Pedley, 1990).

Comprehensive series of tests in the large shear box apparatus were presented for two sample densities, illustrating a good degree of repeatability, therefore giving confidence in the method of sample preparation and test procedure. Boundary data from the large shear box agreed well with data from a medium direct shear apparatus (254 x 153 mm shear plane and 150 mm height) which was used to test the same material (no reinforced

tests were performed in the medium shear box). Tilting of the top half of the apparatus was observed and attributed to an eccentricity of the applied shear force. This resulted in some asymmetry of the applied vertical load about the central plane. However, this phenomenon was not apparent until large relative shear displacements and the cessation of dilation, indicating that the modifications to the boundaries of the large shear box were successful. This conclusion is supported by data from photographic measurements of markers placed in the sand, which indicated good uniformity of shear strain across the central section (Pedley, 1990).

Krahan *et al.* (2007) shear box

The aim of this research was to use a large size (internal size of 1 m x 1 m x 1 m) direct shear apparatus (Figure 3.24) in order to allow interface properties to be quantified, in this specific case filled sandbags in contact with each other and filled sandbags in contact with sod.

The shear box was constructed with equal top and bottom halves comprising 250 mm high steel C section, with a shear plane (1 m²) located at the mid height of the box. At the sliding interface surface between the top and bottom boxes the steel plates were treated with a specially formulated industrial coating to minimise friction and abrasion during shearing. The apparatus was instrumented to record horizontal displacement of the lower half of the box (seated on a set of rollers) while the top container was restrained horizontally.

The load actions were applied by hydraulic actuators: the horizontal load was provided by a 222 kN jack, while a stiffened rigid steel loading plate was used to apply a vertical load to the specimen using a 222 kN capacity jack.

The large size of the direct shear apparatus used in this study allowed interface properties to be quantified for systems exhibiting discrete block behaviour (in this case filled sandbags and filled sandbags in contact with sod) and whose field-scale interface performance could not be determined by using conventional apparatus.

Boundary effects due to local distortion of the sheet products based on how the specimen materials are attached to the test device were also avoided using the large apparatus whose interface area was large enough to reduce local distortions near the specimen edges.

Santana and Estaire (2019) shear box

This study evaluated the shear friction between ballast and bottom surface of sleepers used in railways. The ballast sample had particles with sizes between 25 and 60 mm, with a median diameter (D_{50}) of 40 mm, while the sleepers, having the main role of distributing the rail loads to ballast layer, were made of concrete and for the present study the extremes of one of them were cut to fit into a large direct shear box (shearing plane of 1 x 1 m and able to fit specimens with thickness up to 0.8 m as the box height is 1.2 m). The structure of the apparatus, including the box, was made of steel (Figure 3.25). The maximum vertical and horizontal load that could be imposed to the specimen was 1000 kN. The maximum horizontal displacement of the bottom half of the box was 250 mm, large enough to record peak shear stress. The horizontal load could be imposed at a constant speed, ranging from 0.5 to 45 mm/min, although in this study a speed of 0.8 mm/min was used.

The tests were conducted for ballast-sleeper contact at two different unit weights and five normal stresses (25, 50, 100, 150 and 200 kPa). The large shear box was also used for ballast strength characterisation which was investigated by six tests on compacted ballast specimens with similar unit weight (very close to the one used for the second sample of ballast when testing ballast-sleeper contact) and under normal stresses ranging from 25 to 200 kPa. From both the first and second series of tests it was possible to derive the friction envelop at failure (variation of shear stress at failure with increasing normal stress) and therefore the critical state angle of friction. Despite the horizontal displacement-shear stress curves obtained for the tests concerning ballast-sleeper contact showing a slightly irregular shape and sometimes sudden shear stress drops, it was possible to derive the critical state angle of friction in the ballast-sleeper interface tests and compare it with values obtained from tests with only ballast.

Conclusions

The examples of large shear box apparatus described in this section seem to provide a good solution for testing large particle size material at full scale or specific geotechnical conditions which cannot be tested using standard apparatus (for example soil reinforcement) although the size of the apparatus was not always in line with the limits suggested by modern standards (ASTM D3080, 2011 and/or BS1377-7, 1990). The results obtained from these tests were considered as positive by the authors despite no comparison with small scale tests was undertaken so that it is not possible to derive any

conclusions about scale effects which would be expected to derive from testing the same material in smaller apparatus. The only case where the material was tested at two different scale is described in the study conducted by Pedley (1990) who tested the soil sample (Leighton Buzzard sand with maximum particle size passing the 1.40 mm sieve diameter) both using a large (a cube of internal side 1 m) and a medium (254 x 153 mm shear plane and 150 mm height) shear box. Nonetheless, the conclusion of Pedley (1990) is that results from the large shear box agreed well with data from the medium apparatus (thing which would be expected considering that the size of both the two apparatus was sufficiently large to accommodate the sand sample in accordance with the Standard ASTM D3080 (2011) and the British Standard (BS1377-7, 1990)). Design characteristics of these apparatus were taken into account in Chapter 7 for the design of the large shear box which was manufactured for the purposes of this research.

3.5.4 Scale effects in *in-situ* plate bearing capacity tests

When performing a plate loading test on site it is important to evaluate which size of the testing plate would be the most appropriate. The main concerns in defining the plate diameter are represented by the need to mobilise the plate into the soil and therefore the amount of reaction required and number of particles which would be involved during the test. On that basis, an excessively large plate would lead to an uneconomic test since it would require an elevated reaction load, on the other side the use of a small plate would be less representative of actual conditions imposed by the foundation.

This last problem was pointed out by Ovesen (1979) who studied the results of conventional model tests in which a footing is built to the length scale 1:n and tested on a surface of the same sand (a quartz diluvial sand with particle size ranging from 0.3 to 0.6 mm) as that in the prototype. Results of these tests are shown in Figure 3.26, in which the dimensionless peak load (the peak load measured during test (p_p) normalised by the unit weight of the soil (γ) and diameter of footing (B)) is plotted against the plate diameter (each curve refers to tests carried out on the same model material). The graph shows the presence of a scale effect in conventional model tests: the smaller the diameter of the footing the higher dimensionless peak values.

Ovesen (1979) also undertook plate bearing tests using a centrifuge model. The tests were conducted on the same sand using different acceleration fields and different plate diameters. From the comparison of tests conducted using different acceleration fields (so

that the model plate diameters were representing different prototype plate diameters) it was possible to observe a decrease in bearing capacity and less tendency to peak when increasing the plate diameter (exactly as it was found from conventional model tests). Another comparison was made between tests conducted on the same sand as that in the prototype using different plate diameters (ranging from 7.1 to 113.1 mm) and appropriate corresponding gravity field (ranging from 8.8 to 141.4 times the gravitational acceleration) so that in this case the model plate diameters were representative of the same plate diameter of the prototype (corresponding to 1 m diameter). Taking into account the results of these tests, very similar peak load values were found for plate diameter to average particle size ratios equal to or larger than 30 (corresponding to plate diameters larger than 14.2 mm). Also it was noted that higher values of peak load (about 10-20%) when using very large plate diameters (about 1/5 of the test container diameter) occur indicating a boundary effect as influencing the obtained results.

As previously mentioned in the description of plate loading test procedures, the British Standard (BS 1377-9, 1990) defines a limit in the selection of the plate diameter to be used for the test. This limit requires that the diameter of the plate be a minimum of five times larger than the maximum particle size of the tested material. Conducting tests in accordance with the Standard a reduction of any scale effect is expected so that the values of bearing capacity obtained from the test can be considered reliable.

3.5.5 Scale effects in centrifuge modelling of plate bearing tests

As previously described, the limiting ratio defined in BS 1377-9 (1990) has a huge influence on the reaction load required to undertake tests on working platforms since the bigger the plate the bigger the reaction load to be applied. Considering this problem, the use of centrifuge model experiments can be considered as a viable method to investigate the effect of particle to plate size ratio and verify if the use of a smaller ratio (and thus a smaller plate) would be permissible during testing on site without significant effect on the results.

The centrifuge is a tool by which the characteristics of a prototype can be extrapolated from testing a smaller version (model) of the same scenario. The idea of centrifuge testing of a soil model is simple: a prototype is assumed, a model is built to linear scale $1/n$ so that the prototype and the model form two geometrically similar bodies of the same soil

and the 1/n-scale model is accelerated so that its self-weight increases n times. In this way the stresses at corresponding points in prototype and model should be identical.

The scaling law derives from the need to ensure stress similarity between the model and the prototype (Taylor, 1995). Considering a prototype material of density ρ , the vertical stress at depth h_p can be defined as:

$$\sigma_{vp} = \rho g h_p \quad (3.12)$$

Where g is the Earth's gravity

If an acceleration of N times Earth's gravity is applied to a model material (of the same density ρ), then the vertical stress at a depth h_m in the model correspond to:

$$\sigma_{vm} = \rho N g h_m \quad (3.13)$$

Imposing the same vertical total stress in prototype and model ($\sigma_{vp} = \sigma_{vm}$) it derives that:

$$h_m = \frac{h_p}{N} \quad (3.14)$$

This is the basic scaling law of centrifuge modelling (stress similarity is achieved between the prototype and the model by accelerating the model of scale N to N times Earth's gravity)

When a centrifuge is used to apply the acceleration of Ng on the model an important issue must be considered, which is the fact that the acceleration field requested for physical modelling is given by ωr^2 , where ω is the angular rotational speed of the centrifuge and r is the radius to any element in the soil. This implies that a slight variation in acceleration through the model takes place due to the variation of the radius and therefore a non-linear variation of stress in the model can be found. Consequently, the stress variation with depth in a centrifuge model does not exactly correspond with the stress variation in the prototype (as shown in Figure 3.27).

It can be demonstrated that there is exact correspondence in stress between model and prototype at two-thirds of the model depth so that the effective centrifuge radius (R_c), at which the scale factor N should be calculated, needs to be measured from the central axis to one-third of the depth of the model:

$$R_e = R_t + \frac{h_m}{3} \quad (3.15)$$

Where:

R_t = radius to the top of the model

h_m = height of the model

Unfortunately, the presence of the non-uniform acceleration field created in centrifuge models is just one of the examples of scale effects. It is in fact important to recognise that model studies are not perfect and cannot perfectly reproduce any single aspect of the prototype.

Particularly relevant among scale effects characterising centrifuge models is the particle scale effect deriving from the reduction of soil particle size by a factor of N . This problem occurs mostly when the aim is to model an event in a prototype soil consisting of coarse soil. Considering the limits of model size due to limited apparatus dimensions, the prototype would be reduced to a very small scale when creating the corresponding model so that differences in size would be significant when compared and it is unlikely that the model would mobilise the same stress-strain curve in the soil as would be in the prototype.

A good approach to identify the presence of scale effects is known as “modelling of models” which consists of testing centrifuge models of a same prototype at different scale and corresponding appropriate accelerations (so that they correspond to the same prototype). The model should predict the same behaviour and thus provide a useful internal check on the modelling procedure (Taylor, 1995).

Besides the scale effect arising from using small plate diameters, when plate bearing tests are conducted on a centrifuge model scale effects can derive from the reduction of particle size of the soil sample. In these circumstances, the use of a scaling method is required to reduce the particle size of the prototype whose behaviour has to be modelled. As anticipated in Section 3.5.2, the use of scalping or parallel method might affect the results of the test in a different way and the problem is relevant not only for shear tests but any kind of test which is conducted on large particle size material which cannot fit standard apparatus. Particularly, compression tests like plate bearing tests or oedometer tests can be affected by scaling the particle size of the tested material as much as a direct shear test

would be. In the specific case of plate loading tests an appropriate ratio between plate diameter and particle size should be adopted in order to avoid scale effect. Garnier *et al.* (2015) for example suggested a ratio between plate diameter and D_{50} larger than 35.

3.6 Summary

This literature review was undertaken starting with an initial analysis of the methods commonly used to determine the design of a working platform finding that when the material characteristics of the platform and subgrade are known it is possible to calculate the thickness of the platform simply using a bearing capacity formulation. Difficulties in defining the characteristics of the platform material derive from its coarse nature and the large variability of material components (related to the wide and convenient use of recycled material). Among the characteristics which can influence the design of the platform, the angle of friction of the platform material has the most significant effect on the design and thus it is of vital importance to test the material in order to derive accurate and reliable values of the angle of friction.

The direct shear test and the plate loading test were considered as the most appropriate methods to test the platform material and derive the shear strength characteristics. Difficulties in performing these tests occur due to the presence of scale effects which manifest in different ways in the two test procedures and could lead in both cases to misleading results.

Solutions to scale effect problems in testing large particle size soils would be:

- using a large shear box to test the material at full scale and compare the results with small scale tests so that the small test results would be validated.
- using a centrifuge model for the plate bearing test to evaluate the effect of using different plate diameter to maximum particle size ratios in *in-situ* tests so that a proper ratio could be defined.

Both the test procedures (full/small scale direct shear tests and plate loading tests using a centrifuge model) will be described in the following chapters together with the obtained results.

4. EXPERIMENTAL WORK

4.1 Introduction

The main topic of this chapter is the description of the experimental work which was undertaken during the time of this research work. The chapter is divided in two sections: Section 4.2 provides a description of the tests conducted at small scale (direct shear tests and plate bearing tests using a centrifuge model), Section 4.4 refers to tests conducted on full scale material using a large shear box apparatus whose development and functionality are also described. Test results are provided for each type of test which was conducted and discussion of these results can be found in Chapters 5, 6 and 7.

The main objectives of the experimental work would be:

- Perform small scale tests (plate bearing tests using a centrifuge model and direct shear tests) on downscaled samples of limestone material corresponding to a 6F2 grading and reduced in size in accordance with two scale factors (for comparison).
- Carry out full scale shear tests on the same kind of material (limestone) using a large apparatus.
- Compare the results obtained from small and full scale tests in order to understand the relationship between full size and scale models.
- Using the large apparatus to undertake shear tests on real platform material of different components in order to evaluate the effect of changing material properties.
- Using the large apparatus to evaluate the effect of increasing fines by conducting multiple tests (cycling loads).

Of these objectives only the first three were achieved during this study.

4.2 Description of small scale tests

As previously mentioned above, a series of small scale tests were carried out on two samples of grey Devonian limestone sourced from a quarry in Ashburton (Newton Abbot, UK), whose grading was defined and reproduced in order to represent downsized samples of 6F2 class material. The reason why this particular material was used to conduct the tests was essentially practical due to the fact that a large quantity of this limestone material of small particle size (sand) was available in the laboratory of City, University of London

at the time when the research was started. Furthermore, large particle sizes of the same limestone were easily sourced from the same quarry meaning it was easy to obtain a full scale sample differing from the sand samples only in size. The scale factors used to define the grading curves of the two samples corresponded to fifty and thirty which means that the grading curve representing an average particle size distribution of the class material 6F2 was reduced to particle sizes fifty and thirty times smaller than the ones representing the full scale sample. These scaling factors were arbitrarily selected in order to allow a comparison of the results derived from testing specimens at different scales. The main aim of these series of tests was to find the shear strength characteristics of the two samples, particularly the angle of friction, which will be compared with the values obtained from testing the material at full scale using the large shear box. Furthermore, the results obtained from small scale shear tests were used to inform the design of the large apparatus. A series of small shear box tests was also carried out with the aim of verifying the effect of retesting the material and avoid the preparation of a new sample for conducting the test.

Plate loading tests were also performed in the centrifuge with the second aim of verifying if the limit proposed by the British Standard (BS1377-9, 1990) could be extended to a lower ratio of plate diameter to maximum particle size so that tests on site would require smaller reaction loads and would be more economic. Besides that, these plate loading tests were used to carry out a back calculation of the angle of friction of the tested material which could be compared with the results of the direct shear tests. Finally, a small plate loading test was performed on a layer of the same granular material laying on a soft subgrade in order to verify the validity of the platform design method proposed by Lees (2019).

4.3 Small scale testing material

The material used for these tests is represented by grey Devonian limestone sourced from a quarry in Ashburton, Newton Abbot, UK. The limestone was graded to correspond to two down scaled representations of 6F2 class material (properties of the two samples are summarised in the Table 4.1).

Since the definition of 6F2 material covers a large range of particle size distributions (as discussed in Chapter 3), an average curve, placed between minimum and maximum values of particle size distribution indicated by the “Manual of contractor documents for

Highway Works” for the 6F2 class material (see Table 3.1), was chosen as a representative grading (Highways Agency, 2004). The maximum particle size of the average curve corresponding to 100% passing material was 90 mm and the curve was shifted using the parallel grading method in order to obtain a curve showing the same percentages of passing but for smaller values of sieve size. The maximum particle size of this grading distribution was reduced to 3 mm for the first sample (as shown by the blue curve in Figure 4.1) and 1.8 mm for second sample (as shown by the blue curve in Figure 4.2). It must be noticed from these graphs that the grading curves actually representing the two tested samples (in red) differ from the theoretical curves (in blue) since these ones were adapted according to the size of the sieves which were available in the laboratory. According to the red curves the top particle size of the sieve having 100% passing material would be 4.17 mm for the first sample and 2.5 mm for the second one. Therefore it was decided to define the maximum particle size of these samples as corresponding to the next opening size whose percentage of particle passing was less than 100%. Based on that the maximum particle size of the first sample was taken as equal to 3.35 mm and for the second one a maximum particle size of 2 mm.

The Devonian limestone chosen for testing was therefore properly graded in order to correspond to this particle size distributions (the ones shown in red in Figures 4.1 and 4.2 whose corresponding values are indicated in Tables 4.2). The operation required, firstly, to sieve the available limestone material (using the method for dry sieving described in BS 1377-2, 1990) in order to get a division in particle sizes; once this division was obtained, the different fractions were combined to create the two particle size distributions corresponding to the scaled down samples of 6F2 material.

This operation was undertaken till the sieve size of 0.063 mm for both the samples. The remaining part of the two curves (under this sieve size) was derived from examining the actual particle size distribution of the samples using the sedimentation method for fine-grained soils (BS 1377-2, 1990). This test was conducted on a portion of material (about 30 g, as suggested for sandy soils by BS 1377-2 (1990)) passing the 0.063 mm sieve for both the two samples. No clay (particle size under 0.002 mm) was considered as being present in both the samples of limestone so that no sodium hexametaphosphate solution was used during these tests and the clay percentage was simply considered as being equal to zero. As indicated by BS 1377-2 (1990), the test was conducted in two steps: calibration of the sampling pipette (which was conducted by taking three different samples and

whose results are illustrated in Table 4.3) and sampling operation (results illustrated in Tables 4.4). In order to identify appropriate times for sampling during the sedimentation test, it was necessary to determine the specific gravity of the soil particles using the method provided by BS 1377 (1990). A value of specific gravity (G_s) equal to 2.73 was determined, which was calculated from the results of eight tests (as shown in Table 4.5) conducted on the two samples. Four test were carried out for each sample, two on particles larger than 0.063 mm and other two on the remaining portion of the sample. It was decided to separate the material in this way in order to verify if the possible presence of contaminants in small particles (<0.063) would affect the resulting value of G_s and therefore the time intervals which should be taken into account during the sedimentation test. The exact value of G_s for the entire sample was derived from an average based on the percentage by mass of particles larger and smaller than 0.063 mm (as shown in Table 4.5).

The value of specific gravity was also considered in order to calculate the minimum and maximum index density of the two samples (tests conducted in accordance with ASTM D4253-ASTM D4254 (2016)). Results of these tests are illustrated in Tables 4.6 (for maximum index density) and Tables 4.7 (for minimum index density).

4.4 Description of full scale tests

A series of large scale tests were carried out on the same limestone material used for the small scale tests. The crushed limestone was sourced from the same quarry in Ashburton so that the material properties were maintained constant and only the scale effect could be evaluated. The particle size distribution of this material was selected in order to correspond to an average particle size distribution of the class material 6F2 so that the samples used for the large tests were representing the full size of the samples tested using the small apparatus. The main aim of these tests was to compare the results obtained with the ones derived from testing the same material at small scale. The tests results also allowed to derive conclusions on the performance of the large apparatus and suggestions for improvement and future work.

4.5 Full scale testing material

The material used for large direct shear box tests is represented by limestone material sourced from the same quarry where the soil used for the standard tests was derived. Using the same limestone material allowed to guarantee that no other factor than the

particle size would affect the results of the tests so that the material tested in the large apparatus was a larger scale representation of the sand used for small scale tests. In order to guarantee this correspondence, the particles of limestone were selected in the exact quantity based on their size and mixed together in order to correspond to a grading distribution which was as close as possible to the one representing the full size. This operation was conducted in the quarry from which the material was sourced so that it was possible to purchase and receive the mixed particles ready for the test inside bulk bags which were stored on the strong floor of the university laboratory. The material obtained was characterised by particles smaller than 63 mm and minimum particle size equal to 6 mm, the grading curve is represented in Figure 4.3 (green curve).

5. STANDARD SHEAR BOX TESTS

The main aim of this chapter is to describe the test procedure and results of some direct shear tests performed using a standard shear box apparatus of internal plane size equal to 100 mm² on scaled 6F2 type materials.

The tests were conducted following the standard procedure (as stated by the Standard BS 1377-7, 1990) for direct shear test of soils under consolidated drained conditions and used to determine the shear strength properties of the samples of limestone which were also used during the plate loading tests (first one with a maximum particle size of 3.35 mm and second one equal to 2 mm).

A series of data were obtained from these tests, particularly:

- Peak/critical state angle of friction of the soil sample
- Volumetric strain
- Shear strain

The values of angle of friction were measured in order to:

- compare the results with those obtained from analysis of the plate loading tests;
- verify whether there is any difference in the measured angle when testing the same material at different scale factors.

The levels of volumetric strain and shear strain were used to inform the design requirements of the large shear box apparatus whose design development is fully described in Section 7.1.

5.1 The standard shear box apparatus at City, University of London

The automatic motorised direct shear test apparatus at City, University of London is shown in Figure 5.1. The beam loading device can apply a total vertical load on the specimen of up to 5 kN. This load is applied to the top of the sample using a pressure regulator and transmitted as a vertical stress. This apparatus is supplied with pressure regulating piston and integral 10:1 lever loading.

The machine accepts a shear box assembly which is designed to contain water and includes a square shear box (the one used in these tests had an internal size of 100 mm

square and a maximum sample depth of 44 mm). The box is divided into two halves, it is completed with a vertical loading pad and a retaining plate (Figure 5.2) and placed in a rigid wall box to which the bottom half of the box can be fixed by the use of screws (Figure 5.3). The rigid box is able to move horizontally forward, when the shear load is applied, and then to return to its original position.

During the test, the specimen contained in the box is subjected to a constant normal load whilst horizontally displacing the bottom half of the shear box (the top half remains fixed). The resulting horizontal force is required as the top and bottom halves of the sample shear along the failure plane along the juncture between the box sections.

The horizontal movement is driven by a motor and gear box assembly. The range of speeds at which the bottom half of the sample can be displaced is fully variable between 0.00036 – 1.2 mm/min for forward direction (once the test is completed the reverse movement of the box is allowed by the use of a crank handle). The shear force and the normal load are measured directly by two 5 kN load cells, while two LVDTs (Linear Variable Differential Transformers) are used for vertical and horizontal displacement measurements respectively. Horizontal displacement limits are provided by limit switches.

The Control Unit and Data Acquisition is designed to control the machine and record data from load cells and displacement transducers (fitted to the frame of the machine). All the operations of Data Acquisition and Control System are monitored from a desktop computer. The data collected is in term of loads/displacement vs. time. Test parameters can be defined and the output data related to vertical/horizontal forces and vertical/horizontal displacement can be saved in an Excel document once the test is finished in order to allow further data processing.

5.2 Test description

As noted at the beginning of the chapter, one of the main aims of the series of direct shear box tests was to measure the shear strength properties of two samples made of crushed limestone, properly graded and corresponding to downscaled representations of a possible grading curve of 6F2 class material. The tests were particularly useful to identify the value of angle of friction of the sample which could be compared with the results obtained from plate loading tests and from testing a sample of the same material at full scale in the large direct shear box. In order to design this large apparatus, it was important to have an

understanding of the possible levels of stress dilatancy and shear strain of the material during the test. The standard direct shear box tests on the scaled down material were therefore also an important instrument to evaluate these parameters, which were then used as indicators for the design of the large shear box apparatus.

A total of ten shear box tests were carried out for the sample with a maximum particle size of 3.35 mm (six of them using samples in a denser state and four using looser samples) and nine tests for the sample with maximum particle size equal to 2 mm (six at denser and three at looser state). Specimens prepared at a lower void ratio (denser samples) were sheared under a low level of vertical stress equal to either 100 and 200 kPa, while looser samples were tested at a higher vertical stress of 500 kPa. The reason for this testing approach was an attempt to reduce the number of tests which were necessary to identify the angle of friction of the two samples. In a graph showing shear stress variation (τ) against shear strain (γ_s) (Figure 3.6a as example) of the same soil sample tested at looser and denser states under the same vertical load a straight horizontal line could be drawn representing the level of shear stress at which failure occurs (critical state). In an ideal situation the two curves would join and correspond to this line. The level of shear strain achieved when testing using standard apparatus is limited by the maximum displacement which the apparatus allows. Considering that the maximum displacement allowed by the apparatus used at City, University of London is about 20 mm, the maximum level of shear strain achievable during the test would probably not be sufficient to arrive at the point in which all the curves join the critical state line. On this basis, it was expected the curves obtained from denser samples will approach the horizontal line from above and the curves corresponding to the looser samples will approach the same line from below. Results obtained the end of each test would be then considered as being representative of upper and lower limits of the real critical shear stress level. In this way the critical state line obtained in a graph displaying critical shear stress and applied vertical normal stress would be closer to the real situation as intermediate between the upper and lower limit.

The vertical stress was obtained by dividing the normal force (applied on the sample through the beam loading device and whose value was read by the vertical load cell and adjusted/recorded by the computer software) by the cross-sectional shearing area. This area was calculated considering its variation during shearing as the length of the shear plane was progressively reduced by the horizontal displacement of the lower half of the

box. The shear stress was calculated with the same method dividing the horizontal shear force (read by the horizontal load cell) by the changing shearing plane. A shearing rate of 1 mm/min (Bolton, 1991) was adopted during the test, which was maintained until the maximum displacement allowed by the apparatus was achieved. The choice of the shearing rate was decided based on the characteristics of the test material: a uniformly graded material (20% gravel, 62% sand, 18% silt in case of the sample with a maximum particle size of 3.35 mm and 7% gravel, 70% sand, 23% silt in case of the sample with a maximum particle size of 2 mm) having a very low value of moisture content (which can be assumed as equal to zero). For this reason, it was not necessary to conduct an analysis for the determination of the appropriate shearing rate since no pore pressure would develop in the sample during shearing. Therefore, the shearing rate suggested by Bolton (1991) was taken as appropriate for testing.

Six other tests were carried out using two denser samples of maximum particle size equal to 3.35 mm in order to verify the effects of consecutively retesting the same sample under the three vertical stresses of 100, 200 and 300 kPa. This would give some advantages when testing the material at large scale using the large shear box apparatus since the preparation of the sample would require a considerable amount of effort and time. The first sample was tested under the three stresses in the following order: 100, 200, 300 kPa while the second one was tested in a decreasing stress order: 300, 200, 100 kPa. This made it possible to compare the results of the same type of sample (both had similar void ratios and were made of the same limestone material with equal particle size distribution) when tested under the same vertical stresses in a different order. For example, the results of the first sample tested at 100 kPa were compared with the results of the second sample tested at the same vertical stress but after being tested under 300 and 200 kPa. The same comparison was done with the results obtained by testing the two samples at 200 and 300 kPa. This comparison was necessary in order to verify if retesting of the sample would be allowed without compromising the results so that only one sample could be prepared and tested under three different stresses so that no emptying and refilling of the shear box would be necessary for each test.

5.3 Sample preparation

For the series of small scale tests the crushed limestone was properly graded as previously described (Section 4.3), so that the particle size distributions obtained were representations of scaled down (by a factor of 30 and 50) samples of a possible grading

curve of 6F2 class material. This procedure allowed two samples of limestone material to be obtained with maximum particle size equal to 3.35 mm and 2 mm which were used for the tests.

The first step in the preparation of the test sample for the standard shear box tests, required the two halves of the shear box to be fastened together by tightening the vertical locking screws and inserting the bottom retaining plate in the shear box. Once the box was assembled, a sample of the testing material (approximately 650 g) was weighed and placed into the box. The material was poured into the box and tamped in three approximately equal layers (as recommended by BS1377-7, 1990) using a wooden tamper when a denser sample was to be prepared, while a funnel was used to place the looser sample in the way to minimise the level of compaction.

Once the sample was ready, the loading plate was placed on top and the box was put inside the apparatus and firmly fixed by two horizontal screws. At this point, the beam transmitting the vertical load was properly placed on the upper plate and the transducers were attached to measure the vertical and horizontal displacement during the test.

The height of the sample was measured after the vertical load was applied. In order to record the initial height it was necessary to measure the distance between top of the upper plate and top of the shear box so that from knowing the internal height of the box and thickness of the upper plate it was possible to calculate the initial height and hence the initial void ratio of the sample. For the soil sample with maximum particle size equal to 3.35 mm an average value of void ratio equal to 0.363 ($67\pm 1\%$ relative density) was obtained for the looser samples and an average of 0.285 ($86\pm 3\%$ relative density) for the denser samples. For the sample with maximum particle size equal to 2 mm an average void ratio equal to 0.401 ($58\pm 1\%$ relative density) was obtained for the looser samples and an average equal to 0.287 ($86\pm 2\%$ relative density) for the denser samples.

The last step in preparing the sample consisted of moving apart the two halves of the shear box using two vertical pins placed on opposite corners of the box so that no friction between the two halves would occur during shearing and releasing the two remaining vertical lock screws which had the role of keeping together upper and lower half of the shear box so that the test was ready to start.

5.4 Test results

Once the test was set up, the sample was sheared at constant shearing rate (1 mm/min) whilst monitoring the test from the Labview software that recorded the variation with time of the following parameters:

- Vertical displacement (y)
- Vertical force (F_v)
- Horizontal displacement (x)
- Horizontal force (F_h)

From the outcomes of the test it was possible to calculate the variation of the following parameters during shearing:

- Volumetric strain (ϵ_{vol})
- Effective vertical stress (σ'_v)
- Shear stress (τ)
- Shear strain (γ_s)

The approach of $\Delta\epsilon_{vol}$ to zero was used to identify when the critical state of the soil (corresponding to constant volume state of the sample during shearing) had been achieved.

Once the range of useful data was defined, two graphs were plotted for each test:

- Volumetric strain (ϵ_{vol}) versus shear strain (γ_s), shown in Figures 5.4
- Shear stress (τ) versus shear strain (γ_s), shown in Figures 5.5

From the first graph it was possible to verify the change in volume of the soil and therefore the compression-dilation behaviour of the denser samples and the compression behaviour of the looser samples. Considering the trend of this chart, the critical state of the soil could be identified at the value of γ_s where the curve tends to assume constant value of ϵ_{vol} ($\Delta\epsilon_{vol} = 0$). Once identified, this critical value of γ_s can be used to find out the actual value of critical shear stress (τ_{cr}) using the second graph.

In this section, the outcomes of the tests are analysed and procedures for deriving the results are described step by step. Table 5.1 (referring to the sample with maximum

particle size equal to 3.35 mm) and Table 5.2 (related to the sample with maximum particle size of 2 mm) present the calculated results from the standard direct shear box tests. In Table 5.1, tests 1-6 refer to the specimens which were tested at a denser state, while tests 7-10 correspond to the looser specimens. In Table 5.2, tests 1-6 refer to the specimens which were tested at a denser state, while tests 7-9 correspond to the looser specimens.

After defining the values of critical shear stresses for each applied vertical stress ($\sigma'_v = 100, 200, 500$ kPa), for both denser and looser samples it was possible to plot a third graph showing the trend of the critical state line (Figure 5.6-5.7). From the inclination of the critical state line it was possible to derive the critical state angle of friction of the soil (ϕ'_{cr}), which was found as being equal to 40.8° for the sample with maximum particle size equal to 3.35 mm (Figure 5.6). and 38.1° for the sample with maximum particle size of 2 mm (Figure 5.7). These lines intercepted the vertical axis at 0.46 kPa and 10.31 kPa in the case of smaller and larger sample respectively. In both cases the angles of friction which was derived from these curves were identical to the values which would have been obtained if these lines were forced to pass through the origin of the axis. This result was considered in line with the nature of the material tested, a dry coarse grained material that should not be characterised by any apparent cohesion. For comparison, BS 8004 (2015) gives a method for approximating the critical state and peak friction angle based on PSD, the angularity of the soil and the relative density. Using this method gives an estimated critical state angle of friction of 38° for both of the soil samples tested here.

When an appropriate value of angle of friction has to be decided for the design of a working platform, BRE Report 470 (BRE, 2004) suggests for heavily compacted platform material the use of a characteristic value of this angle, which should exceed the critical friction angle by a value $\Delta\phi'$ (factor depending on normal stress level, void ratio and particle properties). Considering this, another shear strength parameter concerning the denser samples which was looked as useful information to be derived from the direct shear box tests: the peak values of shear stress (τ_{pk}) and the corresponding peak angle of friction (ϕ'_{pk}), which was found out to be 49.6° for the sample with maximum particle size equal to 3.35 mm (Figure 5.6) and 47.8° for the sample with maximum particle size of 2 mm (Figure 5.7) when tested under a confining pressure of 200 kPa. The peak angles were also calculated when a confining pressure of 100 kPa was applied and corresponded to 49.9° and 46.5° for the sample with maximum particle size equal to 3.35 mm and 2

mm respectively (Table 5.1 and Table 5.2). The correlating BS 8004 (2015) calculated peak angle of friction is 44° .

From the difference between the peak angle of friction and the critical state angle was also possible to derive the angle of dilation of the material (indicated with ψ in Figure 5.6-5.7).

Two other important aspects which were verified from the direct shear box tests are represented by: the maximum dilatancy (or compression in case of looser samples) and the peak/critical shear strain of the sample during the test. Both these parameters were expressed in term of percentage (Tables 5.1-5.2) and considered as useful data for the design of the large direct shear box apparatus. The dilatancy/compression of the sample material was evaluated in term of compressive volumetric strain at the critical state ($\max \varepsilon_{vol}$, which was calculated as described in Section 3.3.6):

$$\max \varepsilon_{vol} = \frac{\max y}{h_0} 100(\%) \quad (5.1)$$

Where:

$\max y$ = maximum vertical displacement (mm)

h_0 = initial height of the sample (mm)

The shear strain of the sample (γ_s) previously calculated was considered in term of percentage for both the peak ($\gamma_{s, pk}$) and critical state ($\gamma_{s, cr}$).

From these results it was possible to estimate the maximum volumetric strain which might be expected when testing a sample of similar material and therefore the maximum increase in sample height. Maximum change in height is estimated to be equal to 3.7% the initial height of the tested material. From the critical shear strain, $\gamma_{s, cr}$ (value of shear strain which was necessary to achieve in order to reach the critical state) it was possible to estimate the minimum value of horizontal displacement which would be required during a direct shear test on a similar material to achieve the critical state. This value corresponds to 20-40% of the initial height of the sample. Equally, the peak shear strain, $\gamma_{s, pk}$, can be used to estimate the level of shear strain that a denser sample of similar

material needs to undergo in order to achieve the peak shear stress. This value was found as being equal to 6-16% of the initial height of the sample.

Result from two other series of tests conducted on two denser samples of maximum particle size equal to 3.35 mm are represented in Figure 5.8. These tests were conducted in order to verify the effect of retesting the material so that the option of using the same sample could be evaluated. This option would be very convenient when testing the material at full scale since the emptying and filling operations of the box would represent the hardest part of conducting these tests. The first series of tests on the first sample (series 1) were carried out in the following order of vertical normal stress: 100 kPa (test 1a), 200 kPa (test 1b), 300 kPa (test 1c); while for the second sample the order was inverted: 300 kPa (test 2a), 200 kPa (test 2b), 100 kPa (test 2c). In both cases the same sample was tested at three different vertical stresses in consecutive order so that no fresh sample was made when passing from one increment of vertical stress to another. Comparison of the results was done between test 1a and 2c (both tested under 100 kPa), test 1b and 2b (both tested under 200 kPa) and test 1c and 2a (both tested under 300 kPa). As can be observed from Figure 5.8, when the sample does not undertake any previous shearing (sample 1a or sample 2a) the resulting peak shear strength is higher than the one obtained for the same sample sheared at the same vertical stress after being tested under the other two vertical stresses (for comparison test 2c and test 1c respectively). Particularly, it can be observed that retested samples do not exhibit a peak of shearing resistance but behave as looser samples with a critical state which seems to be joined by the curves of the “fresh” samples (the tests were interrupted after the achievement of the peak of shear resistance so that no real comparison of the critical state can be done). Nonetheless, the order of applied vertical stress does not seem to affect the results of the test. This can be observed by comparison of test 1b and 2b (both tested at 200 kPa) which seem to show the same behaviour despite being previously tested at two different vertical stresses (100 kPa and 300 kPa respectively). It can be concluded that once the material has been sheared enough to pass the peak state (corresponding to the maximum rate of dilation of the sample) it will behave like a looser sample since after the peak is overcome the particles do not exhibit the same initial denser arrangement anymore. Consequently, when the same sample is retested its behaviour will be different from the one showed by a sample with the same properties but tested at its initial denser state. Retesting of the material would affect the results of the test and would not give reliable results. Therefore emptying and filling of the box during large scale shear box tests will be required.

5.5 Conclusions

From the series of tests conducted on limestone material at two different scales it was possible to derive important information regarding the shear strength characteristics of this soil. Particularly important to the aims of this research are:

- Values of angle of friction (peak and critical state angle) which will be used for comparison with the plate loading tests conducted on the same material at the same scale and with large direct shear tests conducted on the same kind of material but at larger scale.
- Maximum values of volumetric strain and shear strain achieved during the tests in order to estimate the maximum vertical and horizontal displacement which could be expected when testing the same kind of material. This information was used to develop the design of the large shear box (described in Chapter 7). Maximum volumetric and shear strain values were used to predict the maximum vertical and horizontal displacement which will be necessary to achieve when conducting the tests on limestone material at full scale in the large shear box apparatus.
- Effect of retesting the material which was useful to verify if the same sample could be used for multiple tests without compromising the results. The results obtained from testing the same sample clearly demonstrate that a reduction of the peak shearing resistance would occur by retesting the sample so that it was possible to conclude that a fresh sample must be used even when testing the material at full scale using the large shear box apparatus. The level of confining pressure was increased when testing the first sample and then decreased when the second sample of the same material was used. Considering that similar results were obtained when testing at the same confining pressure suggests that the factor mainly affecting the difference in results is the rearrangement of the particles during the previous phase of shearing rather than the amount of confining pressure used during the first test.

6. PLATE LOADING TESTS USING A CENTRIFUGE MODEL

The main aim of this chapter is to describe the test procedure and results of plate bearing tests performed at a reduced scale with the use of a geotechnical centrifuge model.

As stated earlier, plate bearing tests are often used to confirm platform design. For the specific purposes of this research the use of a centrifuge model allowed the investigation of three important aspects:

- firstly tests were carried out with the aim of verifying if the plate diameter to particle size ratio, proposed by the British Standard (BS1377-9, 1990) for *in-situ* plate bearing capacity tests, could be reduced without affecting the test results and therefore provide economic advantages. Considering the large particle size of the granular material commonly used for working platforms, the use of a smaller plate diameter would be particularly advantageous since it would require a lower reaction load to conduct the test.
- Secondly, the centrifuge model tests provided information regarding the behaviour of the scaled down material, in particular the bearing capacity near the surface of the ground and the potential settlement under a certain load. From these results a further analysis was carried out, which allowed derivation of the effective angle of friction of the material tested using a simple bearing capacity formulation for a circular shallow foundation.
- Finally, another centrifuge test was performed in order to verify the validity of the design method proposed by Lees (2019).

The angle of friction obtained from these tests represents the most important result for the purposes of this research since the comparison of this value with the ones obtained from other test methods will lead to a better understanding of how the results should be interpreted based on test method and scale size of the tested sample. Once relationship between results and testing method/scale size is understood it will be possible to validate the results obtained from small scale tests and therefore use them to obtain reliable results which can be used in design.

6.1 The geotechnical centrifuge at City, University of London

A geotechnical centrifuge facility has been located at City, University of London since 1989 and has been subject over the years to continuous developments and adaptations. The centrifuge is a 40 g/tonne Acutronic 661 beam centrifuge and can accommodate a maximum package mass of 400 kg at an acceleration of 100g. This capacity reduces linearly with acceleration to allow a maximum package of 200 kg at a maximum acceleration of 200g. Because of the high speed rotation of the centrifuge, necessary to create the required acceleration field, the machine is located within a circular reinforced concrete chamber which guarantees a safe working environment. The internal walls of this chamber are lined with an energy absorbent material to decelerate and retain projectiles in the rare event of any pieces of equipment or large fragments of debris coming loose from the swing during flight. This chamber is closed off by a curved Kevlar door which opens out into a foyer space to enable access to the centrifuge before flight. Located adjacent to this foyer is the centrifuge control room from which the centrifuge is operated, the test is conducted and data is logged from the test. The general arrangement of the Acutronic 661 is shown in Figure 6.1.

This centrifuge is characterised by an asymmetric arm (with model container at a long radius balanced by a more massive counterweight at a smaller radius) and the model package is mounted on a swinging platform attached to one end of the rotor by use of hinges.

The swing platform is located at a radius of 1.8 m when at full rotational speed during the test. During spinning up of the centrifuge and during flight the swing bed rotates such that the radial acceleration field is perpendicular to the now vertical face of the swing bed. The mass of the model, apparatus and swing bed are balanced by a 1450 kg counterweight, which can be adjusted radially on a screw mechanism (according to the mass of the package used for the test). Four strain gauge sensors located at the base of the machine are monitored in real time by the centrifuge control computer, which is able to detect an out of balance of more than the pre-set 15 kN. When this happens the safety system will automatically shut down the centrifuge. This safety system permits unmanned operation of the centrifuge overnight when required.

The centrifuge can accommodate a wide variety of strong model containers (rectangular boxes, cylindrical tubs, etc.). The permitted package volume is 500 mm x 700 mm in plan

and 500 mm height, plus in the central area of the swing a usable height of 970 mm could be exploited.

A slip ring stack, located above the central rotating pillar of the centrifuge, includes: four fluid slip rings and sixteen electrical slip rings. The four fluid slip rings can transmit to the model package compressed air or water up to 10 bar. The sixteen electrical slip rings are used to provide power to: on board control system, instrumentation, cameras, data acquisition (DAQ), motors, lighting and solenoids (as required). Connection to the data acquisition system, motors and cameras used on the model is via Wi-Fi.

Permanent junction boxes mounted on the centrifuge swing are used to collect signals from the instrumentation. These signals are then passed through an on-board signal conditioning unit with the aim of filtering and amplifying them. Amplification gains of 1, 10, 100, 500 or 1000 are available in order to accommodate low output voltage instrumentation (such as strain gauges or pressure transducers).

A PXI computer, mounted on the centrifuge and supplied by National Instruments, captures and stores real time data using a LabView program. This data can be inspected live during tests via a remote desktop connection on a computer situated in the control room.

6.2 Test description

As anticipated in the introduction of this chapter, one of the key aims of these tests was to investigate the effect of plate to particle size ratios to establish if a value of this ratio smaller than five (which is the limit required by the British Standard (BS 1377-9, 1990)) would still allow a reliable test to be performed on site. Plate bearing tests were carried out using crushed samples of a coarse grained limestone which were graded to represent scaled samples of 6F2 material, as described in Section 4.3. The size of the plate was varied for each test in order to change the plate to particle size ratio and the load-displacement response recorded. The measured bearing stress-settlement variation was correlated with the ratio of plate to particle size for both the samples to verify if a scale effect can be associated with the use of a plate diameter that is “too small”.

The maximum particle size of an ideal sample of 6F2 material (assumed, as an average, to be equal to 90 mm) was firstly reduced to a value of 3.35 mm, dictating that the acceleration level chosen to spin up the centrifuge model was equivalent to 30g.

Assuming this acceleration, the plate diameters used (7.8 mm, 12.0 mm, 16.9 mm, 23.8 mm and 39.7 mm) were representative of prototype values of 234 mm, 360 mm, 507 mm, 714 mm and 1191 mm respectively. The corresponding B/d_{\max} ratios (where B represents the plate diameter of the test and d_{\max} the maximum particle size of the samples) were therefore equal to: 2.3, 3.6, 5.0, 7.1 and 11.9 respectively, so that different values (higher and lower than the Standard limit) of B/d_{\max} ratio were tested to verify the effect of the ratio changes on the stress-settlement curve obtained for each test.

After these first results were obtained it was decided to undertake the same kind of operation on a sample of limestone whose maximum particle size corresponded to 2 mm, so that the acceleration level chosen to spin up the centrifuge model was equivalent to 50g. The purpose of testing a second sample having a smaller particle size distribution was to carry out a “modelling of models”, which in this case meant to verify the presence of scale effects due to the reduction of the model size. Considering the acceleration of the model sample being equal to 50g, the plate diameters used (9.0 mm, 12.7 mm, 17.7 mm, 23.8 mm and 39.7 mm) were representative of prototype values of 450 mm, 635 mm, 885 mm, 1190 mm and 1985 mm respectively. The corresponding B/d_{\max} ratios were therefore equal to: 4.5, 6.3, 8.8, 11.9 and 19.9 respectively, so that even in this case a considerable variation of the B/d_{\max} ratio was tested.

Garnier *et al.* (2015) report that, for centrifuge tests on shallow foundations, reliable results may be obtained when $B/D_{50} > 35$. The d_{\max}/D_{50} ratios for both of the samples used here is 6.7 and thus the implied minimum ratio in centrifuge tests, when expressed in the British Standard form of B/d_{\max} , is 5.2. For the tests presented here these two criteria are therefore essentially the same.

The bearing tests were carried out in a circular centrifuge tub (acting as a container for the sample) with a loading frame above, whose function was to drive the plate into the soil at a constant rate of penetration equal to 1 mm/minute. Once the sample, loading apparatus and instrumentation were prepared on the swing bed, the test could be carried out accelerating the system to 30g or 50g (depending on the particle size of the model sample). After compaction (achieved by spinning the sample in the centrifuge for about five minutes in order to ensure that a repeatable, compact sample was obtained for each test) the plate was advanced for about ten minutes such that the total penetration of the plate into the soil corresponded to approximately ten millimetres. This, at prototype scale,

is significantly further than might be expected in a real plate bearing test in order to capture all features of the stress/settlement curve.

The large tub (having an internal height of 300 mm and a diameter of 420 mm) was chosen with the intention of avoiding boundary effects due to the proximity of the plate to the base and sides of the tub. The design chart presented by Ullah *et al.* (2016) (Figure 6.2) provides a method to verify if the model geometry might be affected by boundary effects considering the ratio L_{BD}/B (where L_{BD} is defined as the distance measured from the centre of the plate to the inner edge of the sample container and B is the diameter of the plate). It can be seen from this chart that for the uniform loose sand ($\gamma = 11 \text{ kN/m}^3$) considered in this study the minimum L_{BD}/B ratio allowed is equal to five. Considering that the maximum plate diameter used for the tests was equal to 39.7 mm, the diameter of the tub was considered large enough to prevent or reduce possible boundary effects (L_{BD}/B being 5.3 in this case) although, as stated by Ullah *et al.* (2016), boundary effects would be more significant for dense sand, thus requiring a larger model container for a given foundation size.

The second important component of the testing apparatus, the loading frame, was used to push the plate into the sample and measure the force variation with increasing settlement. The frame, shown in Figure 6.3, consisted of: a motor and screw jack assembly, a loading beam, a force plate and the model test plate.

The motor and screw jack drive the plate into the soil through the stiff loading beam, to which the force plate and the test plate were connected. The force plate is comprised of three load cells sandwiched between two stainless steel plates. Use of three load cells in this arrangement prevented bending moments being induced in the load cells (which may arise from uneven seating of the plate on the test sample) causing false readings. The total force acting on the plate was then simply calculated as the sum of the readings from the three load cells.

Once the test was concluded it was possible to evaluate the settlement of the plate in the sample and calculate the plate bearing stress values in kN/m^2 (from applied load to plate area ratio). Displacement of the plate was not measured directly but rather from knowledge of the precise speed of the jack and the time elapsed (since the test was conducted at constant rate of penetration). For each test, a curve representing the different

stress-settlement curves was generated. The values of stress were compared in order to evaluate the presence of any possible scale effect due to the use of different plate size.

Important information was derived from these tests concerning the bearing capacity of the shallow foundation in the soil, from which it was possible to derive the effective angle of friction of the material tested (analysis explained in Section 6.4).

One more centrifuge test was conducted using the same equipment which was slightly modified in order to drive four foundations into the soil sample. The model was made of soft clay (280 mm height) whose half top was covered with a 10 mm layer of sand limestone. The limestone material chosen for this test was the one having a maximum particle size equal to 2 mm and the reason why it was decided to use this grading is to maximise the plate diameter to particle size ratio and therefore minimise the scale effect deriving from the use of small plates. The model was accelerated at 50g in order to simulate the behaviour of a granular platform of 0.5 m height and made of limestone with a maximum particle size equal to 100 mm.

The test was conducted using foundations of two different diameters (20.5 and 16.5 mm, representing prototype foundation diameters of 1.025 and 0.83 m respectively) which were pushed both into the clay layer and the sand layer overlying the clay so that the bearing capacity of the clay and the net bearing capacity of the granular material on clay could be determined at the same time. Considering the size of the plates which were used, the ratio between plate diameter and maximum particle size of the granular material was equal to 10.3 and 8.3 for the large and small plate respectively so the plate diameters were considered sufficiently large to avoid scale effects. Furthermore, the distance of each foundation from the internal side of the tub was equal to 100 mm, so sufficiently large to avoid boundary effects as indicated by the design chart presented by Ullah *et al.* (2016).

Results of this test were used to derive the “T value” introduced by Lees (2019) using equation 2.18 and compare with the theoretical value derived from equation 2.19-2.21 in order to verify the correspondence between experimental and theoretical value.

The plates used during the test were made of a different thickness (thicker plates were placed on top of the clay layer and thinner plates were used on the side with the granular material on top) so that the force applied by the reaction load system was able to drive the plates into the soil simultaneously at constant rate of displacement. The structure of the reaction frame applying the load was modified by changing the horizontal beam with

a cross element so that the four plates were placed at the each extremity. The load was measured by four triplets of load cells (one for each plate) sandwiched between two stainless steel plates (exactly like in the previous series of tests). The general arrangement of the centrifuge modelling testing equipment and instrumentation for this type of test is shown in Figure 6.4. The plates were pushed into the soil at a constant rate of penetration equal to 1 mm/min and the displacement was gradually increased for about twelve minutes (sufficiently long to allow the reaction system to get in contact with the plates and push the plates to a distance large enough to define the ultimate bearing capacity at the end of the test).

It should be noted that the rate of penetration may not be sufficiently rapid to achieve fully undrained loading of the clay. Finnie and Randolph (1994) proposed the use of a normalised velocity (Equation 6.1) to assess whether an event was drained, partially drained or fully undrained:

$$V = \frac{v_e d}{C_v} \quad (6.1)$$

where:

- v_e = relevant velocity
- d = drainage path length (taken as the diameter of the object pushed into the soil sample)
- C_v = coefficient of consolidation

Based on cone penetrometer experiments, Finnie and Randolph (2004) stated that, in Kaolin clay, drained penetration occurred when $V < 0.03$ and fully undrained behaviour occurred at $V > 30$. In the current experiments, assuming that d is equal to foundation width and using a value of $C_v = 0.05$ (taken from Colreavy *et al.*, 2016), the value of V ranges from approximately 3 to 13, indicating that fully undrained conditions are not met and that the results from these tests may not constitute a lower bound. This may make results obtained here difficult to compare with standard calculation methods but as the method of Lees (2019) uses the ratio of total capacity (of both layers) to the capacity of the clay alone (both measured here) then any rate effects will be negated.

Once the test was concluded, it was possible to derive the shear strength of the clay by using a shear vane. The value of strength was measured at three different height of the

clay layer (at 75, 150 and 200 mm distance from the top) at four different locations. These values corresponded to: 16, 17, 19 kPa at each depth respectively (an average value of undrained shear strength was calculated at each depth based on the readings taken at four different locations) so that an average was taken (corresponding to 17 kN/m²) for the calculation of the T value. The values of undrained shear strength measured were fairly constant at each depth so that it was concluded that drying of the clay sample during the test did not occur.

Using the ultimate bearing capacity of clay and of the granular material on clay obtained from the test and a few input data related to the geometry of the model (thickness of the granular layer and breadth of the foundation) it was possible to calculate the T value from equation 2.18. The value was compared with the one calculated from the shear strength of the two soils (the angle of friction derived from shear box tests in case of the sand limestone and undrained shear strength derived from the vane test for the clay) and effective vertical stress at the base of the granular layer with zero foundation load from equations 2.19-2.21.

6.3 Sample preparation

The same samples used for the standard shear box tests (previously described in Chapter 5) were used for plate loading tests. For the first series of tests, the limestone material was placed into the tub, which was filled up in such a way that the height of sample was the same for each test (approximately 250 mm). The sample was placed in around seven layers, each one comprising about 10 kg of material. The material was distributed inside the tub and each layer was accurately tamped before placing of the next one. The tamping operation was carried out by hitting a heavy circular plate (placed on the soil surface) with a mallet. This led to some variance in compaction near the boundary which was corrected by manually tamping with a wooden block. This method of tamping gave a compact sample characterised by a low void ratio (an average value of 0.336 for the sample with maximum particle size equal to 3.35 mm and average equal to 0.377 for the sample with maximum particle size of 2 mm. That equates to an average unit weight of 20 kN/m³ and 19.5kN/m³ and relative density equal to 74±2% and 61±2% for the two samples, respectively). After the filling procedure, the distance between the top of the tub and sample surface (Δh) was measured in thirteen different positions in order to get an average height of the sample (calculated from the difference between internal height of

the tub and average value of Δh). The height and diameter of the sample were used to evaluate its volume and, therefore, its voids ratio.

Preparation was completed by spinning the sample in the centrifuge for a short time (five minutes) with the intention of compacting the sample before starting the test. This further step ensuring that a repeatable, compact sample was obtained for each test. The height of the sample was checked again in order to ensure an accurate measure of void ratio was obtained before testing.

For the second type of test which was carried out with the aim of calculating the T value presented by Lees (2019), the model was prepared starting from the consolidation of the clay into the tub. In accordance with normal practice at the Research Centre for Multi-scale Geotechnical Engineering at City, University of London the clay sample (Speswhite Kaolin clay) was made from a slurry at a water content of 125% (approximately twice the liquid limit). The slurry was prepared in a mixer using distilled water and the dry Kaolin powder and the operation took about 6 hours. As the tub internal height was 300 mm and the desired height of the clay sample equal to 280 mm, it was necessary to add an extension to the top to allow the consolidation of the sample in the consolidation press. The slurry was then poured into the extended tub whose internal face was covered with water-resistance grease in order to recreate frictionless boundaries. A maximum pressure of 150 kPa was applied on top of the clay sample and a dial gauge placed on top of the loading platen was used to measure changes in vertical displacement and verify the degree of consolidation of the sample. A very low stress was applied to consolidate the sample in order to minimise the resulting shear strength of the soil. This choice was taken with the aim of getting a corresponding high T value meaning a better efficiency of the reinforcement structure. Test results presented by Lees (2019) show how working platforms constructed on very soft subgrades work more efficiently than the ones overlying higher-strength material, consequently the T value results to be inversely proportional to the value of undrained shear strength of the subgrade. Once the consolidation process was completed, the top of the sample was trimmed using a scraper in order to create the space for the layer of limestone material representing the granular platform. This part of the sample preparation process was conducted as quickly as possible in order to prevent the clay from drying. Firstly, the sand was mixed with some distilled water (water content was estimated around 5%) in order to allow a better compaction of the granular material (increased by suction) which was obtained by

tamping the top of the sand layer with a wooden tamper (the same as that normally used for preparing the denser sample for the shear box tests). The relative density of the granular material was equal to 80%. A layer of 10 mm was placed on half of the top of the clay sample so that both the bearing capacity of the clay and the net bearing capacity of the granular material on the clay could be determined during the test. After completing the soil sample preparation, the model was finished by placing the four plates. One pair of small and large diameter plates was placed on top of the granular material and another pair, with the same diameter sizes but greater thickness, on top of the uncovered half of the clay sample. The reaction frame was fixed on top of the tub and the alignment of the plates with the four sandwiched triplets of load cells was verified. At this point the model was ready to be moved to the centrifuge and the test started.

6.4 Test results and back calculation of soil properties

The results of the plate bearing capacity tests are presented in Figure 6.5 which show the variation of the bearing stress (q) against the settlement of the plate (B) for each test. Next to each curve is also indicated the plate diameter to maximum particle size ratio (R).

From Figure 6.5 it can be observed that there is a general increase in plate bearing capacity with increasing plate size (the smallest having a diameter of 7.8 mm and the largest one 39.7 mm) suggesting the presence of a scale effect in the model when tested at different plate diameter (and therefore different plate diameter to maximum particle size ratio). The curves representing the tests number 5, 6 and 7 seem to be characterised by some perturbations probably due to the small size of the plate compared with the particle size of the sample (the plate diameter to maximum particle size ratios in these cases corresponded to 2.3, 3.6 and 5.0). For this reason, the results obtained from these tests were considered not comparable with the other ones and discarded.

The value of bearing capacity for each test was derived from the load obtained at the maximum displacement of the plate which was reached during the test. This decision was taken on the basis that small plate diameters which were used for these tests would require larger displacement than the larger plates which are normally used on site (whose diameter is normally equal to 300-400 mm). On this basis, the calculation of the bearing capacity at settlement equal to 15% the plate diameter which is suggested by the British Standard (BS 1377-9, 1990) is not applicable and larger displacement should be considered. This conclusion was derived from the findings of Palmer *et al.* (2003) who

identified effects of displacement scaling in centrifuge model tests on shallow uplift tests and suggested that displacement should not be scaled. Considering that the amount of displacement required by the small centrifuge model test to reach failure should be comparable with the ones required for the large in situ plates (if 15% of the plate diameter is considered that would correspond to 45-60 mm). Since such a large displacement was not achieved during the centrifuge tests the bearing capacity was taken as the value corresponding to the maximum displacement obtained from the test.

The values of bearing capacity derived from each test were plotted in Figure 6.6 against the diameter of the plate. Results obtained from testing the first sample (with maximum particle size equal to 3.35 mm) are represented in black while the values of bearing stress derived from testing the second sample (maximum particle size equal to 2 mm) are represented in red. Both the results obtained also show the corresponding plate diameter to maximum particle size ratio (R).

The results from these tests seem to show, for each sample, an increase of bearing capacity with increasing the plate diameter (and therefore increasing R) plus the results seem to suggest that the factor mainly influencing the bearing stress is the absolute size of the plate rather than the plate diameter to maximum particle size ratio (R) since, if comparing tests conducted at similar plate diameter and different model particle size, it can be noted that similar results are obtained when using similar plate diameter rather than similar ratio R .

Considering this, another graph was plotted representing the values of ultimate bearing stress against the values of R (Figure 6.7). Also in this case the results are shown in two different colours in order to distinguish the values obtained using two different size samples. As it can be observed from the graph, results obtained from each sample lie close to two parallel lines. Despite these results (which might be ignored), it can be concluded that a scale effect is affecting the results of “downsized” plate loading tests, which means that when testing models at different scale (as in the case of a centrifuge model test), even if using same plate diameter to maximum particle size ratio, the results seem to differ by a constant which depends on the scaling factor which was used to reduce the tested sample.

Based on the analysis of results obtained for each sample grading it is also possible to conclude that despite the limit proposed by the guidance BS1377-9 (1990), there are

discrepancies in bearing capacity results when using different plate diameters during plate loading tests. This would affect not only centrifuge tests but also tests conducted on site. In particular an increase of the resulting ultimate bearing capacity when the test is conducted using larger plates (scale effect) can be expected. A second observation (less important for *in-situ* plate loading tests but relevant to centrifuge models) is that the values of bearing stress at the same ratio R would decrease when the sample is reduced in scale (scale effect).

The most important aspect to consider is the influence of these effects on the estimated angle of friction of the soil sample which can be back calculated from a simple bearing capacity formulation for circular foundations. Description of this calculation and results obtained are in the next section.

6.4.1 Back calculation of soil properties

The general aim of plate loading tests is to determine the bearing capacity near the surface of the ground and hence evaluate the possible settlements of the foundation under a certain load. In the case of a working platform, the aim would be to verify the design of the platform. In addition it is also possible to use the results to back-calculate the properties of the granular material for use in future design. In general, plate loading tests on granular material can continue to support an increasing load with settlements in excess of 50% of the plate diameter, without reaching a definable ultimate load capacity, the value of load which the load-settlement curve indicates uncontrolled settlement. The British Standard (BS1377-9, 1990), describes how to calculate the maximum applied pressure beneath the plate using the following equation (as previously mentioned in Chapter 3):

$$q = \frac{\frac{W_e 9.81}{1000} + P_u}{A} \quad (6.2)$$

Where:

q = maximum applied pressure (kPa);

W_e = total mass of the apparatus acting on the plate before adding the applied load, including the mass of the plate (kg)

P_u = applied force to cause failure (kN)

A = area of the base of the plate (m^2)

Furthermore, with reference to the force P_u the Standard specifies: “*When this is not clearly defined use the force causing a penetration of 15% of the plate width*”.

In practice, plate loading tests on compacted granular working platforms rarely achieve maximum settlements greater than 5% of the plate diameter. Despite the tests carried out on the centrifuge all being loaded sufficiently to ensure maximum settlements well in excess of 15% of the test plate diameter, based on the previous considerations, a larger settlement would be required for the small centrifuge model plates to develop a failure mechanism. The ultimate bearing capacity was therefore calculated considering, for each plate size, the value of load (P) achieved at the end of the test (from which was calculated the corresponding value of q).

Once this value was obtained, it was possible to evaluate the shear strength parameters of the soil sample adopting a back calculation method. BRE (Building Research Establishment) Report 470, “Working Platforms for Tracked Plant” (BRE, 2004), states that when laboratory testing of the platform material is not practicable, in order to select the appropriate design value of ϕ' (ϕ'_d = design angle of friction of the platform material used for the determination of platform thickness) other approaches can be adopted. These methods estimate ϕ'_d taking into account some characteristics of the granular material (for example: angularity of particles, grading, critical state angle of friction). Despite these methods being able to provide a general guide for the selection of a value of ϕ'_d , a great degree of caution is required. A good alternative method is represented by the plate loading test conducted on a trial section of compacted platform material. This test can provide data that will reduce the need to adopt conservative and uneconomic design parameters and will guarantee a more reliable and safer design than any other method based on assumed and untested parameters (Corke and Gannon, 2010). An analysis of the data derived from the series of centrifuge model plate loading tests was carried out in order to calculate the effective angle of friction of the testing material. The analysis utilises a simple bearing capacity formulation for a circular shallow foundation exhibiting the general failure mechanism. The type of failure was established based on the graph shown in Figure 2.4 and visual observation; bulging of the soil in the zone adjacent to the plate, observed for test 3 and shown in Figure 6.8, suggested a failure plane which extended to the surface of the soil sample which is typical of the general failure

mechanism). Using the graph shown in Figure 2.4 it was possible to conclude that a general failure mechanism characterised the series of plate loading tests conducted on the sample with maximum particle size equal to 3.35 mm while a local failure probably occurred when testing the samples with maximum particle size equal to 2 mm. Nonetheless, the difference between the two bearing capacity formulations representing the general and local failure mechanism would only affect the coefficient used for the undrained term which was not considered during the analysis since the value of undrained shear strength of the sample was taken as equal to zero because of the characteristics of sample (a dry coarse grained material). The bearing capacity formulations refer to Terzaghi's bearing capacity theory (Das, 2010):

$$\text{for general failure: } q_u = 1.3s_u N_c + \sigma'_{zD} N_q + 0.3\gamma' B N_\gamma \quad (6.3)$$

$$\text{for local failure: } q_u = 0.867s_u N_c + \sigma'_{zD} N_q + 0.3\gamma' B N_\gamma \quad (6.4)$$

Where:

q_u = ultimate bearing capacity (kPa)

s_u = undrained shear strength (kN/m²)

σ'_{zD} = vertical effective stress at the depth the foundation is laid (kN/m²)

γ' = effective unit weight when saturated or the total unit weight when not fully saturated (kN/m³)

B = diameter of the foundation (m)

N_c, N_q, N_γ = bearing capacity factors (as calculated in equations 6.5-6.8).

The bearing capacity factors can be found using equations below (Das, 2010; Coduto, 2000):

$$N_q = \frac{e^{2(3\pi/4 - \phi'/2)\tan\phi'}}{2 \cos^2\left(45 + \frac{\phi'}{2}\right)} \quad (6.5)$$

$$N_{\gamma} = \frac{2(N_q + 1)\tan\phi'}{1 + 0.4\sin(4\phi')} \quad (6.6)$$

$$N_c = \cot\phi'(N_q - 1) \text{ for } \phi' > 0 \quad (6.7)$$

$$N_c = 5.70 \text{ for } \phi' = 0 \quad (6.8)$$

It should be noted that for plate bearing tests of known geometry, the parameters N_c , N_q and N_{γ} calculation depend only on the effective angle of friction of the granular fill (ϕ') which can be therefore easily back calculated knowing the ultimate bearing capacity, the plate geometry and the bulk unit weight of the platform material. Values of N_c , N_q and N_{γ} could be also derived from other equations presented in literature which might result in slightly different values of ϕ' . The same type of calculation was undertaken using different methods to derive the bearing capacity factors (Davis and Booker, 1971; Vesic, 1973; Meyerhof, 1976) and it was possible to verify that the difference in values would not exceed 2° so that it was decided to use the equations proposed by Das (2010) and Coduto (2000). The angle of friction which is derived from this calculation was considered close to the peak angle of friction since the level of stress which was taken into account to derive this value corresponded to relatively low displacements and therefore the value of the angle could not be considered as critical (this aspect is important to consider when the value is used for design purposes and for comparison with shear box tests conducted on the same soil samples).

The results of this back calculation for each plate diameter are shown in Figure 6.9 in terms of angle of friction (ϕ') against plate diameter to maximum particle size ratio (R). Results represented in black refer to tests conducted on the sample whose maximum particle size was equal to 3.35 mm while those in red represent the results obtained from testing the material with a maximum particle size of 2 mm. From the graph it can be observed that for both the samples the results of tests conducted under a plate diameter to maximum particle size ratio larger than 5.2 (which was considered as limit from Garnier *et al.* (2015) since more conservative than the limit of 5 suggested by the British Standard (BS1377-9, 1990)) seem to lie in a narrow range of values which corresponds to 44.8° - 46.1° for the sample with maximum particle size of 3.35 mm and 42.6° - 43.8° for tests conducted on 2 mm maximum particle size sample. This is in accordance with the limit considered by Garnier *et al.* (2015) and also with the guidance presented in BS1377-9

(1990). Therefore it can be concluded that plate diameter to maximum particle size ratios larger than 5 (which is the limit provided by the British Standard) should be used and provide reliable results.

6.4.2 Results obtained from plate bearing tests on clay and sand overlying clay

The results of the plate bearing tests carried out on a clay and on top of a granular layer overlying the clay using two different plate diameters (20.5 and 16.5 mm) are presented in Figure 6.10 which show the variation of the bearing stress (q) against the settlement of the plate (w). From the graph it is possible to observe:

- A typical punching behaviour of the soft subgrade which shows a slow increase of the bearing stress with increasing the displacement of the plate without reaching an horizontal asymptotic value which could be identified as a failure (at least not for the amount of displacement which was achieved during the test);
- A rapid increase of bearing stress with displacement for the plates placed on top of the granular material overlaying the clay subgrade. The bearing stress in this case showed a small peak of bearing resistance followed by a small reduction and final slow increase towards the end of the test.

In order to verify the validity of the bearing capacity method proposed by Lees (2019), the “T value” introduced by the author was back calculated from equation 2.18 using the experimental ultimate bearing capacity values of the soft subgrade and of the granular soil layer overlaying the subgrade, plus the thickness of the granular layer and diameter of the plate. The ultimate value for the soft subgrade was derived by drawing a best straight fit line through the last part of the bearing stress-displacement curve and the intercept with the y axis was considered as corresponding to the ultimate value of bearing capacity (Figure 6.10). The value derived was compared with the theoretical ultimate bearing capacity of the subgrade calculated from the following equation (BRE, 2004):

$$q_s = s_u N_c s_c \quad (6.9)$$

Where:

- $s_c = 1 + 0.2 B/L$ shape factor for circular foundation (B= breadth of the foundation, L= length of the foundation)

- $N_c = 5.14$
- $s_u =$ undrained shear strength (kPa)

The value of q_s derived from the test and the theoretical value derived from the equation above were very close to each other (equal to 138 kPa) so the method used to derive the ultimate bearing capacity of the subgrade was considered as valid. Nonetheless, it has to be noted that the rate of displacement utilised for this test might have been too small to guarantee undrained penetration of the plates. According to the method described by Finnie and Randolph (2004) to evaluate the transition between the different drainage regimes, the rate of penetration used for this test might have caused the loading conditions to be partially drained. If that is the case, the value of bearing capacity calculated using Equation 6.9 should be increased in order to be representative of the real loading conditions.

The “T value” derived from test results was then calculated from equation 2.18 from knowing the bearing capacity of the subgrade (q_s), the bearing capacity of the granular layer on clay (q_u), the thickness of the granular layer (H) and the diameter of the plate (B). The values of bearing capacity of the granular layer on clay (q_u) were found as equal to 260 kPa for the larger foundation (diameter equal to 20.5 mm) and 280 kPa for the one having a smaller diameter (equal to 16.5 mm). These values of bearing capacity were derived from drawing a best straight fit line passing through the stress-settlement graph in the same way as it was done with the results related to plate tests conducted on clay (Figure 6.10). The “T value” calculated from equation 2.18 was then compared with the one obtained from equations 2.19-2.21. In this last case the value was calculated from knowing the shear strength of the subgrade and granular material and the vertical effective stress at the base of the granular layer with zero foundation load. Furthermore, the peak angle of friction of the granular material was substituted with the critical value since peak values are considered appropriate by Lees (2019) only where the strain level required to cause bearing capacity failure in the clay does not exceed the peak failure strain in the granular layer.

The resulting “T value” calculated from these equations show a very good agreement between the value derived from the experimental ultimate bearing capacity ratio (q_u/q_s) (equal to 0.68 for the larger plate and 0.62 for the smaller plate) and the one calculated from knowing the material properties of the subgrade and granular layer (which was equal to 0.55). On the basis of this correspondence, it was concluded that the “T method”

represents a valid approach to predict the net bearing capacity of two layered soil made of coarse grained material overlaying a fine grained subgrade. Considering the case of a soft ground, the method presented by Lees (2019) could be used for the design of a granular working platform reinforcement.

Once the reliability of the method was verified, the net bearing capacity of a granular layer overlaying a soft subgrade was calculated using both the method presented by Lees (2019) and the one used in the BRE Report 470 (BRE, 2004) which refers to the Meyerhof's bearing capacity theory. Comparison of the two allowed to verify if both the design methods would give the same results in terms of bearing capacity or if one of the two should be preferred to the other one. In order to do this, the ultimate bearing capacity value (q_u) was calculated using the Meyerhof's method (BRE, 2004) considering the same geometric conditions and the same shear strength characteristics of the material adopted for the centrifuge plate bearing test. The results obtained are shown in Figure 6.11.

The results of these calculations clearly show that the method used in the BRE Report 470 (BRE, 2004) gives as a result lower values of bearing capacity if compared with "T method" (bearing capacity equal to 149 kPa and 159 kPa was found for the larger and smaller plate diameter respectively using Meyerhof's method (BRE, 2004) while bearing stresses equal to 169 kPa and 186 kPa were obtained using the same soil parameter/geometry of the centrifuge tests and the equations proposed by Lees (2019)). Furthermore, the method presented by Lees (2019) shows a better agreement with the results obtained from the centrifuge tests so that this method can be considered more accurate and reliable when approaching to the design of a granular working platform on soft subgrade.

6.5 Conclusions

From the first series of bearing capacity tests it was possible to observe that:

- Plate diameter to maximum particle size ratio has an influence on the values of bearing capacity of the soil. In particular, an increase in the plate diameter used to test the material would result in higher values of bearing stress (scale effect). Furthermore, the use plate diameters which are very small compared to the particle size of the sample seem to be characterised by perturbations of the load-settlement curves probably associated with instability of the plate.

- In addition to the effect associated with the use of different plate diameters, a difference in results was found when using different model particle sizes during the test. Particularly, for equal values of plate diameter to maximum particle size ratios (R) the resulting bearing stress is lower when using a centrifuge model representing a smaller scale reproduction of the prototype (scale effect). Results obtained from two different models (maximum particle size equal to 3.35 mm and 2 mm) seem to differ by a constant value when testing the samples at equal plate diameter to maximum particle size ratio (R).
- Angles of friction obtained from back calculations based on the values of ultimate bearing capacity at different ratios (R) seem to lie in a narrow range of values ($\pm 1.2/1.3^\circ$) which depend on the model particle size used during the test, with the exception being the test conducted at $R < 5$. Therefore, concerning the angle of friction, the validity of BS1377-9 (1990), which for *in-situ* plate loading tests impose a plate diameter to nominal particle size exceeding five can be verified. This nominal particle size can be considered to be the maximum particle size in the material. Results of the test could be considered valid also when the value of this ratio is slightly smaller than five (as shown by the results) so that a more economic testing apparatus could be used.
- Differences in results would manifest when testing the material at different scale using different centrifuge models: a reduction of the angle of friction equal to about 2° was found when reducing the factor of scale from 30 to 50 times the size of the prototype. This difference would produce a difference in platform thickness equal to 0.04 m which, for example, in a platform with a surface of 50 m^2 would lead to an increase of 100 m^3 of required platform material with large impact on the economic and environmental aspect of the project.
- It is important to consider these differences when testing the material so that no underestimation/overestimation of the angle of friction would occur during design so that it would be possible to avoid uneconomic design on one hand or reduction of safety on the other one.

From the second type of plate bearing test conducted using a centrifuge model it was possible to conclude that:

- The “T method” developed by Lees (2019) represents a valid and reliable method for the prediction of the net bearing capacity of a granular soil layer overlaying a

soft subgrade since good agreement was obtained between experimental and theoretical results when conducting plate bearing tests using a centrifuge model with two different plate diameters;

- The same test was conducted on top of the clay material alone and the results also showed good correspondence with the ultimate bearing capacity calculated from a traditional bearing capacity equation for undrained loading;
- Comparison of test results with Meyerhof's bearing capacity theory adopted in the BRE Report 470 (BRE, 2004) for the design of working platforms showed how this method can result in a more conservative estimate of the bearing capacity;
- The "T method" seems to be a better approach to the design of granular platforms overlying a soft subgrade as the bearing capacity value predicted by using this method showed better agreement with the results of the tests.

7. LARGE SHEAR BOX TESTS

The aim of this chapter is to describe the design, development, construction and functionality of a large direct shear apparatus which was used for testing at full scale the same limestone material which was used during small scale tests. In addition to a description of the apparatus, the test procedure and results of three tests at different vertical stress levels are presented in this chapter.

7.1 Apparatus design development

The focus of this section is the description of the design process which was undertaken in order to develop a large shear box apparatus capable of testing material with particle sizes up to 100 mm. The section starts with a summary of the conclusions regarding the design criteria from the examples of large shear box apparatus found in literature. This information was taken into account when starting to define the design of the large apparatus which was specifically manufactured for the purposes of this research. In the following is a description of the decisions which were taken about the geometry of the apparatus, forces to be applied on the sample and maximum vertical/horizontal displacement required during the test. This was based on the information found in the literature, knowledge of the maximum particle size of the material to be tested and the results of previous small scale shear box tests. Finally, the general structural arrangement of the shear box is described together with its functionality.

7.1.1 Conclusions derived from examples of large shear box apparatus

Taking the examples of large shear boxes found in the literature (described in Chapter 3), it was possible to derive some conclusions about what were considered the most relevant characteristics of these large apparatus.

Based on these examples, the choice of steel as a material for the construction of a large shear box seems to be the easier solution to guarantee a durable structure able to resist applied large stresses. Except for the specific need of the Davies and Le Masurier (1997) shear box (aimed at testing long reinforcement nails), all reported examples propose the use of a horizontal shear plane for large shear box tests. The use of a horizontal plane might be more practical since it would allow easier sample preparation (basically progressive filling of a box) and enable a simpler load actuator setup compared with a vertical shear plane as adopted by Davies and Le Masurier (1997). The use of joist

sections firmly attached to a strong floor (as described by Davies and Le Masurier, 1997) provide support for the shear box and, at the same time, a low friction surface on which one half of the shear box could move (whilst the other half is fixed). This last feature could be obtained by using the beam sections as runways in which machine skates or similar can slide (as in Davies and Le Masurier, 1997) or treating the interface surface between the shear box and the beam sections with a coating acting to minimise the friction and abrasion during shearing (as used by Krahan *et al.*, 2007 at the interface of the two halves of the box). Based on the literature in regard to the effect of keeping a gap between the two halves of the box and avoiding the development of friction forces during shearing (Section 3.5), the best solution would be to avoid the presence of this gap to prevent loss of material during the test and use some type of lubricant to reduce the friction between each half of the box (as in Krahan *et al.* 2007). Considering the high stress levels required to shear the large sample, a reaction frame (as suggested by Jain and Gupta, 1975) is required in order to resist to shearing and confining stresses applied to the sample.

7.1.2 Geometry of the large shear box apparatus

The first step in the design of the large direct shear apparatus is the definition of the required size of the sample to be tested which, in turn, dictates the size of the box containing it. Among the studies regarding the geometric effects on test results due to the use of a too small sample height/width (or diameter) to particle size ratio (in particular the observed increase in angle of friction), the study conducted by Fu *et al.* (2015) was used as a basis to define an appropriate size for the shear box (see Section 3.5.2). The results obtained from this study (summarised in Table 7.1) are represented in two graphs (Figure 7.1-7.2 respectively) showing: variation of friction angle with W/d_{\max} (where W is the internal diameter of the shear box and d_{\max} the maximum particle size of the sample) at constant value of shear box height and variation of friction angle with H/d_{\max} (where H is the internal height of the shear box) at constant value of shear box diameter. Both the graphs show a vertical red line which defines respectively the limits $W/d_{\max} = 15$ and $H/d_{\max} = 10$, over which the values of angle of friction remain relatively constant.

These ratios were taken into consideration in order to define the internal size of the large shear box and when compared with the proposed limits of ASTM D3080 (2011) it should be noted that the values obtained from the limits provided by Fu *et al.* (2015) are more restrictive, requiring a larger diameter and height. The material proposed for testing is of

6F2 grading (Highways Agency, 2004) since this specification is primarily used for working platforms. Within this specification the maximum particle size of the platform material could be as large as 125 mm (although even at the upper bound of the particle size distribution from the specification particles this size would only comprise 10% of the material, see Table 3.1). For the purposes of these tests it was decided to limit the maximum particle size to 100 mm (this was considered as a limit since the actual maximum particle size of the material used for the full scale tests was expected to be smaller) and therefore the minimum width and minimum height of the large shear box for which the values of friction angle of the sample should not be affected by geometric effects is equal to 1500 mm and 1000 mm respectively.

Once the minimum width/height of the shear box was defined, it was decided to adopt a square geometry in plan instead of a circular container. This decision was taken in order to simplify the design and fabrication of the apparatus, especially with regard to the mounting and use of the loading jacks and actuator devices. The box obtained from these considerations is therefore a large split container of internal dimensions 1 m in height and 1.5 m in length and width with a resulting internal volume of 2.25 m³.

7.1.3 Determination of the vertical and horizontal forces

Once the size and shape of the box were defined, it was necessary to estimate values of vertical and horizontal forces to apply to the sample during the tests. In order to test the soil under conditions close to those experienced in the field, the vertical load was estimated taking as an example the case presented in Appendix E of “Design of granular working platforms for construction plant” (TWf, 2019). This example proposes the case of a piling rig exerting on the platform a maximum foot load of 680 kN over an operational area of about 1.04 m². From these input data it was possible to calculate the normal stress, which was found to be equal to 654 kPa. This was taken as a maximum although it should be noted that, in general, the track loading would be significantly smaller than this (TWf, 2019).

The second step was the estimation of the maximum shear stress required during the test. In order to do this, an angle of friction for the platform material equal to 55° was assumed (this is considered higher than that which might be found in practice). From this angle and the expected normal stress, the corresponding shear stress was calculated using a

simple Mohr-Coulomb failure criterion (assuming dry conditions i.e. no apparent cohesion):

$$\tau = \sigma'_v \tan \phi' + c' \quad (7.1)$$

This gives an estimated maximum shear stress value equal to 934 kPa.

Assuming a shear surface of 1.5 x 1.5 m, it therefore follows that the maximum estimated vertical force required during testing will be equal to 1400 kN while a maximum horizontal force of 2100 kN will be required to shear the sample not accounting for any frictional losses present in the apparatus.

These values were taken as indicative of the maximum vertical and horizontal forces which will be required to conduct the large shear box tests. Nonetheless, it has to be noted that the stress applied vertically at platform surface does not necessarily correspond to the normal stress required for the test since depending on the failure mechanism developed in the platform material this stress could instead represent the shear stress in the soil (for example when punching failure mechanism occurs).

7.1.4 Determination of maximum horizontal and vertical displacement

A series of small scale shear box tests were carried out at City, University of London in order to estimate the magnitude of dilatancy and maximum shear strain required during the test (as described in Section 5.4). Two downscaled representations of 6F2 class material (commonly used in working platforms) were tested under three different vertical stresses of 100, 200 and 500 kPa and different level of compaction using a standard apparatus (a shear box with an internal size of 100 mm square). The particle size distribution of the full scale material was reduced by a factor of 30 and 50 (obtaining two samples with maximum particle size equal to 3.35 mm and 2 mm respectively).

The values obtained for dilatancy and shear strain for these samples were expressed in terms of percentage such that the potential maximum vertical and horizontal displacement of the full scale sample could be estimated. For the denser samples of the tested material it was found that the maximum volumetric strain achieved was in the order of 3.7% and critical state was reached at a shear strain ranging between 20 and 40%. Assuming the initial height of the large shear box sample being equal to 1 m, the corresponding maximum vertical displacement will correspond to 38 mm and the maximum horizontal

displacement (at critical state) will be between 200 and 400 mm. These data were useful in order to verify maximum displacement of the sample and therefore estimate the room needed for the movements of the large shear box during the test.

7.1.5 Preliminary design

On the basis of the considerations outlined in Sections 7.1.1-7.1.4 it was possible to develop a preliminary design for the large shear box apparatus. The components which were defined at this stage are the following:

- A shear box (shown schematically in Figure 7.3a) made of steel and with an internal size of 1.5 m x 1.5 m x 1 m, split in two halves so that a horizontal shear plane would develop during the test. The horizontal shearing force would be applied to the bottom half of the box and the top half would be restrained whilst the vertical force is applied to the top surface of the sample via a stiff steel lid. This simplifies the loading the sample during the test since the normal force would be applied vertically on a surface which is not moving during shearing;
- A base supporting the box and reaction frame (Figure 7.3b), made of steel sections and strong enough to support the structure but also having the advantage of making the apparatus self-contained;
- A reaction frame (Figure 7.3b) made of steel sections capable of supporting the expected maximum horizontal and vertical forces applied to the box;
- Four 500 kN and one 5 MN hydraulic jacks (Figure 7.3b) were available to be used in the laboratory and therefore, based on the level of stresses which would be required during the test, it was decided to utilise the four small jacks to move horizontally the lower half of the box and the large jack to push vertically and downwards on the top lid of the box. The horizontal jacks therefore have a combined capacity slightly lower than the maximum required force calculated above but this was considered acceptable as the assumed maximum stress to be applied was larger than might be realistically used during the testing;
- A horizontal force measuring system (Figure 7.3b) placed between the reaction frame and the upper half of the box in order to measure the resultant horizontal shearing force that the sample would undergo. The use

of a measuring system on the other side of the box is necessary because of the frictional forces that develop between the two halves and at the bottom of the box during shearing. These forces would act against the direction of shearing, consequently reducing the horizontal force applied to the soil sample. The arrangement depicted in Figure 7.3b means that only the friction between the two halves of the box needs to be accounted for when processing the data obtained. As an additional check, the hydraulic pressure supplied to the four jacks could be measured by a pressure transducer enabling the total applied horizontal force to be calculated.

7.1.6 Final design and functionality

Once the general characteristics of the large shear box were defined, it was possible to analyse in detail the design of the apparatus, focusing not only on the shear box structure, but also on other important components (such as load jacks, reaction frames, strong floor base, etc.) and their functionality.

An overall view of the final design is shown in Figures 7.4-7.5. The structure comprises a large split box (internal dimensions 1.5 m x 1.5 m x 1 m) constructed from 254x254x132 UC steel sections and lined with 5mm steel sheet to give a smooth internal surface. For each half of the box, any side is constructed from two sections welded together along the two flanges and with reinforcing gussets positioned internally to prevent deformation from the applied loads. The bottom of the upper half and the top of the lower half of the box are both characterised by the presence of plate extensions whose roles is to prevent any outflow of the material during shearing (Figure 7.6). The upper half of the box is restrained by the presence of a reaction frame, while the bottom half is free to move horizontally in order to shear the sample. The top half contacts the reaction frame by an “extension” of the top side of the box made from a further piece of UC steel section (Figure 7.7) which during shearing reacts against two 1 MN load cells (measuring the horizontal force transmitted through the shear plane). The two load cells are attached to the reaction frame by the use of a rectangular plate (Figure 7.8) and therefore kept in position between the top extension and the vertical frame. Each load cell was provided with a domed piece of steel (Figure 7.9) which was specifically machined in order to perfectly fit the central cavity of the load cell and provide a rounded end. The presence of these rounded ends prevents damage from occurring to the load cells by ensuring no bending moment is applied. This is achieved by having a single point of contact between

the load cell and the top half of the box. In addition, if the displacement of the top half of the box is not perfectly parallel to the frame (as might occur in the early stages of the test) these domed fittings allow for the load being applied at a slight angle from the perpendicular.

The choice of moving the bottom half of the box was mainly related to the practical aspect of applying the vertical load on a stationary lid rather than a moving surface. The structure along which the bottom half moves consists of three long I-beams of 280 mm height which have the role of providing support to the box and a low friction surface on which the movement of the bottom half of the box would be allowed. The friction at the bottom of the shear box and at the contact of the two halves of the box was reduced to a very low value by the use of lubricated acetal sheets which were bonded (using epoxy resin) to the top of the three supporting beams and the top surface of the bottom half of the box (only on the two sides parallel to the direction of shearing) (Figures 7.10-7.11). Besides using acetal sheets to facilitate the sliding of the box on the steel beams, some guides (Figure 7.12) were attached at the bottom of the box in order to prevent the box twisting in plan during horizontal movement. These guides were fabricated in such a way that their smoothed corners would not dig into the beams in the event that the box does twist.

The entire reaction frame and box is manufactured from 254x254x132 UC steel sections with the exception of the top beam which is 356x368x202 UC. The vertical reaction assemblies at the left and right of the frame are welded units which are bolted to the three ground beams using M24 bolts. All bolts are tightened to the specified torque for structural steelwork. The vertical reaction assemblies are reinforced with two inclined supports which are aligned with the forces being applied (one arising from the system applying the horizontal force to the bottom half of the shear box and the other resulting from the top half of the box reacting against the two load cells during shearing).

The shear force is applied to the sample through four 500 kN hydraulic jacks (maintained in their position by the reaction frame, Figure 7.13) which push the bottom half of the box in the horizontal direction at a constant rate of displacement equal to 25 mm/min. The rate of displacement was established in order to create similarity with the shear strain rate used during the small scale shear box tests acknowledging the fact that, as previously explained in Chapter 5, the tested material was dry and made of coarse particles and thus does not require the rate of displacement to be necessarily smaller than 1 mm/min (as recommended for sand by Bolton, 1991). The rate of displacement was adjusted to the

desired level by simply adjusting the flow of the oil (via a needle valve) in the hoses which connect the four horizontal jacks to the activating pump and checking the resultant rate of displacement from the readings of the horizontal displacement measuring system. This was done with the box empty prior to any testing. The maximum horizontal displacement that can be applied by the four jacks is equal to 337 mm (equivalent to a shear strain of approximately 35% in the large shear box). The range of shear strains required to reach critical state in the small shear box tests was between 20% and 40% and therefore, if similarity exists between the samples tested, the displacement possible in the large shear box apparatus was considered sufficiently large to enable the tests to attain a critical state.

If necessary and as a final check, the force applied to the bottom half of the shear box can be calculated from the pressure applied to the four jacks which is recorded by a pressure transducer within the hydraulic system. This pressure divided by the cross sectional areas of the four horizontal jacks gives the total applied horizontal force.

The vertical load is applied by one 5 MN double-acting hydraulic jack (Figure 7.14) attached to the reaction frame and having a maximum stroke equal to 150 mm. The reaction frame is designed to minimise deflections and the upper cross beam is removable (together with the vertical hydraulic jack) to allow for filling and emptying of the container. The top beam is connected to the rest of the reaction frame by ten M24 bolts at each end. Both the capacity and the maximum displacement allowed by the vertical jack were considered sufficient for the purposes of this research. This was established by comparison with the tests conducted at small scale which were carried out under a maximum confining pressure of 500 kPa and showed as result a maximum volumetric strain equal to 3.8% the sample height (which for the large sample would approximately correspond to 38 mm). The volumetric strain from the small scale tests was taken as an indicator for the maximum change in height of the large sample considering that this value would change according to level of compaction and confining pressure.

The vertical jack is actuated by a second hydraulic pump and a servo-hydraulic control system manufactured by MOOG. This system runs at a maximum pressure of 210 bar whereas the jack is rated at 5 MN when operated at 700 bar. Thus the maximum load that can be applied is 1.5 MN which equates to a vertical stress on the sample of 666 kPa. This system measures the hydraulic pressures on either side of the piston and, coupled with data on the internal dimensions of the jack, is capable of adjusting those pressures to

achieve the force required. Should the sample compact or dilate during testing, the system is capable of adjusting to maintain the constant vertical load required. The system was checked by demanding a set value of force and measuring the output with a calibrated load cell underneath the nose of the piston. The force applied was found to be within 5% of the force demanded from the system.

The vertical stress is applied to the sample via a platen comprising a 30 mm thick steel plate stiffened with lengths of 200 mm SHS steel welded to the upper surface which were designed to minimise deflections even at the maximum applied vertical force (Figure 7.15). To ensure that the platen applies the vertical stress evenly to the sample it must act as near as practically possible to a rigid plate. The plate thickness and stiffener arrangement required were determined by a simple finite element model that considered the plate to be acting on an elastic foundation under a central point load. Figure 7.16 shows the stresses on the plate generated under an applied load that would be equivalent to approximately 450 kPa on the sample. There are some stress concentrations arising from the lack of fillets in the model but, in general, stresses are well below yield. The relative deflection of the plate from centre to edge is 1.4 mm and, as such, it can be considered to be acting as a rigid plate for the purposes of these experiments. The load is applied by the vertical hydraulic jack to the top lid through a cup and cone bearing such that small rotations of the top lid will not transmit unwanted forces into the piston potentially causing damage.

Measurements of the vertical displacements of the top lid and horizontal movement of the bottom half of the shear box are obtained by displacement transducers. The four transducers measuring the vertical displacements are positioned at the corners of the top lid. The arrangement of the four vertical displacement transducers was decided in order to monitor and take into account of possible rotation of the top lid during the test which would be evidenced by lifting of the lid on one side and a corresponding downwards movement on the opposite one. These transducers have a maximum travel of ± 100 mm and are kept in position by a frame made using slotted channel section which was assembled in order to create a solid structure which is resting on the strong floor of the laboratory (Figure 7.17). Similar support structures were created for the two displacement transducers (maximum travel equal to ± 300 mm) which were placed in contact with the side of the bottom half of the box (on the opposite side to the four horizontal hydraulic jacks) and kept in contact by the use of magnets connected to the tip of the core extension

rod of the transducer (Figure 7.18). In this way, all of the displacement transducers are mounted completely independently from the shear box itself and are thus not affected by any deflection of the reaction frame or similar effects.

A Data Acquisition System similar to the one used for the standard shear box apparatus was used to collect data from the tests in terms of load/pressure/displacement *vs.* time. In the same way as with the smaller apparatus, the recorded data is transferred to an Excel spreadsheet once the test is finished in order to allow further data processing. Two separate Data Acquisition Systems are used to record the data of the test when a vertical force is applied. The first one is the one recording the vertical and horizontal displacement of the displacement transducers, the reaction force measured by the two load cells on top of the shear box and the pressure activating the four horizontal jacks. The second one belongs to the servo-hydraulic control system of the vertical jack which also allows for the recording of the upper and lower pressure values of the jack through two pressure transducers and the resulting vertical force. This is simply used as a check to ensure that the vertical force applied remains constant throughout the test.

7.2 Evaluation of the frictional forces

The general arrangement of the large shear box means that there will be friction acting between the sliding surfaces of the apparatus which needs to be quantified such that it can be accounted for when processing the results of tests. Friction exists between the supporting beams and the lower half of the box and between the upper and lower halves. The arrangement of the jacks and load cells means that only the friction between the two halves of the box will have an effect on the measured results but the friction between the box and the beams will have an effect on the maximum shear force that the apparatus can apply to the sample.

Appendix B shows some simple calculations on the frictional effects in the apparatus. At an applied vertical stress of 100 kPa the total load acting at the base between the box and the beams (including the deadload from the apparatus and sample) would be around 330 kN. Assuming a conservative steel-steel interface friction coefficient of 0.5 would mean a horizontal force of 165 kN would be required to overcome this friction. There would be additional losses at the interface between the two halves of the box. Appendix B further shows that, assuming an angle of friction of the material tested of 45°, the frictional losses would be significant compared with force required to shear the material.

To reduce this frictional force, it was proposed to use acetal sheets as a bearing surface between the sliding parts of the apparatus. Acetal is a hard plastic available in sheet form but with a low stated coefficient of friction against steel. As it can be noted from the data shown in appendix B, a considerable reduction in F_f to T ratio derives from the use of acetal sheets so that a smaller horizontal force would be needed to shear the sample during the test when these are adopted. Furthermore, the addition of a lubricant was considered in order to further reduce the friction between the steel surfaces and the acetal sheets. Use of plastics sheets was chosen over, for example, machine skates or rollers due to the advantages of low cost and maintenance.

After cutting to size, one side of the acetal sheets was abraded using glass paper (in order increase adherence) and bonded to the three beams and top surface of the lower half of the box. The sheets were stuck to the steel surfaces using a strong epoxy resin and then put under load for about a day by the use of wooden blocks overlaid with 20 kg aggregate bags so that the sheets were firmly attached to the steel surface (Figure 7.19). All sliding surfaces therefore comprise steel acting against these acetal sheets which are additionally coated in waterproof grease.

Once the method for reducing friction was established, a further investigation was undertaken in order to verify the actual frictional forces acting at the bottom surface of the shear box and at the sliding surface between the two halves. This was performed by pushing the entire (empty) box horizontally by the use of the four horizontal hydraulic jacks so that only the friction at the bottom of the box was mobilised (bottom and top half of the box were not displaced from each other). The force required as a function of the mass of the empty box could be calculated from the pressure required in the horizontal jacks. Once the top half of the box came into contact with the load cells on the reaction frame, the load measured is simply that required to overcome the friction between the two halves of the box.

From knowing the total horizontal force required to overcome friction (which corresponded to about 10 kN) and the masses of the various component parts of the apparatus (whose sum corresponded to about 100 kN), it was possible to calculate the actual coefficient of friction ($\mu = 0.1$) which was used to calculate the actual frictional force (about 2.75 kN) acting at the sliding surface of the two halves. During testing, the shear force acting on the soil sample was therefore calculated as the difference between

the sum of the forces measured by the two load cells minus the frictional force acting at the contact surface of the two halves of the box.

Another aspect related to friction is the effect of vertical drag of the soil particles on the internal sides of the box. When the sample is compressed under the vertical load, friction is created between the soil sample and the internal sides of the top half of the box. As a consequence the confining pressure applied on the shear plane is reduced. Based on this assumption, an estimate of the total force which would be lost due to this friction is presented in Appendix C. Nonetheless, this effect occurs only when the two halves of the box are in contact with each other. When conducting the small shear box tests it was possible to observe that lifting of the top half of the box occurred so that the contact between the top and bottom half was lost towards the end of the test. When this happens, the weight of the top half of the box is transferred to the shear plane so that the confining pressure and consequently the shear strength would increase. Considering that this increase in vertical load was not taken into account for the small shear box tests (and is generally neglected in literature) it was concluded that this will not be considered for the large tests in order to keep the consistency of the testing method between small and large scale.

7.3 Apparatus and sample preparation

The preparation of the sample and emptying of the large shear box apparatus at the end of each test represented the longest procedure in the process of conducting the full scale tests. In order to simplify the preparation of the sample, the material was placed into the box and left in a relatively loose state without applying any form of compaction so that the samples obtained from this procedure had an average unit weight equal to 17 kN/m^3 and a void ratio of about 0.55 (precise values for each test are reported in Table 7.2). The void ratio of the sample was compared with the maximum (e_{\min}) and minimum (e_{\max}) index density of the two samples which were used to conduct small scale tests. Considering these values as reference (although some differences can be expected due to the non-exact correspondence in particle shape) it is clear that the large samples are tending to a loose state.

Preparation of the sample started by positioning the two halves of the box. This was to ensure that the top and bottom half were correctly aligned and just a very small gap would separate the side of the top half of the box (the one having the extension) from the load

cells which measure the horizontal force (to prevent any pre-loading of the cells before the test was started). This would allow the bottom of the box to have sufficient travel during shearing so that enough shear strain would develop. The bottom half of the box was moved by pushing it horizontally with the four horizontal jacks (in the case where the box had to be moved towards the load cells) or by two small capacity jacks activated by a manual pump (when the movement was required in the opposite direction). The top half of the box was aligned with the bottom half using the overhead crane.

Once the box was correctly positioned, it was filled with the limestone material which was collected from the quarry and delivered to the laboratory of City, University of London in bulk bags. Each bag contained about 1000 kg of material and was provided with loops which allowed them to be lifted by the use of a crane. One bag at a time was lifted, weighed (using an electronic balance between the hook of the crane and the bag), positioned within the box (the reaction beam and attached vertical hydraulic jack having been removed to facilitate the filling operation) and cut open with a knife at its bottom so that the material could be poured into the box. This procedure was repeated until the box was almost full (a small height of about 75 mm was left empty in order to accommodate the top lid so that it was safely kept in the same position during the test and also so that no loss of material would occur during testing). The total amount of crushed limestone which was used for each test corresponded to about 3500 kg. The material was not compacted in any way and the surface was carefully levelled after which the top lid was lowered into position using the overhead crane.

After this, the beam holding the vertical hydraulic jack was lifted into position and bolted to the vertical reaction frame so that the jack was aligned with the centre of the top lid. For the first test the vertical jack was not used to apply pressure on top of the sample, nonetheless it was necessary to secure the horizontal beam to the vertical components of the reaction frame in order to guarantee the correct functionality of the structure.

Once the sample was ready for the test, the last step in the preparation was setting up the vertical and horizontal displacement transducers. These were attached to their respective frames, positioned as necessary and zeroed within the data logging program.

At this point the test was ready to be started. For tests that involved a vertical load being applied, the control system was set to apply the required force and allowed to stabilise as well as taking up any initial compaction of the sample. At this stage, in line with common

practice, the initial height of the sample was measured from the distance between the top of the lid and the top of the shear box which was subtracted to the sum of the internal height of the box and the thickness of the lid. Shear force was applied by operating the pump connected to the four horizontal hydraulic jacks to shear the sample at a constant rate of displacement. Displacements, pressures and loads were recorded by transducers and load cells respectively. Once the test was complete and sufficient horizontal displacement was achieved, the bottom half was pushed backwards to its original position by the use of the two small capacity jacks which were placed between the reaction frame and the side of the bottom half of the box (in the opposite direction to the four jacks previously used to move the bottom half of the box and shear the sample).

At this point the horizontal beam holding the vertical jack and top lid were removed and the box was emptied. As previously explained in Chapter 5, complete emptying of the box (rather than just removing the material around the shearing plane) was considered necessary in order to guarantee preparation of a new undisturbed sample for the following test since the extension of the shearing zone was difficult to estimate. Additionally, completely emptying the box ensures an accurate measurement of the mass of material placed back into the box. This operation was made possible by placing a wooden platform (Figure 7.20) around the bottom half of the shear box so that the top half could be lifted and the material which was inside released. The wooden platform was provided with walls around its perimeter allowing it to retain the material which was pushed through the platform by shovels so it was possible to collect it into bulk bags similar to the ones used for filling- the box. The rest of the crushed limestone contained in the bottom half of the shear box was shovelled out and stored in bulk bags as well.

7.4 Testing programme

The large shear box apparatus was designed and manufactured with the aim of testing large particle size material and comparing the results with those obtained from testing the same material at smaller scale using a standard shear box apparatus. In order to compare the shear properties of the material at different scales, three large scale tests were performed at vertical stresses of 11, 104 and 185 kPa on three samples of limestone with similar initial void ratio (Table 7.2) and maximum particle size equal to 63 mm (particle size distribution shown in Figure 4.3), which were sheared at constant rate of displacement. The lowest of these values represents a test performed with only the

deadload of the platen applied and no additional load from the vertical jack. A summary of the testing program using the large shear box apparatus is provided in Table 7.2.

The first full scale test in the large shear box apparatus was conducted under a vertical stress corresponding to the sum of the self-weight of the material above the shear plane and weight of the top lid which has a mass of 991 kg (i.e. no further vertical load was applied by the vertical hydraulic jack). The resulting vertical stress at the shear plane during the test was therefore equal to 11 kPa (at the beginning of the test) and the sample was sheared at constant rate of displacement. This allowed a preliminary test to be conducted before the large vertical jack set up was completed.

The second large test was conducted on a sample of the same material which was prepared using the same procedure adopted for the first sample (by pouring the material from the top of the shear box) so that a loose sample with similar void ratio was obtained. In this case the vertical force applied by the hydraulic jack on top of the sample was equal to 390 kN. The self-weight of the material above the shear plane, the weight of the top lid and of the bearing cup of the jack were added to this force so that a total vertical force equal to 417 kN was applied on top of the shear plane. The resulting normal stress was calculated from the cross sectional area of the sample at the beginning of the test and corresponded to 185 kPa.

A third test was finally conducted on a third sample of the same properties applying through the hydraulic jack a vertical force equal to 208 kN so that a total vertical force equal to 235 kN was applied on top of the shear plane. The resulting normal stress at the start of the test is therefore 104 kPa.

Test results and their interpretation are presented in the following sections.

7.5 Test results

The Data Acquisition System of the large shear box apparatus records the following parameters during the test (with respect to time):

- Displacement of the four vertical transducers;
- Pressure applied to the vertical jack;
- Displacement of the two horizontal transducers;
- Pressure applied to the four horizontal jacks;

- Resultant horizontal force applied to the load cells by the top half of the box.

Monitoring the vertical and horizontal displacements was particularly important during the test to verify that the bottom half of the box was moving horizontally and that the vertical displacement transducers were correctly measuring the change in volume of the sample without reaching the maximum range allowed by the instrument. This problem occurred towards the end of the first test (conducted without any vertical load on top of the platen and thus at a low vertical stress). The absence of an additional vertical force from the jack allowed the lid to rotate considerably so that the vertical displacement transducers placed at one side of the lid (the one moving upwards) needed some adjustment during the test. When the transducers reached the limit of their travel (corresponding to ± 50 mm) it was necessary to move them to an appropriate height so that measuring of the vertical displacement of the top lid could continue till the end of the test.

The data recorded by the Data Acquisition System were used to derive the following parameters:

- Average vertical displacement of the top lid;
- Vertical force (F_v , calculated from the lower and upper pressure applied to the vertical jack and lower and upper cross sectional area of the jack);
- Average horizontal displacement of the bottom half of the box (x , from the average of the readings derived from the two horizontal displacement transducers);
- Horizontal force (F_h , calculated from the sum of the forces recorded by the two horizontal load cells minus the frictional force developed between the two halves of the shear box, as explained in Section 7.2);

From these measurements it was possible to calculate the variation of the following parameters during shearing in a similar fashion to the data from the small shear box tests:

- Volumetric strain (ϵ_{vol});
- Effective vertical stress (σ'_v);
- Shear strain (γ_s);
- Shear stress (τ);

7.5.1 Test 1

The first full scale test in the large shear box apparatus was conducted under a vertical stress corresponding to the sum of the self-weight of the material above the shear plane and weight of the top lid so that no further vertical load was applied by the vertical hydraulic jack. The resulting vertical stress at the shear plane when the test was started was therefore equal to 11 kPa and the sample was sheared at constant rate of displacement.

The first observation from the results of this test was the large rotation of the top lid during shearing (Figure 7.21). Rotation of the top lid appeared visibly evident while executing the test and the large amount of rotation was associated with the absence of a vertical load on top of the sample such that the lid was completely free to move vertically during the test and, in places, lost contact with the sample. Lifting of the lid occurred on the side which was placed farther from the position of the four horizontal jacks while the opposite side was moving downwards. The phenomenon can be clearly observed from the readings of the four vertical displacement transducers (Figure 7.22). From Figure 7.22 it can be seen how the transducers placed on the side of the lid which was moving upwards (V_1 and V_3) were recording negative values of displacement (meaning upwards movement of the lid) while an opposite direction was followed by the other side of the lid (as indicated by V_2 and V_4). This phenomenon seemed to visibly increase during the last phase of shearing and this was confirmed by plotting a graph which shows the variation during shearing of the difference in displacement between the two sides of the top lid (Figure 7.23). The difference in vertical displacement between the two sides was derived from the average of the displacements calculated for each side respectively (average of V_1 and V_3 minus the average of V_2 and V_4). Particularly, what can be observed from Figure 7.23 is a rapid increase of the rate of rotation starting from level of shear strains larger than 6%-7% and the maximum difference in height which was reached at the end of the test was corresponding to 120 mm.

In order to allow for a more representative calculation of the volumetric strain of the sample (ϵ_{vol}) it was decided that the vertical displacement would be calculated to correspond with the mid-point of the shear plane (considering that this length would reduce during shearing) rather than from the average of the readings of the four vertical displacement transducers. The average vertical displacements previously calculated for both sides of the top lid were used to derive the position of the pivot point of rotation of

the lid (calculated from the similitude between triangles considering its variation during shearing as shown in Figure 7.24). This was compared with the position of the middle of the shearing zone (also calculated in accordance with the increase in horizontal displacement (Δx) of the lower half of the box) which was used to calculate the corresponding value of vertical displacement (V_r , also shown in Figure 7.22). The definition of the vertical displacement aligned with the mid-point of the shear zone (V_r) allowed for a better understanding of the overall vertical movement of the sample and was used to identify the volumetric behaviour of the sample during shearing. The calculated value of vertical displacement (V_r) was therefore used to derive the volumetric strain of the sample during the test (Figure 7.25). The graph shown in Figure 7.25 (representing the variation of the volumetric strain, ε_{vol} , with the shear strain of the sample, γ_s) shows a short phase of compression followed by dilation. The sample continued to dilate until the end of the test without reaching a constant value (critical state). The dilation, typical of dense samples, was explained by the absence of confining pressure applied to the sample (i.e. the stress applied to the shear plane resulted from the weight of the top lid and self-weight of the material above it only). This would make the relatively loose sample (unit weight equal to 17.25 kN/m^3) behave like a dense sample at these very low stresses i.e. the sample moves towards critical state displaying dilation and strain softening. Considering that the maximum shear strain which was possible to apply to the sample during the test was equal to 31%, it was concluded that further displacement would be probably needed in order to reach the critical state.

From the graph showing the variation of the shear stress with shear strain of the sample (Figure 7.26), it can be observed that the shear stress is constantly increasing for the duration of the test without showing a peak value (which might be expected based on the soil state and the low stress level) indicating that it cannot have reached a critical state. The graph shows that the increase in shear stress is showing a relatively smooth curve up to levels of shear strain (γ_s) corresponding to 10% the height of the sample, after that some perturbations in the curve start to develop. Comparing this curve with the one showing the amount of rotation of the top lid (Figure 7.23) suggests that from this point onwards the results might have been affected by the excessive rotation of the top lid and it may therefore be necessary to consider only the data up to and including shear strains of 10% as reliable for this test.

7.5.2 Test 2

The second test was carried out on a loose sample (given bulk unit weight equal to 17.36 kN/m^3) of the same material on which a vertical load was applied by the use of the hydraulic jack. In addition to performing the test at a higher stress level, it was assumed that some of the issues with the rotation of the platen would be mitigated by the vertical load acting on top. A vertical force of 225 kN was demanded from the servo-hydraulic control system which, when coupled with the deadload of the apparatus and sample, would have resulted on a vertical stress of around 110 kPa. However, subsequent to the test, an error in the calibration of the control system was discovered and, after applying a correction for this, it was found that the vertical force applied on the sample was in fact equal to 390 kN. Combined with the self weight of the material above the shear plane, the weight of the top lid and the weight of the bearing cup of the jack the total vertical force during this test was therefore equal to 417 kN which corresponded to an initial vertical stress of 185 kPa.

The first thing observed during the execution of the test was that despite the presence of vertical load applied by the jack, rotation of the top lid still occurred during shearing, nonetheless this appeared to be less pronounced than in the first test (Figure 7.27). The phenomenon can be better visualised by the graph of Figure 7.28 showing the difference in displacement between the two sides of the top lid during shearing. From the graph it is confirmed that the rotation of the lid was lower than in the first test and that, in this case, the rotation gradually increased during shearing without showing a sudden increase (as observed during the first test). The maximum difference in height between the two sides of the box was reached at the end of the test and corresponded to about 64 mm, almost half of the value reached during the first test. Based on the conclusions from the first test, the vertical displacement of the sample was also in this case calculated in correspondence with the mid-point of the shearing plane whose position was again derived by means of simple calculations. The displacement recorded by the four vertical displacement transducers and the amount of vertical displacement calculated above the mid-point of the shear plane are shown in Figure 7.29. From this figure, an upwards movement of the lid on one side can be observed (V_1 and V_3 , as in the first test) and corresponding downward movement of the lid on the opposite side (V_2 and V_4). The values of displacement calculated in the middle of the shear plane (V_T) suggests an overall compression of the sample. The change in volumetric strain during shearing (ϵ_{vol}) was

therefore derived from the variation of the vertical displacement V_r and plotted in a graph shown in Figure 7.30. From Figure 7.30 it is possible to observe an increase in compression with shearing till a maximum value equal to about 1% corresponding to an amount of shear strain equal to 10%. After reaching the maximum level of compression, the sample starts to dilate exhibiting a reduction in that compression until the end of the test but without exceeding the value of voids ratio corresponding to its initial state (i.e. the sample never exhibits an overall dilation). It can be concluded that the addition of the vertical load applied to the sample through the top lid had a positive effect in reducing the rotation of the top lid so that the reading of the vertical displacements of the sample (and therefore the change in volumetric strain during shearing) would be more reliable when a vertical load is applied. Overall, the sample is compressing during shear, commensurate with a relatively loose sample at a relatively high level of vertical stress.

Examining the graph showing the variation of shear stress with the increase in shear strain (Figure 7.31) again shows that the values seem to increase without the curve reaching a constant value of shear stress although for shear strains larger than 20% the rate of increase in shear stress seems to reduce when compared with the initial part of the curve suggesting that proximity to the critical state might have been reached.

The same observation is valid for the curve showing the variation of the volumetric strain during shearing (Figure 7.30) where it can be noted how the reduction in compression is less pronounced for values of shear strains larger than 20% suggesting proximity to the point where the sample would reach a constant volume (critical state).

7.5.3 Test 3

The third test was conducted with a vertical load applied by the jack on top of the sample. Having corrected the calibration in the vertical load control system, the magnitude of this load was chosen such that the normal stress applied would be between the values applied during the first and second test (corresponding to 11 kPa and 185 kPa respectively). The sample was prepared using the same method which was adopted for the other tests so that a loose sample of unit weight equal to 17.09 kN/m^3 was obtained (as indicated in Table 7.2). The sample was sheared under a force of 208 kN (applied by the vertical jack) so that the total vertical force applied on the shear plane was equal to 235 kN which corresponded to a confining pressure of 104 kPa.

The data recorded was processed in the same way as that from the previous tests. From the graph (Figure 7.32) showing the difference in vertical displacement between the two opposite sides of the top lid rotation of the lid during the test can again be observed which, nonetheless, seems to be much less pronounced than in the first test and also slightly smaller than the second test. The maximum difference in height between the two sides of the lid at the end of this test corresponded to about 48 mm. The same method used for the previous two tests for calculating the global vertical displacement of the top lid was adopted for this test as well. The values of the resultant vertical displacement (V_r) is shown in Figure 7.33 together with the displacements measured at the corners of the top lid. From this value of displacement (V_r), it was possible to calculate the volumetric strain and observe its variation during shearing (Figure 7.34). The results show that the sample initially compressed, reached a maximum volumetric strain equal to 0.6% at a corresponding shear strain of about 5%, then started to dilate until reaching a minimum volumetric strain of about -1% towards the end of the test. The rate of dilation of the sample seemed to gradually increase until values of shear strains reach about 25%, after this point the increase in dilation seemed to reduce but without reaching a constant value (which would correspond to the critical state of the sample). Nonetheless, the increase in dilation was much more contained than in the first test due to the presence of the vertical load applied by the jack.

The variation of the shear stress during shearing is shown in Figure 7.35. The shear stress in this case is increasing until shear strains reach about 15%, after which the stress-strain curve seems to reach a relatively constant value of shear stress till further strains are achieved and the stress starts increasing again. When approaching the end of the test it was possible to observe the lifting of the top lid from the surface of the sample so that it can be concluded that the values of shear stress obtained at large shear strains cannot be considered as reliable. Again, a clear definition of the critical state of the sample is not possible for this test since both volumetric strain and shear stress values did not seem to reach a constant value.

7.6 Summary

Based on the literature and the results of the tests conducted at small scale using a standard shear box apparatus, a design for a large shear box apparatus was developed which would allow testing of samples containing large particles of up to 100 mm in size.

After the design and functionality of the large apparatus were defined, the shear box was manufactured and delivered to the laboratory of City, University of London in order to conduct a series of tests on crushed limestone with maximum particle size equal to 63 mm. The material represented a full scale version of the samples used for the small scale tests and was sourced from the same quarry so that the intrinsic material properties (such as mineralogy and angularity) would be the same.

Three large shear box tests were conducted on relatively loose samples of the same material using three different normal stresses. These stresses were corresponding to (in order of testing) 11, 185 and 104 kPa and were calculated from the sum of the vertical load applied by the vertical jack and its loading cup (not present for the first test), the weight of the top lid and the weight of the material above the shearing plane.

The results obtained from the first test indicated a considerable rotation of the top lid during shearing associated with the absence of a vertical load applied on top of the lid. This assumption was confirmed by the results of the other two tests which were conducted with a vertical load applied and showed a significant reduction in the rotation of the top lid.

In order to allow for a better understanding of the volumetric behaviour of the samples during the test, the global vertical displacement of each sample (V_r) was calculated for each test above a point corresponding to the mid-point of the shearing plane (whose position was obtained by consideration of the horizontal displacement of the lower half of the box during the test). The global vertical displacement was calculated from the values of displacement which were measured at the four corners of the top lid by using a simple calculation. From this value of vertical displacement it was possible to obtain the variation of volumetric strain showing the compressive/dilatant behaviour of the samples during the test. The results obtained from the first test (where no vertical force was applied) showed a short phase of compression at the beginning of shearing followed by dilation which continued until the end of the test. For the second sample (which was tested under a normal stress equal to 185 kPa) the volumetric strain increased during the first phase of shearing and then reduces towards the end of the test. Nonetheless, the increase in volume of the sample during the last phase of shearing was not large enough to increase the void ratio of the sample over the initial value measured before the test was started. The third test (during which a vertical normal stress equal to 104 kPa was applied) showed again a compressive behaviour at the beginning of shearing followed by a small dilation

of the sample during the last part of the test so that the final value of void ratio was larger than the one corresponding to the initial state of the sample.

The curve representing the variation of shear stress during the first test shows a general increase in shear stress throughout the test. It is not possible to identify a peak or constant value of shear stress (critical state) from this curve so that no conclusion about the values of peak/critical state angle of friction could be derived from this curve. From the values of volumetric strain which were recorded for this test it is possible to observe a dilatant behaviour typical of dense samples. This was associated with the absence of a vertical load on top of the sample, which allowed the sample to dilate considerably after a small initial phase of compression.

Test results obtained from the second test showed a constant increase in shear stress with shearing without the curve reaching a constant value which could be interpreted as critical state. Comparing with the curve showing the volumetric strain, an overall compression of the sample was observed without reaching a constant value. Therefore, even in this case no critical state could be identified.

For the third test the shear stress increased until levels of shear strain corresponding to 15%, after that a relatively constant value of shear stress was reached followed by a sudden increase during the last part of the test. The values of volumetric strain suggest a dilatant behaviour of the sample even if it is more limited than in the first test. Even in this case therefore, no peak or critical state angle of friction could be identified from the stress-strain curve.

Considering the results obtained from the three tests conducted at full scale it was concluded that no angle of friction at peak or critical state could be identified from the curves showing the variation of the shearing stress with shear strain. In order to derive these parameters and allow for the interpretation and comparison of the tests with small scale tests another method was required. The method used for interpreting the results is described in the following section.

8. DISCUSSION

8.1 Introduction

The aim of this chapter is to describe the method used for interpreting the results obtained from the three large shear box tests so that a comparison with the small scale tests could be carried out.

As noted in Chapter 7, it was not possible to identify peak or critical state angles of friction directly from the large shear box test results because:

- the values of shear stress continually increased during shearing without reaching a constant value,
- the volumetric strain observed during shearing continuously varied without reaching a state of constant volume.

These observations clearly indicate that the material failed to reach a critical state.

The results obtained do not lend themselves to interpretation in the way the results from the small shear box did, i.e. from the graphs of shear stress and volumetric strain versus shear strain it is not possible to easily identify peak or critical states. It is possible that the maximum shear strain that the apparatus could apply was insufficient for the samples to reach a critical state or that the observed rotation of the lid affected the results at high levels of shear strain. Therefore a different method of analysis would be required to determine appropriate values for critical state friction angles. In order to compare the results with those obtained from the small scale tests, it was decided to obtain the values of the critical state angle of friction using a stress-dilatancy approach which considers the work done during shearing as the sum of two contributions, one required to overcome the friction between the particles and another one related to volume changes during shearing (Wood, 1991). A description of this method and the results obtained from applying it to both small and large scale shear box test results are described in this Chapter.

The results obtained by applying this method to large shear box test results were compared with those derived from small scale shear box tests. Differences between the scale models helped to identify how much the size of the sample (i.e. maximum particle size) can affect the results of direct shear tests. The results obtained were also compared with those obtained from small scale plate bearing tests conducted on the same material using a centrifuge model.

Based on the comparison of these results a strategy was developed in order to interpret the results obtained from small scale tests so that they could be safely used for the design of working platforms when a large scale apparatus is not available for testing the material at full scale.

8.2 Overview of the results obtained from large scale tests

In order to derive the conclusions about the effect of testing the material at different scale and with the use of different testing methods it was first necessary to interpret the results obtained from the large shear box tests.

The first comparison between the three large tests was undertaken by considering the rotation of the top lid during shearing. This is shown for all tests in Figure 8.2. From this graph it is evident that the first test shows significantly larger rotations of the top lid compared with the other tests, which started to increase considerably after a shear strain of about 7%. Contrary to the other two tests, the amount of rotation kept increasing until the end of the test while for the other tests, the rate of rotation increased rapidly in the first phase of shearing but reduces towards the end. The responses provided by the results of the second and third test are very similar until shear strain is equal to about 15%, for larger strain the rotation of the lid appears larger in the second test despite this being the test with the highest vertical load applied to the lid. In both cases the total amount of rotation during the first phase of shearing is larger than in the first test but significantly lower towards the end of the test. Particularly, it can be noted that in both cases the presence of the vertical load on top of the lid reduces the total amount of rotation to about 50% of the amount seen in the case of no vertical load applied (test 1).

The effect of applying a vertical load can be also identified by comparing the curves representing the variation of the volumetric strain of the sample during shearing (Figure 8.3). From this graph it can be seen how the absence of a vertical load during the first tests allowed the sample to dilate considerably after a small initial phase of compression, while the other two samples (tests 2 and 3) showed a larger amount of compression followed by a small increase in height during the last phase of shearing. Particularly, this increase was smaller for higher levels of vertical load (test 2) and slightly larger for the test conducted under a medium value of vertical load (test 3, in which overall response of the sample was dilatant).

Consistency between level of confining pressure and behaviour of the sample is also maintained in terms of resulting shear stresses. In fact, as can be observed from Figure 8.4, as would be expected, the maximum level of shear stress reached by the sample increases with the increase in vertical load.

Nonetheless, as previously mentioned in Chapter 7, the three curves shown in Figure 8.4 suggest continuously increasing shear stress without reaching a constant value (although, due to reasons of scale, the results from Test 1 look to be constant in this Figure). In conjunction with the curves representing the variation of volumetric strain during shearing (Figure 8.3), it can be noted that no constant volume state is reached by any of the three samples for these level of shear strains and therefore, as a consequence, no critical state (and therefore critical state angle of friction) can be determined from these graphs in the way that they could for small scale tests (Chapter 5).

8.3 Rotation of the top lid in shear box tests

Considering that the rotation of the top lid seemed to have a significant impact on the results of the test further literature sources have been explored in order to clarify if this phenomenon was previously identified by other authors and what solutions have been proposed.

Rotation of the apparatus during shearing was early identified and measured by Assadi (1975), Dyer (1985) and Airey (1987). A series of tests on dense sand were also conducted by Palmeira (1987) with the use of three different arrangement: a fixed top platen (symmetrical arrangement), a free rigid top platen (conventional arrangement) and a free rigid top platen loading a pressure bag. The results derived from these tests (Figure 8.5) showed that increased freedom for sample rotation increases the measured peak shearing resistance and reduces the peak rate of volume change measured at the sample boundaries. The shear displacement required to mobilise the peak shearing resistance also increases.

Based on the results derived by Palmeira (1987), Jewell (1980) suggested that improvement can be achieved by firmly securing the rigid top loading platen to the top half of the apparatus after applying the vertical load so that the upper half of the apparatus moves as a unit during shear.

Non uniform stress distribution due to the rotation of the sample during the test was also reported by Pedley (1990). The author identified the problem in the apparatus used by Palmeira (1987) and suggested to fix the top loading platen to the upper half of the large

shear box which was used in his study in order to obtain symmetrical boundary conditions. Pedley (1990) also conducted a series of direct shear tests using a medium sized apparatus to provide a datum with which to assess the effectiveness of modifications to the large shear box. During these tests the author observed a rotation of the top half which seemed to increase with shear displacement, the vertical displacement falling at the front of the shear box compared with that at the rear of the box. According to Pedley (1990) this rotation is due to a counter clockwise moment resulting from the eccentricity between the shear load and the centroid of the sample. As a consequence of this, the load applied in the front of the shear box would drop whereas the load in the rear would increase. The author suggested that in order to overcome small fluctuations in the vertical load the mobilised shear stress should be normalised with respect to the vertical stress acting on the central plane. Furthermore, reduction in rotation may be possible by using a shear jack which can compensate for the eccentricity of the shear force or a separate control of the load when using multiple vertical loading jacks.

Potts (1987) investigated the effect of allowing rotation of the top lid by the use of finite element analysis. The author compared the results obtained from tests conducted using a standard shear box loading plate able to rotate and another one in which the plate was allowed to move vertically but was prevented from rotating. Based on the results obtained from this analysis, it was concluded that freedom of the top cap to rotate had little influence on the behaviour and rotations were less than half a degree. Freedom of the top plate gave slightly less stiff pre-peak load-displacement behaviour in all the analysis and caused a reduction of the peak shearing resistance of 3%. The conclusion drawn by the author is that restraint of the top plate might be desirable when testing soils which exhibit severe strain softening.

Bareither *et al.* (2008) also reported rotation of the top lid as a consequence of particle movements during shear which were schematically represented in Figure 8.6. Dilation was identified at the front of the box and contraction at the back. Based on a series of discrete element model studies previously conducted by other authors (Liu, 2006, Cui and O'Sullivan, 2006, Zhang and Thornton, 2007) Bareither *et al.* (2008) observed that these particle movements may create particle-to-particle force concentrations at the front of the upper shear box and back of the lower shear box during shearing. These forces are transferred to the particle-box interface increasing the measured shear resistance which was found to increase at larger horizontal displacement in some of the large shear box tests. Also, the author observed that this phenomenon was more accentuated in the larger

box compared to the smaller one and explained this as due to a greater number of particles moving within the shear band in the larger scale tests. Evaluation on the type of arrangement to use for applying the vertical load on top of the sample during shearing was also studied by Kim et al. (2012). The author considered three different types of shear box apparatus (Figure 8.7).

In the case of Type A the loading plate is able to rotate and move up and down because the loading plate and upper half of the shear box are independent from each other. The author explained that in this case it is especially easy to induce a moment during shearing because the loading plate and piston are connected with a hinge which is not fixed. In the case of Type B the loading plate and the upper shear box are rigidly fixed after the consolidation process. In this case the rotation is prevented during shearing and the variation of the opening between the two halves of the box is induced by the change in volume of the sample during the test. The problem with Type B is the outflow of the specimen through the gap when a large dilation is reached. The Type C is suggested by the author as better solution. In this case the upper half of the box is kept separated from the loading plate and the loading plate is fixed to the piston. In this way although the loading plate is able to move vertically a rotation is barely induced during shearing.

Conclusions derived from this series of studies is that rotation of the top lid becomes critical when testing large samples and should be prevented by the use of a rigid connection between the plate and the system applying the vertical load. Failure from limiting the rotation of the lid would cause a change in boundary conditions of the sample during the test with consequent increase in the measured shear resistance.

The following presents the analysis of the results obtained in the tests conducted. The issue of rotation of the lid is summarised in the conclusions and further work.

8.4 Method for interpreting the results obtained from large scale tests

In order to allow comparison with the small scale test results, the use of a different approach based on dilatancy theory was required in order to derive the value of the angle of friction from the large shear box tests. This approach considers the work done during shearing as the sum of two contributions, the first one is the work done to overcome the friction between the particles and the second one is required for producing volume changes during shearing.

Simplified equations based on this approach are presented by several authors (for example Atkinson, 2007) and relate the variation of the stress ratio during shearing (τ/σ'_v) to the critical friction angle (ϕ'_{cr}) and the angle of dilation (ψ):

$$\tau/\sigma'_v = \tan (\phi'_{cr} + \psi) \quad (8.1)$$

Where, $\tan \psi = - dy/dx$

It can be seen from Equation 8.1 that when $dy/dx = 0$:

$$\tau/\sigma'_v = \tan \phi'_{cr} \quad (8.2)$$

This condition, corresponding to zero change in volume of the sample, can occur during two different phases of shearing (Figure 8.8): at the point of maximum compressive strain (pre-peak strength phase, when the soil behaviour changes from compression to dilation) and at the critical state (post-peak strength phase, when the soil is shearing at constant volume and constant shear stress) (Wood, 1991).

Considering that no critical state was achieved during the large shear box tests, the use of this method was taken into account in order to derive the values of stress ratio (τ/σ'_v) corresponding to $dy/dx = 0$ reached by the samples during the first phase of shearing (pre-peak strength phase). The corresponding critical state angle of friction was therefore calculated.

Rotation of the top lid during the large scale tests affected the distribution of the normal stress applied on top of the samples (dilation of the sample was unrestrained on the side rising and reduced on the opposite side so that the stress distribution in the samples is assumed to be non-uniform) so that caution should be taken even when adopting this alternative method for interpreting the results, since both stress ratio and dilatancy were affected by the phenomenon. Nonetheless, considering that the rotation of the top lid was significant only towards the last part of the tests it was concluded that the results obtained from the initial phase of shearing could be considered as valid in order to identify the critical state angle of friction (calculated from the first intercept of the curve with the vertical axis).

In order to verify the validity of the method for laboratory tests, it was decided to firstly apply this theory to the results obtained from small scale tests and compare the angles of friction derived from the stress-dilatancy method with the values calculated from the

stresses reached at critical state (which in case of small scale tests was possible to identify by observing a zero change in volumetric strain when the soil was shearing at constant shear stress).

Following the method proposed by Wood (1991), the values of stress ratios (τ/σ'_v) obtained from the results of the shear box tests conducted with the 3.35 mm and 2 mm maximum particle size samples were plotted against the values of dy/dx (calculated from the vertical and horizontal displacement of the samples during shearing) (Figures 8.9). Considering the large number of tests which were conducted at small scale it was decided to plot only three tests for each particle size corresponding to the three different vertical stresses used during these tests (100, 200 and 500 kPa).

In these plots, the points at which the curves cross the stress ratio (τ/σ'_v) axis at $dy/dx=0$ indicate a stress ratio at which only frictional forces between the soil grains are resisting shearing so that the corresponding angle of friction (calculated from that value of stress ratio) would be equal to the critical state angle. Considering that the tests conducted at lower confining pressure (100 kPa and 200 kPa) were carried out on dense samples while loose samples were tested at higher vertical stress (500 kPa), the initial phase of compression of the dense samples was followed by dilation while loose samples showed only a compressive behaviour during shearing. As consequence, the curves plotting the values of stress ratio vs. dy/dx for the dense samples would be expected to intercept the vertical axis twice at the same point while the loose samples would reach the vertical axis only at critical state. What is observed in Figure 8.9 is that, for dense samples, the values of interception of the curves with the y axis at the point of maximum compression are lower than those at critical state. This observation is consistent with experimental data presented by Wood (1991) which explained the phenomenon as due to elastic deformation of the soil particles during the early phase of shearing. The work done by the shear load in causing these elastic deformations is not accounted for in the derivation of Equation 8.1 and therefore that would explain the discrepancy between the two values of interception of the curves with the vertical axis.

The first intercept of the curves with the vertical axis was equal to 0.65 and 0.81 for the 3.35 mm maximum particle size sample, 0.64 and 0.79 for the sample with maximum particle size equal to 2 mm (for values of confining pressure equal to 100 and 200 kPa respectively). These stress ratios correspond to angles of friction equal to 33° and 39° for the sample with maximum particle size equal to 3.35 mm, 33° and 38° for the sample

with maximum particle size equal to 2 mm. Considering the higher points of interception of the curves (Figures 8.9), corresponding to the critical state of the samples, the values obtained are approximately 0.9 and 0.8 for the 3.35 mm and 2 mm maximum particle size samples respectively. These stress ratios correspond to a critical state angle of friction of 42° for the sample with maximum particle size equal to 3.35 mm and 39° for the 2 mm sample. The values are very close to those reported in Table 5.1-5.2 and confirm the validity of the method for identifying the critical state angle of friction. Consistency can also be found with the values of peak angle of friction derived from the maximum stress ratios reached by the curves representing the dense samples which were tested at confining pressure of 100 and 200 kPa. As previously mentioned, the values of stress ratio obtained by considering the first intercept with the vertical axis (at the point of maximum compression of the dense samples) were smaller than the ones obtained at critical state (second interception with the vertical axis). Nonetheless, it is possible to observe from Figure 8.9 that the difference between these two values reduces for higher values of confining pressure (200 kPa).

The same method was used to derive the critical state angle of friction from the tests conducted using the large shear box apparatus. The variation of the stress ratio (τ/σ'_v) was plotted against the values of dy/dx obtained during the three tests.

The first observation from these results (Figure 8.10) is that the curves intercept the vertical axis only once during the test which confirms the fact that larger shear strains would be required for the sample to reach the critical state or that the rotation of the lid affected the results at high levels of shear strain. The only value of stress ratio which could therefore be used to derive the critical state angle of friction (and thus allow a comparison with the small scale test results) is the one obtained from the first intercept of the curves with the y axis (corresponding to the maximum compression of the sample). As observed in the small scale test results, this value is not the same for the three tests and the reason for that can again be attributed to the different amount of elastic deformation of the particles for the three samples during the early stage of shearing. The data shows that, as with the small tests, the intercepts for the higher vertical stress are probably closer to the critical state angle of friction if in the tests shearing could have been continued to that point. On this basis, the values of intercept obtained for test numbers 2 and 3 (being conducted at higher vertical stress levels) should be considered closest to the true critical state angle. The values of intercept results to be fairly evenly

spaced and were defined by drawing for each curve a straight line through the initial portion of the results and seeing where it crossed the vertical axis. These values were equal to 0.8, 0.93 and 1.12 for test number 1, 3 and 2 respectively and correspond to a critical state angle of friction of 39° for test 1, 43° for test 3 and 48° for test 2.

8.5 Comparison of the results with small scale shear tests

Using the method based on the dilatancy theory of soil during shearing it was possible to analyse the results obtained from small and large scale shear box tests and derive the critical state angle of friction of the material tested at different scales.

As discussed above, the results obtained from the small scale shear box tests were plotted in terms of stress ratio (τ/σ'_v) against rate of dilation (dy/dx), Figures 8.9. The curves obtained showed two different values of interception with the vertical axis for the dense samples due to the presence of elastic deformation of the soil particles during the first phase of shearing. The discrepancy is more pronounced for lower levels of confining pressure and it was concluded that the values of the critical state angle derived from considering the stress ratio at the first point of interception of the curves (corresponding to the point of maximum compression of the dense samples) would be more reliable for tests carried out at higher levels of vertical stress.

The same approach was used to derive the critical state angle of the material from the results of the large shear box tests. In this case the intercepts were obtained only at the point of maximum compression of the samples.

The pre-peak values of intercept obtained from large and small scale tests are shown in Table 8.2 and correspond to: 0.65 and 0.81 (under a vertical stress equal to 100 and 200 kPa respectively) for the sample with maximum particle size equal to 3.35 mm; 0.64 and 0.79 (under a vertical stress equal to 100 and 200 kPa respectively) for the sample with maximum particle size equal to 2 mm; 0.8, 0.93 and 1.12 (under a vertical stress equal to 11, 104 and 185 kPa respectively) for the sample with maximum particle size equal to 63 mm.

These values of stress ratio were used to derive the corresponding angles of friction (Table 8.2) which were equal to: 33° and 39° for the 3.35 mm maximum particle size sample; 33° and 38° for the 2 mm maximum particle size sample; 39° , 43° and 48° for the 63 mm maximum particle size sample.

Based on the conclusions derived from the previous section, it was decided to compare only the values of angle of friction obtained from testing the material under higher level of vertical stress (200 kPa for the small scale tests and 185 kPa for the large scale test). This gave as result an angle of friction equal to 38° for the sample with maximum particle size equal to 2 mm, 39° for the sample with maximum particle size equal to 3.35 mm and 48° for the sample with maximum particle size equal to 63 mm.

Nonetheless, the angle of friction obtained from test 3 was also considered for the comparison with the values obtained from the small scale tests conducted under similar confining pressure (100 kPa for the small scale tests and 104 kPa for test 3). The decision was taken on the basis that the stress ratio-dilatancy curve for test 3 showed a better linear trend than the one obtained for test 2 and the confining pressure used for test 3 was higher than the one adopted during test 1. This resulted in an angle of friction equal to 33° for both the samples tested at small scale and 43° for the sample with maximum particle size equal to 63 mm.

From the comparison of these results it is possible to conclude that a scale effect exists when testing the material at different scale so that the increase in particle size determines an increase in the angle of friction of the material. This difference in results is very low when testing samples of the same material with similar particle size (3.35 mm and 2 mm maximum particle size for example) but becomes significant when the scale of the sample is largely increased (in this case a difference of about 10° when using a sample of 63 mm maximum particle size). The results obtained are also consistent with the finding of other authors, for example FHWA (2013) reported a difference in the angle of friction up to 8° when testing aggregate material with relatively large particle size. In this case the tests were conducted using a large scale shear box apparatus of internal size equal to 305 mm square and 203 mm high. The critical state angles of friction were calculated using a different analysis technique than the one used in this research but similarly referring to sample dilation during shearing. The values obtained from this approach ranged between 46° - 54° for samples with maximum particle sizes between 10-38 mm.

8.6 Comparison of the results with small plate loading tests

The results obtained from the three large scale shear box tests were also compared with the ones obtained from the small scale plate bearing tests conducted on the same material by the use of a centrifuge model.

For the small scale plate tests the mobilised angle of friction of the material was back calculated from the values of bearing capacity corresponding to the maximum displacement reached by the plates during the test (in accordance with the conclusions derived from Palmer *et al.* 2003). The values obtained were different for each plate diameter used to test the material since the bearing capacity increases with the diameter of the plate. Nonetheless, it was found that the values of the mobilised angle of friction derived from the bearing capacity of each plate are restricted to a certain range for both the two models (one having maximum particle size equal to 3.35 mm and the other one equal to 2 mm) for plate diameter to maximum particle size ratio larger than 5. In case of tests conducted with a plate diameter to maximum particle size ratio smaller than 5 the results seemed to indicate instability of the plates while penetrating the sample so that it was decided to discard these results. The mobilised angles of friction ranged between 46.1°-44.8° for the sample with maximum particle size equal to 3.35 mm and between 43.8°-42.6° for the sample with maximum particle size equal to 2 mm. It was concluded that a difference of about two degrees derived from testing the material at these two different scales.

As discussed in Chapter 6, the mobilised angles of friction derived from the plate loading tests cannot be considered as equivalent to the critical state angle of the material since the values of bearing capacity used for their calculation corresponded to a small displacement of the plate which was not sufficiently large to be considered as close to the failure of the material. Assuming that for this displacement the level of shear stresses in the sample would be equal to the ones achieved during a pre-peak phase, the derived mobilised angles should have values in between the critical state angle and the peak angle. Considering the values of peak and critical state angles of friction obtained from the small scale tests (Tables 5.1 – 5.2) it was possible to conclude that the results obtained from the plate loading tests were in fact corresponding to mobilised angles of friction with values in between the critical and peak angles.

It was therefore possible to conclude that a scale effect existed even when using the plate loading tests which resulted in an increase of the mobilised angle of friction equal to 2° when increasing the maximum particle size of the sample from 2 mm to 3.35 mm (Figure 6.8). The values obtained were higher than the critical state angle derived from testing the same samples in the standard shear box apparatus but smaller than the peak angles and the reason of that was associated with the fact that the bearing capacity considered for the

calculation of the mobilised angle was derived in correspondence of a small amount of displacement of the plate.

Considering that the mobilised angles of friction derived from the plate loading tests were not equal to the critical state angles, a direct comparison between small plate loading tests and large shear box tests was not possible. Nonetheless, given that the plate loading tests are consistent with the results obtained from the small scale shear tests (i.e. a reduction of the angle of friction of about 2° was found when reducing the maximum particle size of the sample from 3.35 mm to 2 mm) it can be concluded that the same scale effect affected the results obtained.

8.7 Summary

A series of small scale tests (shear box and plate loading tests) were conducted on two samples of crushed limestone whose particle size distribution was recreated in order to represent reduced scales of real platform material. The maximum particle size of the two samples corresponded to 3.35 mm and 2 mm.

From the small shear box tests it was possible to derive the critical and peak angles of friction of the two samples while the results obtained from the plate bearing tests were used to back calculate the angle of friction of the material corresponding to the maximum settlement reached during the tests. The critical and peak angles obtained from the direct shear tests were respectively equal to 41° and 50° for the 3.35 mm maximum particle size sample and equal to 38° and 48° for the 2 mm maximum particle size sample.

Two ranges of values for the back calculated angles of friction (depending on the diameter of the plate) were derived for both the samples and corresponded to 46° - 45° for the 3.35 mm maximum particle size sample and 44° - 43° for the 2 mm maximum particle size sample. The angles obtained from the plate loading tests were higher than the critical state angles but smaller than the peak values derived from the results of the small shear box tests. The reason for this being associated with the small amount of displacement at which the bearing capacity of the plate and corresponding angle of friction were calculated.

Therefore, the results obtained from small scale tests are consistent and identify the presence of a scale effect when testing the material at a different scale. In this specific case a decrease of the angle of friction of about 2 degrees was obtained when reducing the maximum particle size of the sample from 3.35 to 2 mm.

A series of large scale shear box tests were then conducted on three samples of the same limestone material with maximum particle size equal to 63 mm. The particle size distribution used for the large tests represented a full scale version of the samples used for the small scale tests.

The level of shear strain allowed by the large apparatus or the excessive rotation of the top lid during the last phase of the test made impossible to identify the critical state angle of friction directly derived from the test. Another method based on dilatancy theory was used to interpret the results obtained from the large tests. The method was applied to both small scale and large scale shear box tests and allowed the results to be compared. A difference of 10° was found when reducing the maximum particle size of the sample from 63 mm to 3.35 and 2 mm.

9. CONCLUSIONS

9.1 Introduction

A series of small and large scale tests were conducted on crushed limestone in order to identify the effect on the angle of friction of the material derived from testing at different scale and using different test methods. In this chapter the key findings of this research are presented along with concluding remarks concerning the implications of the research on platform design. The conclusions are followed by some discussion on the limitations of the work and recommendations for further research are proposed.

9.2 Experimental procedure

A series of small scale tests (shear box tests using a standard apparatus and plate loading tests conducted on centrifuge models) were carried out on two samples of crushed limestone at two different scales so that the maximum particle size corresponded to 3.35 mm and 2 mm respectively. The results obtained from the small scale tests were compared with those obtained from testing at full scale a sample of the same material with maximum particle size equal to 63 mm.

9.2.1 Small scale shear box tests

Small scale shear box tests were conducted using a standard apparatus and from the test results it was possible to derive the critical and peak angle of friction of two samples of crushed limestone with maximum particle size equal to 3.35 and 2 mm. The particle size distributions of the two samples were obtained by reducing the particle size distribution of the full scale sample of a factor of 30 and 50 respectively by the use of the parallel grading method. The grading curve of the full scale sample was taken as equal to the average particle size distribution of the class material 6F2. After this, the grading curves of the two small samples were slightly modified in accordance to the size of the sieves which were available in the laboratory. The limestone material was sieved and divided in particle sizes which were later combined in the right proportions to create the particle size distributions which were required.

The samples were tested under confining pressure equal to 100, 200 and 500 kPa and a small scale effect was observed which resulted in a measured difference of about 2° for both the critical and peak angles of friction with higher values for the sample with larger particles.

A sample of the same limestone with maximum particle size equal to 3.35 mm was also used to identify the effect of retesting the material. Conclusions derived from this series of tests is that retesting of the same sample would lead to different results than the ones derived from testing fresh samples so this option was excluded for both small and large scale tests.

9.2.2 Plate loading tests using centrifuge models

The plate loading tests were conducted on two centrifuge models of the same samples used for small shear box tests (one having maximum particle size equal to 3.35 mm and the other one equal to 2 mm). The tests were carried out using different plate diameters and the bearing capacity of each plate was derived. From the values of bearing stress obtained at the end of each test it was possible to back calculate the mobilised angle of friction of the material. The values obtained were restricted to a certain range for plate diameter to maximum particle size ratios larger than 5 for both the two models. A difference of about 2° was again found between the two ranges of values associated with the two models so that it was concluded that consistency in the scale effect due to the particle size exists even when adopting a different test method.

A plate loading test was also conducted on a layer of crushed limestone (maximum particle size equal to 2 mm) overlaying soft clay. The test was carried out using two different plate diameters and demonstrated the validity of the design method proposed by Lees (2019). The results showed good agreement with the theory presented by Lees (2019) and confirmed the validity of this method.

9.2.3 The large shear box apparatus

In order to identify the difference in angle of friction of the material when testing at large and small scale (using a standard apparatus) a large shear box apparatus (1.5 m square in plan and 1 m high) was designed and manufactured in order to test the same limestone at full scale (so that the particle size of the sample tested would be representative of real working platform material) and compare the results with the ones obtained from the small scale tests. The design characteristics of the large apparatus were defined based on the results obtained from the small scale tests and examples of large apparatus from literature.

9.2.4 Large scale shear box tests

Three full scale tests were carried out using the large shear box apparatus. The tests were conducted on samples prepared by pouring the material from above the top of the shear box so that loose samples of similar density were obtained. The material was tested under a confining pressures of 11, 104, 185 kPa.

The results obtained from the first test (confining pressure equal to 11 kPa) identified a large rotation of the top lid during shearing which was associated with the absence of a vertical load on top of the sample. This rotation resulted in a loss of contact between the lid and the soil over a small area and some interpretation of the vertical movement data was required to obtain volumetric strains. A significant amount of dilation was observed in the sample, after an initial small amount of compression, which continued to increase until the end of the test.

The second test was conducted under higher value of confining pressure which limited the dilation of the sample (an overall compressive behaviour was obtained). Nonetheless, an error in the calibration of the hydraulic system resulted in the load applied being higher than expected so that the confining pressure was equal to 185 kPa. Post-test analysis of the system showed that the vertical force applied by the jack took some time to stabilise and there was likely to have been some small fluctuations in the force whilst the test was carried out.

A third test (confining pressure equal to 104 kPa) was conducted using the correct calibration of the hydraulic system and the vertical load applied on top of the sample was sufficiently large to limit the rotation of the lid. Based on this, the results obtained from the third test were considered as more reliable than the other ones.

For all the three tests the results obtained showed a constant increase in shear stress with shearing without the curves reaching a constant value and the same phenomenon was observed for the curves showing the volumetric strain so that no critical state could be identified. The possible reasons for this was the limited amount of shear strain allowed by the large apparatus or the large rotation of the top lid at high levels of shear strain. In order to compare the results with the ones obtained from small scale tests an alternative method based on the dilatancy theory was adopted. The use of this method identified a critical angle of friction corresponding to 39°, 43° and 48° for the tests conducted under a confining pressure of 11, 104 and 185 kPa respectively. A value of 43° was taken as

critical state angle of friction of the full scale sample considering that the test from which this value was calculated was not affected by a large rotation of the top lid or errors in the calibration of the vertical hydraulic jack (both factors which might have affected the results of the other full scale tests).

9.3 Conclusions and implications for working platform design

From the series of shear box tests conducted using a standard (small) apparatus it was possible to obtain consistent values of the angle of friction of the material for both of the scaled samples. The critical state angles obtained corresponded to 41° for the 3.35 mm maximum particle size sample and 38° for the sample with maximum particle size equal to 2 mm. The difference in the two values indicates the presence of a scale effect (also reported in the literature) when changing the size of the sample. In this case, this would equate to an increase in the angle of friction of 2° when increasing the maximum particle size.

The values of angle of friction which were back calculated from the plate bearing capacity tests performed on the centrifuge can be divided into two ranges of values depending on the maximum particle size of the material tested (this despite the fact that the models were aiming to represent the same prototype particle size). The angles of friction ranged between 46° - 45° for the sample with maximum particle size equal to 3.35 mm and between 44° - 43° for the sample with maximum particle size equal to 2 mm. Again, a difference of 2° was found between the two different maximum particle size of the tested material. In both cases the values obtained were larger than the critical state angles measured in the small shear box tests but smaller than the peak values (50° and 48° for the larger and smaller sample respectively). The reason for this is associated with the level of displacement and hence, the shear strain applied to the material, at which the bearing capacity of the plate and corresponding angle of friction were calculated. The implication of this result for safe platform design is that angles of friction above critical could be routinely adopted.

The results obtained from the large shear box tests conducted on samples with maximum particle size equal to 63 mm which were interpreted using the method based on the stress-dilatancy theory gave a critical state angle of friction equal to 43° . It was therefore concluded that reducing the scale of the tested material produces a reduction in the measured angle of friction. The values of friction angles given in piling platform guidance

are consistent with the ones obtained from the small scale tests on scaled down material. They are likely to be low compared with the real situation (i.e. when using large particle size material) and that would lead to inefficient design. Based upon the results obtained during this research it is possible to conclude that the values of the angle of friction used in current design guidance are maybe conservative as derived from standard shear box tests. Adoption of higher angles of friction (which seem to be more appropriate considering the conclusions derived from this study) would lead to a reduced platform thickness or a design that would normally require a geotextile being possible to construct without.

9.4 Limitations of the current work and recommendations for further research

The work conducted within this study developed a method for testing large particle size material which, besides working platforms, is widely used in many other engineering applications. The research aimed to determine the angle of friction of crushed limestone material tested at different scales using different testing methods and compare the results. The results obtained clearly showed the presence of a scale effect affecting the derived angle of friction when the material is tested at smaller scale and this would lead to inefficient design.

The tests conducted using the large shear box experienced a problem with the apparatus associated with the top lid. Rotation of the lid occurred during all the tests especially during the test conducted without any vertical load applied. As a result, the measurements of the vertical displacement of the sample (which was obtained from the four vertical displacement transducers on top of the lid) were likely affected by the rotation of the lid and this led to unreliable results towards the end of the test where the amount of rotation became considerable. It was calculated that in the three tests the maximum tilt angles reached by the top lid were equal to 4.2° , 2.4° and 1.8° for tests number 1, 3 and 2 respectively, with higher values of the angle for lower levels of confining pressure. In order to avoid this phenomenon, it is suggested that a fixed top platen should be provided by creating a rigid connection between the vertical hydraulic jack and the lid so that no rotation would be allowed during shearing. Another method which could be used to avoid this rotation is presented by Bradfield *et al.* (2015). The authors conducted a series of shear box tests on mine spoil using a 750 mm^2 shear box and investigated on the tilt of the lid during shearing. In this case the use of three jacks applying the vertical load on the top cap of the lid limited the tilting angle to less than 2° .

The large shear box tests presented in this thesis considered one sample preparation method and hence one value of voids ratio. Different methods of preparing the sample should be investigated which would allow a denser sample to be tested. This could be achieved (as in the small shear box tests) by compacting several layers of the material until complete filling of the box is achieved. All tests presented here were carried out on dry samples and the influence of moisture (as might be expected in a real working platform) should also be examined.

The tests described in this research were conducted on fresh crushed limestone however any material with maximum particle size up to 100 mm could be tested using the large apparatus avoiding the presence of scale effects on the results. Working platforms are generally constructed from material of different composition and particle size including construction demolition waste (CDW). Further tests should be conducted using real platform material in order to verify the observed effect of testing at different scales. CDW is generally characterised by the prevalence of crushed concrete and brick components which are likely to have a lower intrinsic strength than limestone. In this case the material probably would be affected by crushing during shearing, the effect of which was ignored for the limestone used for this study. Crushing of the particles will change the particle size distribution which will have an effect on the performance and measured properties of the material. Comparison of small and large scale tests for this type of material could provide more clarity about the scale effects affecting the angle of friction and determine what measures to take in order to define an appropriate value for the design.

APPENDIX A

EXAMPLE OF DESIGN CALCULATIONS FOR WORKING PLATFORM ON FIRM CLAY SUBGRADE (BRE, 2004)

Introduction:

This example of calculation from BRE Report 470 takes under consideration the case of a working platform placed on a fine grained subgrade. This example was considered as more representative since most of London ground material is made of clay.

The bearing resistance R of a fine grained subgrade when a load is applied at the surface is:

$$R_s = s_u N_c s_c$$

Where:

s_u = undrained shear strength of the fine subgrade (kN/m²)

N_c = bearing capacity factor for a fine grained subgrade ($N_c = 2 + \pi$, i.e. the conventional value of bearing capacity factor for undrained loading)

s_c = shape factor (when the load is applied at ground surface over a rectangular area of dimensions W and L , $s_c = 1 + 0.2(W/L)$)

The bearing resistance R of a coarse grained subgrade when a load is applied at the surface is:

$$R_s = 0.5 \gamma'_s W N_{\gamma s} s_{\gamma}$$

Where:

γ'_s = effective unit weight of the subgrade (kN/m³)

W = track width of the plant (m)

$N_{\gamma s}$ = bearing capacity factor for a coarse grained subgrade (which is a function of the design value of the angle of shearing resistance of the subgrade ϕ' : $N_{\gamma s} = 2 \tan \phi' (1 + e^{\pi \tan \phi'} \tan^2(45 + (\phi'/2)))$)

s_γ = shape factor (when the load is applied at ground surface over a rectangular area of dimensions W and L , $s_\gamma = 1 - 0.3(W/L)$)

In a typical situation where a working platform of relatively shallow thickness is placed on a weak subgrade, a simple approach to the design calculations can be based on the analysis of punching failure. In this analysis the bearing resistance (R_{tot}) is considered to be the sum of the shear required to punch through a vertical plane in the coarse grained platform material and the bearing capacity of the subgrade. Using the simplified analysis developed by Meyerhof and his co-workers for a shallow foundation punching through dense sand layer overlying soft clay, the following expression is obtained for the bearing resistance of a platform on a fine grained subgrade:

$$R_{tot} = s_u N_c s_c + (\gamma_p D^2 / W) K_p \tan \delta s_p$$

Where:

γ_p = bulk unit weight of the platform material (kN/m^3)

D = thickness of the platform material (m)

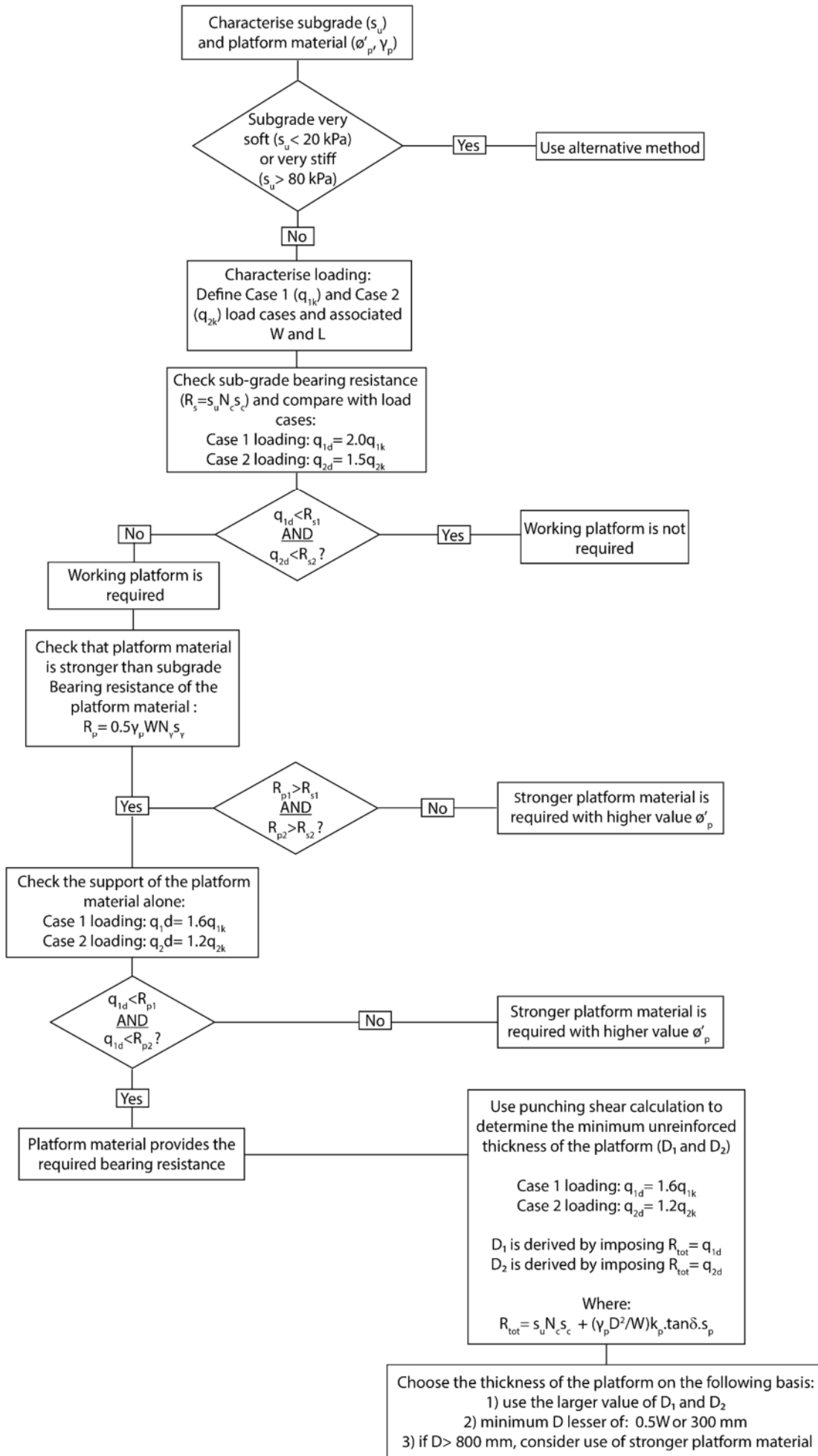
$K_p \tan \delta$ = punching shearing resistance coefficient (values of K_p taken from BS EN 1997-1 (2004), Figure C.2.1 and δ as a function of the design value of the angle of shearing resistance of the dense sand (ϕ'): $\delta = 2/3 \phi'$, as suggested by Meyerhof (1974))

s_p = shape factor which can be derived from the geometry of the volume of soil undergoing punching shear ($s_p = 1 + (W/L)$)

In order to define the loading conditions of the platform, the calculation of the applied plant track load should be done using the weight and centres of gravity of the various components of the particular item of plant, along with the most critical orientation of the body of the rig or crane with respect to the orientation of the tracks. This will produce loading which varies with either a triangular or trapezoidal distribution over the length of

the track that is in contact with the ground. For use in this design process, the triangular or trapezoidal loading is converted to an equivalent rectangular loading using the method of Meyerhof (1953) described in Section 2.2.3.

In the design process, two loading conditions are considered, which are termed case 1 (applied when the operator is unlikely to be able to aid recovery from an imminent platform failure. Operations could include: standing, travelling, handling) and case 2 loading (applied when the operator can recover from an impending collapse by interrupting the driving or extracting activity thus reducing the load to an acceptable level. Operations could include: installing casing, drilling, extracting an auger, extracting casing, rig travelling or slewing with a fixed mast which has a foot or fixed load). The most adverse situation should be used for design purpose for each of the two loading conditions in order to define the characteristic values for case 1 loading q_{1k} and case 2 loading q_{2k} .



Calculation example:

Initial data:

1) Design values for ground properties:

It is proposed that the values of factors for ground properties should be unity, therefore the design value of a ground parameter is the same as the characteristic value.

- Subgrade: $s_{ud} = s_{uk} = 48 \text{ kPa}$
- Working platform: $\phi'_{pd} = \phi'_{pk} = 35^\circ$ $\gamma_{pd} = \gamma_{pk} = 20 \text{ kN/m}^3$

2) Design values for track width and effective length:

It is recommended that the values of the factors for the track dimensions should be unity, so that:

- $W_d = W_k = 0.7 \text{ m}$
- $L_{1d} = L_{1k} = 3.6 \text{ m}$
- $L_{2d} = L_{2k} = 3.1 \text{ m}$

3) Characteristic values of load:

- Case 1 loading: $q_{1k} = 190 \text{ kPa}$
- Case 2 loading: $q_{2k} = 280 \text{ kPa}$

4) Bearing capacity factors and shape factors:

- $N_c = 2 + \pi = 5.14$
- $N_{\gamma p} = 2 \tan \phi' (1 + e^{\pi \tan \phi'} \tan^2(45 + (\phi'/2))) = 48$
- Case 1 loading: $s_{c1} = 1 + 0.2[W/L] = 1.04$

$$s_{\gamma 1} = 1 - 0.3[W/L] = 0.94$$

$$s_{p1} = 1 + [W/L] = 1.19$$

- Case 2 loading: $s_{c2} = 1 + 0.2[W/L] = 1.05$
 $s_{\gamma2} = 1 - 0.3[W/L] = 0.93$
 $s_{p2} = 1 + [W/L] = 1.23$

5) Punching shear resistance coefficient: $K_p \tan \delta = 3.1$

Calculation:

1) Check that subgrade cannot provide required bearing resistance without a working platform (i.e. the bearing resistance without a working platform is smaller than the bearing resistance that is required to support the plant):

Bearing resistance without working platform: $R_{sd} = s_{ud} N_c s_c$

- $R_{sd1} = s_{ud} N_c s_{c1} = 48 \times 5.14 \times 1.04 = 256 \text{ kPa}$
- $R_{sd2} = s_{ud} N_c s_{c2} = 48 \times 5.14 \times 1.05 = 258 \text{ kPa}$

The design values for loading are calculated by applying a factor to the corresponding characteristic value:

- Case 1 loading: $q_{1d} = 2.0q_{1k} = 2 \times 190 = 380 \text{ kPa}$
- Case 2 loading: $q_{2d} = 1.5q_{2k} = 1.5 \times 280 = 420 \text{ kPa}$

Now: $q_{1d} > R_{sd1}$ and $q_{2d} > R_{sd2}$

therefore, a working platform is required for plant support.

2) Check that platform material is stronger than subgrade:

Bearing resistance of platform material: $R_{pd} = 0.5 \gamma_{pd} W_d N_{\gamma p} s_{\gamma}$

- $R_{pd1} = 0.5 \gamma_{pd} W_d N_{\gamma p} s_{\gamma1} = 0.5 \times 20 \times 0.7 \times 48 \times 0.94 = 317 \text{ kPa}$
- $R_{pd2} = 0.5 \gamma_{pd} W_d N_{\gamma p} s_{\gamma2} = 0.5 \times 20 \times 0.7 \times 48 \times 0.93 = 313 \text{ kPa}$

Bearing resistance of subgrade: $R_{sd} = s_{ud} N_c s_c$

- $R_{sd1} = s_{ud} N_c s_{c1} = 48 \times 5.14 \times 1.04 = 256 \text{ kPa}$ (as previously calculated)

- $R_{sd2} = s_{ud} N_c s_{c2} = 48 \times 5.14 \times 1.05 = 258 \text{ kPa}$ (as previously calculated)

Now: $R_{pd1} > R_{sd1}$ and $R_{pd2} > R_{sd2}$
 therefore, platform material is stronger than subgrade.

3) Check support of platform material alone:

The proposed platform material should provide the required bearing resistance when placed at a thickness sufficient to ensure that the subgrade does not materially affect bearing capacity.

Bearing resistance of platform material:

- $R_{pd1} = 317 \text{ kPa}$ (as previously calculated)
- $R_{pd2} = 313 \text{ kPa}$ (as previously calculated)

The design values for loading are calculated by applying a factor to the corresponding characteristic value:

- Case 1 loading: $q_{1d} = 1.6q_{1k} = 1.6 \times 190 = 304 \text{ kPa}$
- Case 2 loading: $q_{2d} = 1.2q_{2k} = 1.2 \times 280 = 336 \text{ kPa}$

Now: $q_{1d} < R_{pd1}$ but $q_{2d} > R_{pd2}$
 therefore, the chosen platform material cannot provide the required bearing resistance however thick it is made.

4) If the previous check is not satisfied a stronger material is required:

A better quality platform material should be used: $\phi'_{pd} = 40^\circ$

Therefore:

- $N_{\gamma p} = 109$
- $K_p \tan \delta = 5.5$

For this better quality material the bearing resistance is equal to:

- $R_{pd1} = 0.5 \gamma_p W_d N_{\gamma p} s_{\gamma 1} = 0.5 \times 20 \times 0.7 \times 109 \times 0.94 = 721 \text{ kPa}$
- $R_{pd2} = 0.5 \gamma_p W_d N_{\gamma p} s_{\gamma 2} = 0.5 \times 20 \times 0.7 \times 109 \times 0.94 = 714 \text{ kPa}$

Now: $q_{1d} < R_{pd1}$ and $q_{2d} < R_{pd2}$

therefore, this material can provide the required bearing resistance.

5) Calculate required thickness of platform for the two loading conditions, based on punching failure through the platform material:

- Case 1 loading (imposing $R_d = q_{1d} = 1.6q_{1k}$):
 - $D_1 = \{W_d [q_{1d} - s_{ud} N_c s_{c1}] / [\gamma_p K_p \tan \delta s_{p1}]\} 0.5$
 - $D_1 = \{0.7 [(1.6 \times 190) - 257] / [20 \times 5.5 \times 1.19]\} 0.5 = 0.50 \text{ m}$
- Case 2 loading (imposing $R_d = q_{2d} = 1.2q_{2k}$):
 - $D_2 = \{W_d [q_{2d} - s_{ud} N_c s_{c2}] / [\gamma_p K_p \tan \delta s_{p2}]\} 0.5$
 - $D_2 = \{0.7 [(1.2 \times 280) - 259] / [20 \times 5.5 \times 1.23]\} 0.5 = 0.64 \text{ m}$

6) Determine the thickness of the platform on the following bases:

- Use the larger value of D_1 and D_2 for design purposes
- Minimum thickness should be the lesser of $0.5W_d$ or 300 mm
- When the calculations indicate that a platform of considerable thickness is required ($D > 800 \text{ mm}$), consider the use of a stronger platform material or structural geosynthetic reinforcement

Therefore $D = 0.64 \text{ m}$ is required.

List of symbols used in Appendix A:

s_{ud} = design value of undrained shear strength of fine grained subgrade

s_{uk} = characteristic value of undrained shear strength of fine grained subgrade

D = thickness of platform material

D_1 = thickness of platform material required for case 1 loading conditions

D_2 = thickness of platform material required for case 2 loading conditions

δ = taken as $2/3\phi'$ in calculation of punching shear resistance coefficient

ϕ' = angle of shearing resistance of coarse grained material

ϕ'_{pd} = design angle of shearing resistance of platform material

ϕ'_{pk} = characteristic angle of shearing resistance of platform material

γ_p = bulk unit weight of platform material

γ_{pd} = design bulk unit weight of platform material

γ_{pk} = characteristic bulk unit weight of platform material

γ'_s = effective unit weight of subgrade

K_p = horizontal component of passive earth pressure coefficient

L = effective track length of plant

L_{1d} = design effective track length of plant under case 1 loading

L_{1k} = characteristic effective track length of plant under case 1 loading

L_{2d} = design effective track length of plant under case 1 loading

L_{2k} = characteristic effective track length of plant under case 1 loading

N_c = bearing capacity factor for fine grained subgrade

$N_{\gamma p}$ = bearing capacity factor for platform material

$N_{\gamma s}$ = bearing capacity factor for coarse grained subgrade

q_{1d} = design value for case 1 loading

q_{2d} = design value for case 2 loading

q_{1k} = characteristic value for case 1 loading

q_{2k} = characteristic value for case 2 loading

s_c = shape factor associated with bearing capacity factor for fine grained subgrade

s_{c1} = shape factor associated with bearing capacity factor for fine grained subgrade under case 1 loading

s_{c2} = shape factor associated with bearing capacity factor for fine grained subgrade under case 2 loading

s_{γ} = shape factor associated with bearing capacity factor for the platform material or a coarse grained subgrade

$s_{\gamma 1}$ = shape factor associated with bearing capacity factor for the platform material or a coarse grained subgrade under case 1 loading

$s_{\gamma 2}$ = shape factor associated with bearing capacity factor for the platform material or a coarse grained subgrade under case 2 loading

s_p = shape factor associated with punching shear resistance coefficient

s_{p1} = shape factor associated with punching shear resistance coefficient under case 1 loading

s_{p2} = shape factor associated with punching shear resistance coefficient under case 2 loading

R_{pd} = design bearing resistance of the platform material

R_{pd1} = design bearing resistance of the platform material under case 1 loading

R_{pd2} = design bearing resistance of the platform material under case 2 loading

R_s = bearing resistance of the subgrade

R_{sd} = design bearing resistance of the subgrade

R_{sd1} = design bearing resistance of the subgrade under case 1 loading

R_{sd2} = design bearing resistance of the subgrade under case 2 loading

R_{tot} = bearing resistance of a platform on a fine grained subgrade

W = track width of plant

W_d = design track width of plant

W_k = characteristic track width of plant

APPENDIX B

ESTIMATION OF THE FRICTION FORCES ACTING ON THE SLIDING SURFACES OF THE LARGE SHEAR BOX APPARATUS.

Introduction:

These simple calculations aim to demonstrate the benefits obtained from the use of acetal sheets on the sliding surfaces of the shear box apparatus. The reason for this concern derives from the attempt to reduce the friction of steel against steel and therefore the force needed to shear the sample during the test. The same kind of calculation was applied twice: firstly to estimate the friction forces acting on contact surface of the two box halves and secondly at the contact between the bottom of the box and the three beams which sustain the entire apparatus.

Initial data:

- Shear plane (m^2) = 2.25
- Shear box internal height (m) = 1
- Unit weight of the tested sample (kN/m^3) = 18
- Assumed angle of friction of the sample tested ($^\circ$) = 45

Calculation:

- 1) Calculation of the horizontal force necessary to shear the sample (T) at different levels of vertical stress (σ'_v):

σ'_v (kPa)	assumed τ (kPa)	T (kN)
18	18	40.5
36	36	81.0
54	54	121.5
90	90	202.5

180	180	405.0
-----	-----	-------

2) Calculation of the vertical force (F_{n1}) acting on the sliding surface between the two halves of the box:

- Mass of the top half (kg) = 2800
- Corresponding force F_{n1} (kN) = $(2800/1000)*10 = 28$

3) Calculation of the vertical force (F_{n2}) acting on the bottom surface of the shear box:

- Mass of the top half (kg) = 2800
- Mass of the bottom half (kg) = 3200
- Mass of the soil tested (kg) = $2.25*1*(18/1000*10) = 4050$
- Mass of the top lid (kg) = 991
- Corresponding force F_{n2} (kN) = $((2800 + 3200 + 4050 + 991)/1000)*10 = 110$

4) Determination of the frictional forces acting at the sliding surface between the two halves of the box (F_{f1}) and at the bottom surface of the shear box (F_{f2}):

Interface type	Friction coefficient (μ)	$F_{f1} = F_{n1} * \mu$ (kN)	$F_{f2} = F_{n2} * \mu$ (kN)
steel/steel	0.5	14	55
steel/acetal	0.04	1.12	4.4
acetal/acetal	0.04	1.12	4.4

5) Frictional force acting at the sliding surface between the two halves of the box to shearing force ratio (F_{f1}/T):

T (kN)	F_{f1}/T (%) steel/steel interface	F_{f1}/T (%) steel/acetal
40.5	35	2.8
81.0	17	1.4
121.5	12	0.9
202.5	7	0.6

405.0	3	0.3
-------	---	-----

6) Friction force acting on the sliding surface between the two halves of the box to horizontal force ratio (F_{f2}/T):

T (kN)	F_{f2}/T (%) with steel	F_{f2}/T (%) with acetal
40.5	135	10.9
81.0	68	5.4
121.5	45	3.6
202.5	27	2.2
405.0	14	1.1

APPENDIX C

ESTIMATION OF THE FRICTION FORCES ACTING ON THE INTERNAL SIDES OF A SHEAR BOX APPARATUS.

Introduction:

The aim of these calculations is to estimate the value of frictional force which would be generated between the soil sample and the internal surfaces of the top half of a shear box when the sample is subjected to a vertical confining pressure. This force would cause a reduction of the normal load applied to the sample through the top lid when the contact between the two halves of the box is maintained during the test. An estimate of this force for the large shear box apparatus used in this study is here presented.

Initial data:

- Assumed angle of friction of limestone (ϕ') = 44° (BS 8004 (2015))
- Assumed coefficient of friction between steel material and limestone (μ) = $\tan(25^\circ) = 0.47$ (Ziogos *et al.*, 2021)
- Assumed confining pressure (σ_n') = 100 kPa
- Internal height of the top half of the large shear box (h) = 0.45 m
- Internal width/length of the large box (w) = 1.5 m

Calculation:

- 1) Calculation of the lateral earth pressure coefficient at rest (K_0) and lateral pressure (σ_h'):
$$K_0 = 1 - \sin(\phi') = 1 - \sin(44) = 0.31$$
$$\sigma_h' = K_0 * \sigma_n' = 31 \text{ kPa}$$
- 2) Calculation of the frictional stress (τ) developed on the internal surface of the top half of the box:

$$\tau = \mu * \sigma_h' = 0.47 * 31 = 14.5 \text{ kPa}$$

- 3) Calculation of the frictional force (F_f) reducing the vertical load applied to the sample through the top plate (when contact is maintained between the two halves of the box):

$$F_f = \tau * 4 * h * w = 14.5 * 4 * 0.45 * 1.5 = 39 \text{ kN}$$

- 4) Calculation of the vertical load applied to the sample through the top plate (F_v):

$$F_v = \sigma_n' * w * w = 100 * 1.5 * 1.5 = 225 \text{ kN}$$

- 5) Calculation of the vertical force (F_v) lost in friction:

$$\% \text{ lost in friction} = F_f / F_v * 100 = 39 / 225 * 100 = 17\%$$

REFERENCES

- Airey, D. W. (1987). Some observations on the interpretation of shear box test results. Technical report CUED/D-SOILS/TR 196, University of Cambridge.
- Arthur, J. R. F. and Menzies, B. K. (1972). Inherent anisotropy in a sand. *Geotechnique*, Vol. 22, No. 1, pp 115-128.
- Assadi, A. (1975). Rupture layers in granular materials. PhD thesis, University of London.
- ASTM D1194 (1994). Standard Test Method for Bearing Capacity of Soil for Static Load and Spread Footings. ASTM International. West Conshohocken, PA, USA.
- ASTM D3080/D3080M (2011). Standard Test Method for Direct Shear Test of Soils Under Consolidated Drained Conditions. ASTM International. West Conshohocken, PA, USA.
- ASTM D4253 (2016). Standard Test Methods for Maximum Index Density and Unit Weight of Soils Using a Vibratory Table. ASTM International. West Conshohocken, PA, USA.
- ASTM D4254 (2016). Standard Test Methods for Minimum Index Density and Unit Weight of Soils and Calculation of Relative Density. ASTM International. West Conshohocken, PA, USA.
- Atkinson, J. (2007). *The Mechanics of Soils and Foundations* (2nd edition). Taylor and Francis, London.
- Bagherzadeh-Khalkhali, A., Mirghasemi, A. A. (2009). Numerical and experimental direct shear tests for coarse grained soil. *Particuology* 7(1):83-91.
- Bareither, C. A., Benson, C. H., Edil, T. B. (2008). Comparison of shear strength of sand backfills measured in small-scale and large-scale direct shear tests. *Canadian Geotechnical Journal* 45: 1224-1236.
- Barr, B. I. G., Davies, M. C. R., Jacobs, C. D (1991). A large direct shear box - some initial results of tests on soil nails. *Ground Engineering*.

Bishop, A. W. (1948). A large shear box for testing sands and gravels. Proceedings of the 2nd International Conference on Soil Mechanics and Foundation Engineering, Rotterdam, the Netherlands, 21–30, 207–211.

Bolton, M. D. (1991). A Guide to Soil Mechanics. Cambridge: M.D and K. Bolton.

Bond, A., Harris, A. (2008). Decoding eurocode 7. CRC Press LLC, 1st edition.

Bradfield, L. R., Fytius, S. G., Simmons, J. V. (2015). Large scale testing of mine spoil. Proceedings of 12th Australia New Zealand Conference on Geomechanics, Wellington, New Zealand.

BS 1377-2 (1990). British Standard Methods of Test for Soils for Civil Engineering Purposes: Part 2. Classification Tests, BS 1377. British Standards Institution, London.

BS 1377-7 (1990). British Standard Methods of Test for Soils for Civil Engineering Purposes: Part 7. Soils for civil engineering purposes, BS 1377. British Standards Institution, London.

BS 1377-9 (1990). British Standard Methods of Test for Soils for Civil Engineering Purposes: Part 9. *In Situ* Tests, BS 1377. British Standards Institution, London.

BS 8004-2 (2015). Code of practice for foundation: Part 2. Design for foundations. British Standards Institution, London.

BS EN 1997-1 (2004). British Standard Eurocode 7: Geotechnical design: Part 1. General rules, BS EN 1997. British Standards Institution, London.

BS EN 1997-2 (2004). British Standard Eurocode 7: Geotechnical design: Part 2. Ground investigation and testing, BS EN 1997. British Standards Institution, London.

Budhu, M. (2010). Soil mechanics and foundations. John Wiley & Sons, 3rd edition.

Burd, H. J., Frydman, S. (1997). Bearing capacity of plane-strain footings on layered soils. Canadian Geotechnical Journal. 34: 241-253.

Cerato, A. B., Lutenecker, A. J. (2006). Specimen Size and Scale Effects of Direct Shear Box Tests of Sands. Geotechnical Testing Journal, Vol. 29, No. 6.

Coduto, D. P. (2000). Foundation Design: Principles and Practice. Prentice Hall; 2nd edition.

Colreavy, C., O'Loughlin, C. D., Randolph, M. F. (2016). Estimating consolidation parameters from field piezoball tests. *Géotechnique*, 66(4), 333-343.

Corke, D., Gannon, J. (2010). Economic design of working platforms for tracked plant. Technical note. *Ground Engineering*.

Cui, L., O'Sullivan, C. (2006). Exploring the macro and micro scale response of an idealised granular material in the direct shear apparatus. *Geotechnique*, 56(7): 455-468.

Das, M. J. (2010). *Principles of foundation engineering*. Stamford, CT: Cengage Learning. 7th edition.

Davis, E. H., and Booker, J. R. (1971). The bearing capacity of strip footings from the standpoint of plasticity theory. *Proc. First Australia– New Zealand Conference on Geomechanics*, Vol. 1, 276–282.

Davies, M. C. R., Le Masurier, J. W (1997). Soil/Nail Interaction Mechanisms from Large Direct Shear Tests. *Ground improvement geosystems* *Densification and reinforcement*, pp 492-499. January 1997.

Day, R. W. (2010). *Foundation engineering handbook: design and construction with the 2009 international building code*. Chapter 6. The McGraw-Hill Companies. 2nd edition.

Dyer, M. R. (1985). Observation of the stress distribution in crushed glass with applications to soil reinforcement. DPhil thesis, University of Oxford.

Estaire, J., Olalla, C. (2005). Analysis of shear strength of armourstone based on 1 m³ direct shear test. *VII coastal Engineering 2005*, pp 341-350. April 2005.

FHWA (Federal Highway Administration) (2013). *Friction Angles of Open-graded aggregates from large-scale direct shear testing*.

Finnie, I. M. S, Randolph, M. F. (1994). Punch-through and liquefaction induced failure of shallow foundations on calcareous sediments. *Proceedings of the International Conference on Behavior of Offshore Structures, BOSS '94*, Boston, USA, 217-230.

Fluet, J. E. (1988). *Geosynthetics for soil improvement: a general report and keynote address*. *Proceedings of the Symposium on Geosynthetics for Soil Improvement*. Tennessee, USA, pp. 1–21.

Fu, X., Zheng, X., Lei, X., Deng, J. (2015). Using a modified direct shear apparatus to explore gap and size effects on shear resistance of coarse grained soil. *Particuology* 23, 82–89.

Garnier, J., Gaudin, C., Springman, S. M., Culligan, P.J., Goodings, D., Konig, D., Kutter, B., Phillips, R., Randolph, M. F. and Thorel, L. (2015). Catalogue of scaling laws and similitude questions in geotechnical centrifuge modelling. *International Journal of Physical Modelling in Geotechnics*. Volume 7, Issue 3, pp. 01-23.

Giroud, J. P., Ah-Line, A., Bonaparte, R. (1984). Design of unpaved roads and trafficked areas with geogrids. *Proceedings of the symposium on polymer grid reinforcement*, London, pp. 116-127.

Gorasia, R. J. (2013). Behaviour of ribbed piles in clay. PhD thesis, City, University of London.

Halai, H. (2018). Compensation grouting to control deep excavation ground movements. PhD thesis, City, University of London.

Hamidi, A., Azini, E., Masoudi, B. (2012). Impact of gradation on the shear strength dilation behaviour of well graded sand-gravel mixtures. *Scientia Iranica A*, 19 (3), 393–402.

Hanna, A. M., (1981). Foundations on strong sand overlying weak sand. *Journal of the Geotechnical Engineering Division*, 107(7):915-927.

Hanna, A. M., Meyerhof, G. G. (1980). Design charts for ultimate bearing capacity of foundations on sand overlying soft clay. *Canadian Geotechnical Journal*, Vol. 17, No 2, pp 300-303.

Highways Agency (2004). *Manual of Contract Documents for Highway Works – Volume 1 Specification 6 for Highway Works*. The Stationary Office, London.

Jacobs, C. D. (1993). An investigation of soil nail reinforcement using a large direct shear box. PhD thesis, University of Wales, College of Cardiff.

Jain, S. P., Gupta, R. C. (1975). Large shear box for tests on river bed material. *Indian Geotechnical Society*.

Jewell, R. A. (1980). Some effects of reinforcement on the mechanical behaviour of soils. PhD thesis, University of Cambridge. Jewell, R. A. and Wroth.

Jewell, R.A. (1996). Soil Reinforcement with Geotextiles. Construction Industry Research and Information Association, London, CIRIA, Special Publication 123. Jewell and Wroth (1987).

Kim, D., Ha, S. (2014). Effects of Particle Size on the Shear Behaviour of Coarse Grained Soils Reinforced with Geogrid. *Materials* 2014, 7(2), 963-979.

Kim, B., Shibuya, S., Park, S., Kato, S. (2012). Effect of Opening on the Shear Behaviour of Granular Materials in Direct Shear Test. *KSCE Journal of Civil Engineering* 16(7):1132-1142.

Koerner, R. M. (2005). *Designing with Geosynthetics*. Fifth Edition, Prentice Hall, New Jersey, USA.

Krahn, T., Blatz, J., Alfaro, M., Bathurst, R. J. (2007). Large-scale interface shear testing of sandbag dyke materials. *Geosynthetics International*, 14, No. 2, 119–126.

Kumar, J., Chakraborty, M. (2015) Bearing capacity of a circular foundation on layered sand-clay media, *Soils and Foundations* 55(5): pp 1058–1068.

Lawson, N., Douglas, I., Garvin, S., McGrath, C., Manning, D., Vetterlein, J. (2001). Recycling construction and demolition wastes- a UK perspective. *Environmental Management and Health*, 12, 2/3, 146-157.

Lees, A. S. (2019). The bearing capacity of a granular layer on clay. *Proceedings of the Institution of Civil Engineering – Geotechnical engineering* 173(1): pp. 13-20.

Lee, K., K., Cassidy, M. J., Randolph, M. F. (2013). Bearing capacity on sand overlying clay soils: experimental and finite-element investigation of potential punch-through failure. *Géotechnique* 63(15): pp 1271–1284.

Linden, T., Dettenborn, T., Klläinen, A., Forsman, J., Kolisoja, P. (2019). Utilization of crushed concrete aggregate in light rail construction. *Proceedings of the XVII European Conference on Soil Mechanics and Geotechnical Engineering*.

Liu, S. H: (2006). Simulating a direct shear box test by DEM. *Canadian Geotechnical Journal*, 43(2): 155-168.

Marsal, R., J. (1973). Mechanical properties of rockfill, embankment dam engineering. Casagrande Volume, Wiley, New York. USA

Meyerhof, G., G. (1953). The bearing capacity of foundations under eccentric and inclined loads. Proceedings of 3rd International conference on soil Mechanics and foundation Engineering, Zurich, Vol 1, pp 440-445.

Meyerhof, G., G. (1963). Some Recent Research on the Bearing Capacity of Foundations. Canadian Geotechnical Journal, 1, 16-26.

Meyerhof, G., G. (1974). Ultimate bearing capacity of footings on sand layer overlying clay. Canadian Geotechnical Journal, Vol 11, no 2, May, pp 223-229.

Meyerhof, G. G. (1976). Bearing capacity and settlement of pile foundations. J. Geotech. Eng. Div. ASCE, 102(GT3), 195–228.

Moulay Smaïne, G., Gueye, B., Zoubir, B. (2014). Influence of Grain Size Coarse Soil on Shear Strength. International Congress on Materials and Structural Stability. MATEC Web of Conferences Volume 11.

Nakao, T., Fityus, S. (2008). Direct Shear Testing of a Marginal Material Using a Large Shear Box. Geotechnical Testing Journal, Vol. 31, No. 5.

Okamura, M., Takemura, J., Kimura, T. (1997) Centrifuge model tests on bearing capacity and deformation of sand layer overlying clay. Soils and Foundations 37(1): pp 73–88.

Okamura, M., Takemura, J., Kimura, T. (1998) Bearing capacity predictions of sand overlying clay based on limit equilibrium methods. Soils and Foundations 38(1): pp 181–194.

Ovesen, N. K. (1979). The scaling law relationship- panel discussion. Proceedings 7th European Conference on Soil Mechanics and Foundation Engineering, 4; pp. 319-323.

Palmer, A. C., White, D. J., Baumgard, A. J., Bolton, M. D., Barefoot, A. J., Finch, M., Powell, T., Faranski, A. S., Baldry, J. A. S. Uplift resistance of buried submarine pipelines: comparison between centrifuge modelling and full-scale tests. Geotechnique 53, No. 10, pp. 877-883.

Palmeira, E. M. (1987). The study of soil-reinforcement interaction by means of large

scale laboratory tests. PhD thesis, University of Oxford.

Palmeira, E. M., Milligan, G. W. E. (1989). Scale Effects in Direct Shear Tests on Sand. Proceedings of the 12th International Conference on Soil Mechanics and Foundation Engineering, Vol. 1, No. 1. pp. 739–742.

Parsons, J. D. (1936). Progress Report on an Investigation of the Shearing Resistance of Cohesionless Soils. Proceedings of the 1st International Conference on Soil Mechanics and Foundation Engineering, Vol. 2, pp. 133–138.

Pedley, M. J. (1990). The performance of soil reinforcement in bending and shear. PhD thesis, Oxford University.

Pereira, P. M., Vieira, C. S., Lopes, M. L. (2019). Degradation assessment of recycled aggregates from construction and demolition waste through wet-dry cycles. Proceedings of the XVII European Conference on Soil Mechanics and Geotechnical Engineering.

Pinto, M. I. M. (2003). Discussion. Applications of geosynthetics for soil reinforcement. Ground Improvement, 7, No. 2, 61-72.

Potts, D. M., Dounias, G. T. & Vaughan, P. R. (1987). Finite element analysis of the direct-shear box test. Geotechnique 37, No. 1, 11-23. Roscoe, K. H. (1970).

Powrie, W. (2010). Soil Mechanics: Concepts and Applications. CRC Press. 3th edition.

Q181C (1994, rev. 2002). Effective Angle of Internal Friction at Constant Volume Conditions for Granular Materials. Draft. Queensland Main Roads, Brisbane Old, Australia.

Santana, M., Estaire, J. (2019). Test results of friction resistance in the sleeper – ballast contact. Proceedings of the XVII European Conference on Soil Mechanics and Geotechnical Engineering.

Shiau, J. S., Lyamin, A. V., Sloan, S. W. (2003). Bearing capacity of a sand layer on clay by finite element limit analysis. Canadian Geotechnical Journal 40(5), pp. 900–915.

Shukla, S. K. (2002). Shallow foundations. Chapter 5, Geosynthetics and Their Applications, Shukla, S.K., Editor, Thomas Telford, London, pp. 123–163.

Shukla, S. K. (2004). Discussion of “Applications of geosynthetics for soil reinforcement” by M.I.M. Pinto’ *Ground Improvement*, 8, 4, pp. 179–181.

Shukla, S. K. (2016). *An introduction to geosynthetic engineering*. CRC Press.

Simoni, A., Houlsby, G. T. (2006). The direct shear strength and dilatancy of sand–gravel mixtures. *Geotechnical and Geological Engineering*, 24, 523–549.

BRE (2004). *Working platforms for tracked plant*. BR470.

Sobol, E., Sas, W., Szymanski, A. (2015). Scale effect in direct shear tests on recycled concrete aggregate. *Studia Geotechnica et Mechanica*, Vol. 37, No. 2.

Steele, D. P. (2004). Ground engineering as potential end uses for recycled and secondary aggregates. *Recycled and Secondary Aggregates*. Waste and Resources Action Programme, Banbury, UK.

Taylor, R. N. (1995). *Geotechnical Centrifuge Technology*. CRC Press.

Taylor, D.W., Leps, T. M. (1938). Shearing properties of Ottawa standard sand as determined by the MIT strain-controlled direct shearing machine. *Record of Proceedings of Conference on Soils and Foundations*, US Corps of Engineers, Boston.

Terzaghi, K., Peck, R. B., Mesri, G. (1996). *Soil mechanics in engineering practice*. Chapter 9. John Wiley and Sons.

Terzaghi, K. (1943). *Theoretical Soil Mechanics*. Wiley, New York.

TWf (2019): *Design of Granular Working Platforms for Construction Plant – A guide to good practice*. Temporary Works Forum c/o Institution of Civil Engineers, London.

Ullah, S. N., Hu, Y., Stanier, S. and White, D. (2016). Lateral boundary effects in centrifuge foundation tests. *International Journal of Physical Modelling in Geotechnics* 17(3): 144-160.

Valsangkar, A. J., Meyerhof, G. G. (1979). Experimental study of punching coefficients and shape factor for two-layered soils. *Canadian Geotechnical Journal*, Vol. 16, pp 802-805.

Vesic, A. S. (1963). Bearing capacity of deep foundations in sand. Highway Research Record, No. 39, 112-153.

Vesic, A. S. (1973). Analysis of ultimate loads of shallow foundations. Journal of the soil mechanics and foundations division, 99, 45-73.

Wei, K. M., Zhu, S. H., Yu, X. H. (2014). Influence of the scale effect on the mechanical parameters of coarse grained soils. IJST, Transactions of Civil Engineering, Vol. 38, No. C1, pp 75-84.

Wood, D.M. 1991. Soil behaviour and critical state soil mechanics. Cambridge University Press, Cambridge.

Worbes, R, Moormann, C. (2018). Geotechnical model tests on bearing capacity of working platforms for mobile construction machines and cranes. Physical Modelling in Geotechnics – McNamara *et al.* (Eds). Taylor & Francis Group, London.

Zhang, L., Thornton, C. (2007). A numerical examination of the direct shear test. Geotechnique, 57(4): 343-354.

Ziogos, A., Brown, M. J., Ivanovic, A., Morgan, N (2021). Understanding rock-steel interface properties of use in offshore applications. Proc. Inst. Of Civil Engineers: Geotechnical Engineering Journal.

TABLES

sieve size (mm)	percentage passing (%)
125	100
90	80 – 100
75	65 – 100
37.5	45 – 100
10	15 – 60
5	10 - 45
0.6	0 – 25
0.063	0 – 12

Table 3. 1 Particle size distribution of 6F2 material, data obtained from Highways Agency (2004).

Grading	α (°)	β (°)
base sample	45.4	44.8
scalped sample	43.9	42.6
parallel sample	36.4	33.9

Table 3. 2 Values of α and β coefficients proposed by Hamidi *et al.* (2012) for the determination of the maximum and constant volume friction angles of the base material.

Shear box characteristics	Davies and Le Masurier	Jain and Gupta	Pedley	Krahn <i>et al.</i>	Santana and Estaire
box internal size (m)	3 x 1.5 x 1.5	1.2 x 1.2 x 1.2	1 x 1 x 1	1 x 1 x 1	1 x 1 x 0.8
shear plane surface (m ²)	2.25	1.44	1	1	0.8
box material	steel	concrete	steel	steel	steel
side thickness (mm)	6	450	25	-	-
gap (mm)	80	160	6	-	-
maximum particle size of tested material (mm)	0.75	200	1.4	< 2	60
shear plane direction	vertical	horizontal	horizontal	horizontal	horizontal
moveable shear box half	right	upper	upper	lower	lower
normal load system provider	air bags (pressure up to 400 kPa)	two 500 kN hydraulic jacks	four 80 kN hydraulic jacks	one 222 kN hydraulic jack	one 1000 kN hydraulic jack
shear load system provider	one 500 kN hydraulic jack	one 1000 kN hydraulic jack	one 600 kN hydraulic jack	one 222 kN hydraulic jack	one 1000 kN hydraulic jack
shear rate displacement (mm/min)	-	-	0.5	5	0.8
maximum shear displacement achieved (mm)	250	75	70	300	250

Table 3. 3 Large shear boxes in literature.

Properties	Value (sample with maximum particle size equal to 3.35 mm)	Value (sample with maximum particle size equal to 2 mm)
Minimum void ratio (e_{min})	0.229	0.136
Maximum void ratio (e_{max})	0.640	0.757
Specific gravity (G_s)	2.73	2.73
Scaling factor	30	50
D_{50} (mm)	0.5	0.3
d_{max} (mm)	3.35	2
d_{min} (mm)	0.006	0.020
γ_d , average for direct shear tests, denser samples (kN/m^3)	21.3	21.2
γ_d , average for direct shear tests, looser samples (kN/m^3)	20.0	19.5

Table 4. 1 Properties of testing samples representing scaled versions of the grading required for the 6F2 class material.

Down scaled (theoretical)		Down scaled (actual)	
sieve size (mm)	percentage passing (%)	sieve size (mm)	percentage passing (%)
3.00	100	4.17	100
1.25	72.5	3.35	95
0.33	37.5	2.4	82.5
0.17	27.5	1.2	72.5
0.02	12.5	0.3	36
0.00	6	0.18	28
-	-	0.063	18.77
-	-	0.020	0.336
-	-	0.006	0.028
-	-	0.002	0.000

a)

Down scaled (theoretical)		Down scaled (actual)	
sieve size (mm)	percentage passing (%)	sieve size (mm)	percentage passing (%)
1.8	100	2.5	100
0.75	72.5	2	93
0.2	37.5	1.18	79.1
0.1	27.5	0.6	66.2
0.01	12.5	0.425	57.5
0.001	6	0.3	48.5
0.000	0	0.15	33
-	-	0.063	24
-	-	0.020	0.065
-	-	0.006	0
-	-	0.002	0

b)

Tables 4. 2 Theoretical and actual particle size distributions of the small-scale samples of maximum particle size equal to (a) 3.35 mm and (b) 2 mm.

Sample 1	
beaker (g)	65.250
beaker + water (g)	77.347
water in the pipette (ml)	12.097
Sample 2	
beaker (g)	65.250
beaker + water (g)	77.321
water in the pipette (ml)	12.071
Sample 3	
beaker (g)	65.250
beaker + water (g)	77.351
water in the pipette (ml)	12.101
Volume of water in the pipette (average) (ml)	
12.090	

Table 4.3 Calibration data of the sampling pipette used for the sedimentation test (according to BS 1377-2, 1990).

Sample 1	
d_{\max} (mm)	3.35
sample weight (g)	30.928
bottle 1 (g)	27.283
bottle 2 (g)	24.987
bottle 3 (g)	32.323
bottle 1 + W_1 (g)	27.295
bottle 2 + W_2 (g)	24.991
bottle 3 + W_3 (g)	32.326
W_1 (g)	0.12
W_2 (g)	0.004
W_3 (g)	0.003
M_1 (g)	0.496
M_2 (g)	0.165
M_3 (g)	0.124
medium silt (0.02-0.006 mm) (%)	1.1
fine silt (0.006-0.002 mm) (%)	0.1

(a)

Sample 2	
d_{\max} (mm)	2
sample weight (g)	30.422
bottle 1 (g)	26.229
bottle 2 (g)	32.739
bottle 3 (g)	32.961
bottle 1 + W_1 (g)	26.232
bottle 2 + W_2 (g)	32.740
bottle 3 + W_3 (g)	32.962
W_1 (g)	0.003
W_2 (g)	0.001
W_3 (g)	0.001
M_1 (g)	0.124
M_2 (g)	0.041
M_3 (g)	0.041
medium silt (0.02-0.006 mm) (%)	0.27
fine silt (0.006-0.002 mm) (%)	0.00

(b)

Table 4. 4 Data and results of the sedimentation tests conducted on the samples with (a) maximum particle size equal to 3.35 mm and (b) maximum particle size of 2 mm.

Sample 1		Sample 2		Sample 3		Sample 4	
d _{max} (mm)	3.35	d _{max} (mm)	3.35	d _{max} (mm)	0.063 (from d _{max} = 3.35 mm)	d _{max} (mm)	0.063 (from d _{max} = 3.35 mm)
bottle reference number	134	bottle reference number	177	bottle reference number	134	bottle reference number	177
W ₁ (g)	22.365	W ₁ (g)	22.339	W ₁ (g)	23.706	W ₁ (g)	23.534
W ₂ (g)	27.343	W ₂ (g)	27.336	W ₂ (g)	28.756	W ₂ (g)	28.938
W ₃ (g)	49.928	W ₃ (g)	50.092	W ₃ (g)	51.631	W ₃ (g)	51.73
W ₄ (g)	46.777	W ₄ (g)	46.927	W ₄ (g)	48.434	W ₄ (g)	48.301
G _{s1}	2.724	G _{s1}	2.727	G _{s2}	2.725	G _{s2}	2.736
Sample 5		Sample 6		Sample 7		Sample 8	
d _{max} (mm)	2	d _{max} (mm)	2	d _{max} (mm)	0.063 (from d _{max} = 2 mm)	d _{max} (mm)	0.063 (from d _{max} = 2 mm)
bottle reference number	134	bottle reference number	177	bottle reference number	134	bottle reference number	177
W ₁ (g)	23.706	W ₁ (g)	23.532	W ₁ (g)	23.706	W ₁ (g)	23.532
W ₂ (g)	29.372	W ₂ (g)	29.219	W ₂ (g)	29.531	W ₂ (g)	29.031
W ₃ (g)	52.02	W ₃ (g)	51.904	W ₃ (g)	52.128	W ₃ (g)	51.801
W ₄ (g)	48.434	W ₄ (g)	48.301	W ₄ (g)	48.434	W ₄ (g)	48.301
G _{s1}	2.724	G _{s1}	2.729	G _{s2}	2.733	G _{s2}	2.751

Table 4. 5 Data and results for the determination of the specific gravity (G_s) of the two soil samples used to conduct small scale tests (*continued*).

G_s total sample (d_{max}= 3.35 mm)				
Mass ₁ (%) > 0.063mm	Mass ₂ (%) < 0.063mm	G _{s1}	G _{s2}	G _{stot}
81	19	2.73	2.73	2.73
G_s total sample (d_{max}= 2 mm)				
Mass ₁ (%) > 0.063mm	Mass ₂ (%) < 0.063mm	G _{s1}	G _{s2}	G _{stot}
76	24	2.73	2.74	2.73

Table 4. 5 Data and results for the determination of the specific gravity (G_s) of the two soil samples used to conduct small scale tests.

Determination of e_{min} - Sample 1	
Initial test data	
d _{max} (mm)	3.35
average mould internal height (mm)	115.51
average mould diameter (mm)	104.62
mould cross sectional area (cm ²)	85.64
mould volume (cm ³)	989.1
mould mass (kg)	3.216

Table 4. 6(a) Data and results of maximum index density (e_{min}) tests conducted on the sample with maximum particle size equal to 3.35 mm (*continued*).

Test 1		Test 2		Test 3	
specimen mass (g)	1301.9	specimen mass (g)	1316.27	specimen mass (g)	1293.57
h_0 (mm)	178.9	h_0 (mm)	178.9	h_0 (mm)	178.9
h_1 (mm)	247.8	h_1 (mm)	247.8	h_1 (mm)	247.4
specimen height (mm)	68.9	specimen height (mm)	68.8	specimen height (mm)	68.5
specimen volume (cm ³)	589.7	specimen volume (cm ³)	589.5	specimen volume (cm ³)	586.8
ρ_{\max} (g/cm ³)	2.21	ρ_{\max} (g/cm ³)	2.23	ρ_{\max} (g/cm ³)	2.2
Test 4		Test 5		Test 6	
specimen mass (g)	1328.18	specimen mass (g)	1250.58	specimen mass (g)	1350.92
h_0 (mm)	178.9	h_0 (mm)	178.9	h_0 (mm)	178.9
h_1 (mm)	248.6	h_1 (mm)	244.8	h_1 (mm)	249.2
specimen height (mm)	69.6	specimen height (mm)	65.9	specimen height (mm)	70.3
specimen volume (cm ³)	596.42	specimen volume (cm ³)	564.14	specimen volume (cm ³)	601.89
ρ_{\max} (g/cm ³)	2.23	ρ_{\max} (g/cm ³)	2.22	ρ_{\max} (g/cm ³)	2.24
Results					
average ρ_{\max} (g/cm ³)		2.22			
γ_{\max} (kN/m ³)		21.79			
G_s		2.73			
e_{\min}		0.229			

Table 4. 6(a) Data and results of maximum index density (e_{\min}) tests conducted on the sample with maximum particle size equal to 3.35 mm.

Determination of e_{\min} - sample 2	
Initial test data	
d_{\max} (mm)	2
average mould internal height (mm)	115.51
average mould diameter (mm)	104.62
mould cross sectional area (cm ²)	85.64
mould volume (cm ³)	989.1
mould mass (kg)	3.216

Table 4. 6(b) Data and results of maximum index density (e_{\min}) tests conducted on the sample with maximum particle size of 2 mm (*continued*).

Test 1		Test 2		Test 3	
specimen mass (g)	1376.66	specimen mass (g)	1431.29	specimen mass (g)	1328.34
h0 (mm)	178.9	h0 (mm)	178.9	h0 (mm)	178.9
h1 (mm)	253.9	h1 (mm)	243.9	h1 (mm)	248.4
specimen height (mm)	74.9	specimen height (mm)	64.9	specimen height (mm)	69.5
specimen volume (cm ³)	641.7	specimen volume (cm ³)	556.1	specimen volume (cm ³)	595
rmax (g/cm ³)	2.15	rmax (g/cm ³)	2.57	rmax (g/cm ³)	2.23
Test 4		Test 5		Test 6	
specimen mass (g)	1349.24	specimen mass (g)	1343	specimen mass (g)	1333.66
h0 (mm)	178.9	h0 (mm)	178.9	h0 (mm)	178.9
h1 (mm)	246.6	h1 (mm)	241.7	h1 (mm)	237.8
specimen height (mm)	67.7	specimen height (mm)	62.7	specimen height (mm)	58.9
specimen volume (cm ³)	579.85	specimen volume (cm ³)	537.22	specimen volume (cm ³)	504.62
rmax (g/cm ³)	2.33	rmax (g/cm ³)	2.5	rmax (g/cm ³)	2.64
Results					
		average rmax (g/cm ³)	2.4		
		gmax (kN/m ³)	23.57		
		Gs	2.73		
		emin	0.136		

Table 4. 6(b) Data and results of maximum index density (e_{min}) tests conducted on the sample with maximum particle size of 2 mm.

Determination of e_{max} - sample 1	
Initial test data	
d_{max} (mm)	3.35
average mould internal height (mm)	115.51
average mould diameter (mm)	104.62
mould cross sectional area (cm ²)	85.64
mould volume (cm ³)	989.1
mould mass (kg)	3.216
Test 1	
specimen mass (g)	1664.460
specimen volume (cm ³)	989.1
ρ_{max} (g/cm ³)	1.68
Test 2	
specimen mass (g)	1637.970
specimen volume (cm ³)	989.1
ρ_{max} (g/cm ³)	1.66
Test 3	
specimen mass (g)	1634.970
specimen volume (cm ³)	989.1
ρ_{max} (g/cm ³)	1.65
Test 4	
specimen mass (g)	1671.550
specimen volume (cm ³)	989.1
ρ_{max} (g/cm ³)	1.69
Test 5	
specimen mass (g)	1638.500
specimen volume (cm ³)	989.1
ρ_{max} (g/cm ³)	1.66
Test 6	
specimen mass (g)	1632.660
specimen volume (cm ³)	989.1
ρ_{max} (g/cm ³)	1.65
Results	
average ρ_{max} (g/cm ³)	1.66
γ_{max} (kN/m ³)	16.33
G_s	2.73
e_{max}	0.640

(a)

Table 4. 7(a) Data and results of minimum index density (e_{max}) tests conducted on the sample with maximum particle size equal to 3.35 mm.

Determination of e_{max} - sample 2	
Initial test data	
d_{max} (mm)	2
average mould internal height (mm)	115.51
average mould diameter (mm)	104.62
mould cross sectional area (cm ²)	85.64
mould volume (cm ³)	989.1
mould mass (kg)	3.216
Test 1	
specimen mass (g)	1536.460
specimen volume (cm ³)	989.1
ρ_{max} (g/cm ³)	1.55
Test 2	
specimen mass (g)	1518.610
specimen volume (cm ³)	989.1
ρ_{max} (g/cm ³)	1.54
Test 3	
specimen mass (g)	1539.850
specimen volume (cm ³)	989.1
ρ_{max} (g/cm ³)	1.56
Test 4	
specimen mass (g)	1545.820
specimen volume (cm ³)	989.1
ρ_{max} (g/cm ³)	1.56
Test 5	
specimen mass (g)	1539.190
specimen volume (cm ³)	989.1
ρ_{max} (g/cm ³)	1.56
Test 6	
specimen mass (g)	1538.190
specimen volume (cm ³)	989.1
ρ_{max} (g/cm ³)	1.56
Results	
average ρ_{max} (g/cm ³)	1.55
γ_{max} (kN/m ³)	15.23
G_s	2.73
e_{max}	0.757

(b)

Table 4. 7(b) Data and results of minimum index density (e_{max}) tests conducted on the sample with maximum particle size equal to 2 mm.

Test No.	d_{max} (mm)	e	Peak values				Critical values				max ϵ_{vol} (%)
			σ'_v (kPa)	τ_{pk} (kPa)	ϕ'_{pk} (°)	$\gamma_{s,pk}$ (%)	σ'_v (kPa)	τ_{cr} (kPa)	ϕ'_{cr} (°)	$\gamma_{s,cr}$ (%)	
1	3.35	0.281	103	119	49.9	9.7	111	101	40.8	30	-1.9
2		0.288	105	128		9.7	110	87		28	-2.4
3		0.283	105	123		13.1	116	94		42	-3.3
4		0.282	209	237	49.6	12	224	189		25	-2.6
5		0.297	212	249		16.3	224	208		32	-2.2
6		0.277	210	254		14.7	224	201		32	-2.4
7		0.362	-	-	-	-	575	491		29	2.8
8		0.361	-	-		-	565	492		28	2.2
9		0.363	-	-		-	575	506		36	2.8
10		0.368	-	-		-	565	473		31	1.4

Table 5. 1 Results of the standard direct shear box tests on scaled down 6F2 material (maximum particle size equal to 3.35 mm).

Test No.	d_{max} (mm)	e	Peak values				Critical values				max ϵ_{vol} (%)
			σ'_v (kPa)	τ_{pk} (kPa)	ϕ'_{pk} (°)	$\gamma_{s,pk}$ (%)	σ'_v (kPa)	τ_{cr} (kPa)	ϕ'_{cr} (°)	$\gamma_{s,cr}$ (%)	
1	2	0.28	103	105	46.5	8.3	111	90	38.1	22	-1.5
2		0.287	103	107		6.1	109	99		18	-2
3		0.29	103	113		8.7	115	87		37	-1.7
4		0.281	214	238	47.8	15.9	223	179		29	-3.2
5		0.293	209	227		14.2	228	192		39	-2
6		0.293	211	234		14.5	220	180		25	-2.1
7		0.403	-	-	-	-	556	433		29	2.5
8		0.402	-	-		-	579	435		26	3.7
9		0.399	-	-		-	547	439		22	2.8

Table 5. 2 Results of the standard direct shear box tests on scaled down 6F2 material (maximum particle size equal to 2 mm).

d_{\max} (mm)	W (mm)	H (mm)	W/d_{\max}	H/d_{\max}	Friction angle ($^{\circ}$)
5	200	100	40	20	46
	150		30		46
	100		20		46
	61.8		12.36		49
	200	50	40	10	47
		100		20	46
		150		30	46
		200		40	47
10	200	100	20	10	46
	150		15		46
	100		10		49
	61.8		6.18		51.5
	200	50	20	5	53
		100		10	46
		150		15	47
		200		20	47

Table 7. 1 Initial data and friction angle results obtained from the study of Fu *et al.* (2015) (values of friction angles scaled from the graphs presented by the author).

Test No.	d_{\max} (mm)	γ (kN/m ³)	e	D_r (%)	σ'_v (kPa)
1	63	17.25	0.552	21	11
2		17.36	0.542	24	185
3		17.09	0.567	18	104

Table 7. 2 Summary of the tests conducted using the large shear box apparatus.

Test No.	σ'_v (kPa)	τ (kPa)	mobilised angle of friction ($^{\circ}$)
1	11	26	67.07
3	104	180	59.98
2	185	380	64.04

Table 8. 1 Mobilised angles of friction for each test conducted with the large shear apparatus and stress values used for their calculation.

Test No.	d_{\max} (mm)	σ_v (kPa)	τ/σ'_v at $dy/dx=0$	ϕ'_{cr} (°)
3	2	100	0.64	33
5		200	0.79	38
1	3.35	100	0.65	33
5		200	0.81	39
1	63	11	0.8	39
3		104	0.93	43
2		185	1.08	48

Table 8. 2 Summary of the results obtained from applying the principals of the stress dilatancy theory (Wood, 1991) to the data derived from small and large scale tests.

FIGURES

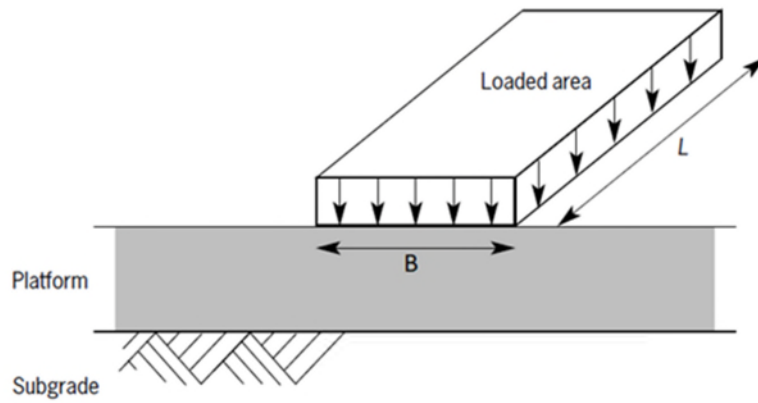


Figure 2. 1 Platform design method (BRE, 2004).

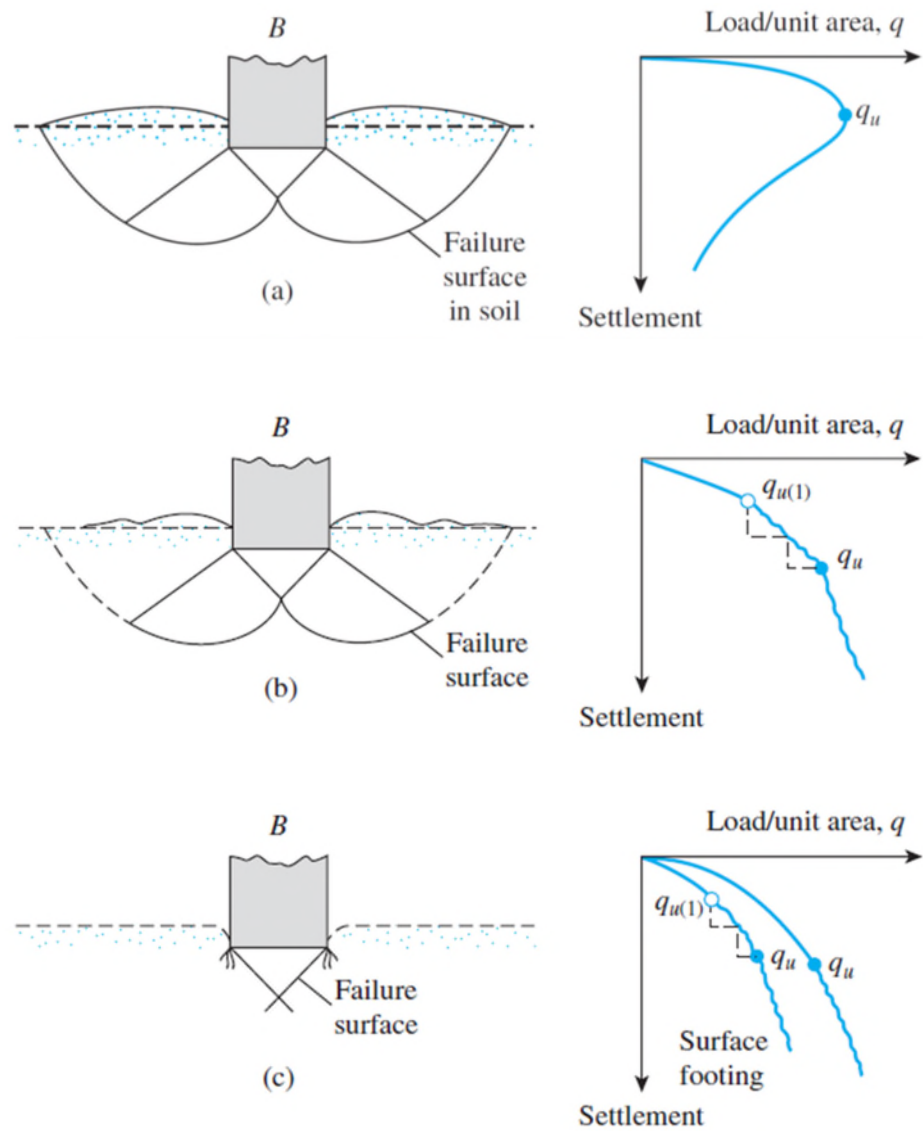


Figure 2. 2 General (a), Local (b), Punching (c) shear failure mechanisms (Das, 2010).

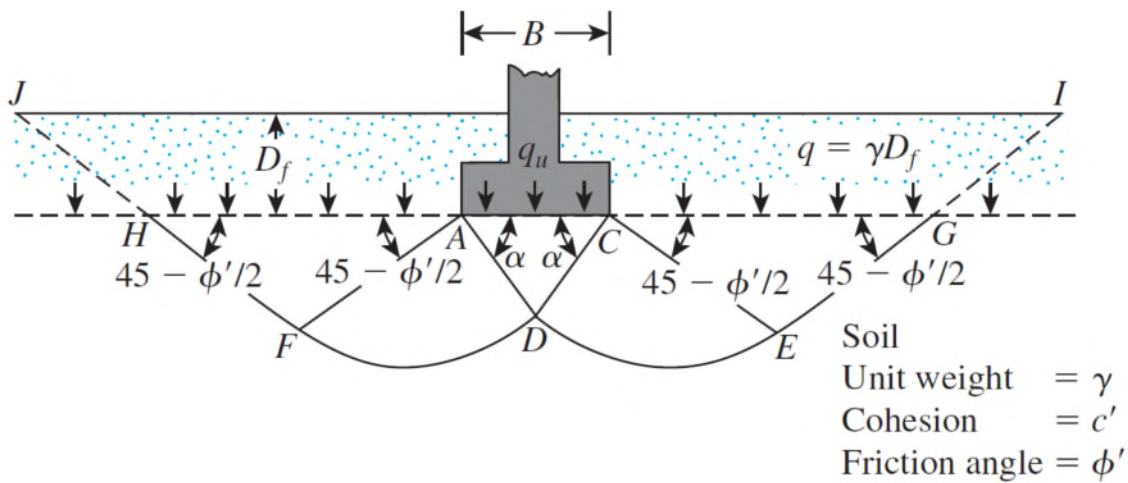


Figure 2.3 Bearing capacity failure in soil under a rough rigid strip foundation (Das, 2010).

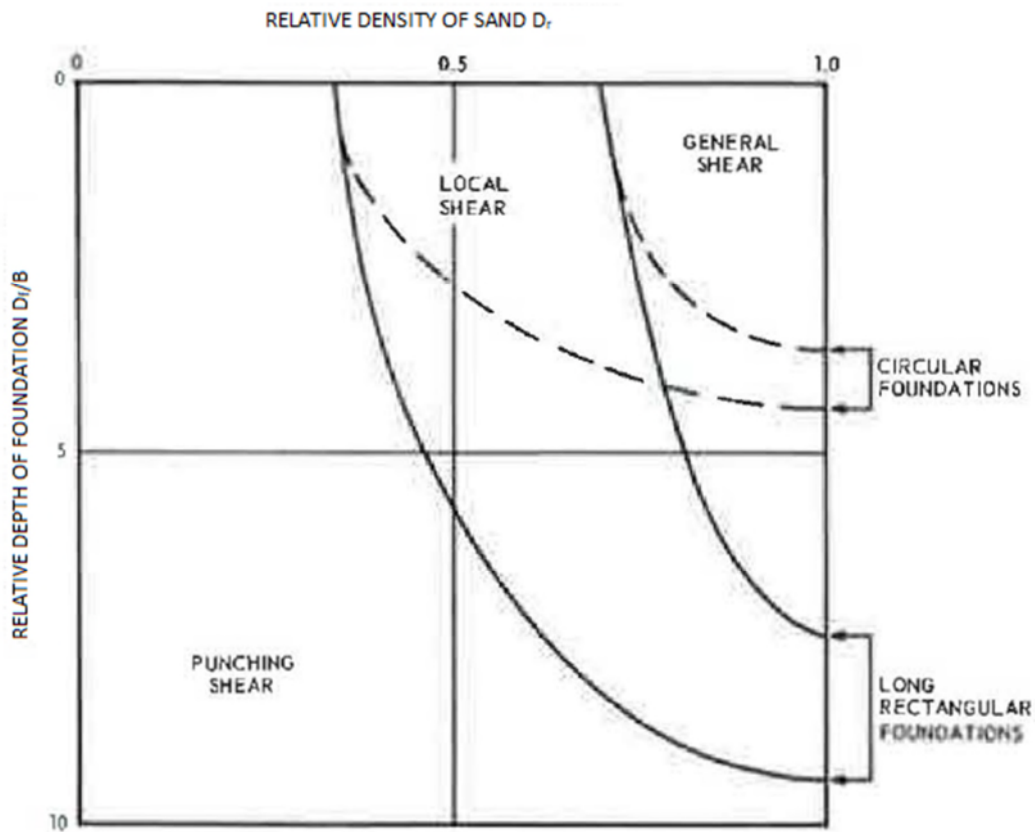


Figure 2.4 Types of failure at different relative depth D_f/B of foundations in sand (Vesic, 1963).

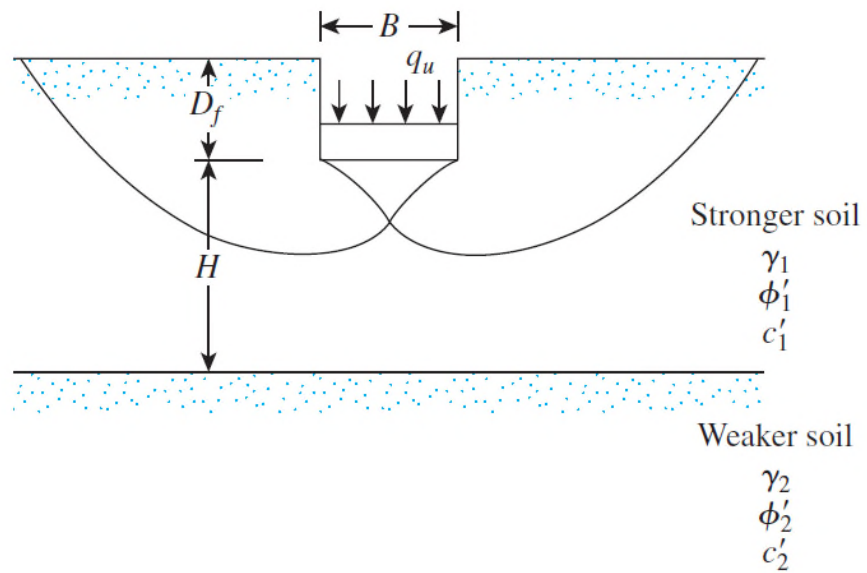


Figure 2. 5 Bearing capacity of a strip foundation on layered soil (stronger soil underlain by weaker soil) where the depth H is relatively large compared with the foundation width (B) (Das, 2010).

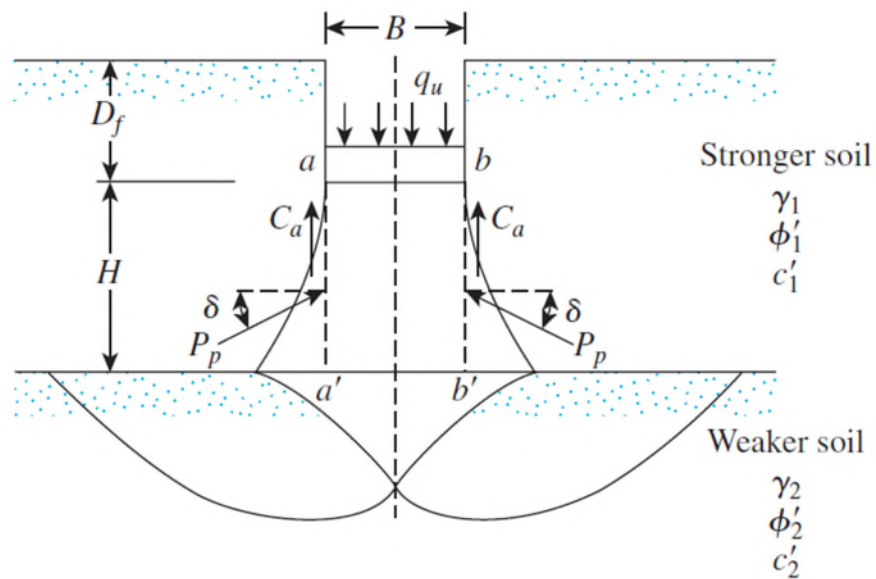


Figure 2. 6 Bearing capacity of a strip foundation on layered soil (stronger soil underlain by weaker soil) where the depth H is relatively small compared with the foundation width (B) (Das, 2010).

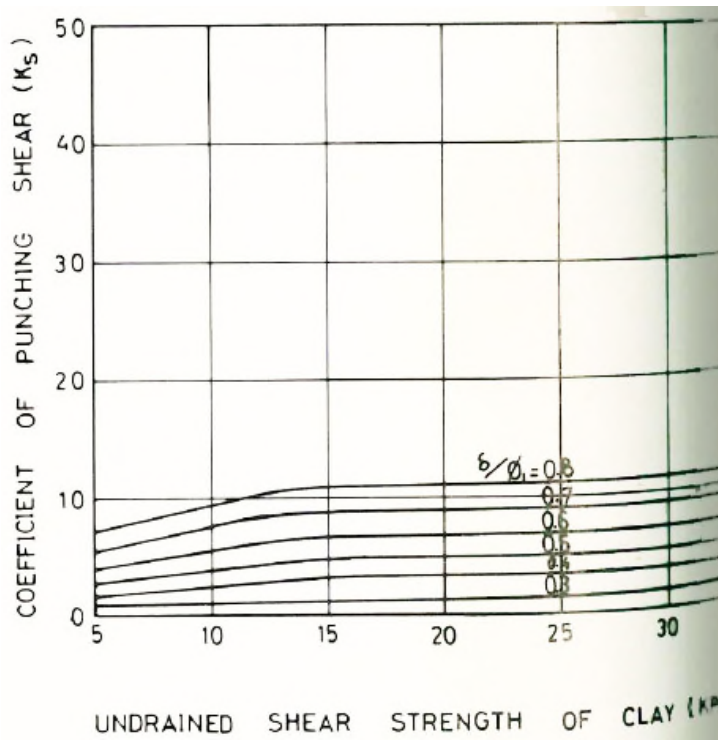


Figure 2. 7 Coefficient of punching shear (K_s) expressed as function of the undrained shear strength of clay and the ratio δ/ϕ_1' . Chart showing the results for a sand top layer with $\phi_1' = 40^\circ$ (Hanna and Meyerhof, 1980).

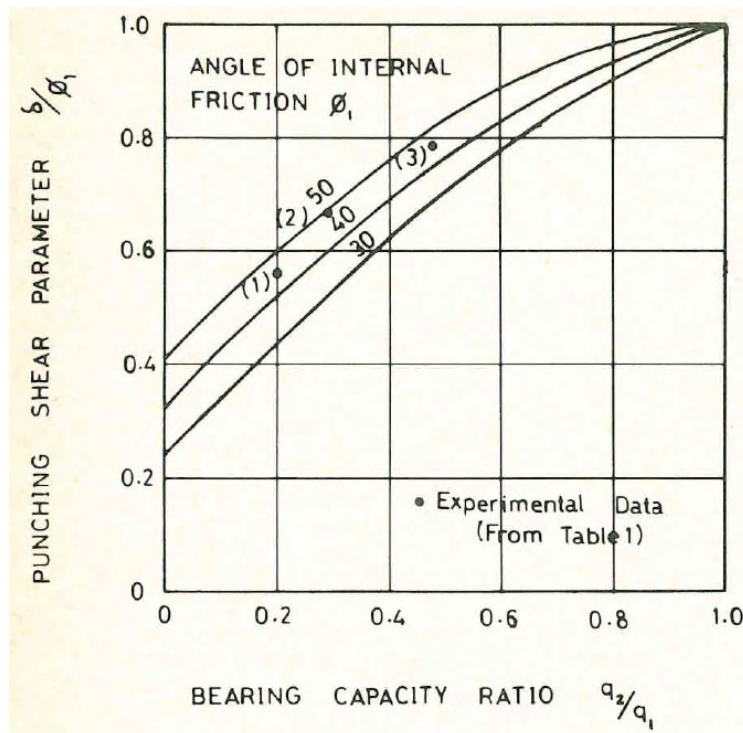


Figure 2. 8 Punching shear parameter (δ/ϕ_1') expressed as function of the ratio q_2/q_1 and the angle of friction of the top granular layer (ϕ_1'), Hanna and (Meyerhof, 1980).

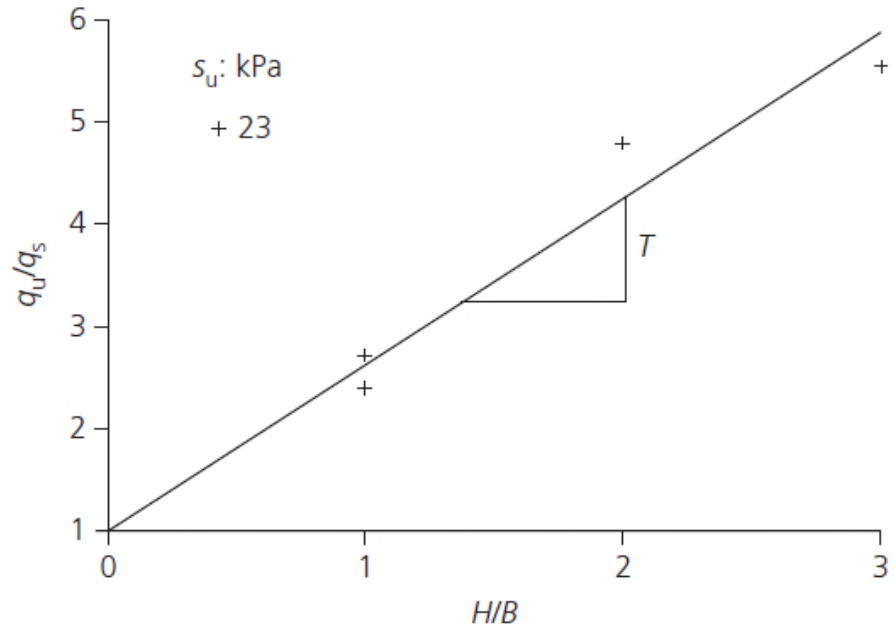


Figure 2. 9 Plots of bearing capacity ratio against H/B from centrifuge testing reported by Okamura et al. (1997) in case of strip footings.

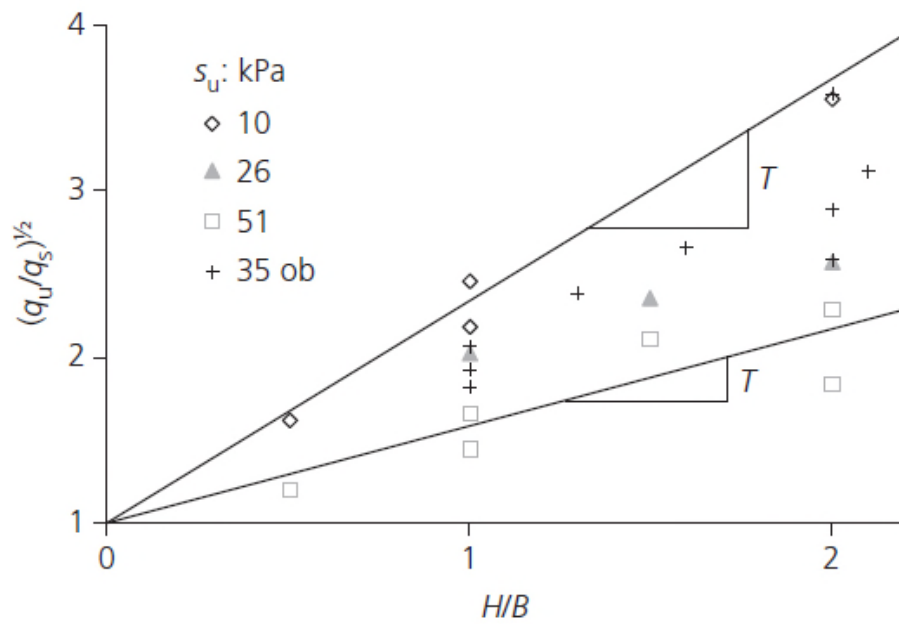


Figure 2. 10 Plots of bearing capacity ratio against H/B from centrifuge testing reported by Okamura *et al.* (1997) in case of circular footings (Lees, 2019).

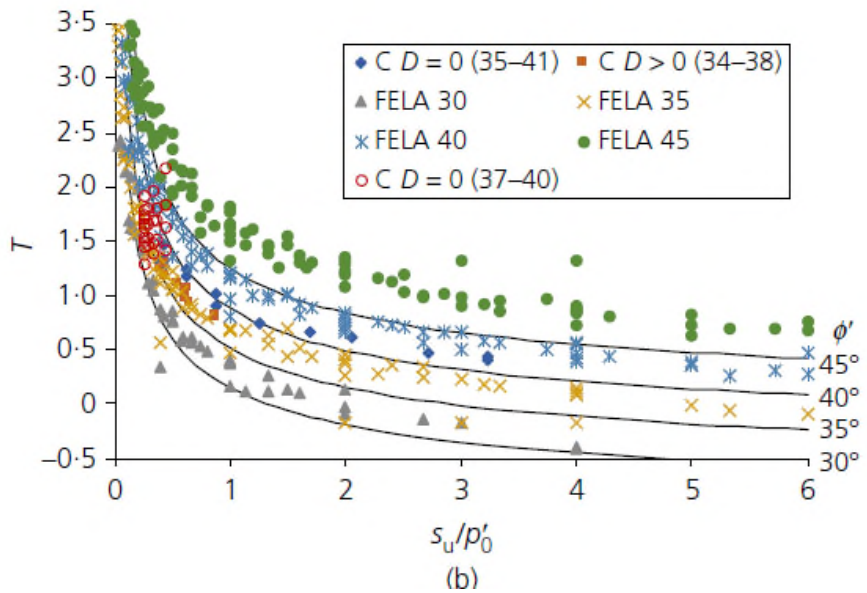
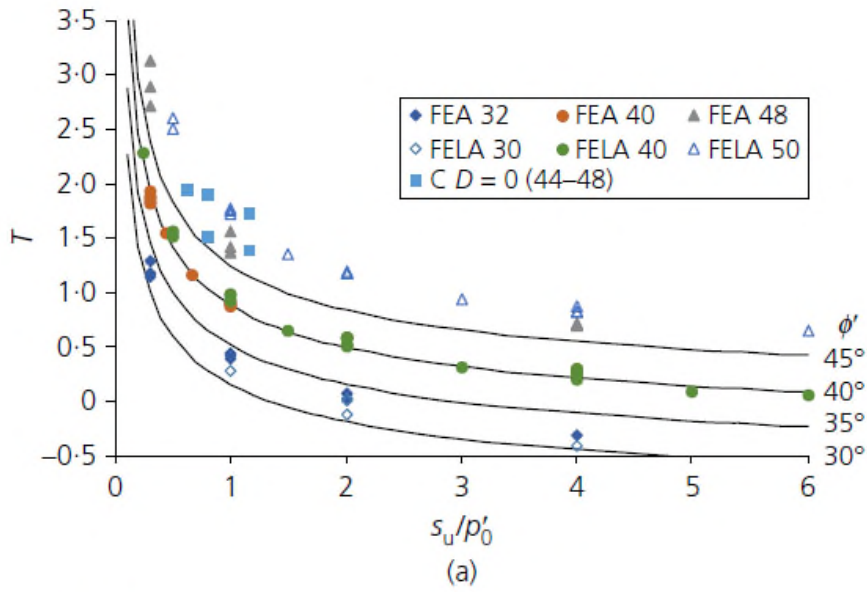


Figure 2. 21 Variation of T with s_u and ϕ' for: (a) strip footing; (b) square footing (Lees, 2019).

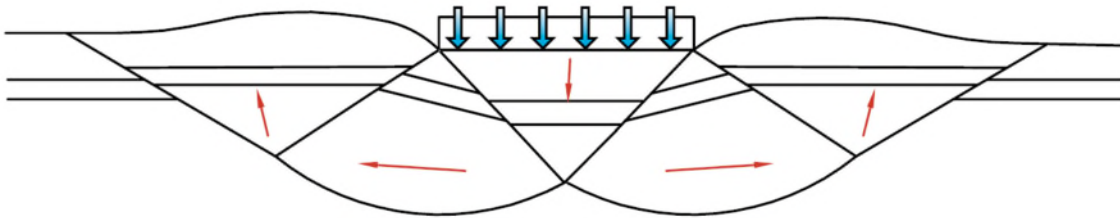


Figure 2. 12 General failure mechanism (TWf, 2019).

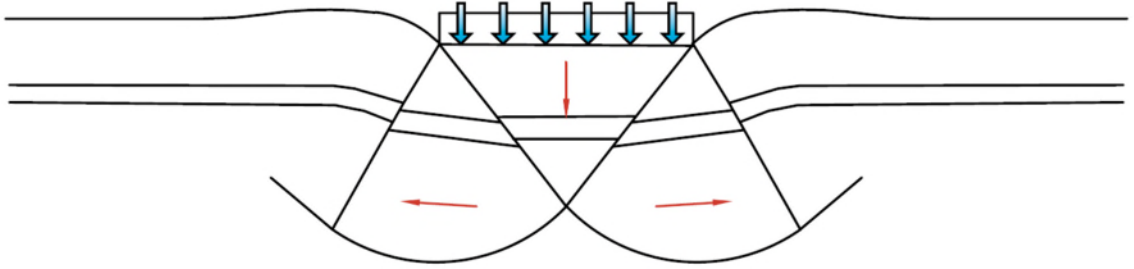


Figure 2. 13 Local failure mechanism (TWf, 2019).

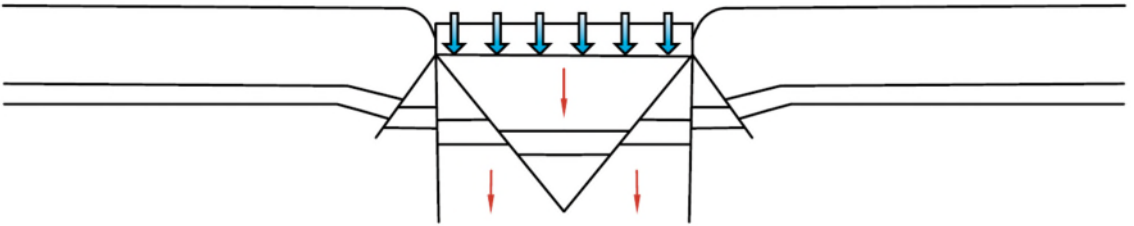


Figure 2. 14 Punching failure mechanism (TWf, 2019).

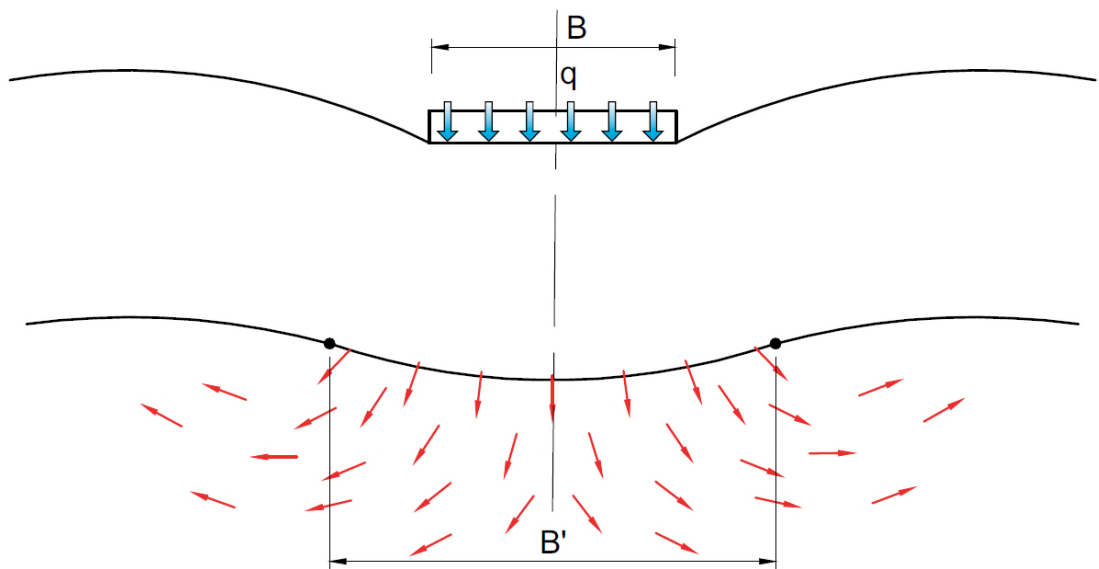


Figure 2. 15 Displacement of the loaded platform and subformation (TWf, 2019).

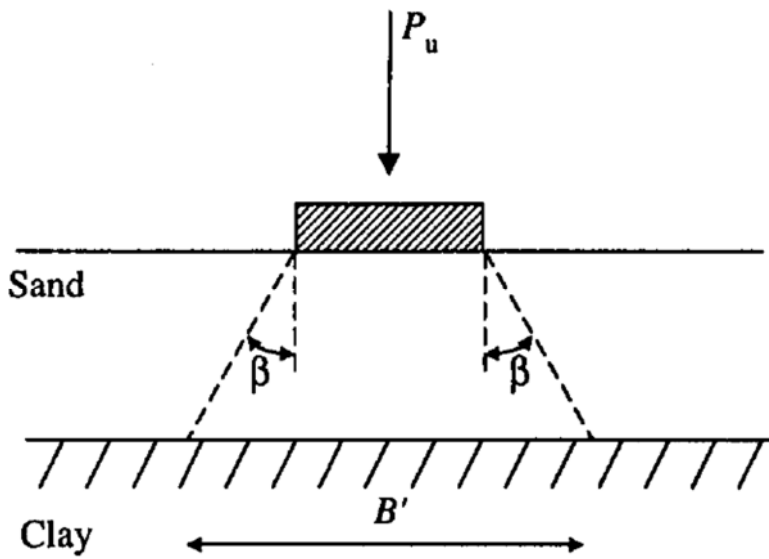


Figure 2. 16 Load spread model in bearing capacity method (Burd and Frydman, 1997).

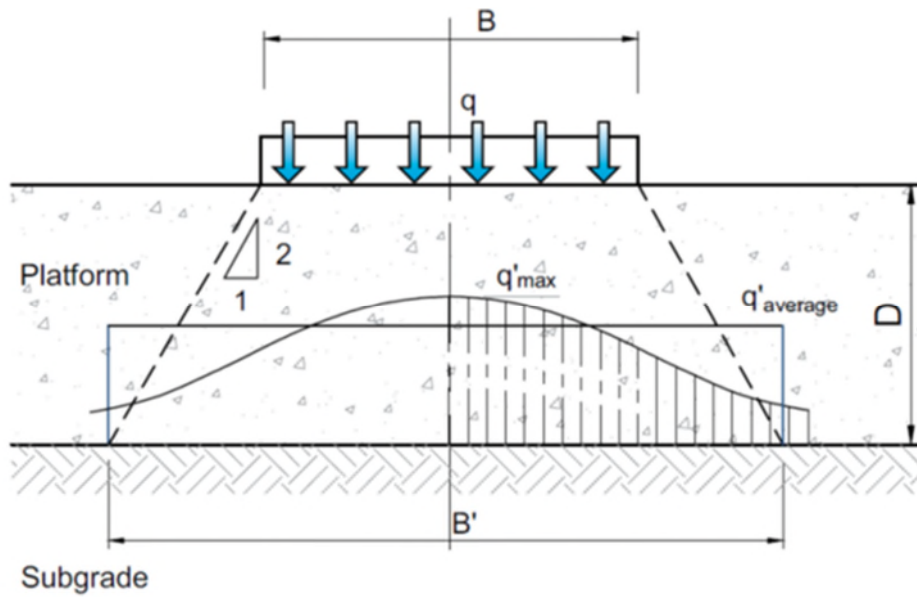


Figure 2. 17 Actual pressure on formation compared with average derived from load spread method (TWf, 2019).

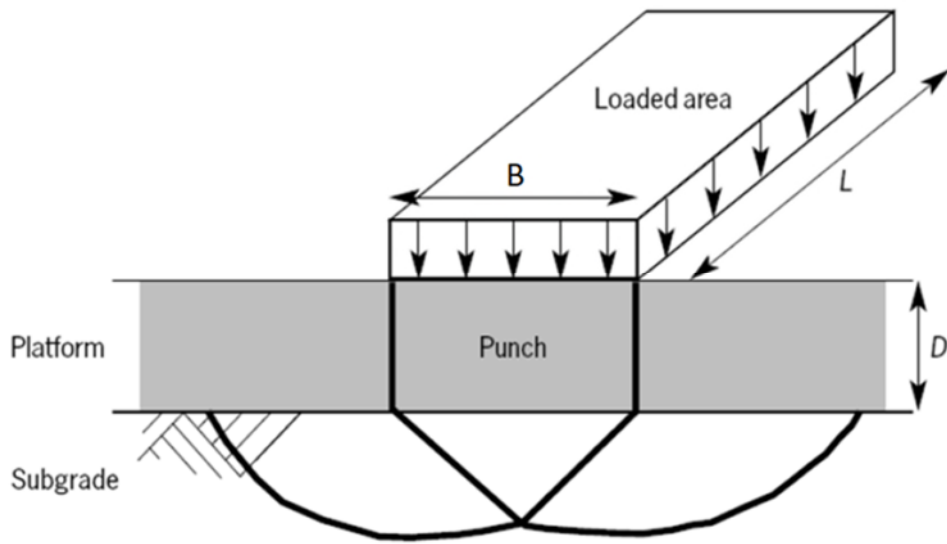


Figure 2. 18 Punching shear model (BRE, 2004).

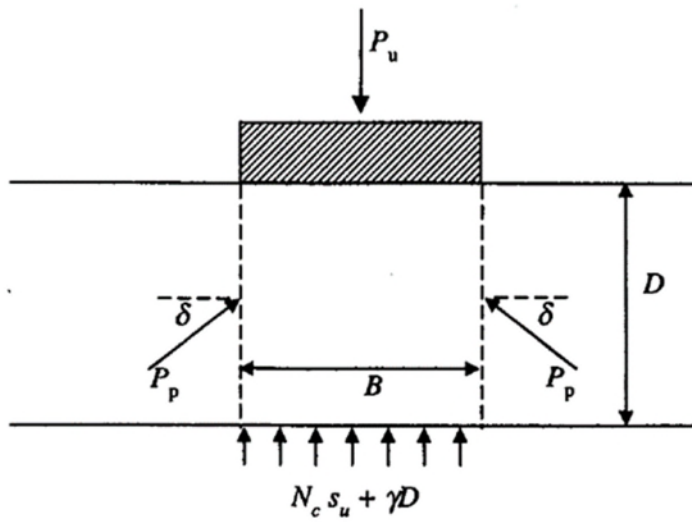


Figure 2. 19 Punching shear model (Burd and Frydman, 1997).

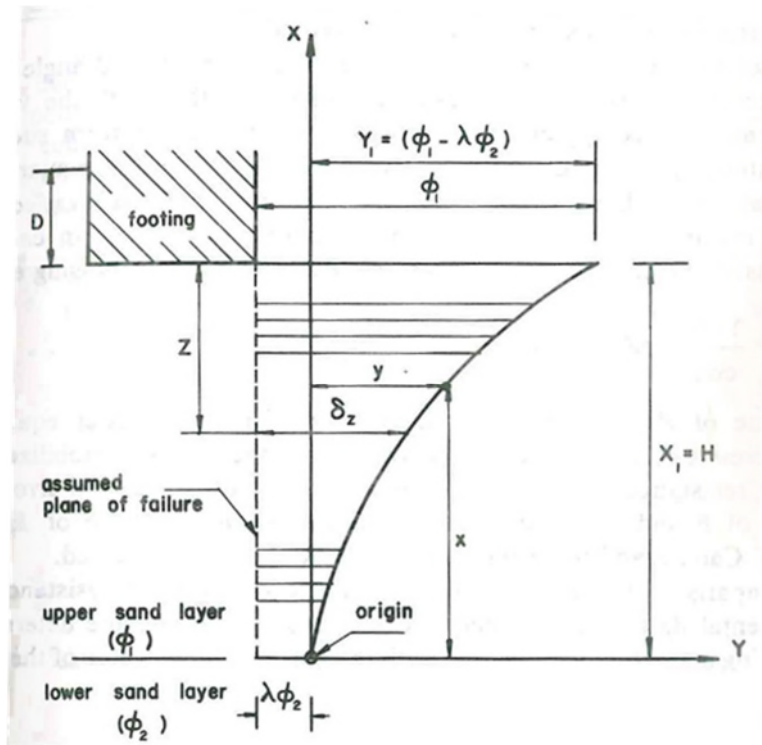


Figure 2. 20 Comparison between assumed and actual plane of failure developing in a strong soil layer underlain by weaker soil (Hanna, 1981).

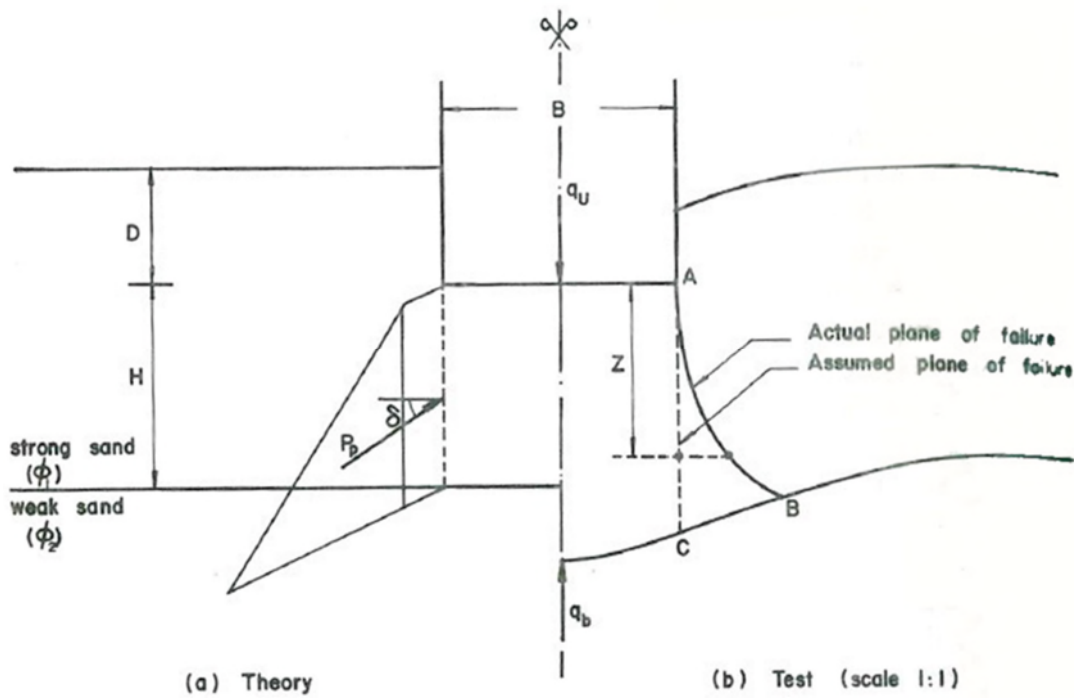


Figure 2. 21 Variation of the angle of inclination (δ) of the passive pressure (P_p) within the upper strong layer (Hanna, 1981).

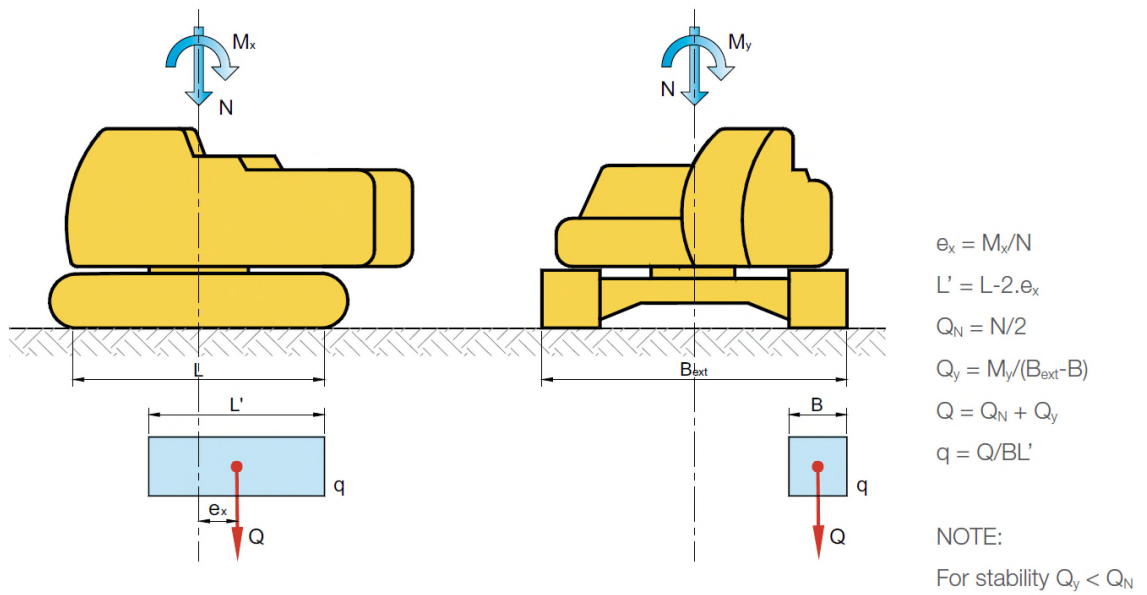


Figure 2. 22 Determination of the single forces acting on each track (Q) and loaded area on which the ground pressure is distributed (TWf, 2019).

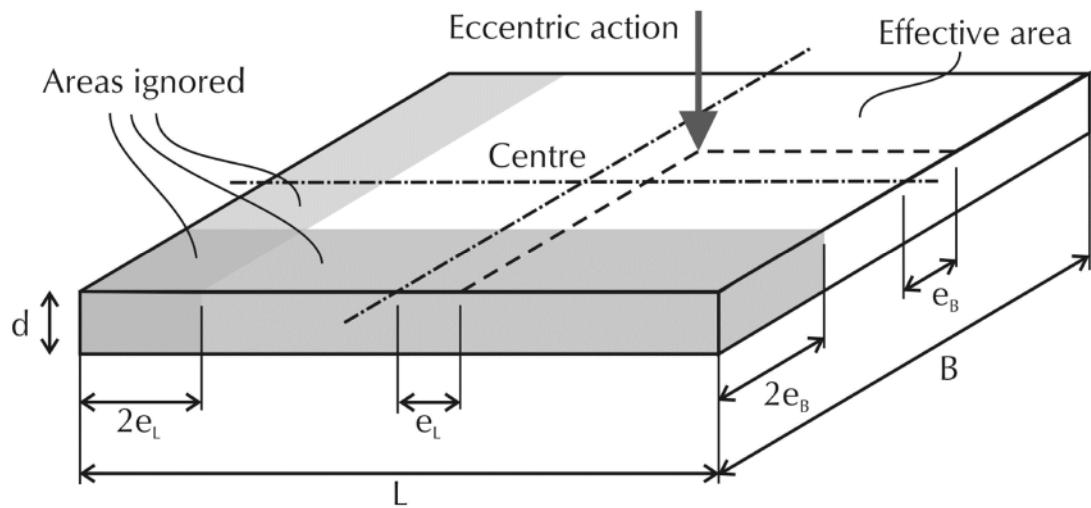


Figure 2. 23 Determination of the effective area of spread foundation (A') (Bond and Harris, 2008).

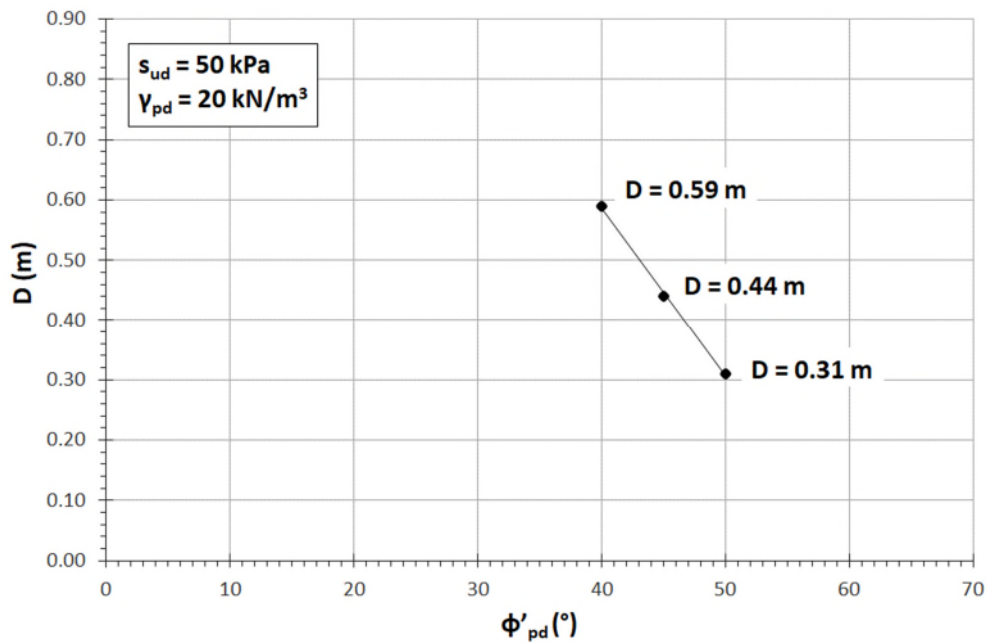


Figure 2. 24 Variation of thickness of platform material (D) with design angle of shearing resistance of the platform (ϕ'_{pd}), at constant design values of undrained shear strength of fine grained subgrade (s_{ud}) and bulk unit weight of platform material (γ_{pd}).

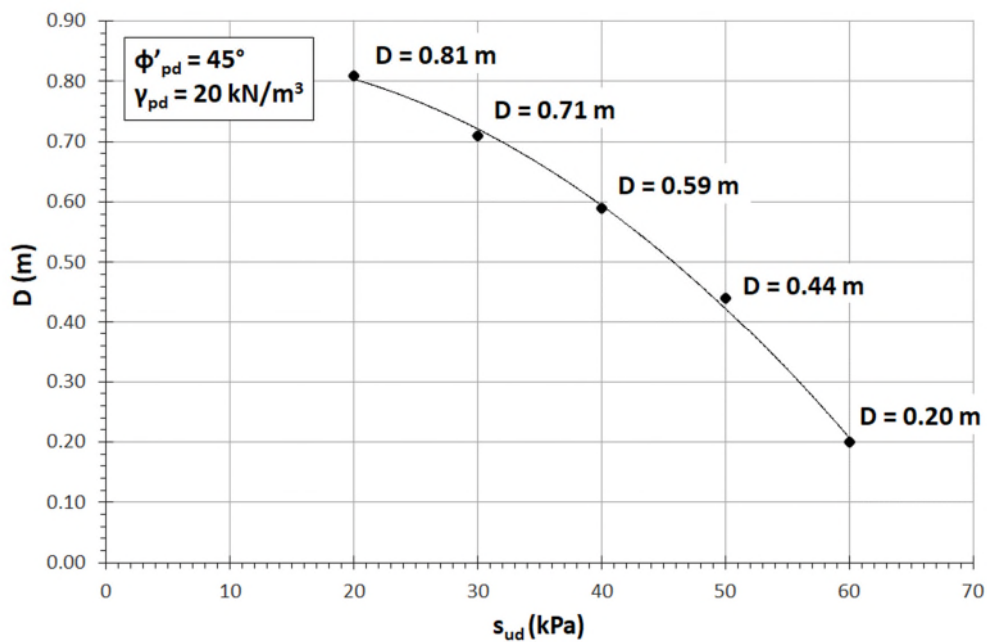


Figure 2. 25 Variation of thickness of platform material (D) with design undrained shear strength of fine grained subgrade (s_{ud}), at constant design values of angle of shearing resistance of the platform (ϕ'_{pd}) and bulk unit weight of platform material (γ_{pd}).

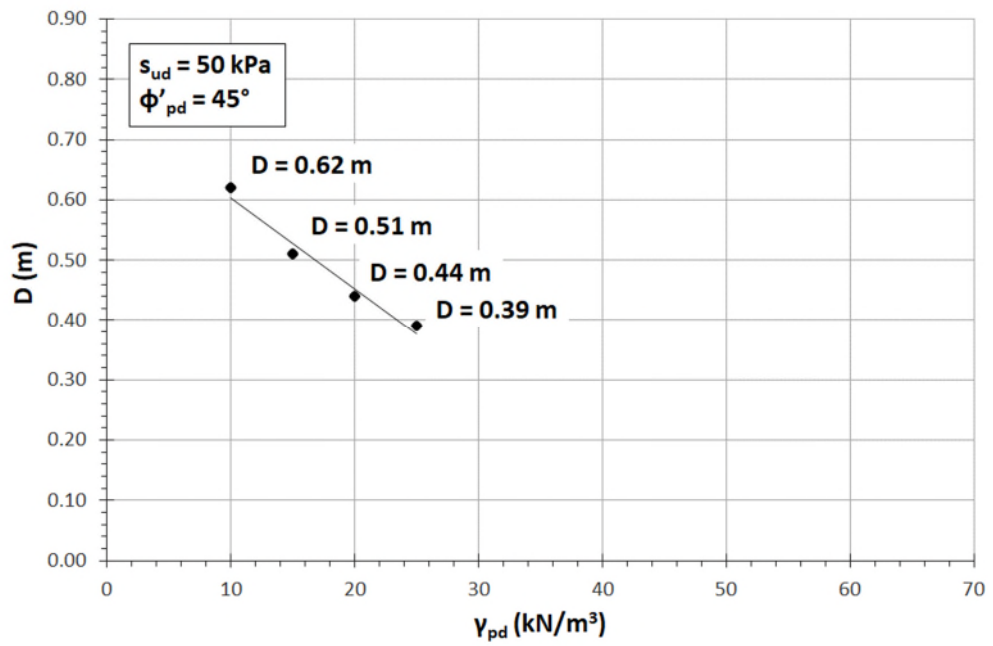


Figure 2. 26 Variation of thickness of platform material (D) with design bulk unit weight of platform material (γ_{pd}), at constant design values of undrained shear strength of fine grained subgrade (s_{ud}) and design angle of shearing resistance of the platform (ϕ'_{pd}).

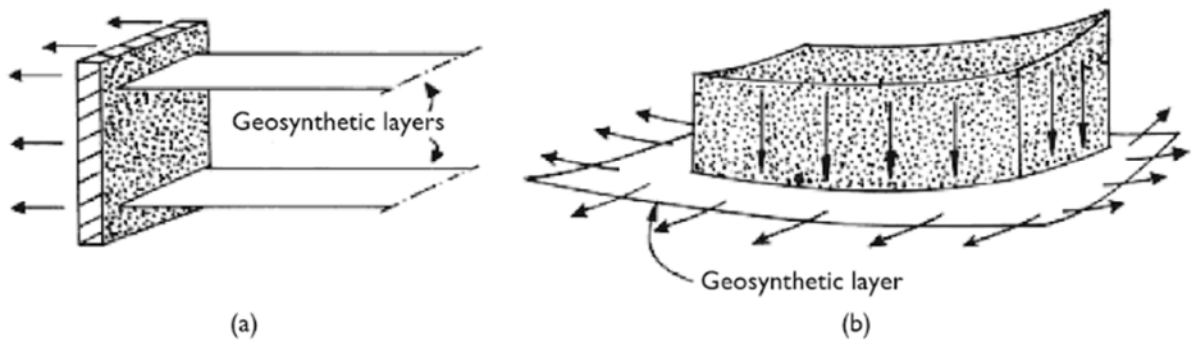


Figure 2. 27 Reinforcement function: (a) tensile member; (b) tension member (Shukla, 2016).

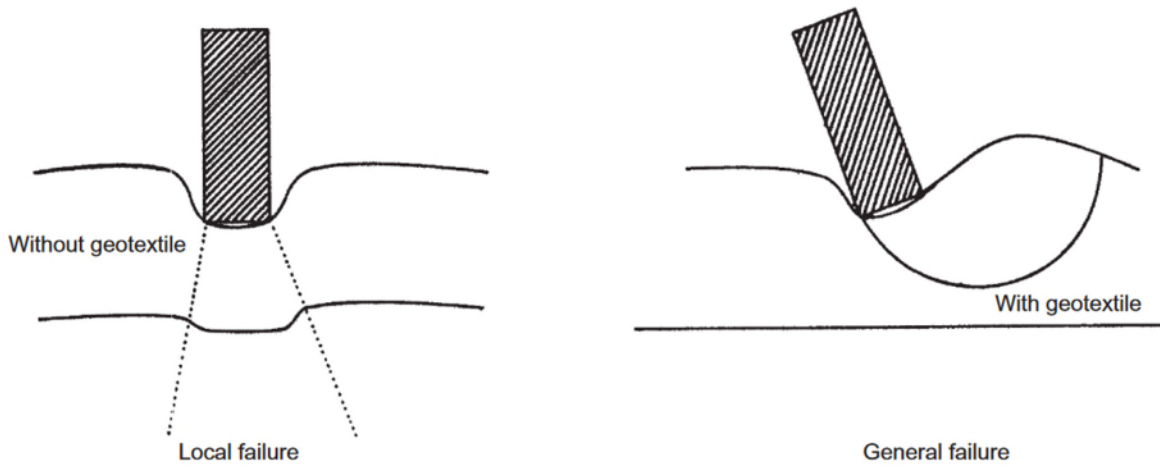


Figure 2. 28 Shear stress reduction effect of geosynthetics (Shukla, 2016).

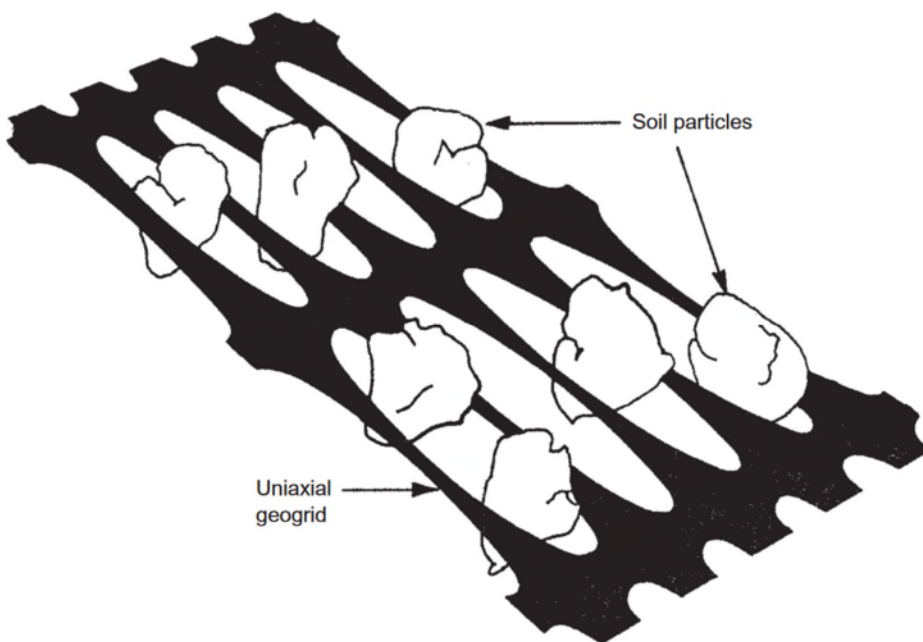


Figure 2. 29 Interlocking effect of geosynthetics (Shukla, 2016).

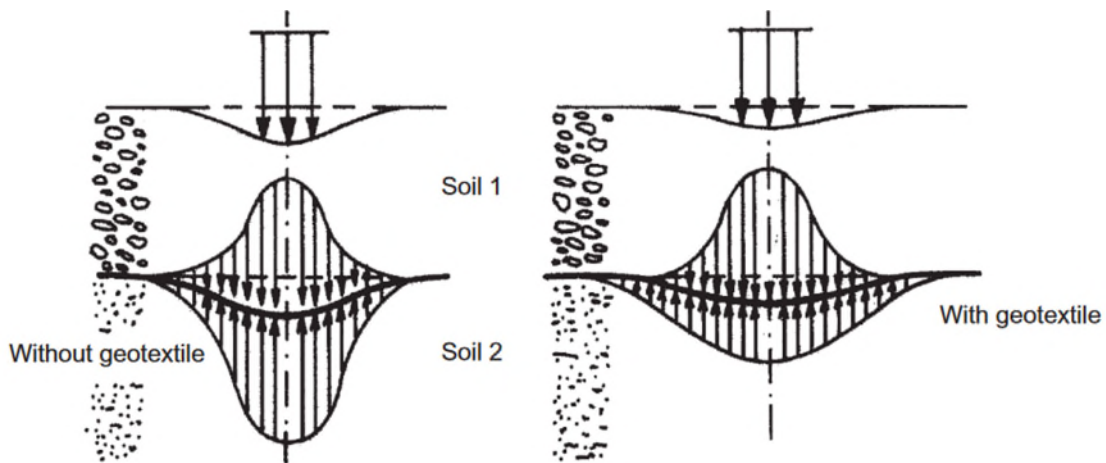


Figure 2. 30 Slab or confinement effect of geosynthetics (Shukla, 2016).

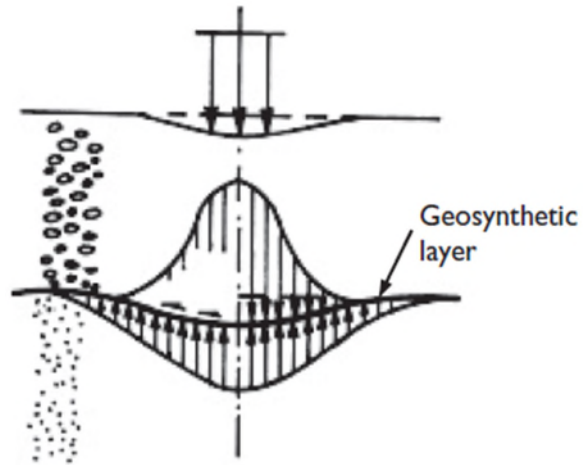


Figure 2. 31 Membrane effect of geosynthetics (Shukla, 2016).

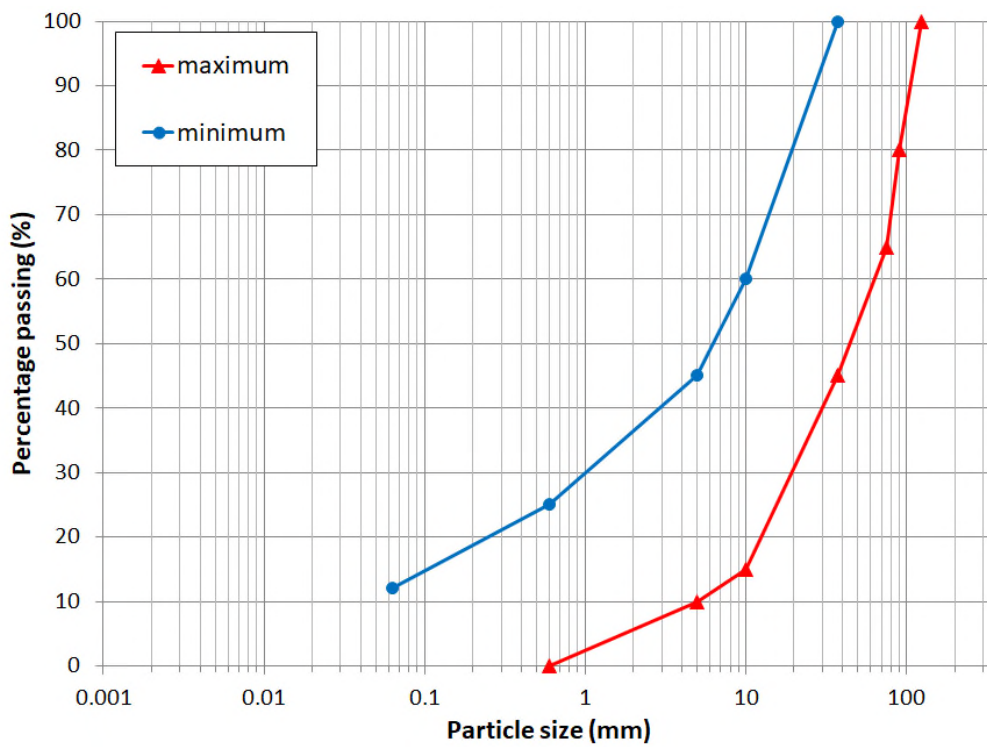


Figure 3. 1 Particle size distribution of 6F2 material, data obtained from Highways Agency (2004).

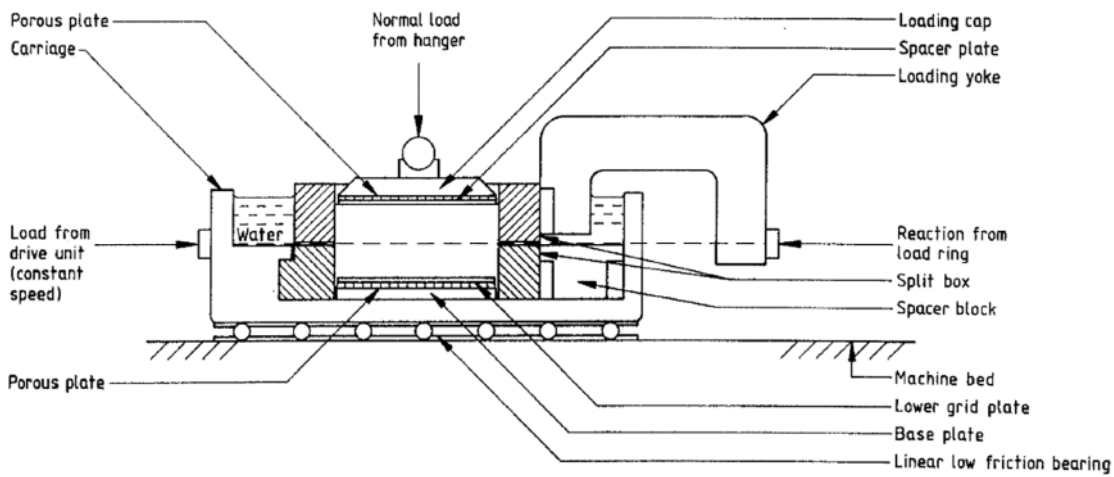


Figure 3. 2 Typical general arrangement of shear box apparatus (BS 1377-7, 1990).

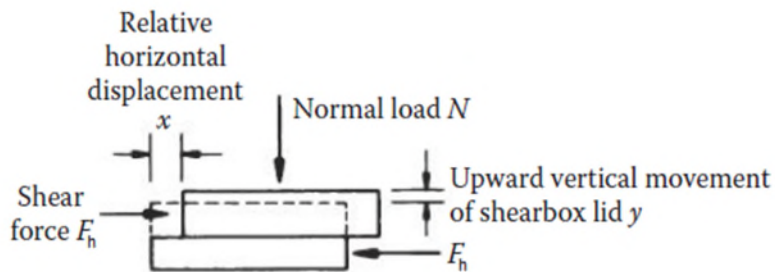


Figure 3. 3 Displacement of the sample during shear (Powrie, 2010).

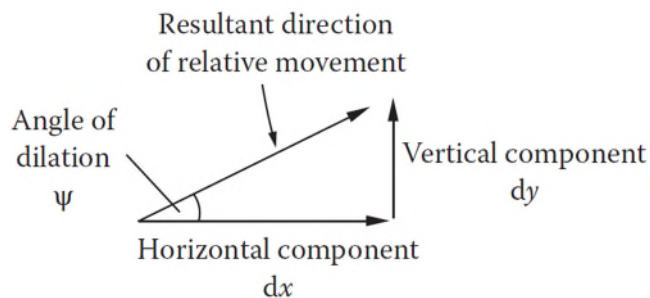


Figure 3. 4 Definition of angle of dilation $\psi = \tan^{-1}(dy/dx)$ from the relative horizontal (dx) and vertical (dy) displacement of the shear box lid during the test (Powrie, 2010).

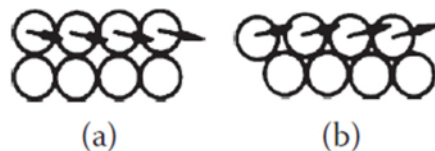


Figure 3. 5 Conceptual model for: (a) compression of an initial loose sample and (b) dilation of an initial dense sample during shear (Powrie, 2010).

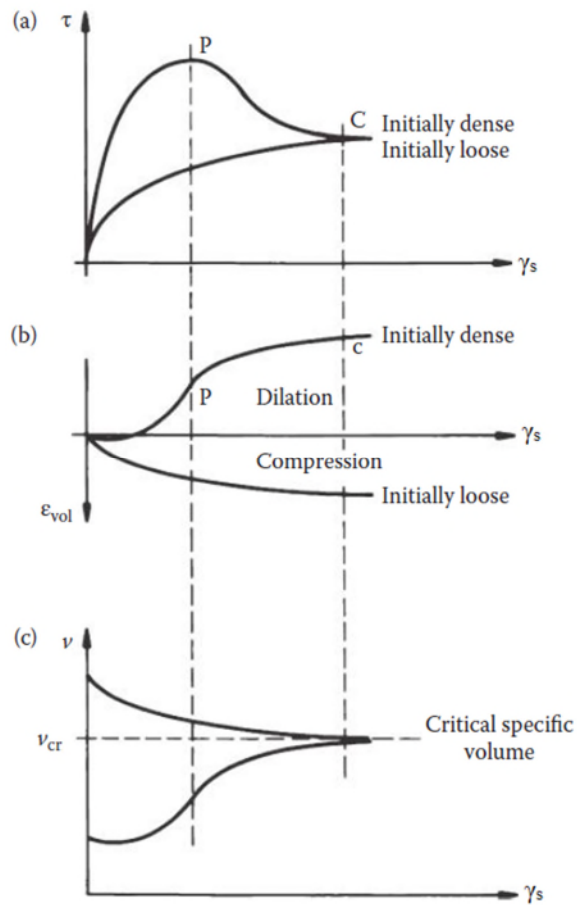


Figure 3. 6 Idealised shear box results conducted under the same value of normal effective stress (σ'_v) on an initial dense and loose sample, showing (a) variation of shear stress (τ) with the sample strain (γ_s), (b) variation of volumetric strain (ϵ_{vol}) with strain (γ_s) and (c) variation of specific volume with strain (γ_s) (Powrie, 2010).

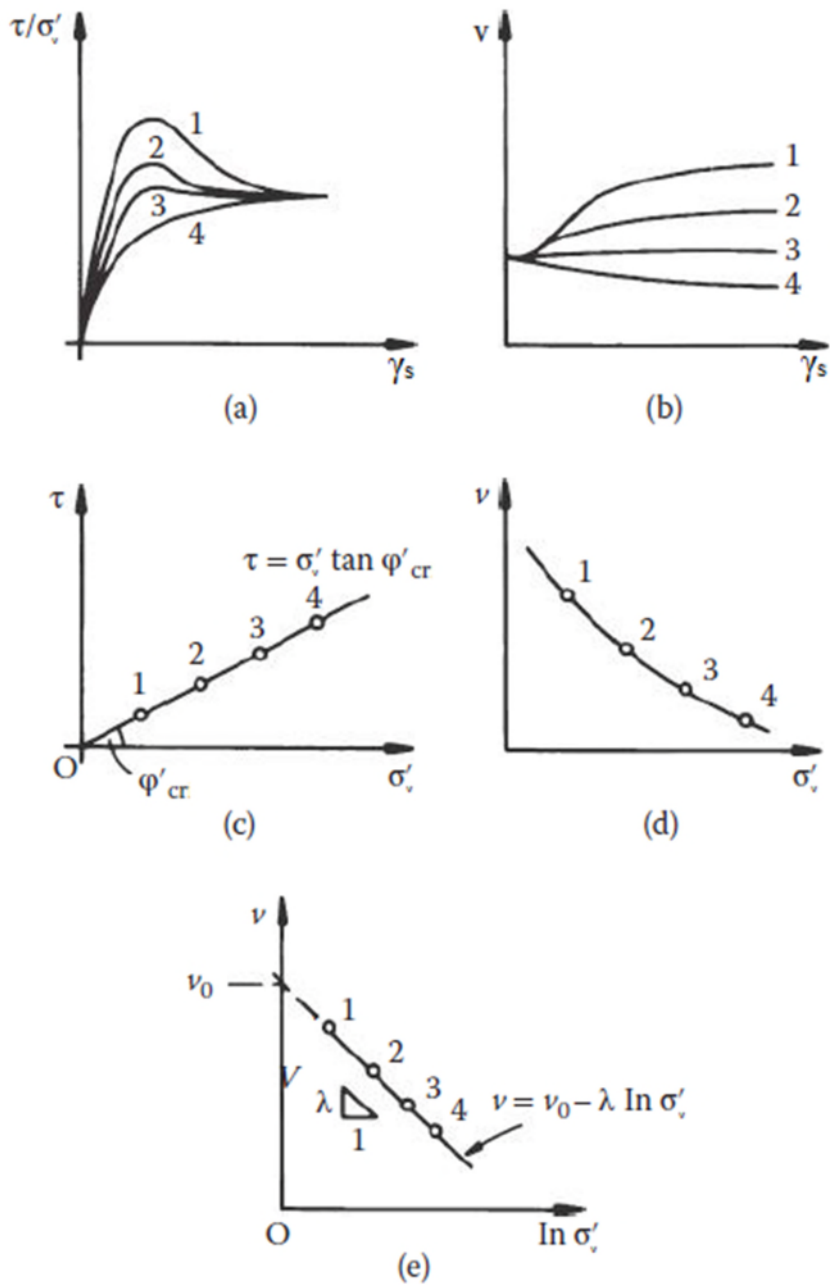


Figure 3.7 Idealised results from shear box tests, carried out at different normal effective stresses, on four samples having the same initial void ratio: (a) stress ratio τ/σ'_v vs. γ_s ; (b) specific volume v vs. γ_s ; (c) critical states (end points of tests); τ vs. σ'_v ; (d) critical states; v vs. σ'_v ; (e) critical states; v vs. $\ln \sigma'_v$ (Powrie, 2010).

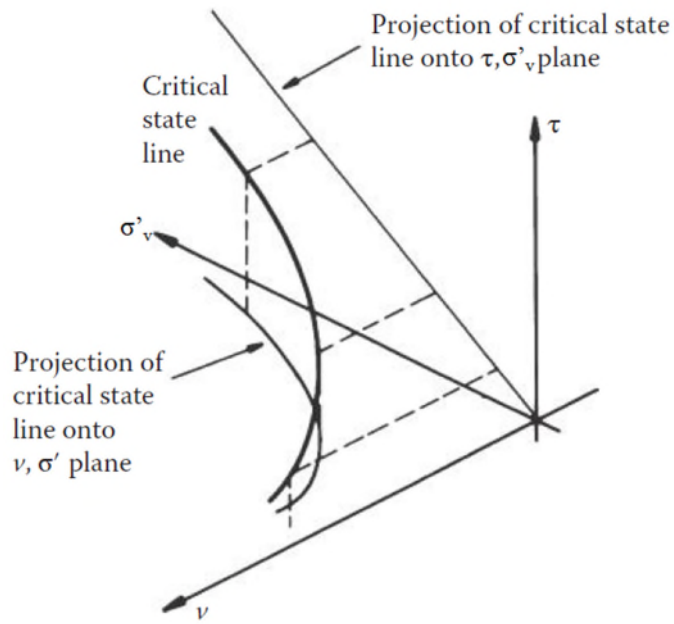


Figure 3. 8 Critical state line in (σ'_v, τ, v) space with projections onto (τ, σ'_v) and (v, σ'_v) planes (Powrie, 2010).

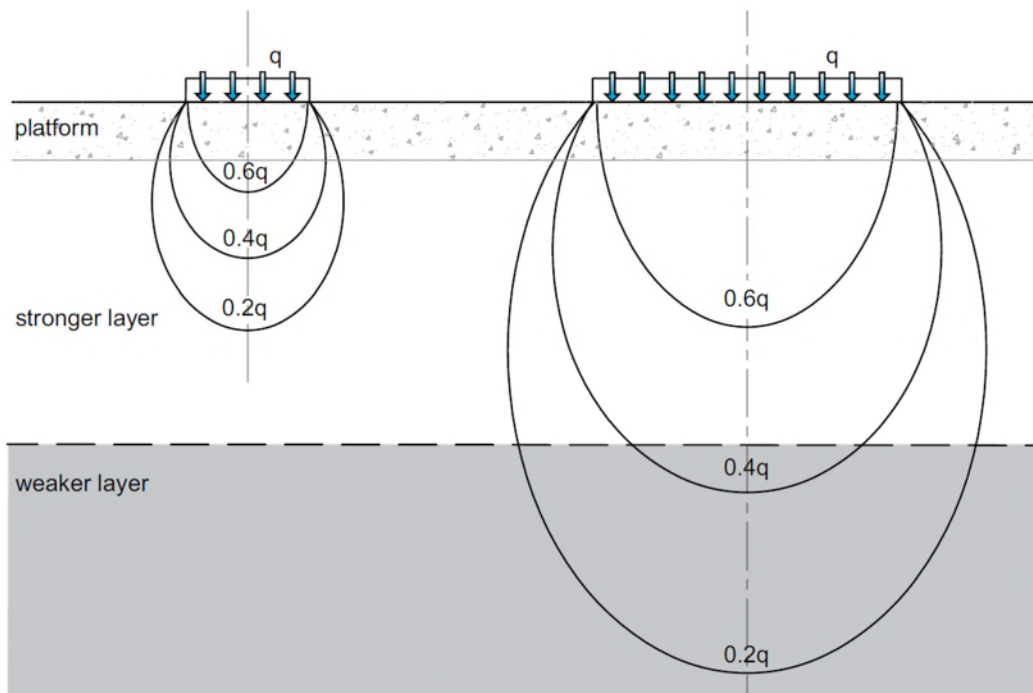


Figure 3. 9 Depth of influence defined by pressure bulbs generated by the Boussinesq formula (TWf, 2019).

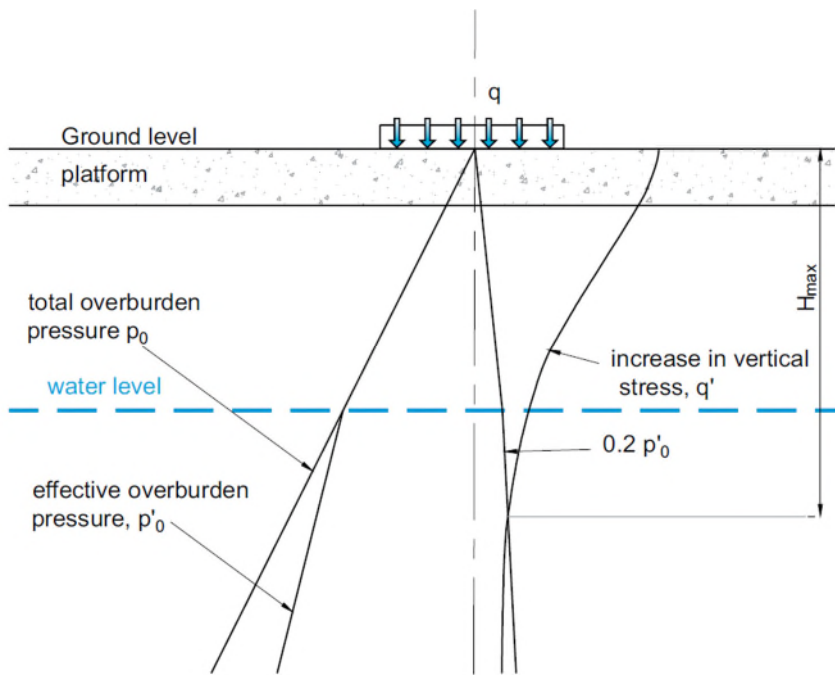


Figure 3. 10 Depth of influence for settlement defined by effective overburden pressure (p'_0) and increase in vertical stress (q') (TWf, 2019).

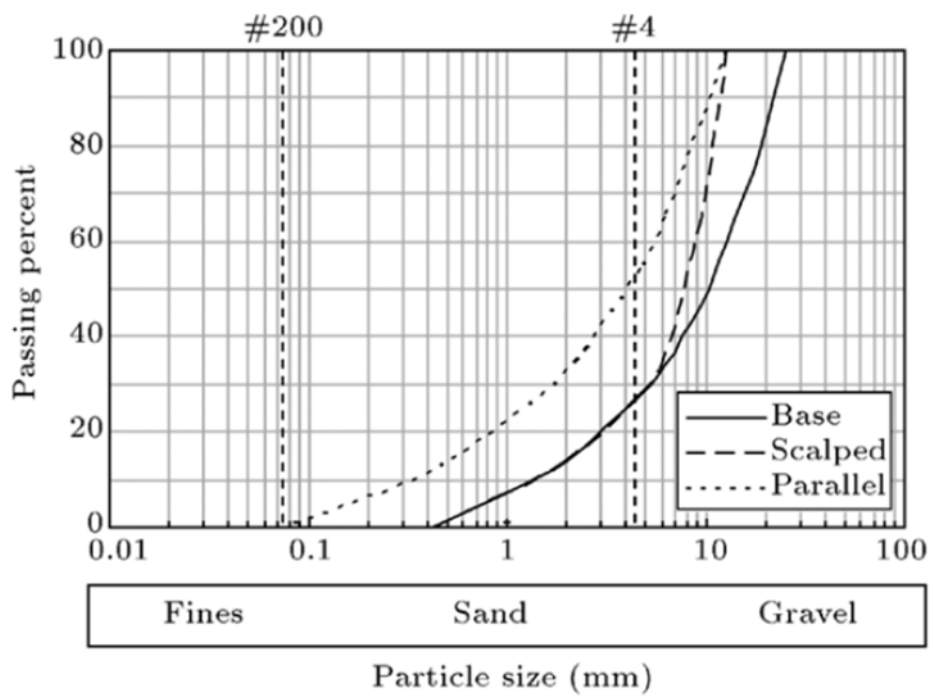


Figure 3. 11 Grading curves for the base, scalped and parallel gradations (Hamidi *et al.*, 2012).

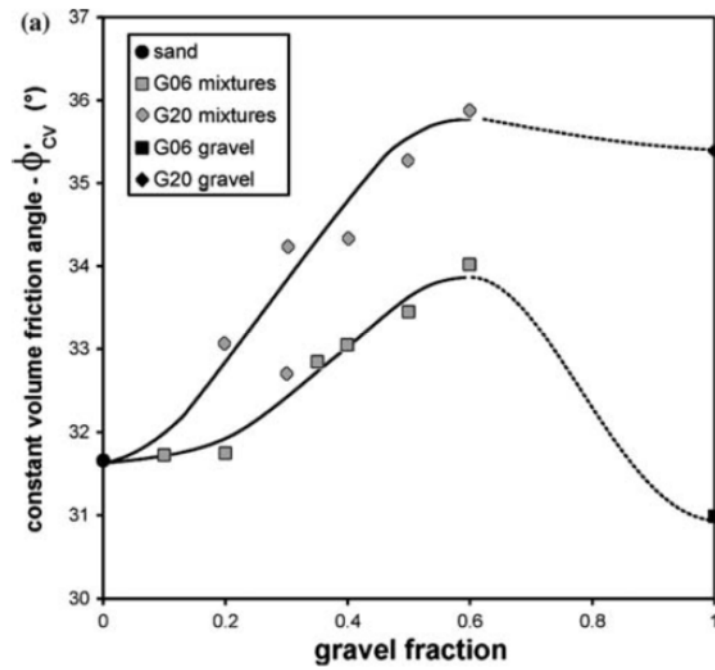


Figure 3. 12 Results of critical state friction angle determination versus gravel fraction (Simoni and Houlsby, 2006).

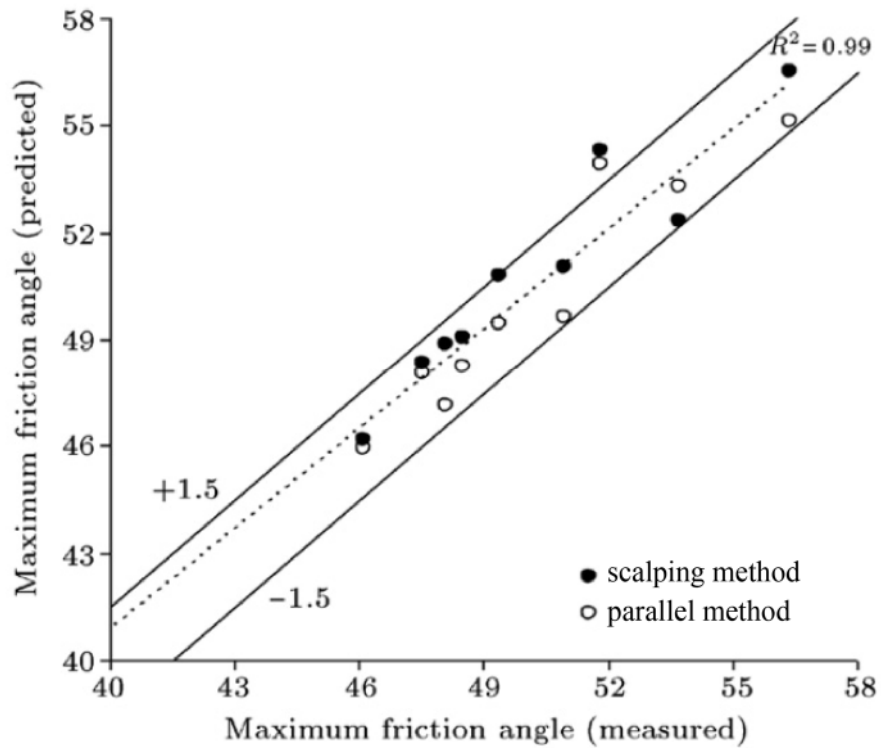


Figure 3. 13 Comparison of results between experiments and empirical equations for maximum friction angle of sample tested at three different relative densities and three different surcharge pressures (Hamidi *et al.*, 2012).

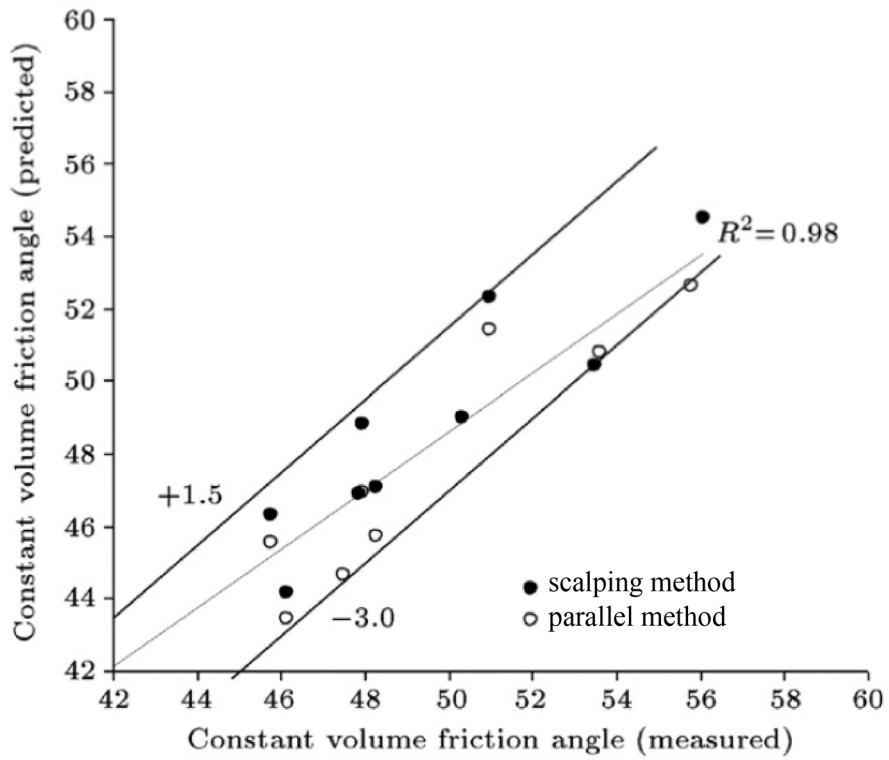


Figure 3. 14 Comparison of results between experiments and empirical equations for constant volume friction angle of sample tested at three different relative densities and three different surcharge pressures (Hamidi *et al.*, 2012).

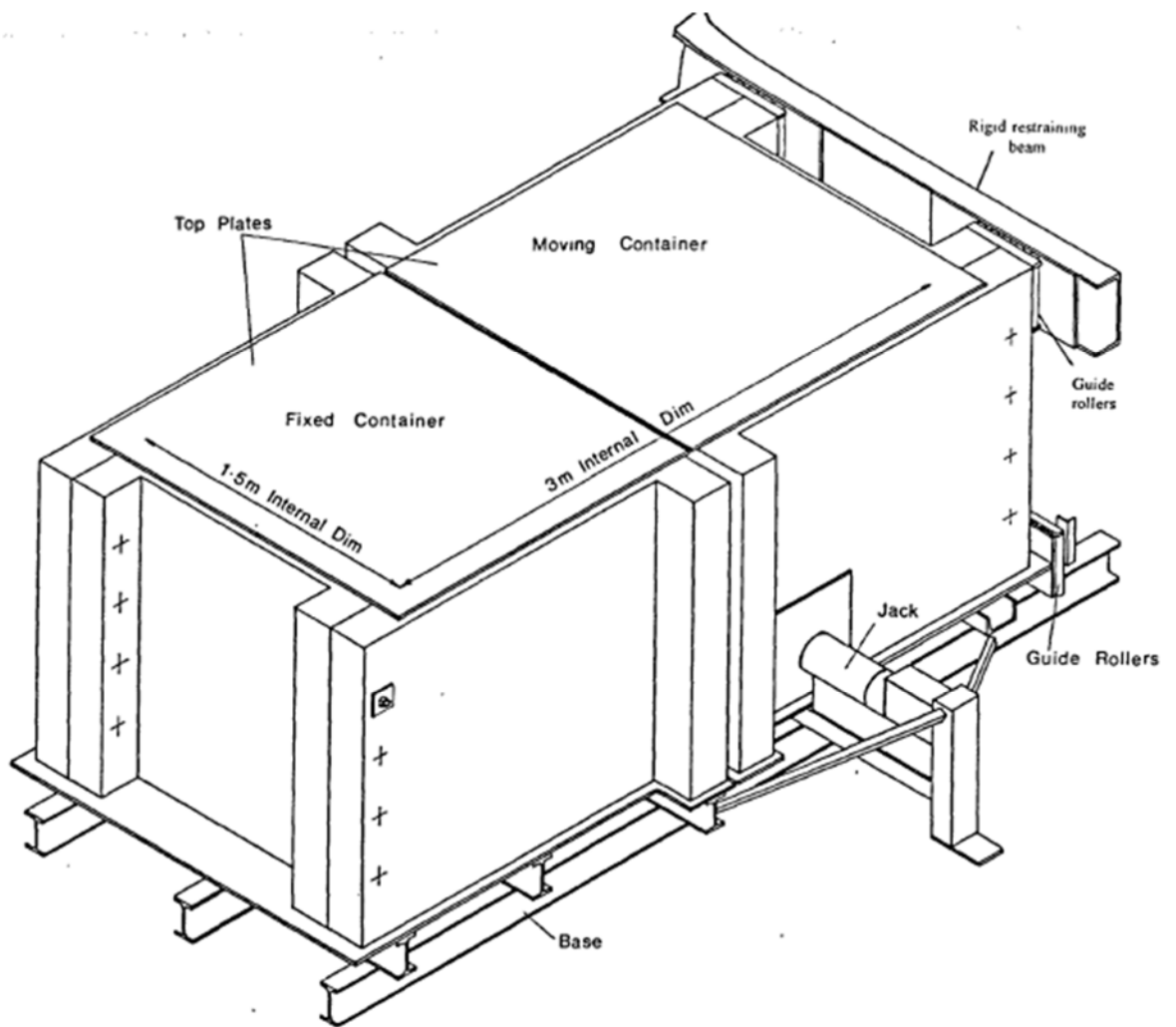


Figure 3. 15 Major features of the concrete shear box designed and manufactured at the University of Wales, College of Cardiff (Jacobs, 1993).

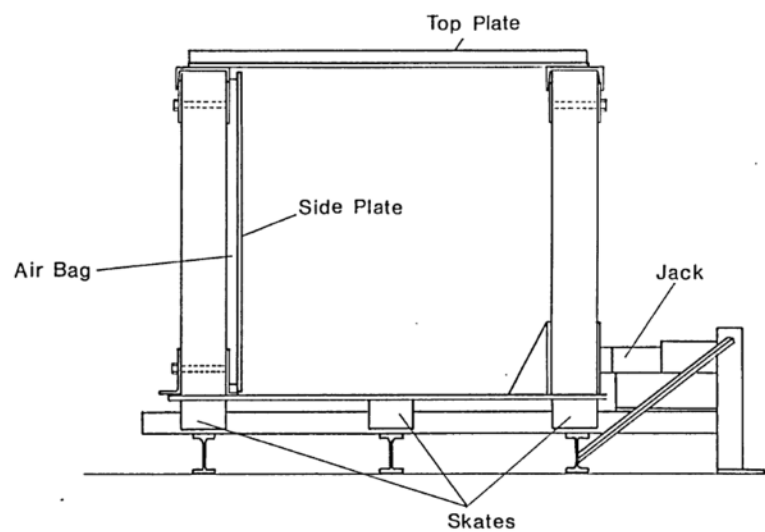


Figure 3. 16 Section through the concrete shear box designed and manufactured at the University of Wales, College of Cardiff (Jacobs, 1993).

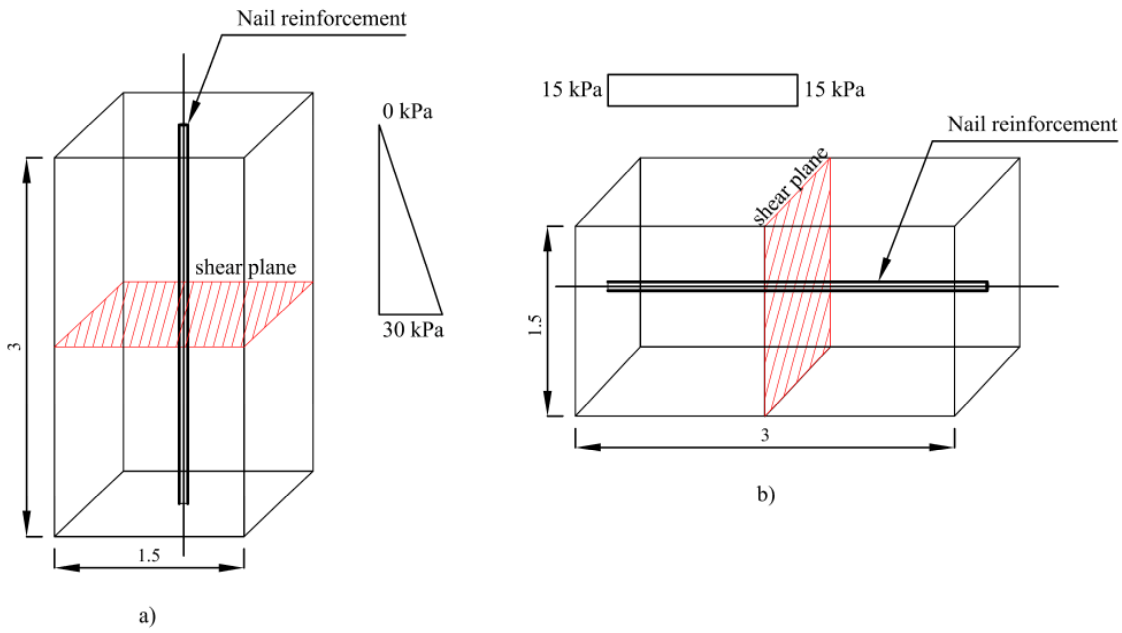


Figure 3. 17 Variation of the vertical stress in the direction of the nail reinforcement in case of (a) horizontal and (b) vertical shear plane alignment.

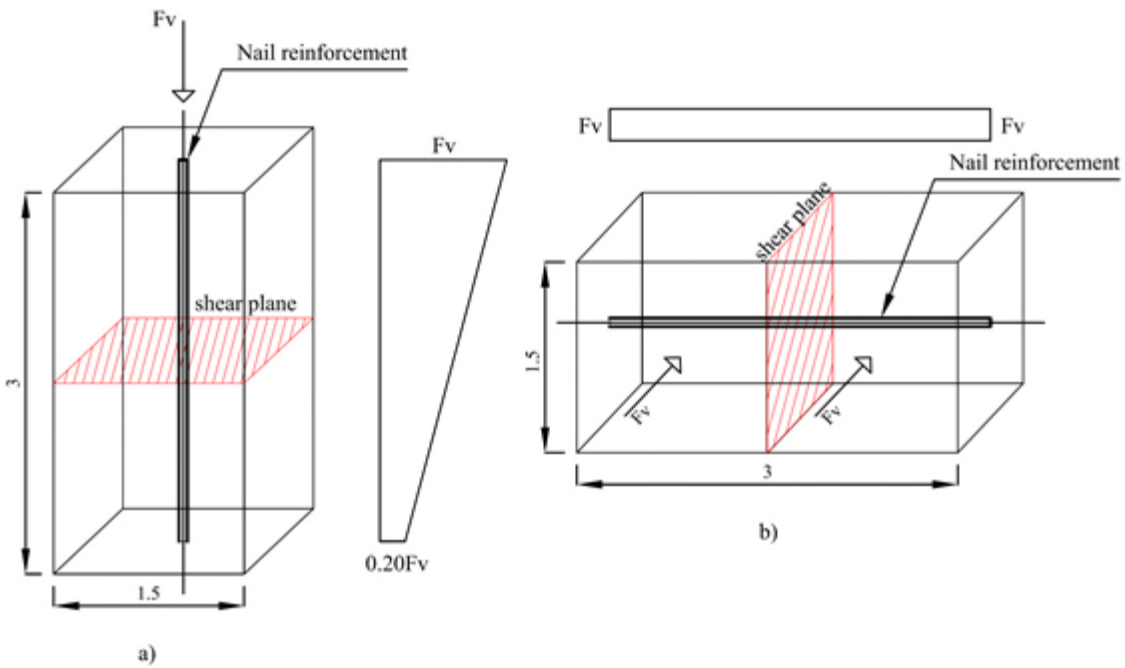


Figure 3. 18 Variation of the normal stress along the nail in case of (a) horizontal and (b) vertical shear plane alignment.

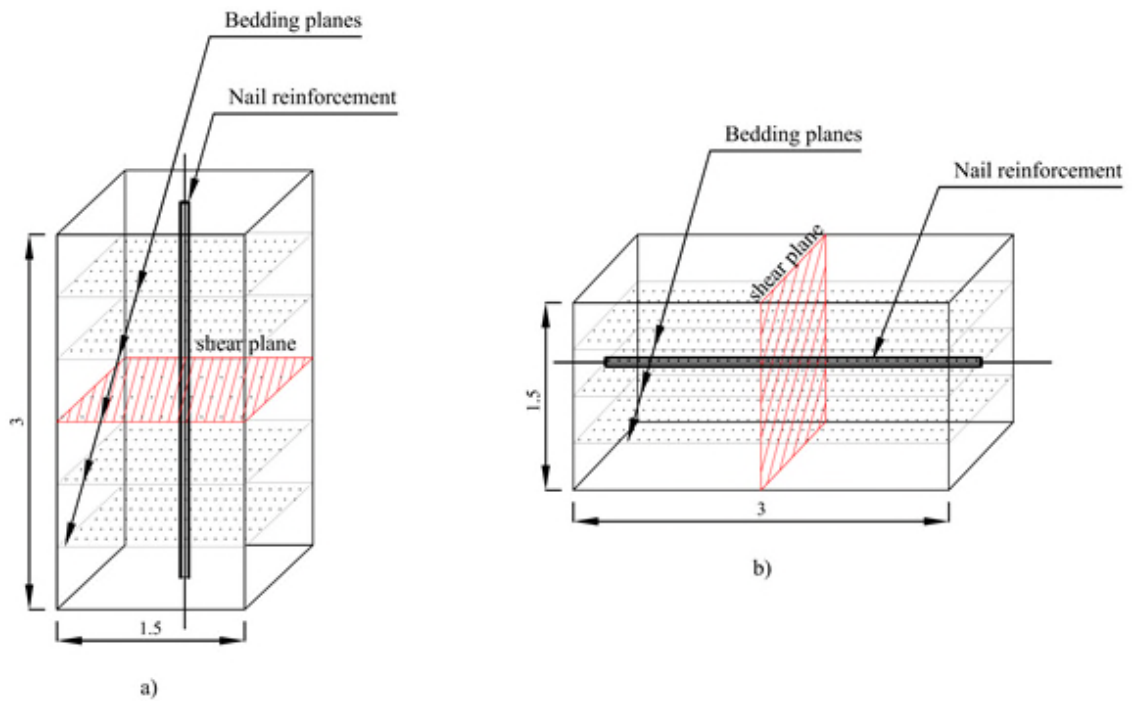


Figure 3. 19 Variation of the bedding planes distribution in the shear box in case of (a) horizontal and (b) vertical shear plane alignment.

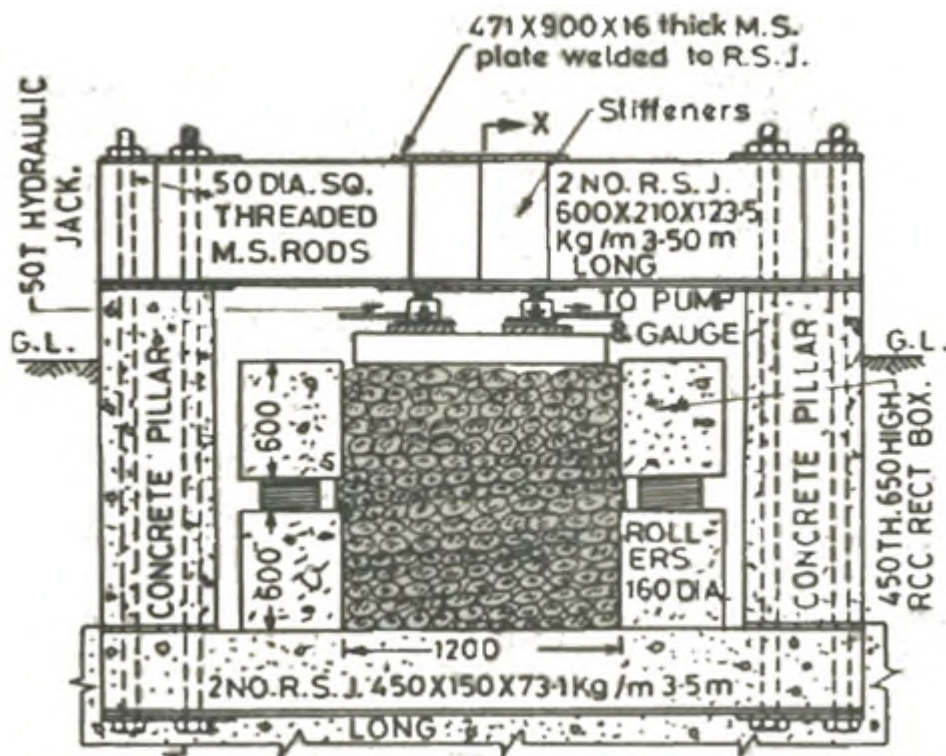


Figure 3. 20 Compression system of the Jain and Gupta (1975) shear box.

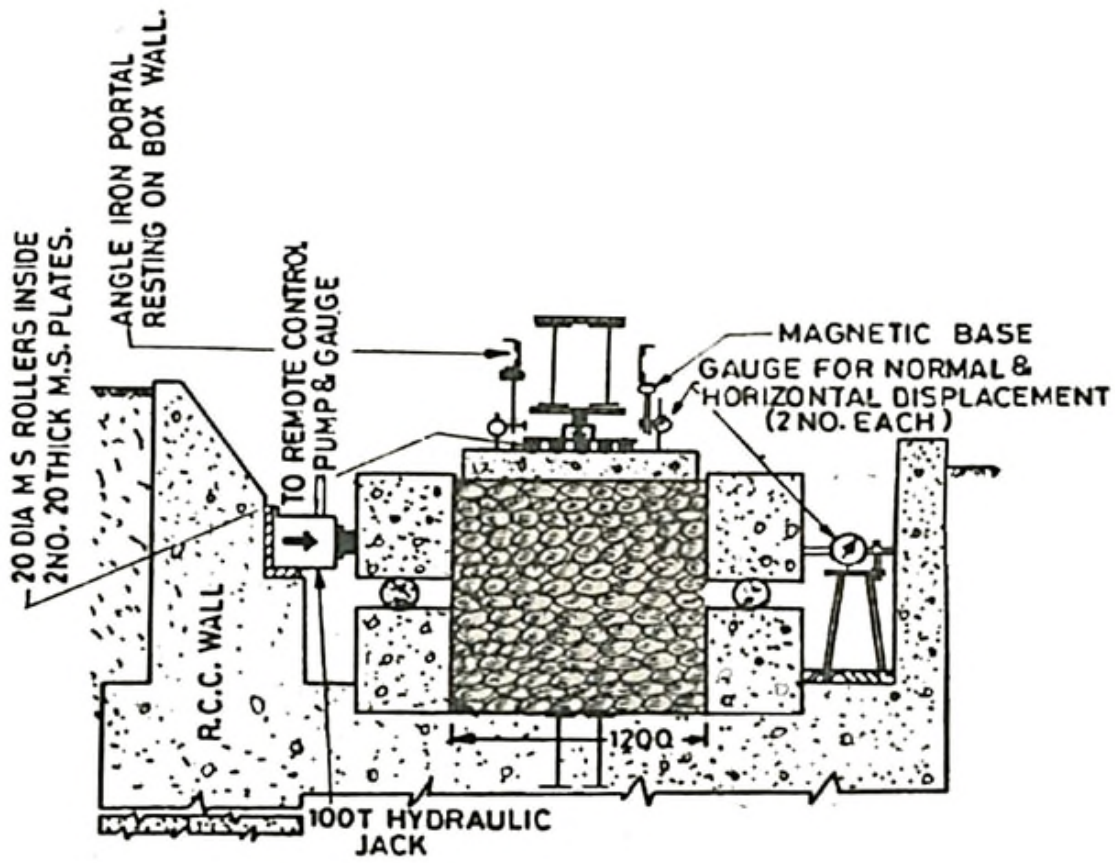


Figure 3. 21 Shear system of the Jain and Gupta (1975) shear box.

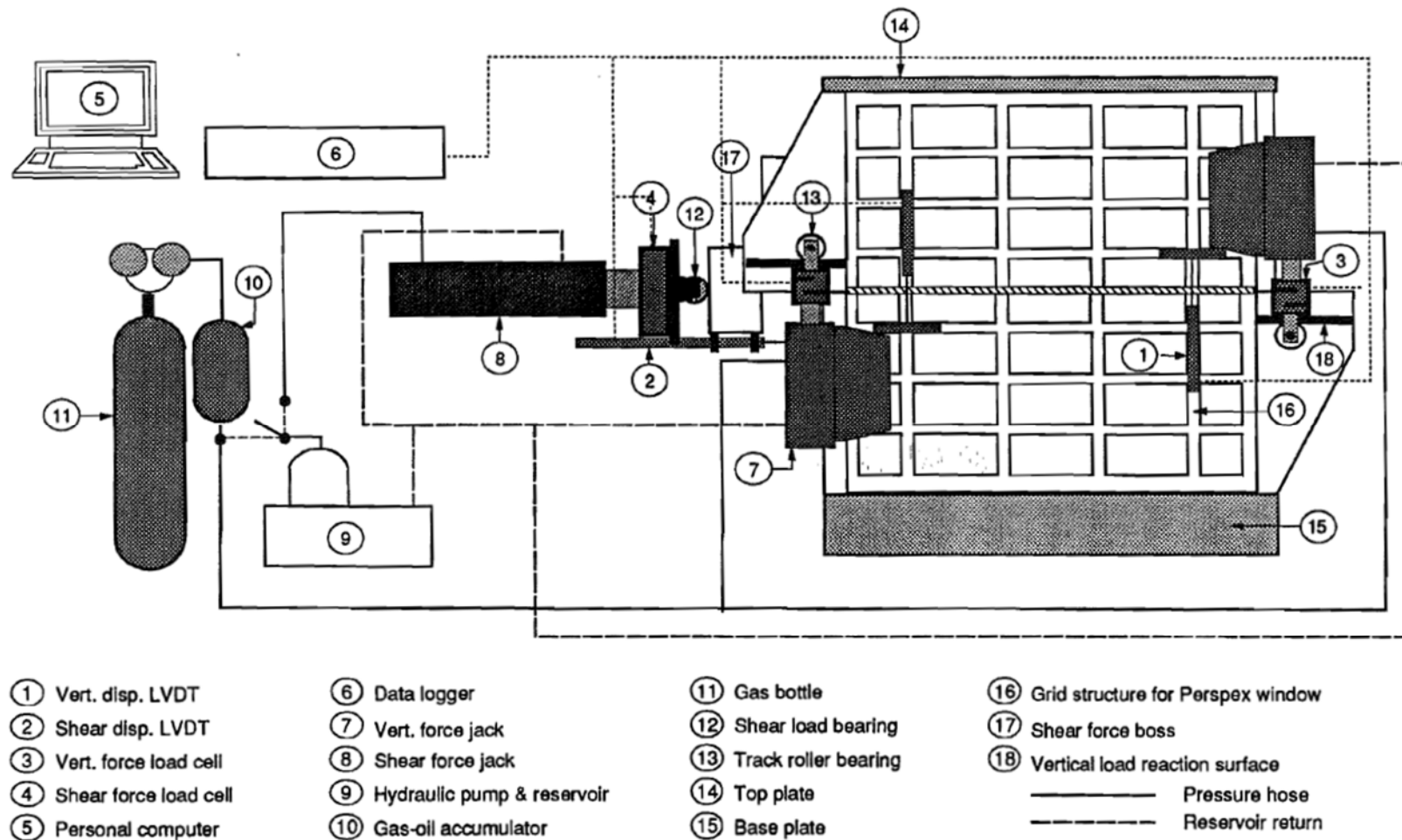


Figure 3. 22 Pedley (1990) shear box.

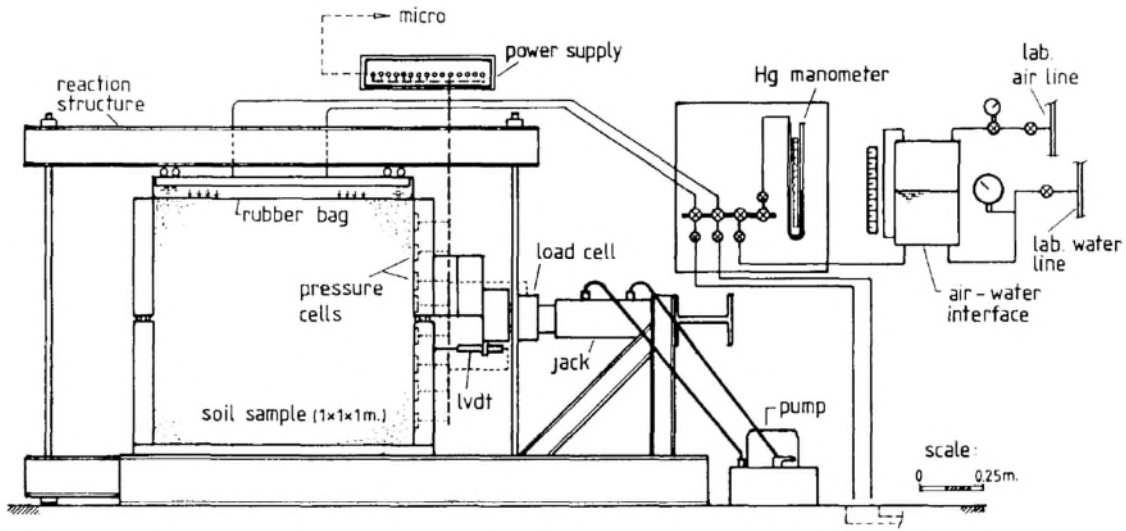


Figure 3. 23 Palmeira (1987) shear box.



Figure 3. 24 Krahan *et al.* (2007) shear box.



Figure 3. 25 Santana and Estaire (2019) shear box (Estaire and Olalla, 2006).

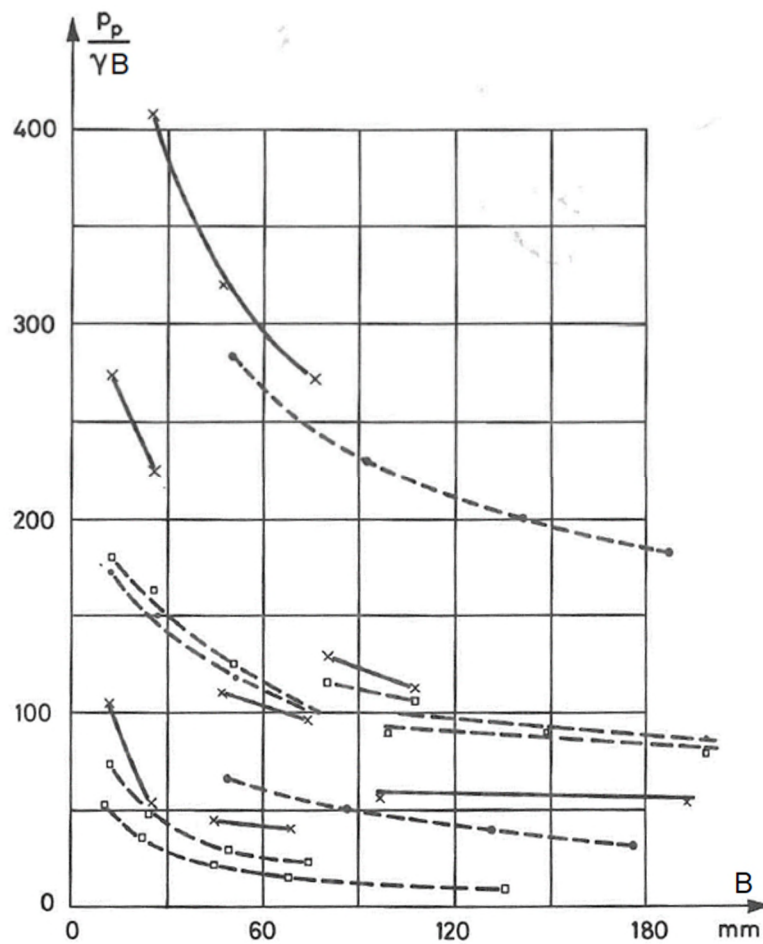


Figure 3. 26 Dimensionless peak loads (peak load measured during test (P_p) normalised by the unit weight of the soil (γ) and diameter of footing (B)) against plate diameter (B) (Ovesen, 1979).

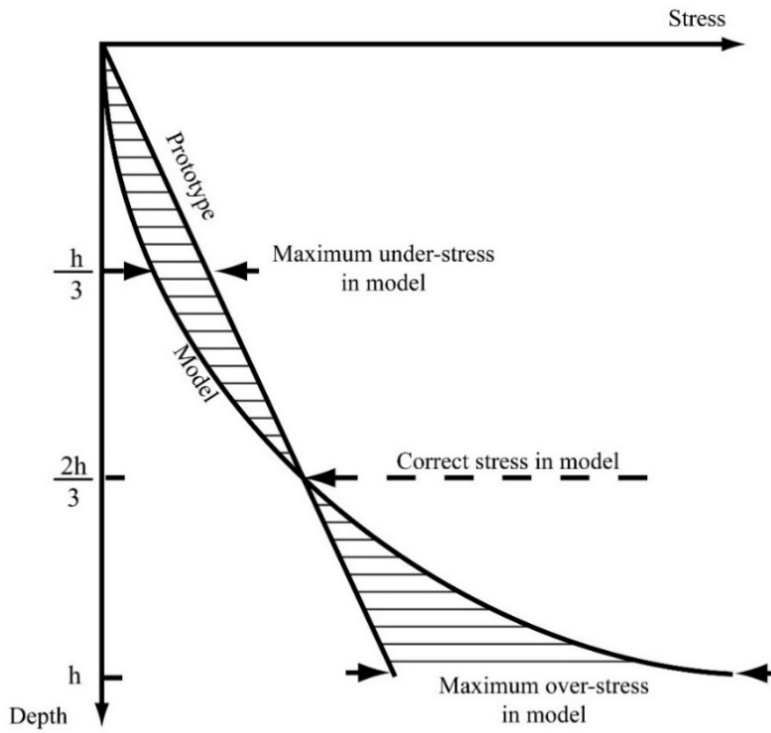


Figure 3.27 Comparison of stress variation with depth (h) in a centrifuge model and its corresponding prototype (Taylor, 1995).

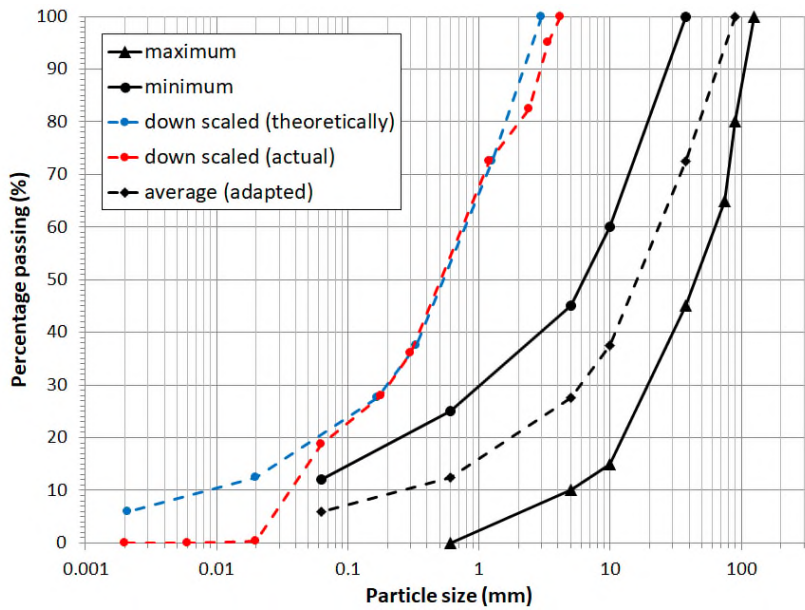


Figure 4.1 Grading curves representing minimum - maximum particle size values for 6F2 (solid black lines) and the particle size distribution chosen to be scaled down for the test material (dashed black line). Dashed red line indicates the effective grading curve of the sample with maximum particle size of 3.35 mm.

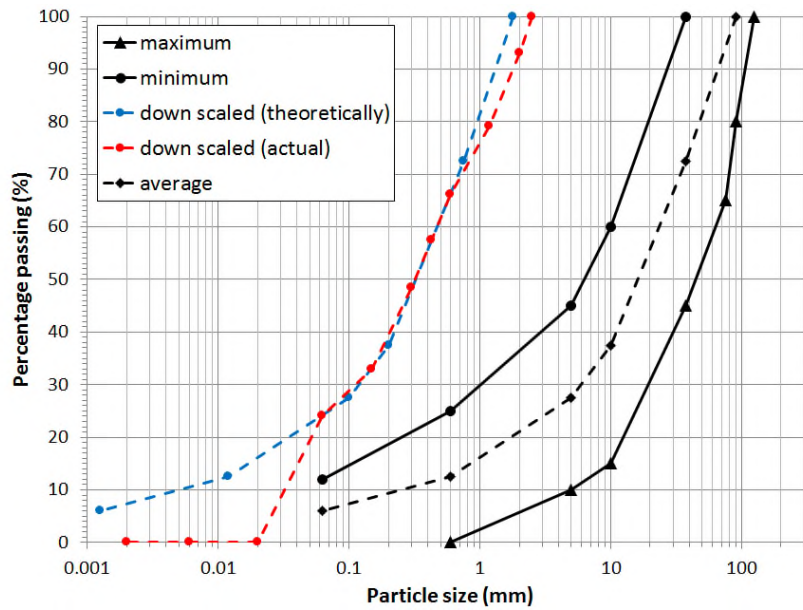


Figure 4. 2 Grading curves representing minimum - maximum particle size values for 6F2 (solid black lines) and the particle size distribution chosen to be scaled down for the test material (dashed black line). Dashed red line indicates the effective grading curve of the sample with maximum particle size of 2 mm.

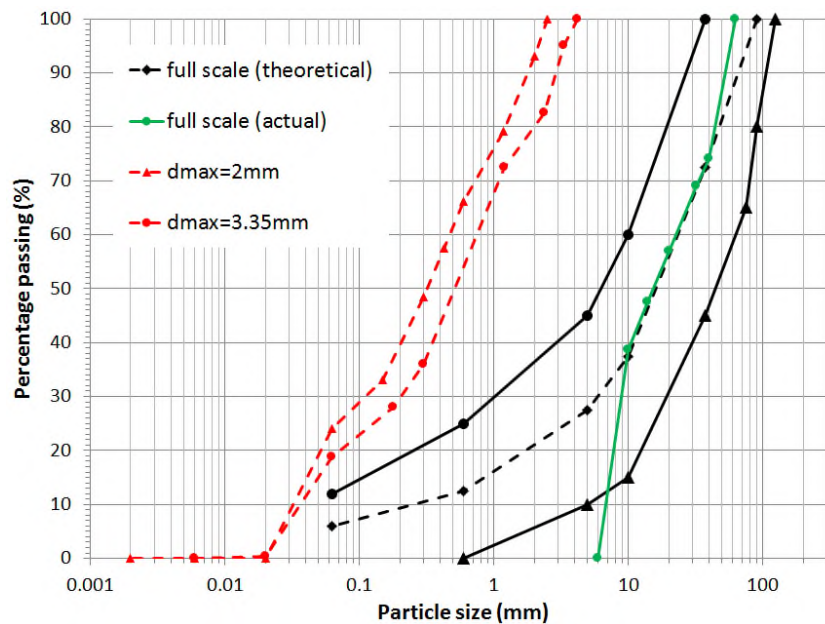


Figure 4. 3 Grading curves representing minimum - maximum particle size values for 6F2 (solid black lines) and the particle size distribution chosen to be scaled down for the test material (dashed black line). Dashed red lines indicates the effective grading curve of the samples used for small scale tests having a maximum particle size of 2 mm and 3.35 mm. In green is the grading curve of the material used for large scale shear box tests.

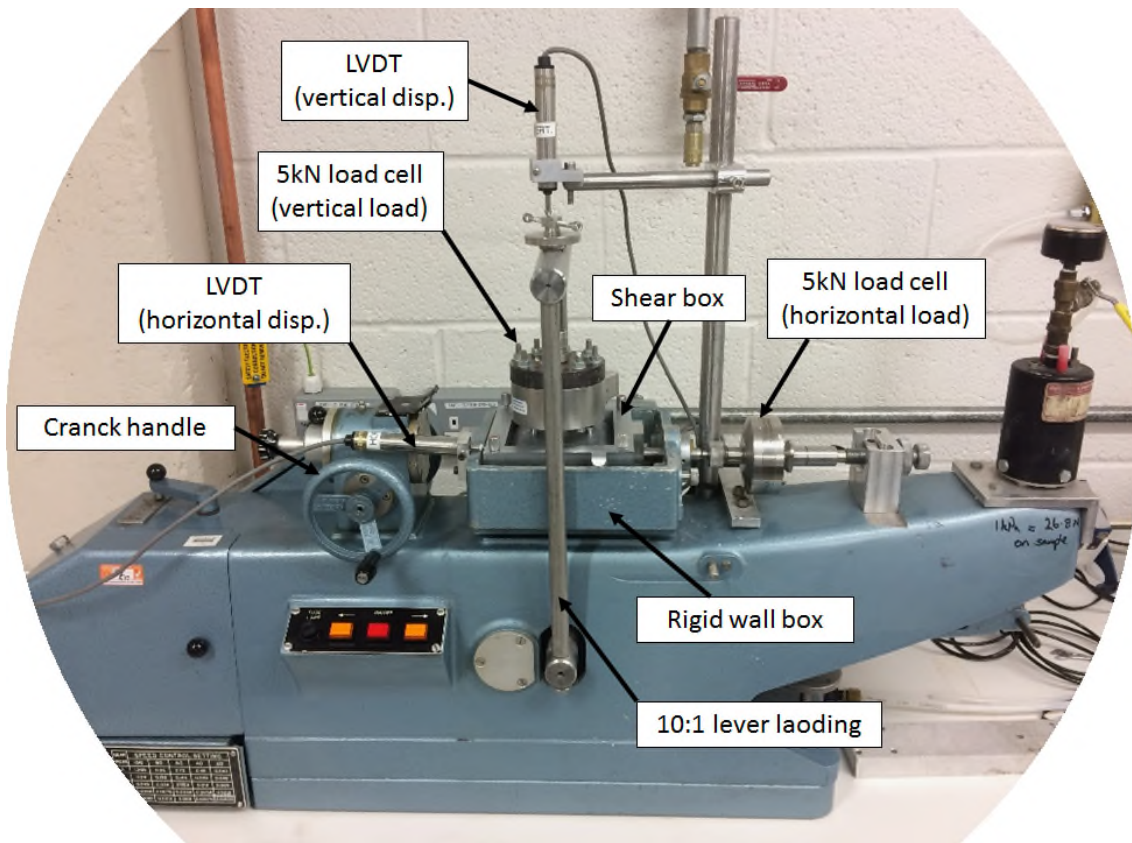


Figure 5. 1 Standard direct shear box test apparatus at City, University of London.

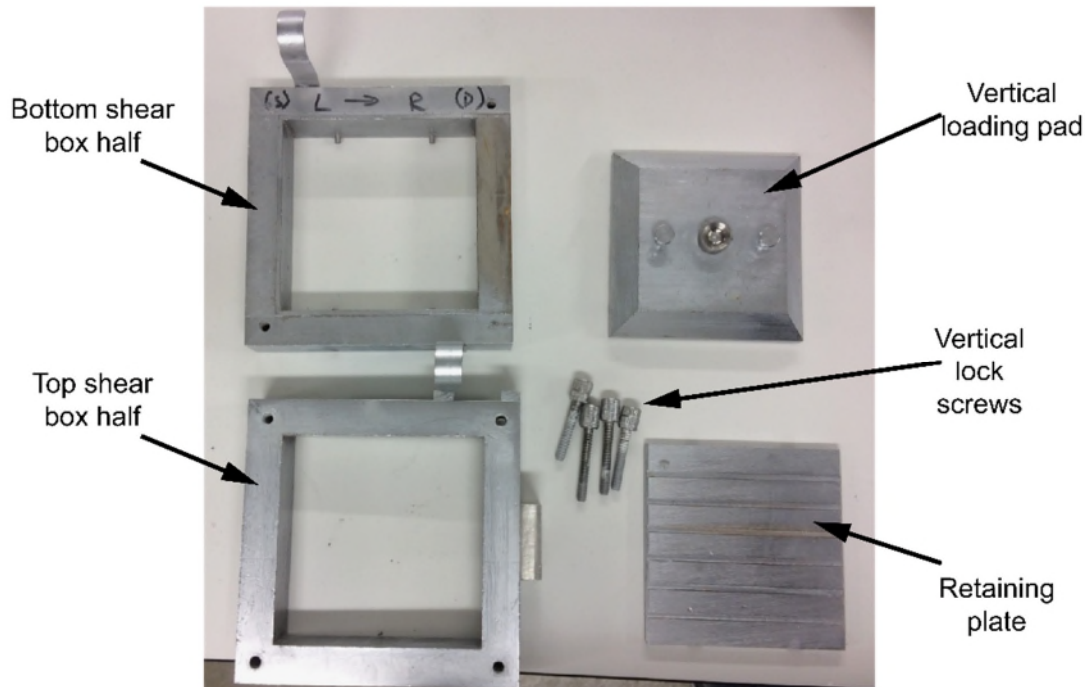


Figure 5. 2 Main components of the 100 x 100 mm shear box used for standard tests at City, University of London.

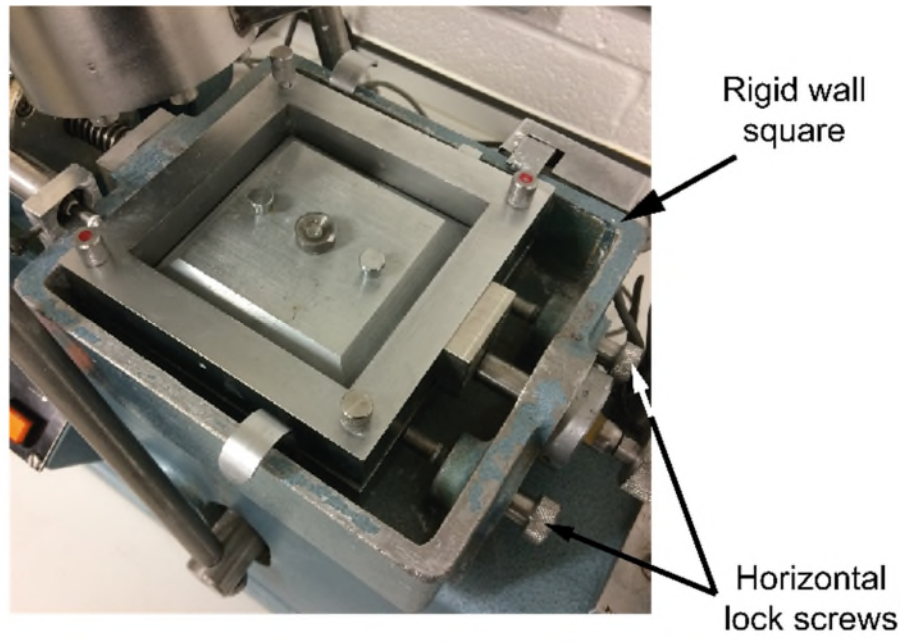


Figure 5. 3 Shear box components placed in the rigid wall square and fixed by two horizontal screws.

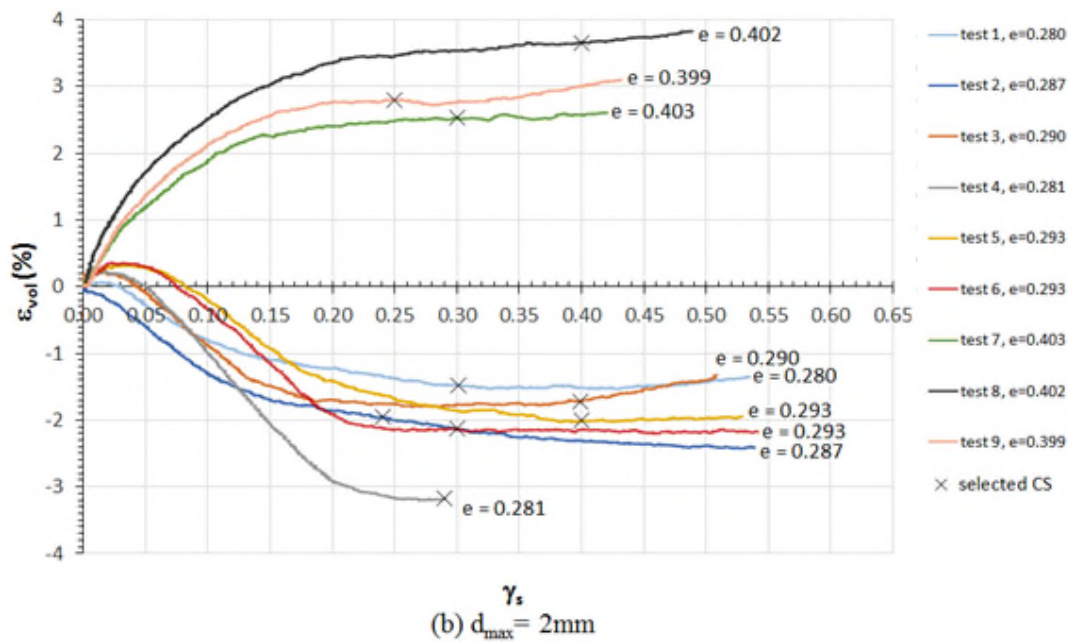
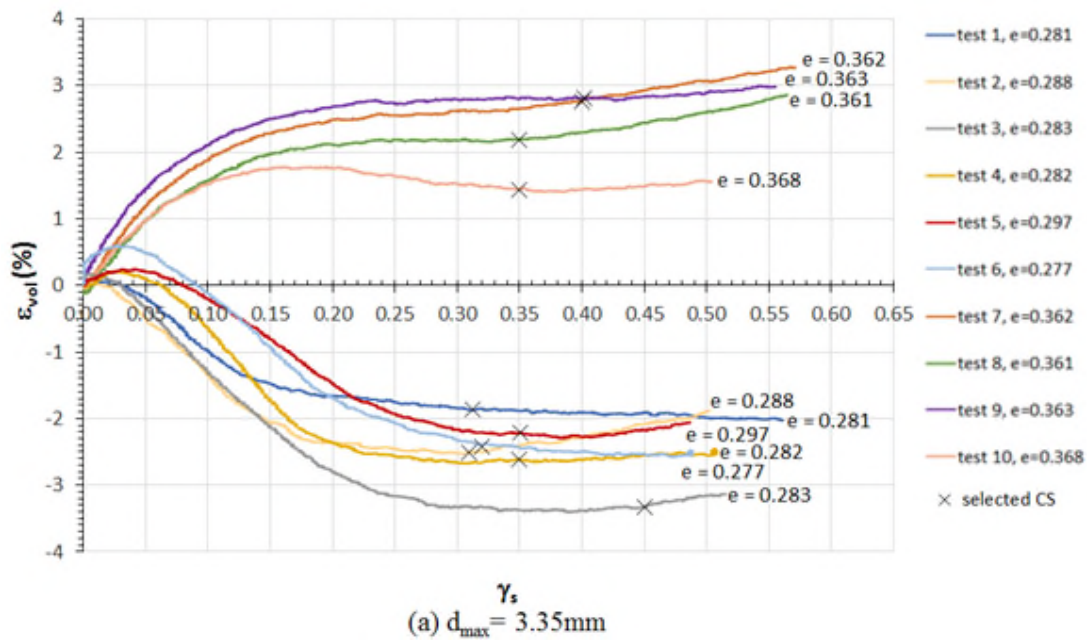


Figure 5. 4 Volumetric strain (ϵ_{vol}) versus shear strain (γ_s) results for standard shear box tests conducted at 100 kPa and 200 kPa vertical stress on dense samples and at 500 kPa on looser samples of limestone material with maximum particle size equal to (a) 3.35 mm and (b) 2 mm. Cross sign indicates where the values of critical state were selected for each test.

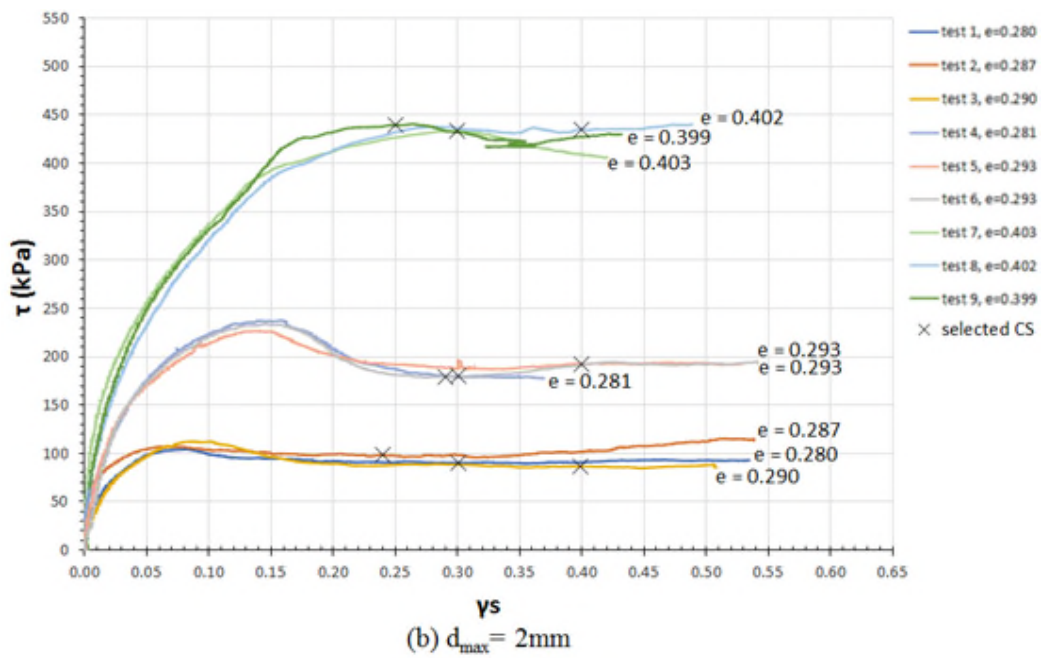
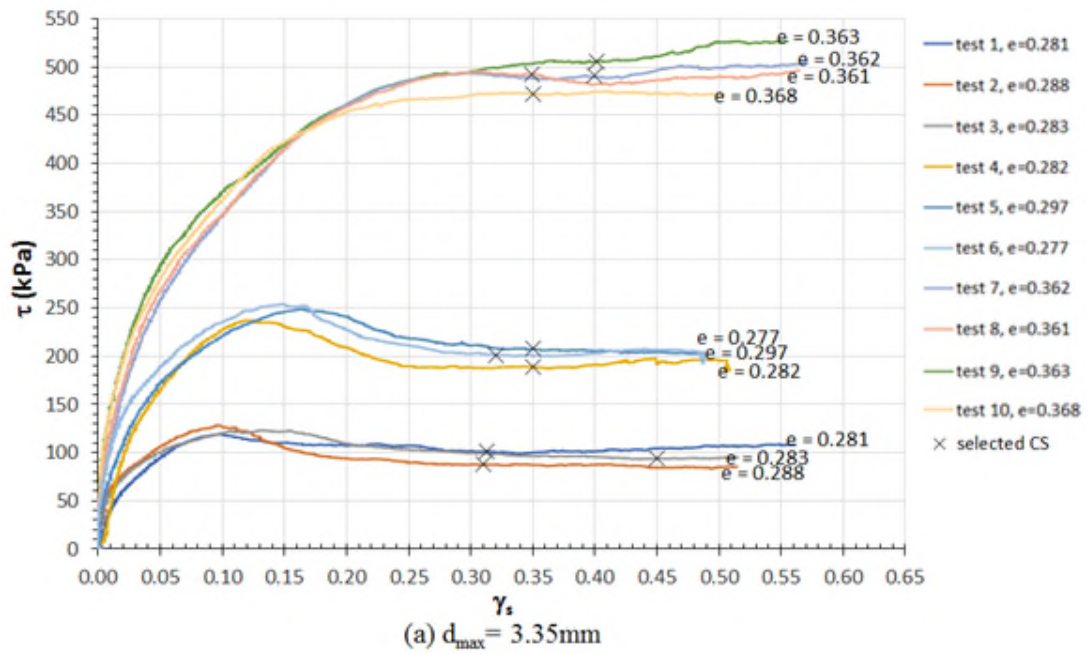


Figure 5. 5 Shear stress (τ) versus shear strain (γ_s) results for standard shear box tests conducted at 100 kPa and 200 kPa vertical stress on dense samples and at 500 kPa on looser samples of limestone material with maximum particle size equal to (a) 3.35 mm and (b) 2 mm. d_{\max} Cross sign indicates where the values of critical state were selected for each test.

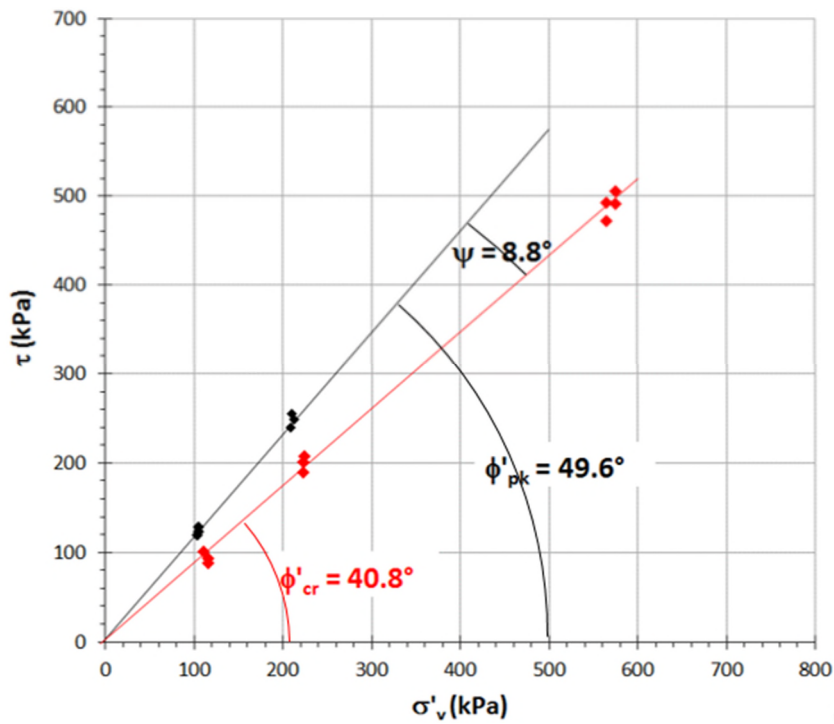


Figure 5. 6 Critical state angle of friction (ϕ'_{cr}), peak angle (ϕ'_{pk}) and angle of dilation (ψ) derived plotting the values of critical shear stress (τ_{cr}) and peak shear stress (τ_{pk}) at the variation of vertical stress (σ'_v) for all test conducted on the sample of maximum particle size equal to 3.35 mm.

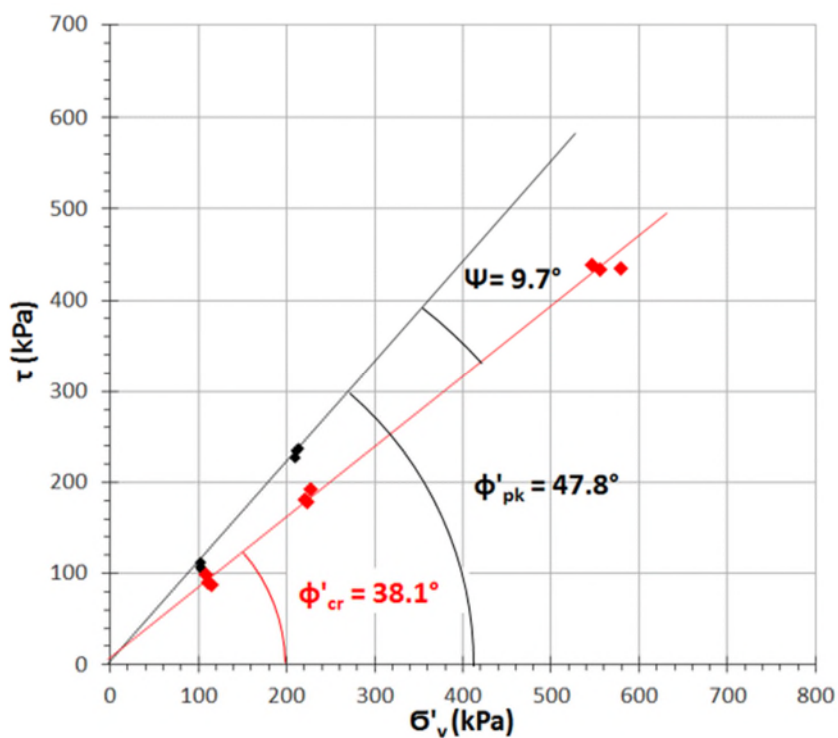


Figure 5. 7 Angle of friction (ϕ'_{cr}), peak angle (ϕ'_{pk}) and angle of dilation (ψ) derived plotting the values of critical shear stress (τ_{cr}) and peak shear stress (τ_{pk}) at

the variation of vertical stress (σ'_v) for all test conducted on the sample of maximum particle size equal to 2 mm.

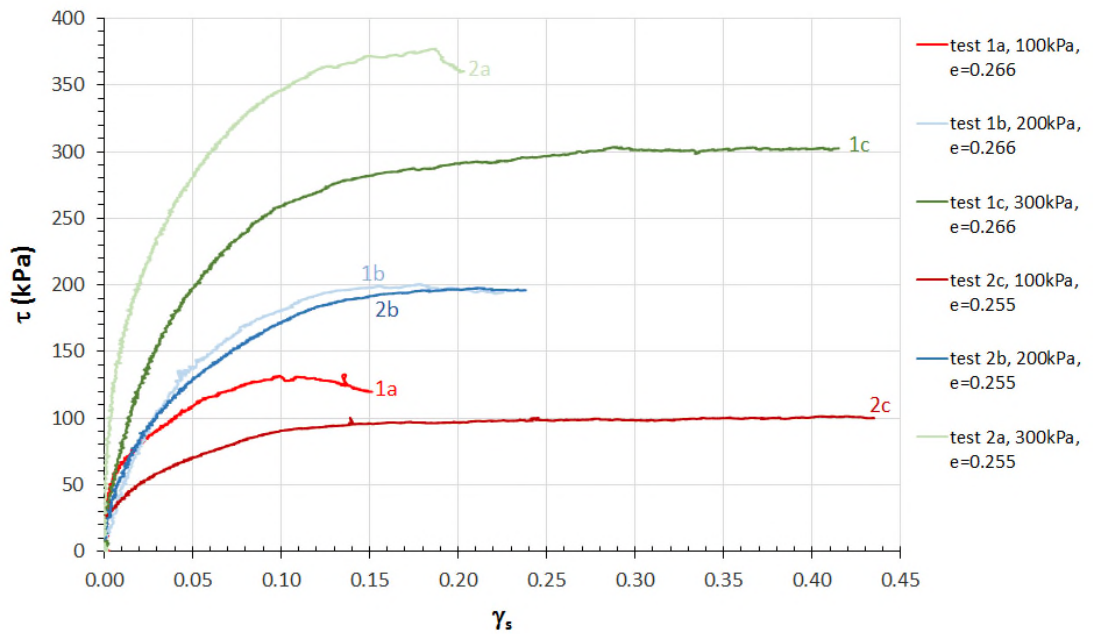


Figure 5. 8 Shear box test series carried out using two sample of limestone material which were retested in two different order of normal vertical stress: 100, 200, 300 kPa (series 1) for the first sample and 300, 200, 100 kPa (series 2) for the second one.

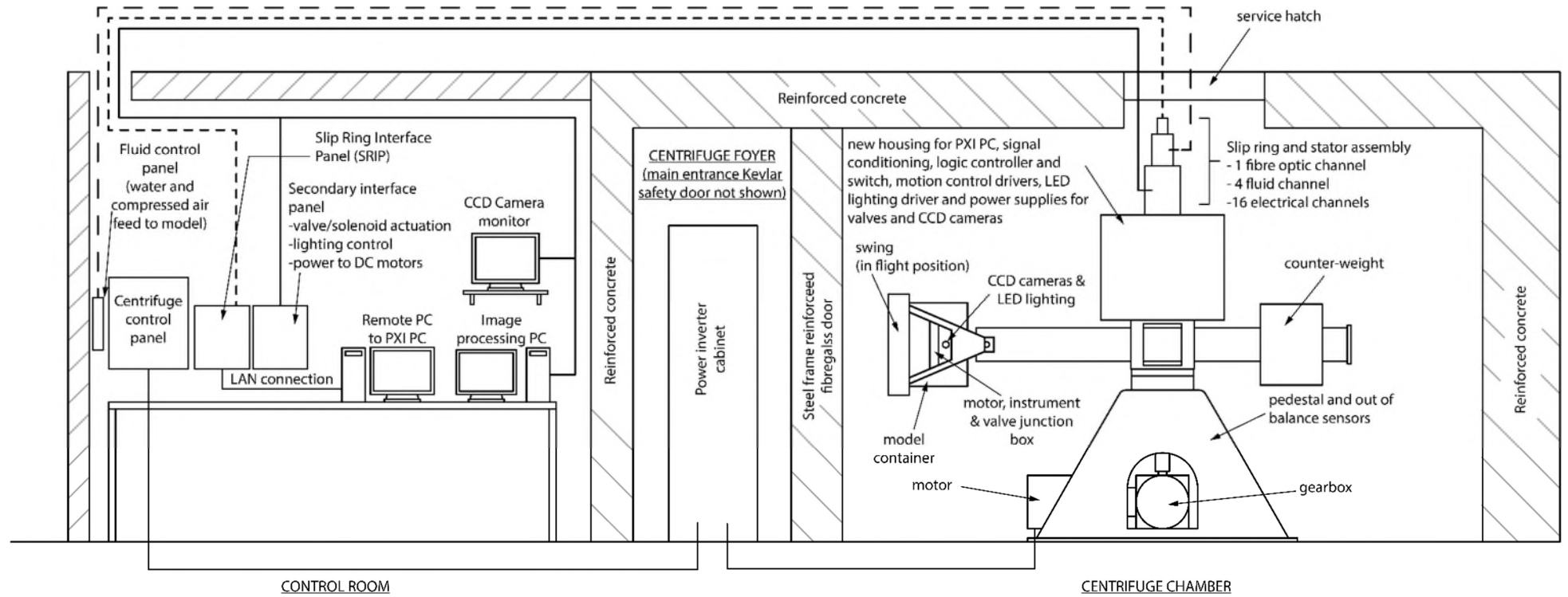


Figure 6. 1 Geotechnical centrifuge facility at City, University of London (Halai, 2018).

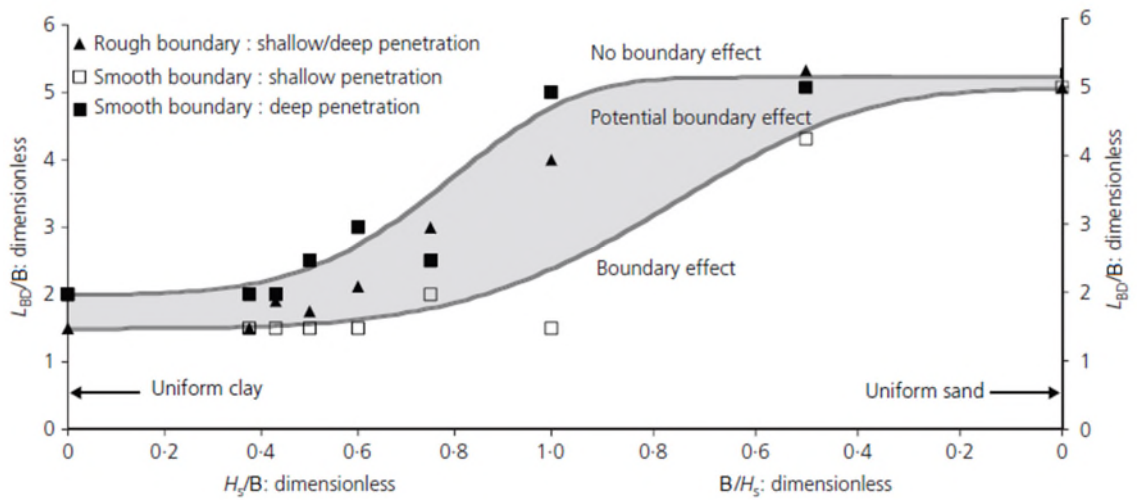


Figure 6.2 Centrifuge test design chart for estimating the safe normalized lateral boundary distance (L_{BD}) based on plate diameter (B) and thickness of the sand layer (H_s) (Ullah *et al.*, 2016).

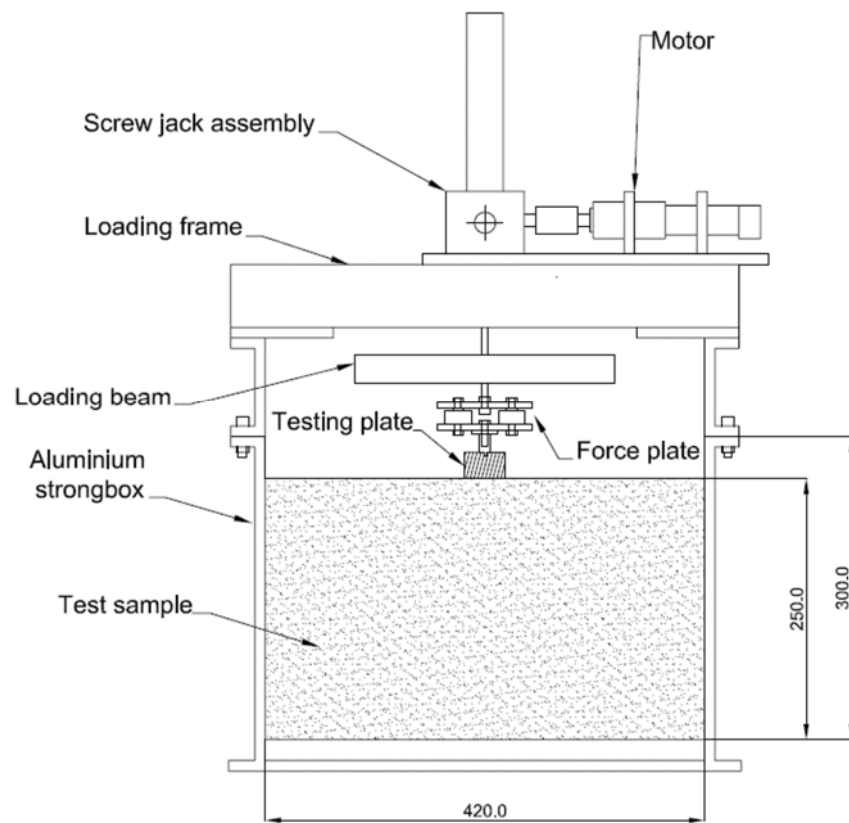


Figure 6.3 Centrifuge modelling testing equipment and instrumentation for the plate bearing capacity tests (based upon Gorasia, 2013).

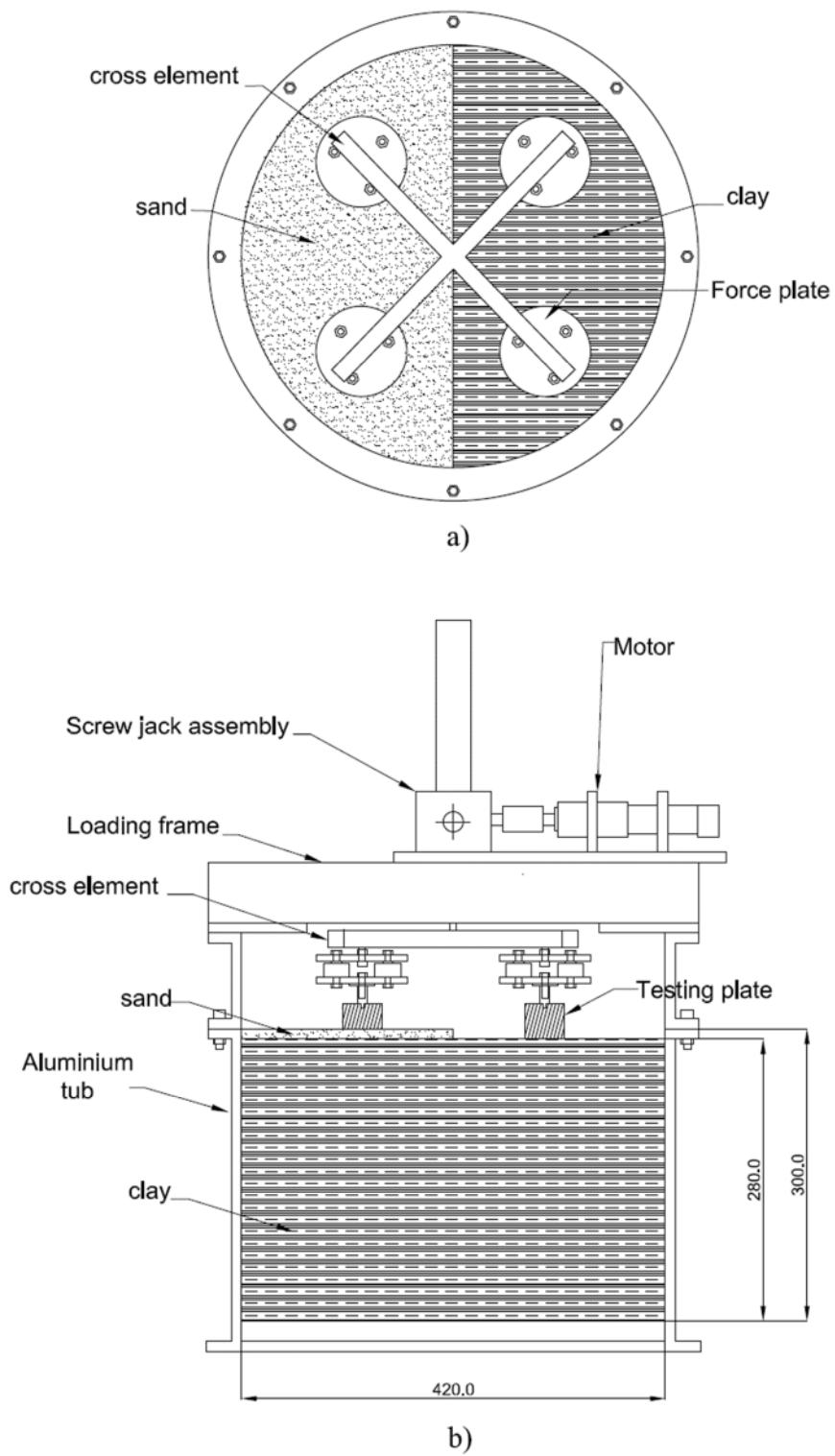


Figure 6. 4 Centrifuge modelling testing equipment and instrumentation for the plate bearing capacity test conducted on clay and sand on clay using four plates.

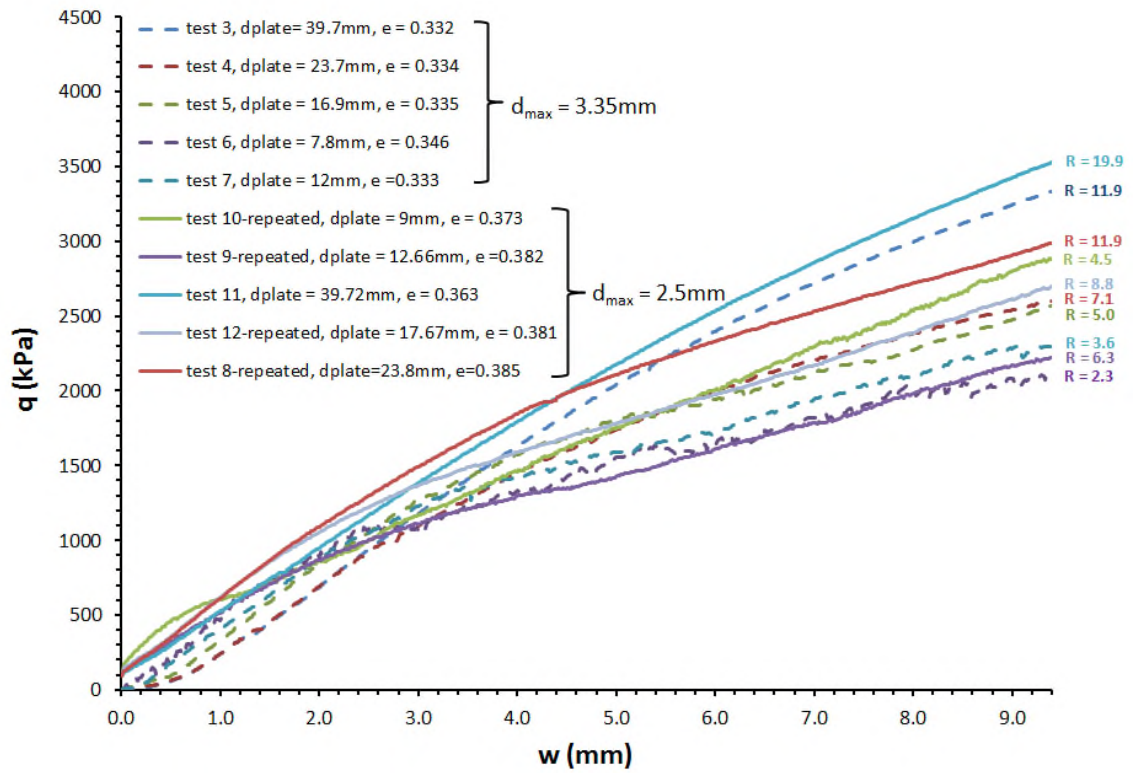


Figure 6.5 Bearing stress (q) variation with displacement (w) obtained from testing the samples with maximum particle size (d_{max}) equal to 3.35 mm and 2 mm, tested at different plate to maximum particle size ratios (R).

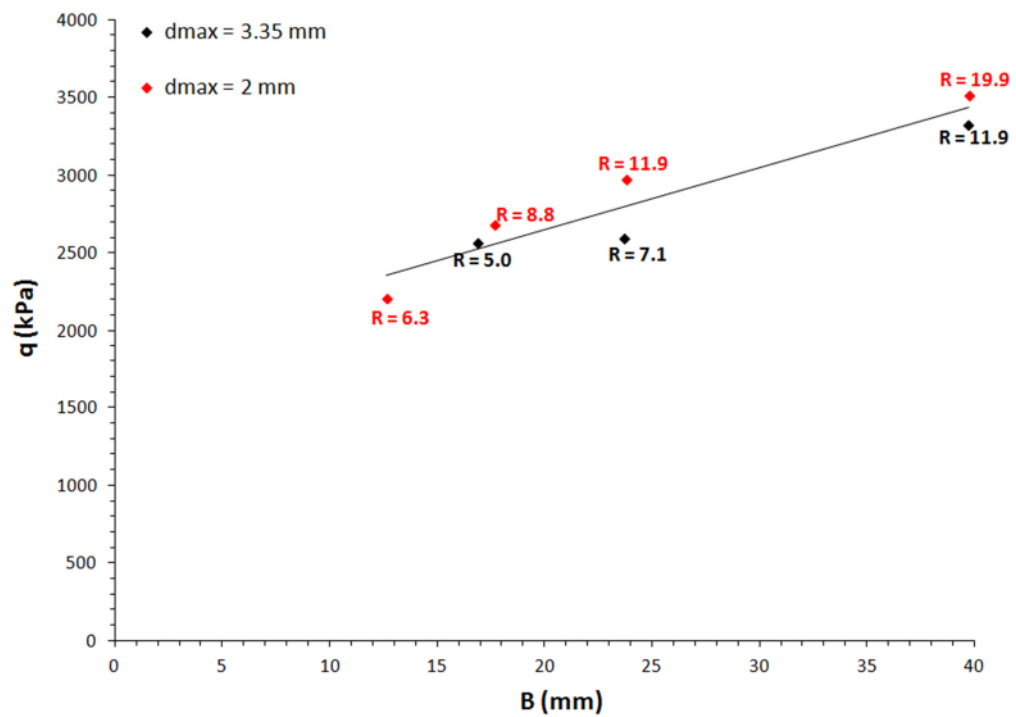


Figure 6.6 Variation of the value of bearing stress obtained at the maximum displacement reached during the test against size of the plate (B), obtained

from testing two samples with maximum particle size (d_{max}) equal to 3.35 mm (in black) and 2 mm (in red).

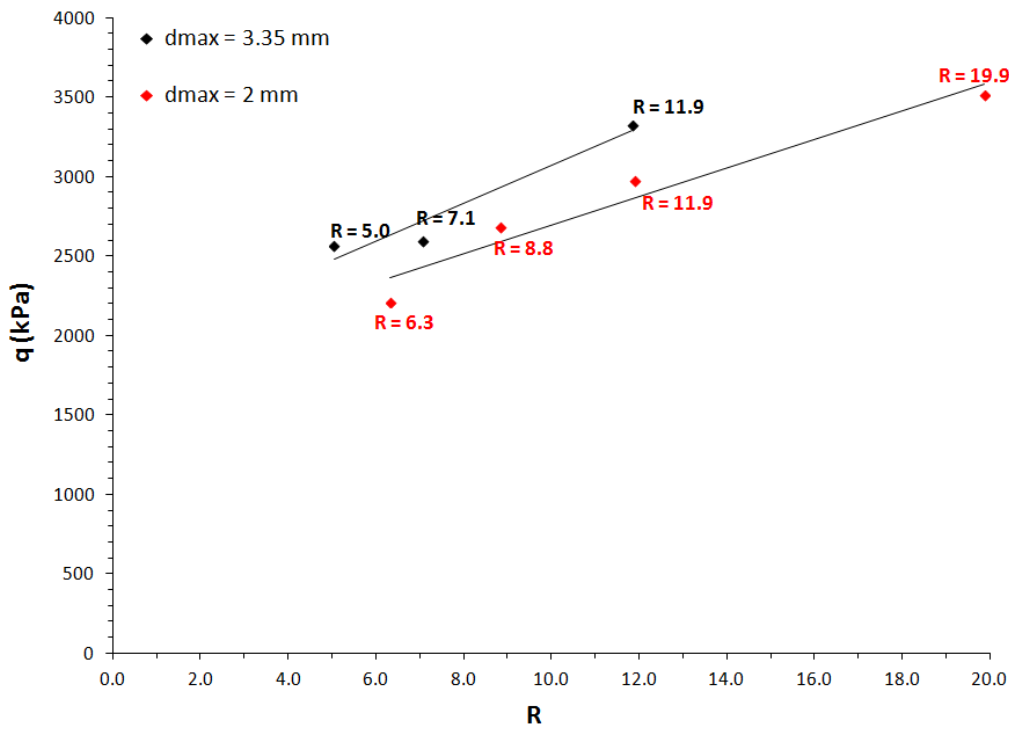


Figure 6. 7 Variation of the value of bearing stress obtained at the maximum displacement reached during the test against plate diameter to maximum size ratio (R), obtained from testing two samples with maximum particle size (d_{max}) equal to 3.35 mm (in black) and 2 mm (in red).



Figure 6. 8 Bulging of the soil in the zone adjacent to the plate typical of the general failure mechanism.

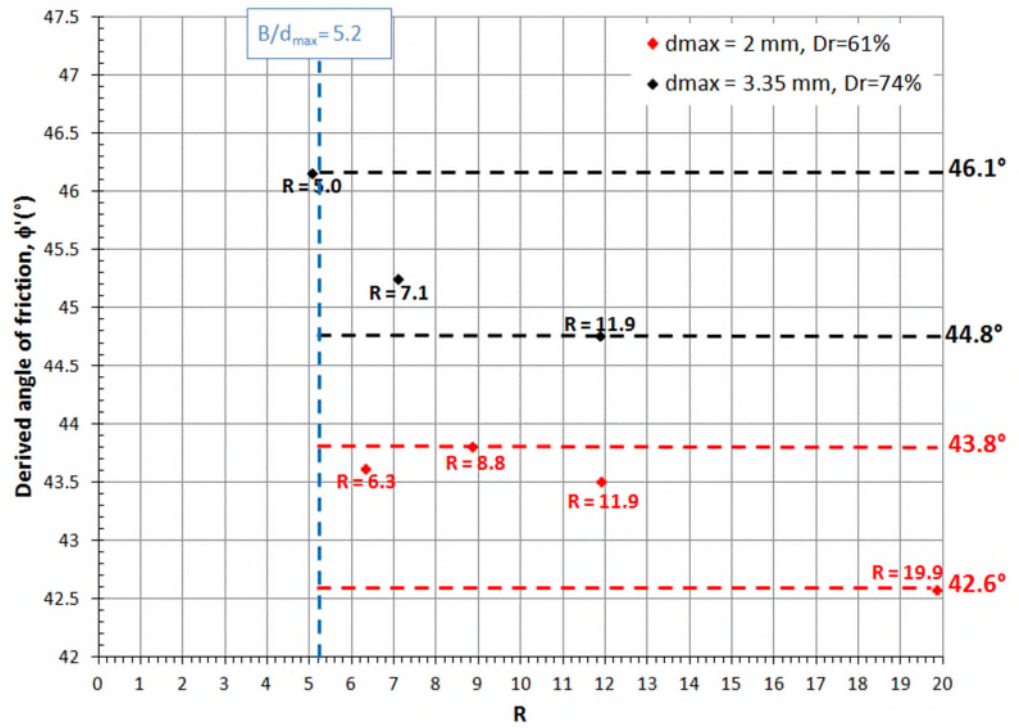


Figure 6.9 Variation of the angle of friction (back calculated) against plate diameter to maximum size ratio (R), obtained from testing two samples with maximum particle size (d_{max}) equal to 3.35 mm (in black) and 2 mm (in red).

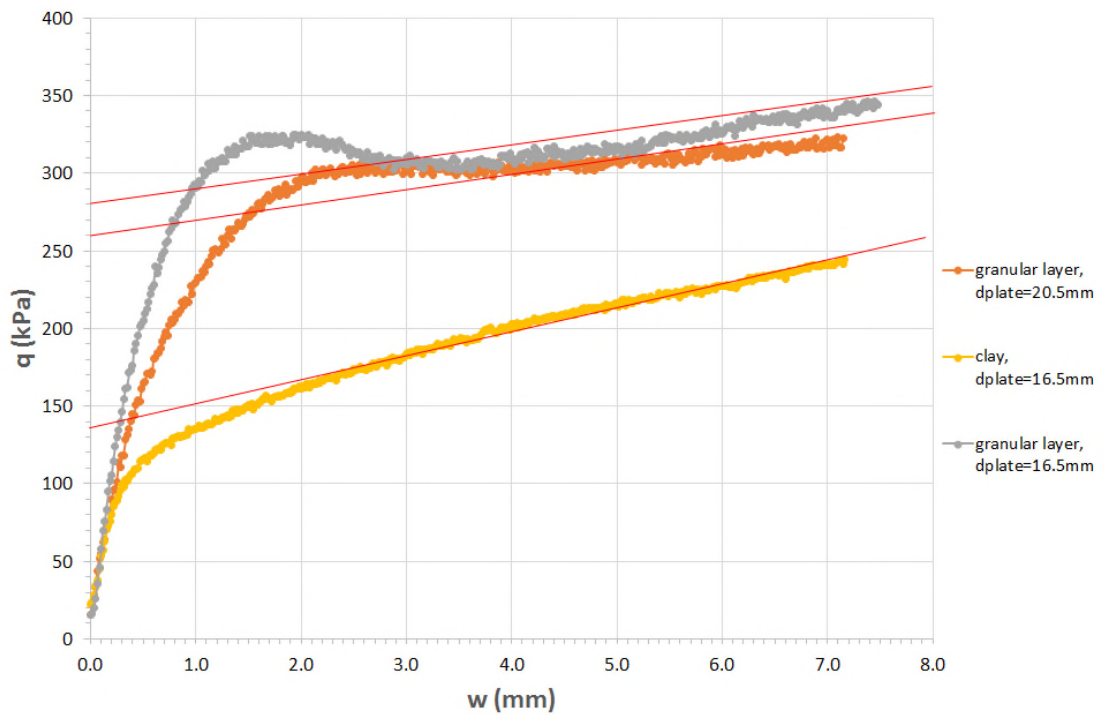


Figure 6.10 Bearing stress (q) variation with displacement (w), obtained from the second plate bearing test conducted on clay and granular material on clay.

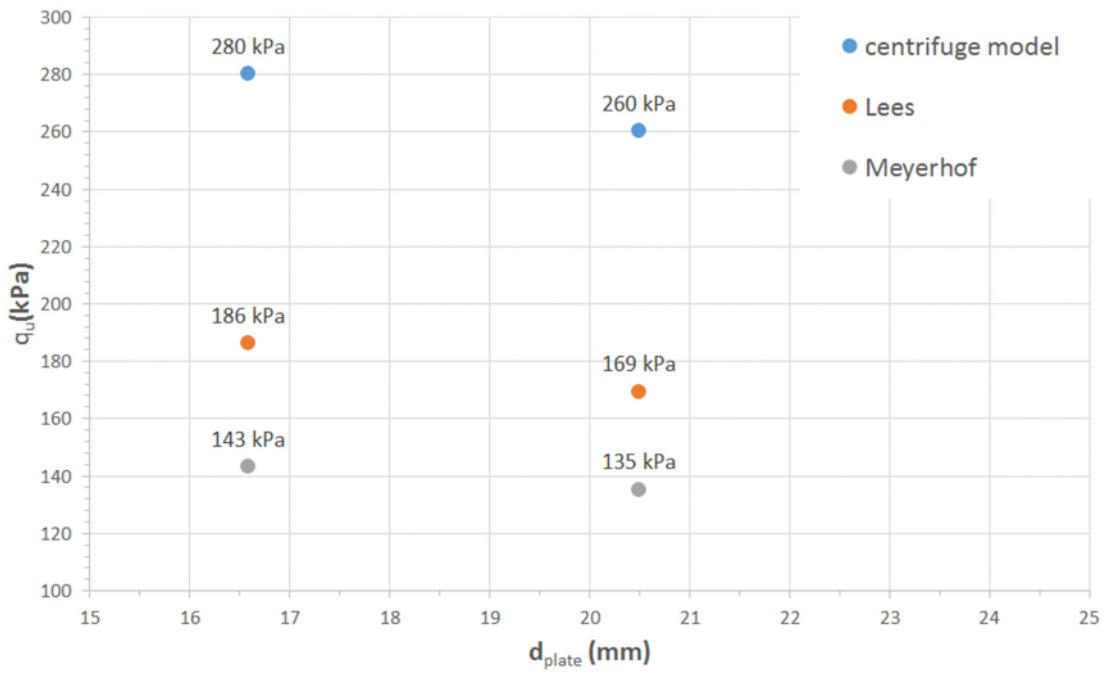


Figure 6. 11 Comparison of the values of ultimate bearing capacity (q_u) obtained from centrifuge model plate loading test on sand overlying clay (d_{plate} indicates the diameter of the plate) with the values derived from the theoretical methods described by Lees (2019) and Meyerhof (BRE, 2004).

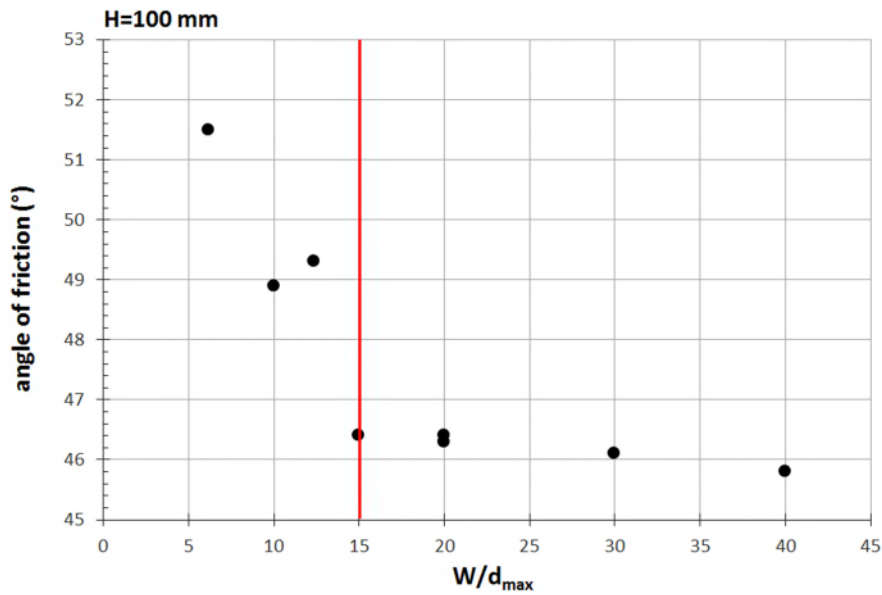


Figure 7. 1 Variation of the angle of friction with W/d_{max} ratio at constant value of H , data obtained from the study of Fu *et al.* (2015) (values of friction angles scaled from the graphs presented by the author).

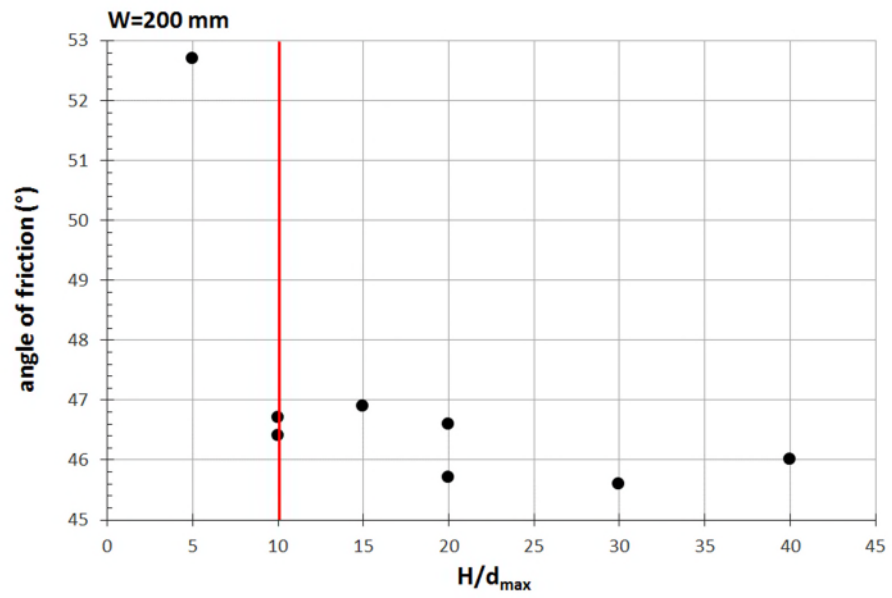
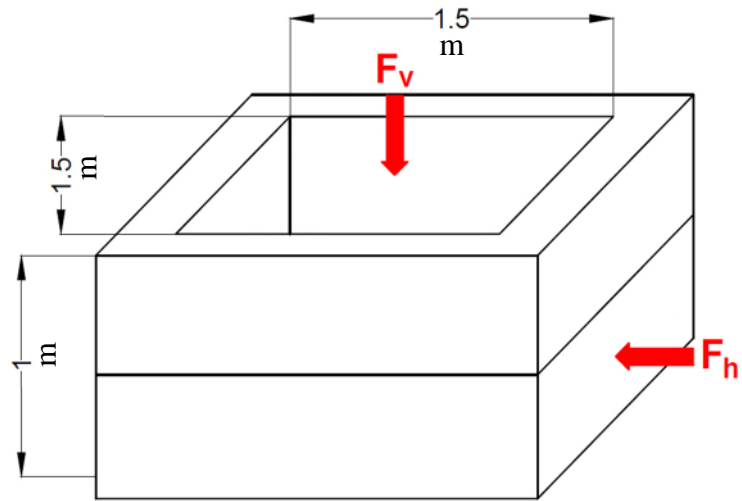
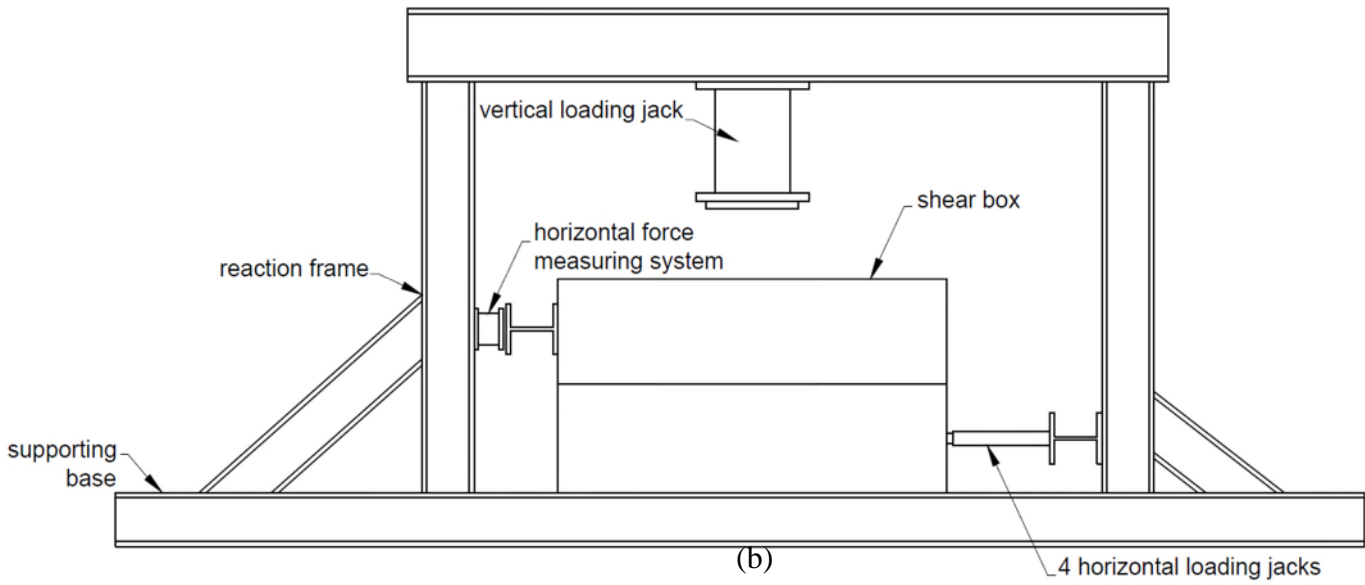


Figure 7. 2 Variation of the angle of friction with H/d_{\max} ratio at constant value of W , data obtained from the study of Fu *et al.* (2015) (values of friction angles scaled from the graphs presented by the author).

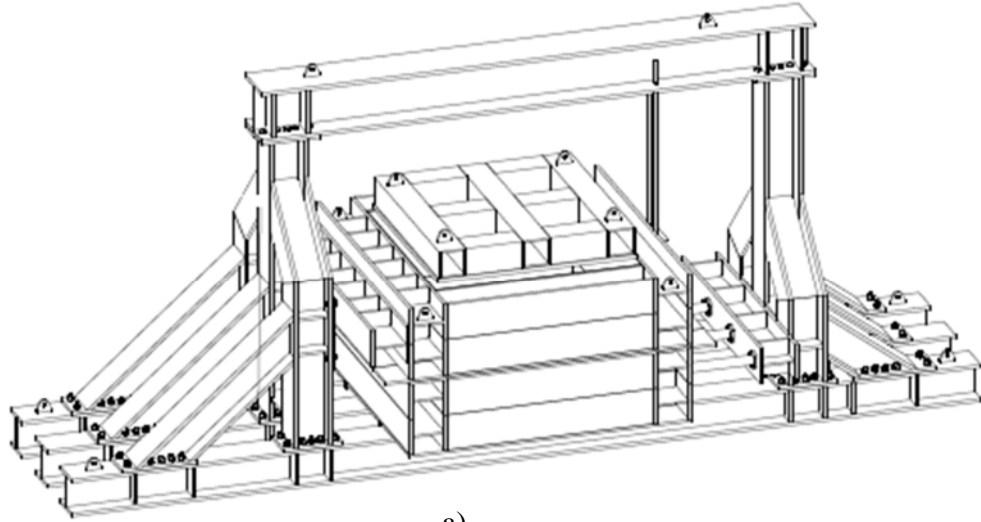


(a)

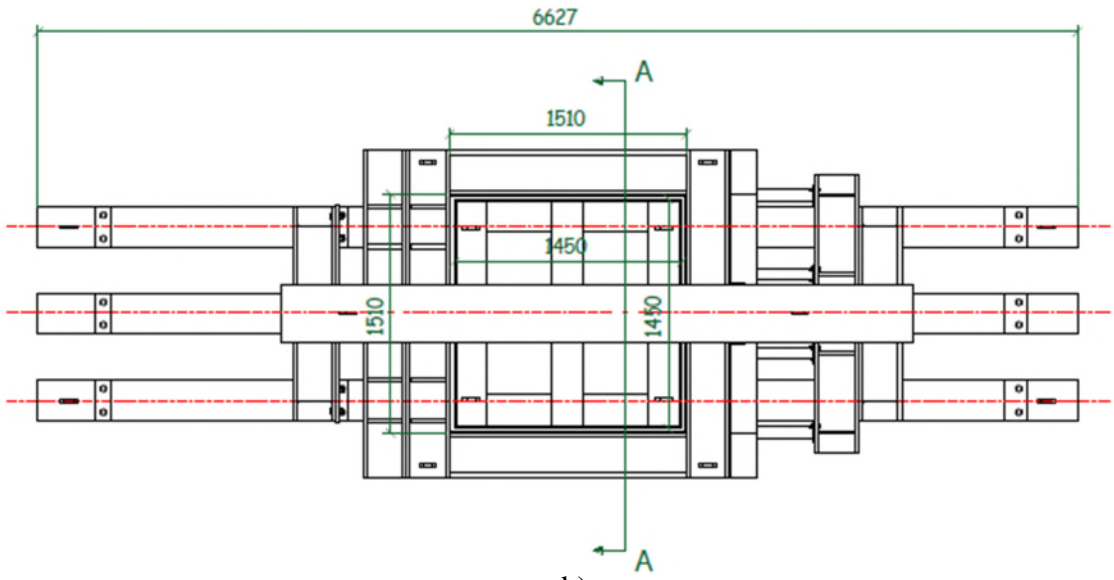


(b)

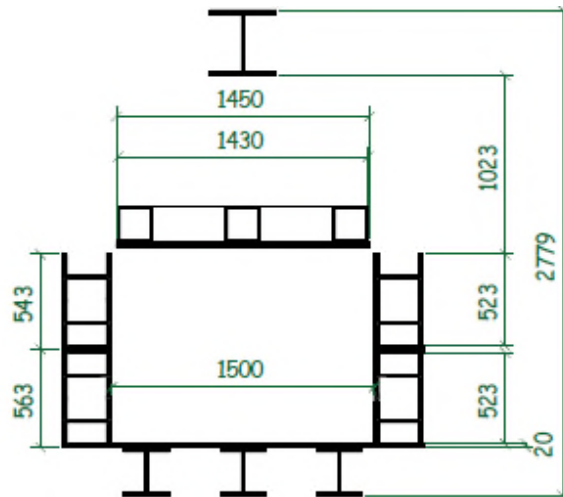
Figure 7.3 Preliminary sketch of (a) the large shear box and (b) of entire apparatus.



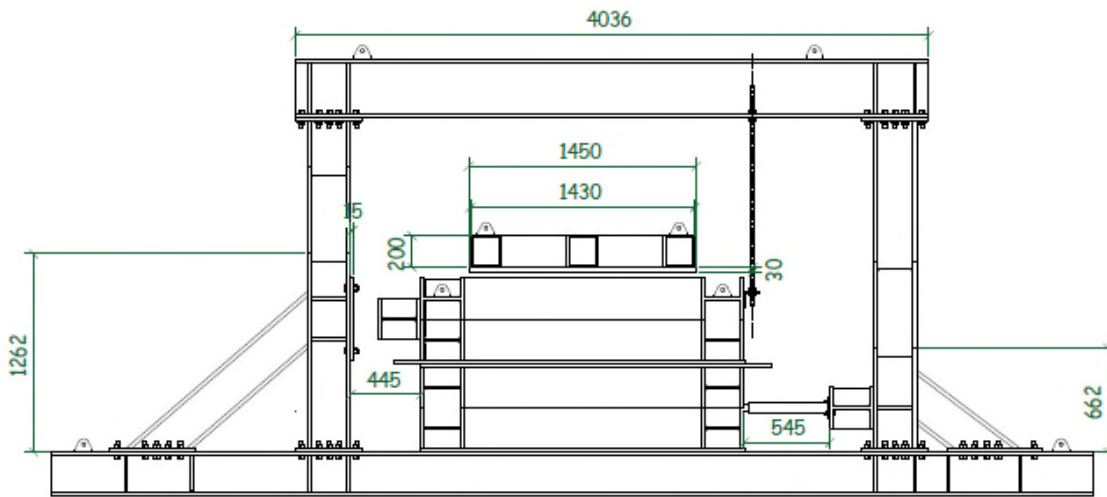
a)



b)



c)



d)

Figure 7.4 Details of the large shear box apparatus design: a) 3D illustration of the apparatus; b) plan; c) section; d) elevation. All dimensions are expressed in mm.



Figure 7.5 Large shear box apparatus (final arrangement).



Figure 7.6 Plate extensions having the role of preventing outflow of the material.



Figure 7.7 Extension of the top half of the box reacting against the two horizontal load cells during shearing.

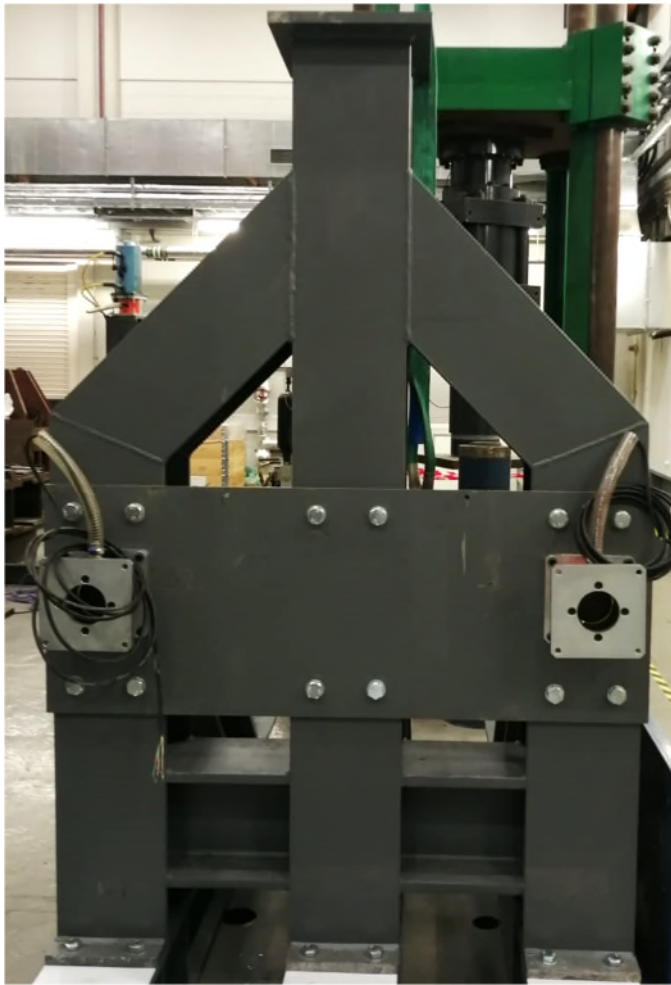


Figure 7. 8 Load cells attached to the vertical reaction frame by the use of a steel plate connected to the frame by bolts.

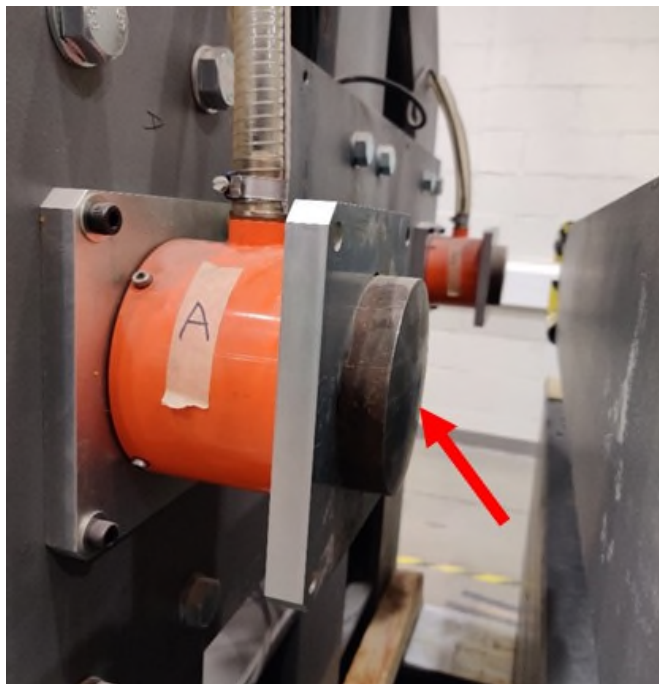


Figure 7. 9 Domed piece of steel machined to provide a rounded end for the load cells.



Figure 7. 10 Acetal sheets on top of the three beams supporting the shear box.



Figure 7. 11 Acetal sheets placed on the top surface of the bottom half of the box and lubricated before starting the test.



Figure 7.12 Guides attached to the bottom of the box in order to facilitate the movement of the box during shearing.



Figure 7.13 Second reaction frame holding and reacting against the four 500 kN hydraulic jacks.



Figure 7. 14 5 MN hydraulic jack attached to the horizontal beam before the latter was bolted to the vertical components of the reaction frame.



Figure 7. 15 Platen comprising a stiffened 30 mm thick plate reinforced with crossed sections (to minimise plate deflection).

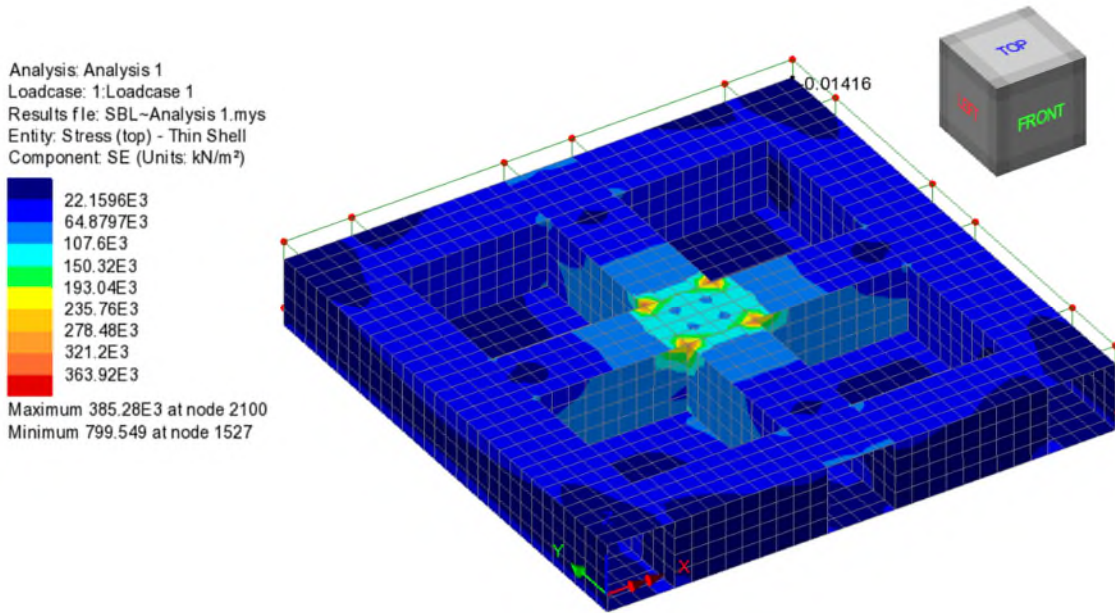


Figure 7. 16 Stresses generated on the top plate of the large shear box apparatus under an applied load equal to approximately 450 kPa when resting on top of the sample.



Figure 7. 17 Rigid frame holding the four vertical displacement transducers above the top of the shear box.



Figure 7. 18 Rigid frame holding one of the horizontal displacement transducers.



Figure 7. 19 Acetal sheet glued on top of the lower half of the shear box and put under load by the use of wooden blocks and aggregate bags.

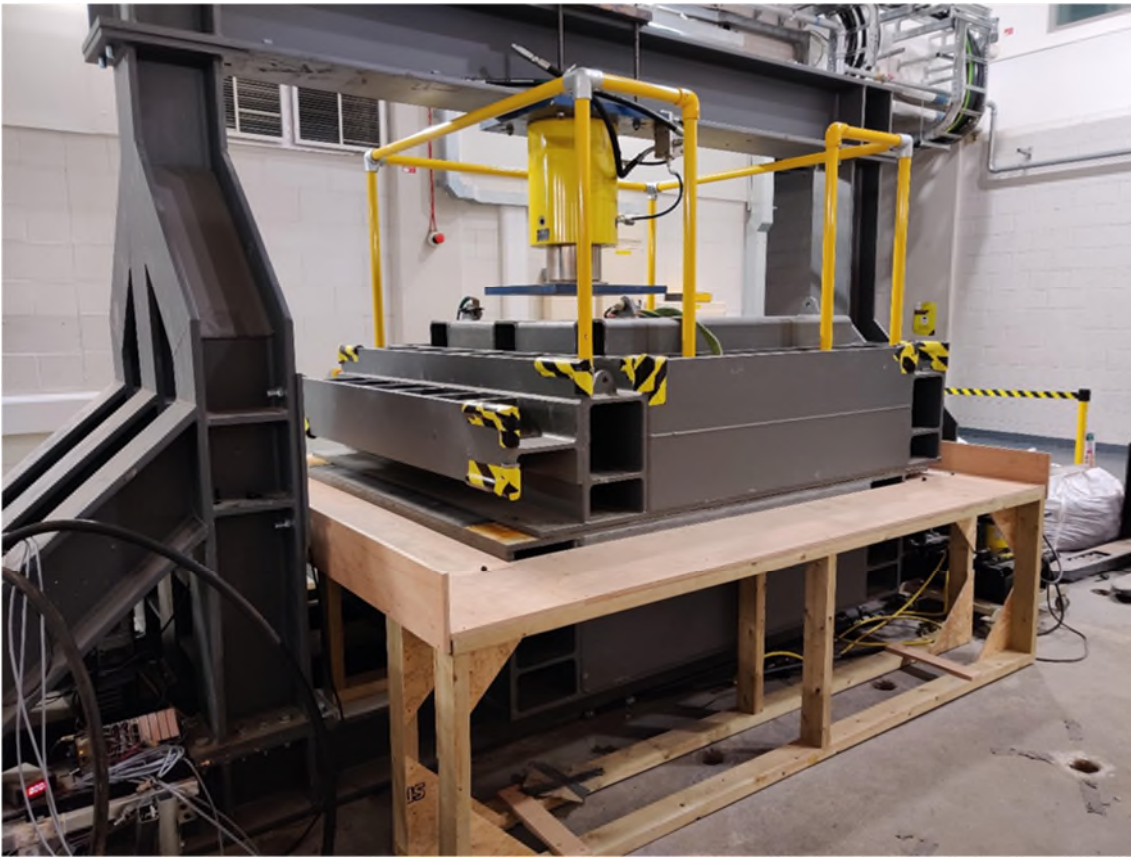


Figure 7. 20 Wooden platform placed around the bottom half of the shear box in order to collect the material contained in the top half.



Figure 7. 21 Rotation of the top lid during the first large scale shear box test ($\sigma'_v = 11$ kPa).

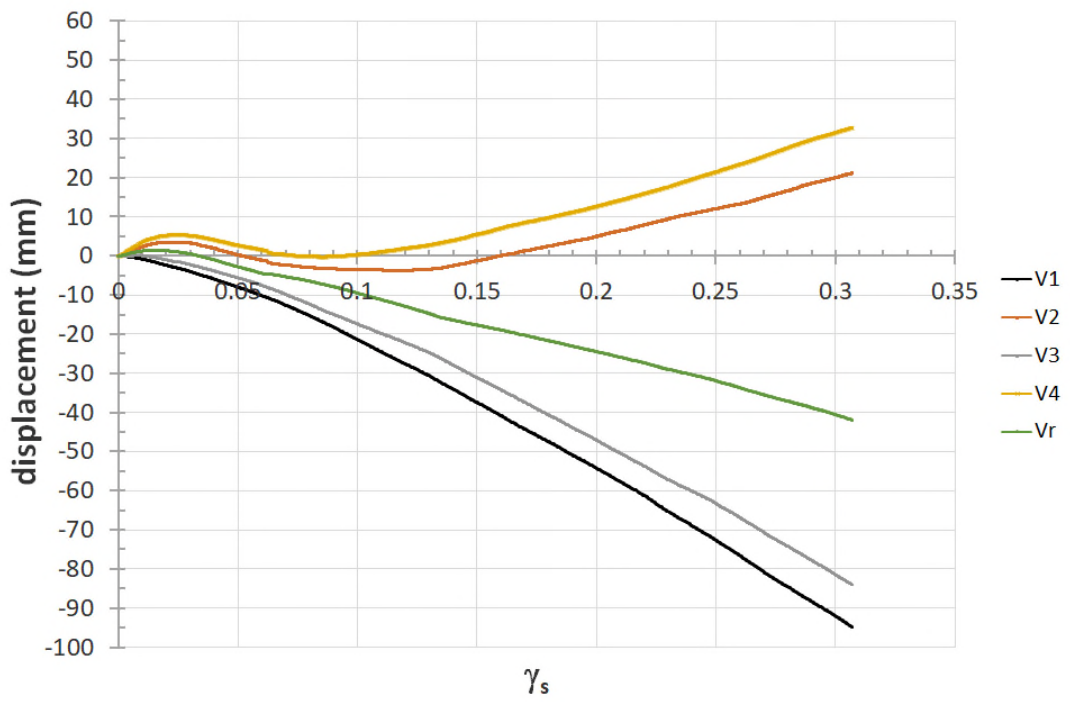


Figure 7. 22 Readings of the four vertical displacement transducers and derived vertical displacement Vr during the first large shear box test ($\sigma'_v = 11$ kPa).

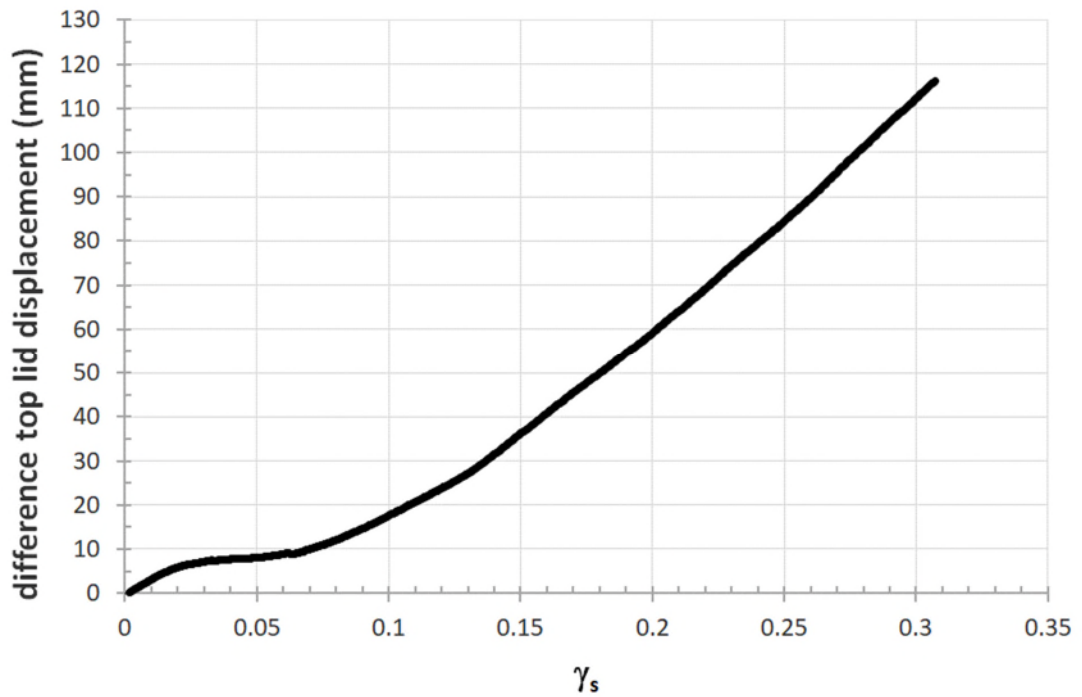


Figure 7. 23 Variation of the difference in vertical displacement between the two sides of the top plate during the first large shear box test ($\sigma'_v = 11$ kPa).

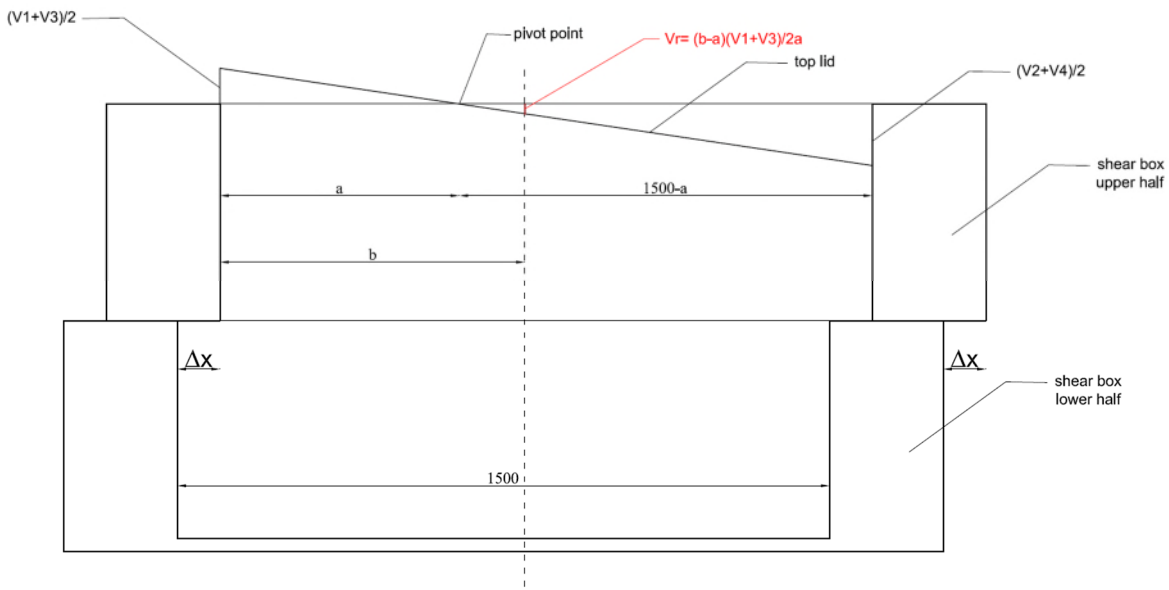


Figure 7. 24 Method for determining the vertical displacement (V_r) of the soil sample in correspondence of the middle of the shearing zone.

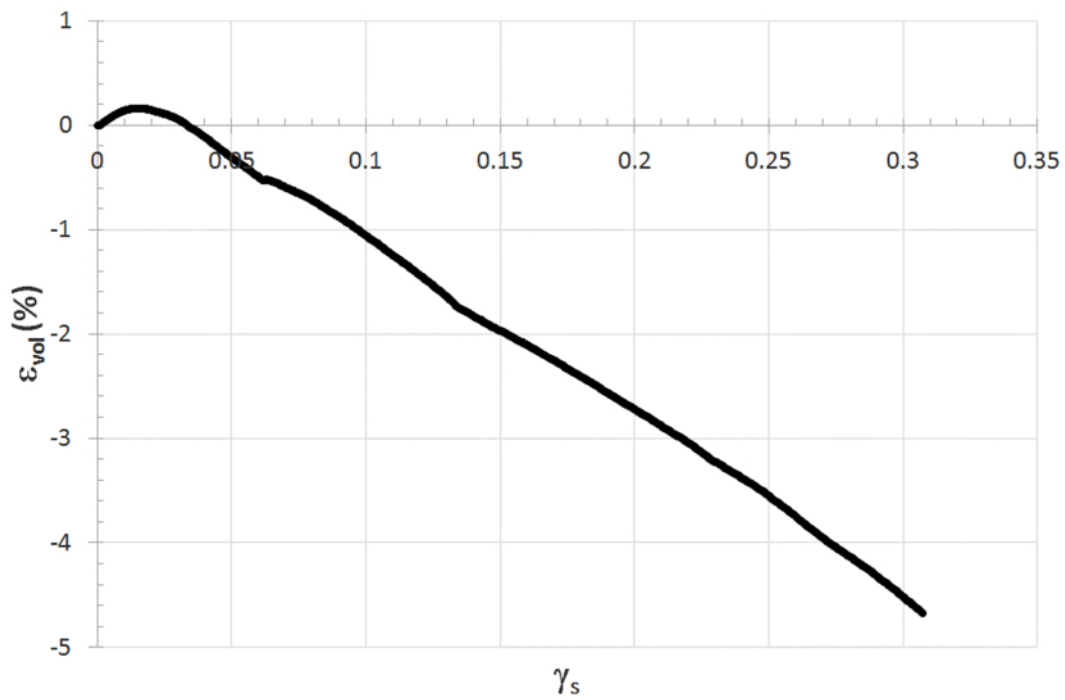


Figure 7. 25 Volumetric strain (ϵ_{vol}) versus shear strain (γ_s) results derived from the first large shear box test ($\sigma'_v = 11$ kPa).

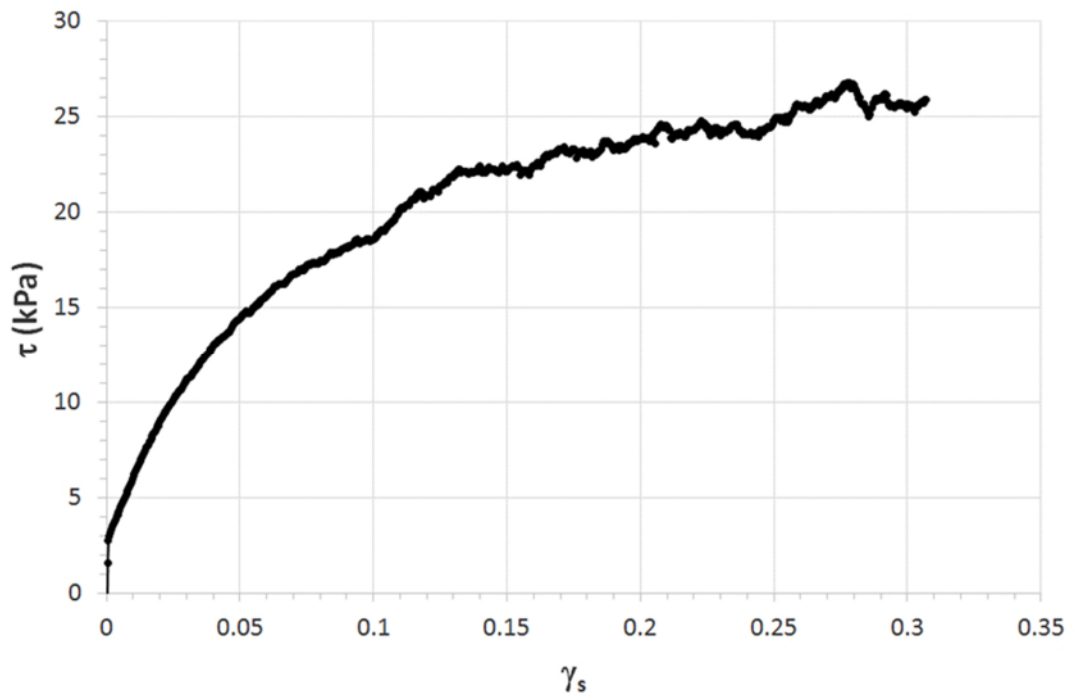


Figure 7.26 Shear stress (τ) versus shear strain (γ_s) results derived from the first large shear box test ($\sigma'_v = 11$ kPa).



Figure 7.27 Rotation of the top lid during the second large scale shear box test ($\sigma'_v = 185$ kPa).

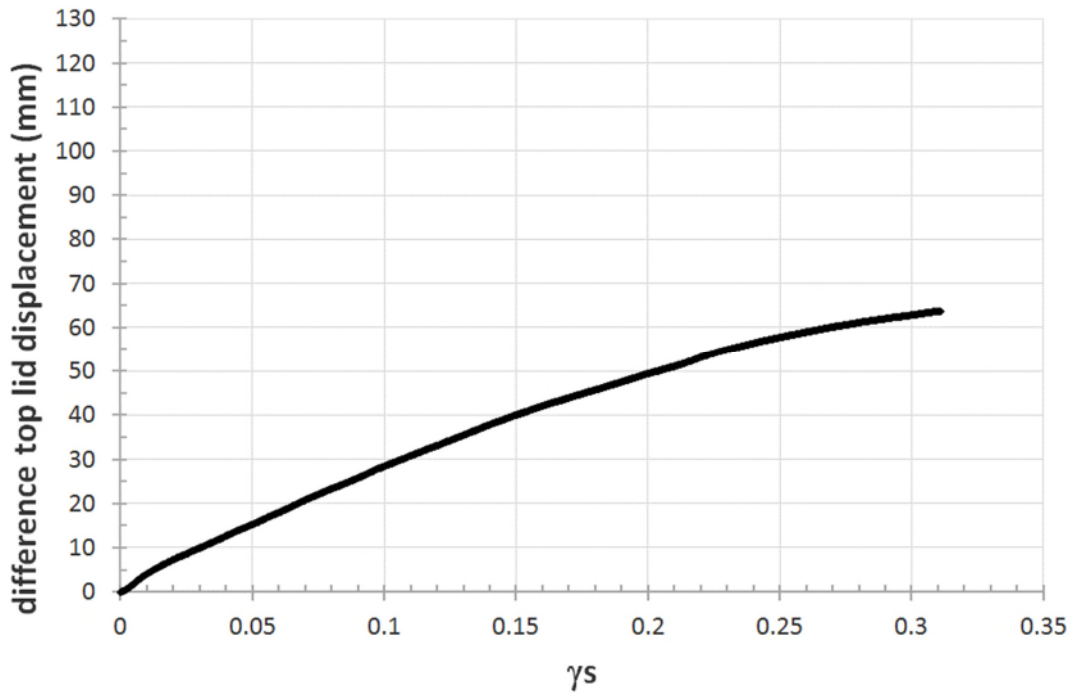


Figure 7.28 Variation of the difference in vertical displacement between the two sides of the top plate during the second large shear box test ($\sigma'_v = 185$ kPa).

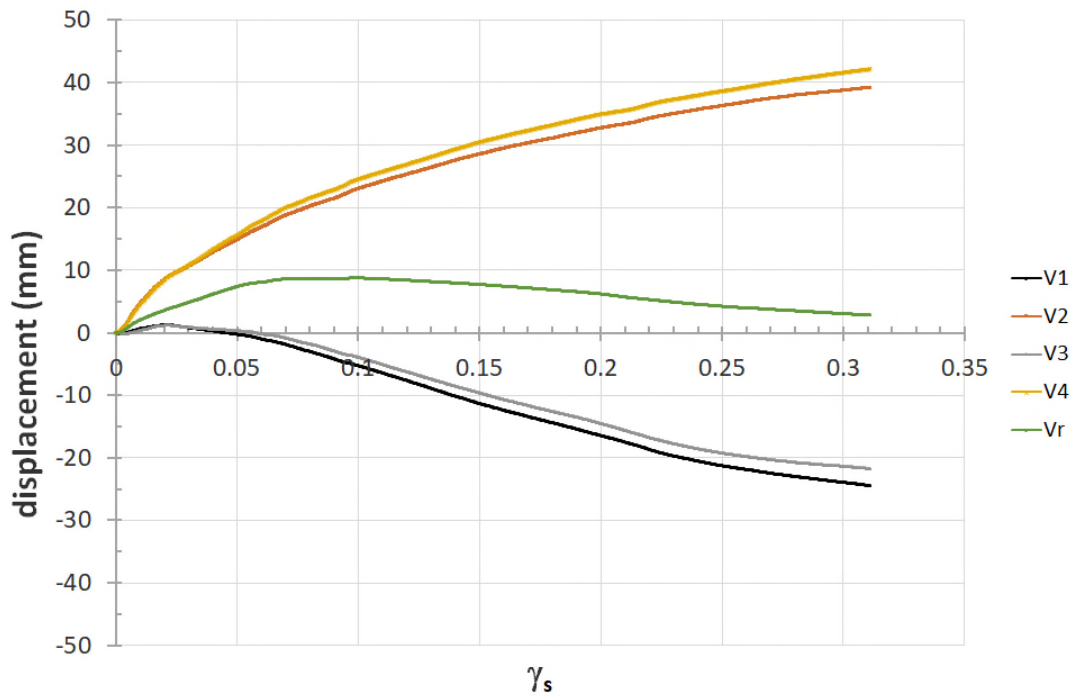


Figure 7.29 Readings of the four vertical displacement transducers and derived vertical displacement Vr during the second large shear box test ($\sigma'_v = 185$ kPa).

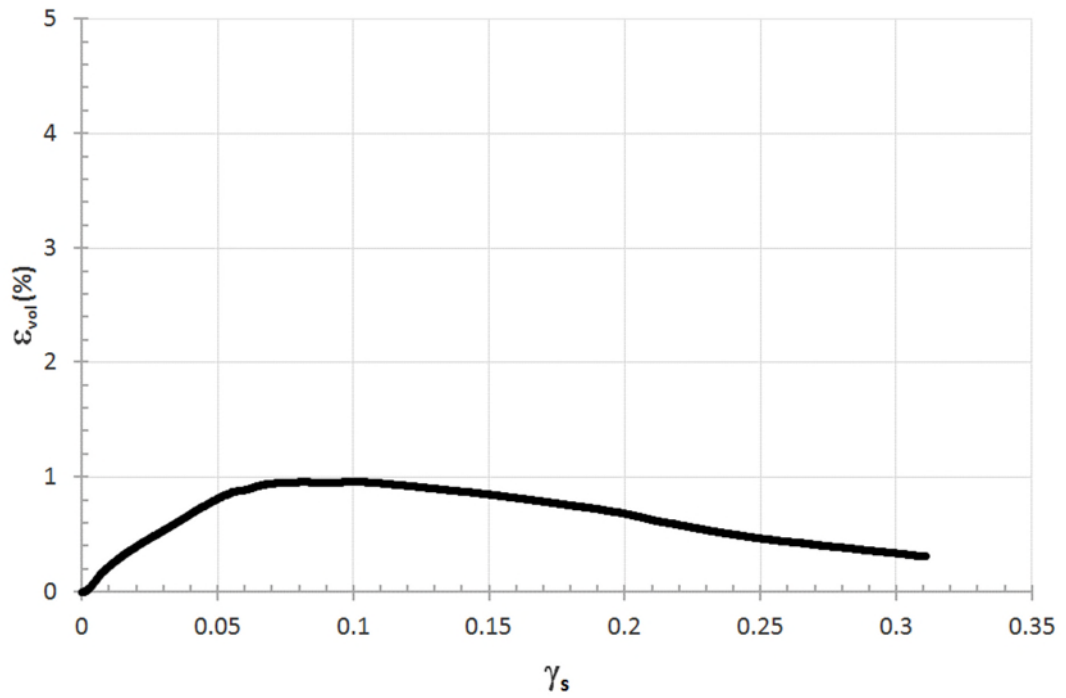


Figure 7.30 Volumetric strain (ϵ_{vol}) versus shear strain (γ_s) results derived from the second large shear box test ($\sigma'_v = 185$ kPa).

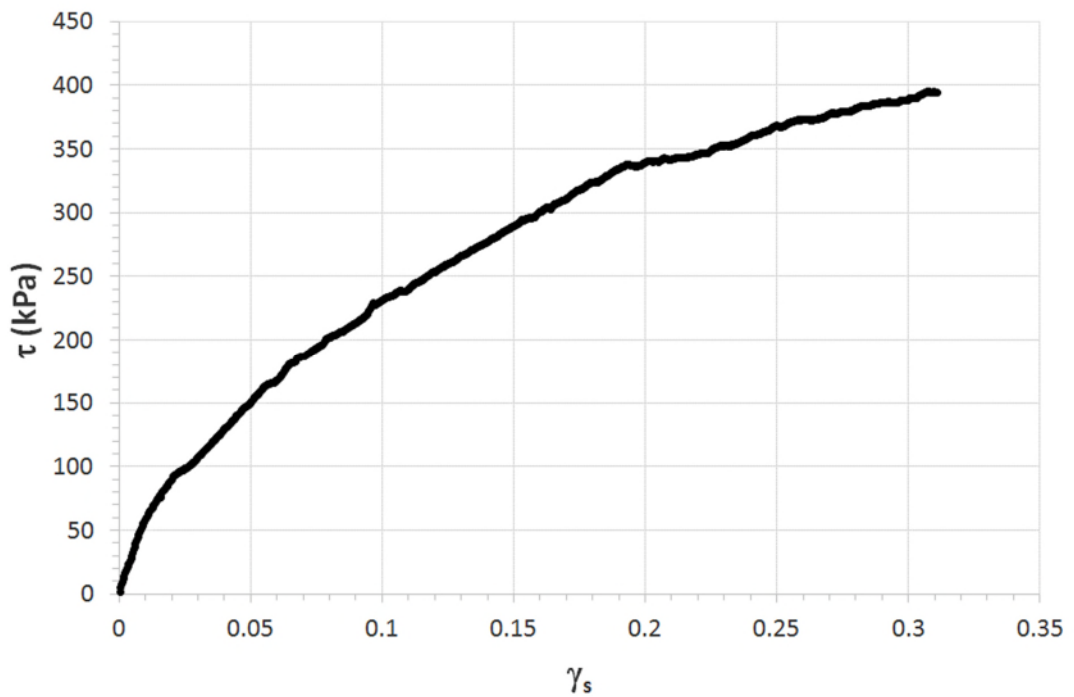


Figure 7.31 Shear stress (τ) versus shear strain (γ_s) results derived from the second large shear box test ($\sigma'_v = 185$ kPa).

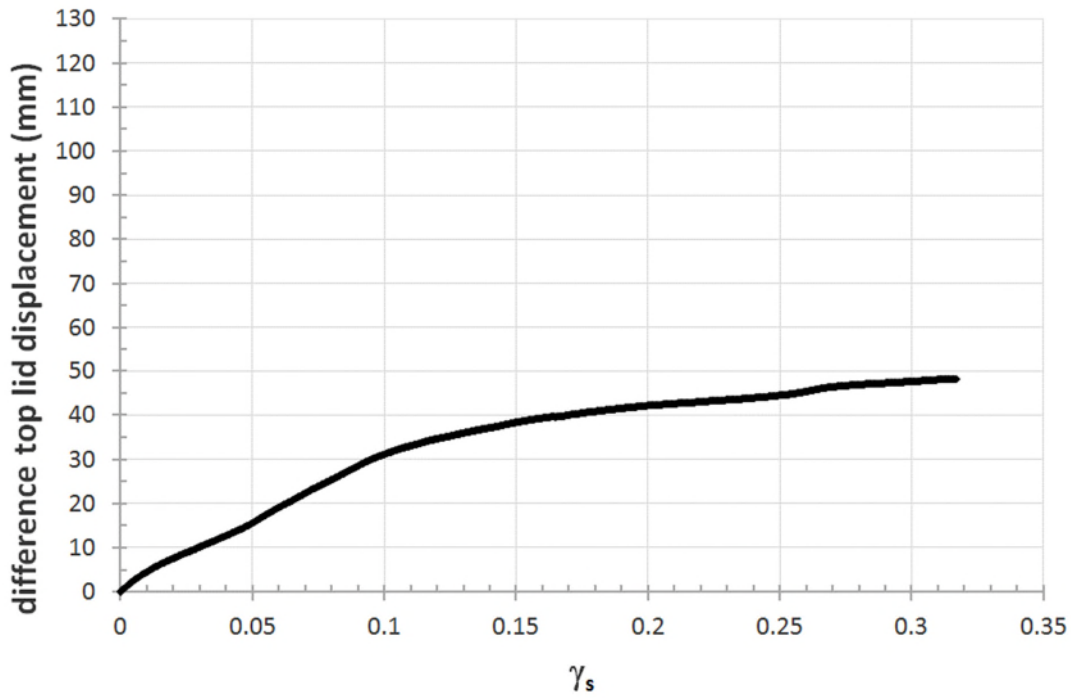


Figure 7. 32 Variation of the difference in vertical displacement between the two sides of the top plate during the third large shear box test ($\sigma'_v= 104$ kPa).

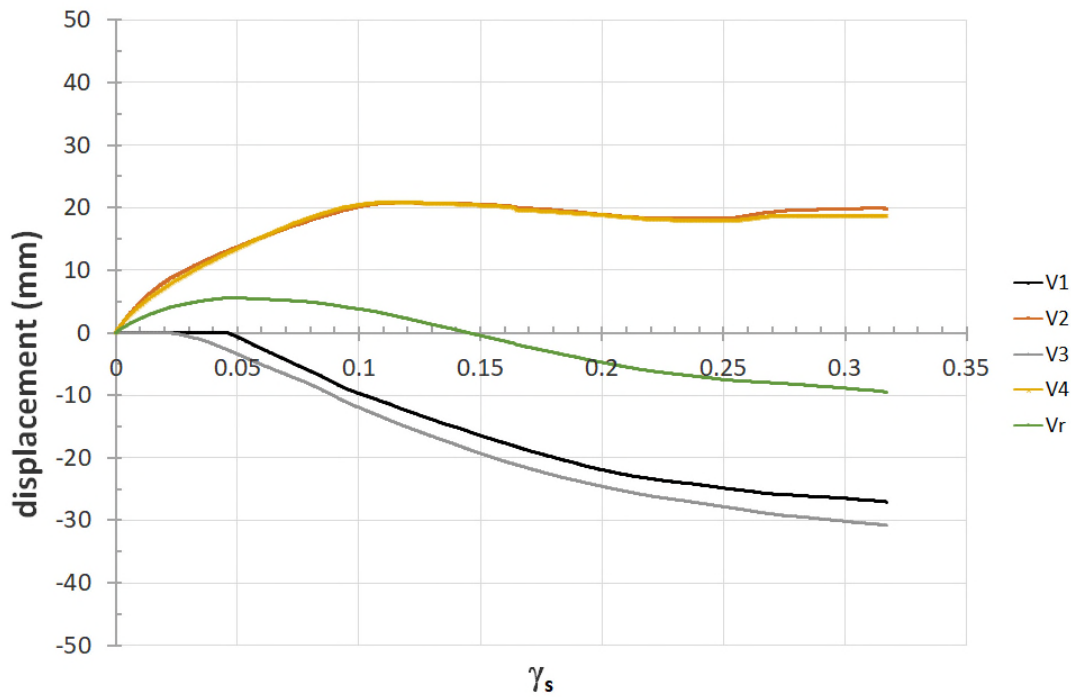


Figure 7. 33 Readings of the four vertical displacement transducers and derived vertical displacement Vr during the third large shear box test ($\sigma'_v= 104$ kPa).

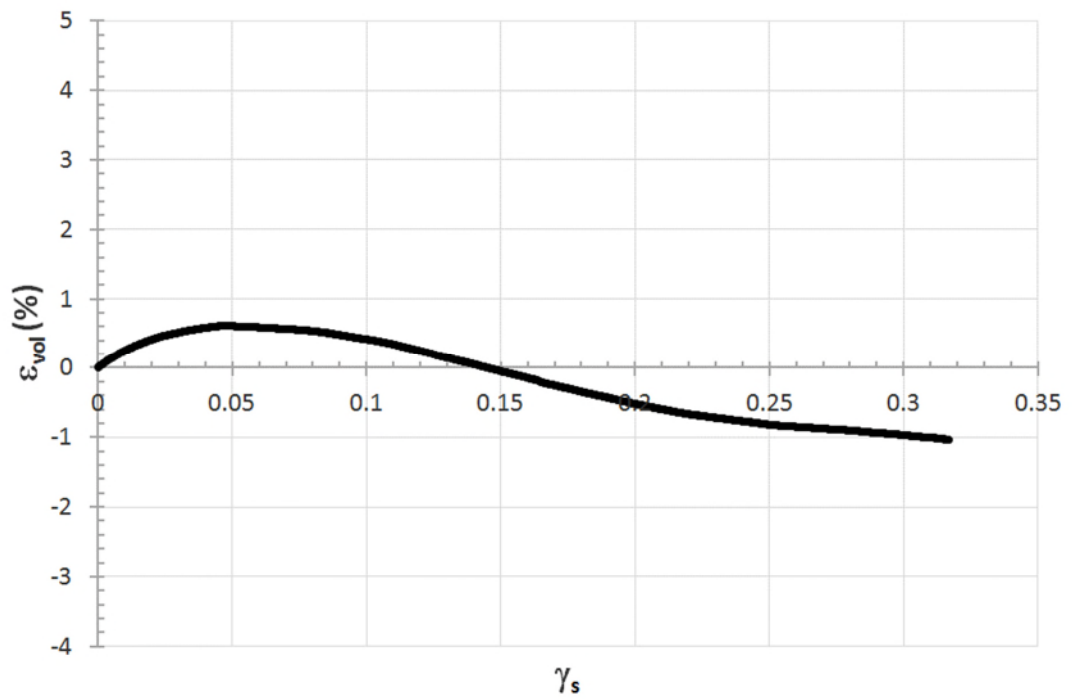


Figure 7. 34 Volumetric strain (ϵ_{vol}) versus shear strain (γ_s) results derived from the third large shear box test ($\sigma'_v = 104$ kPa).

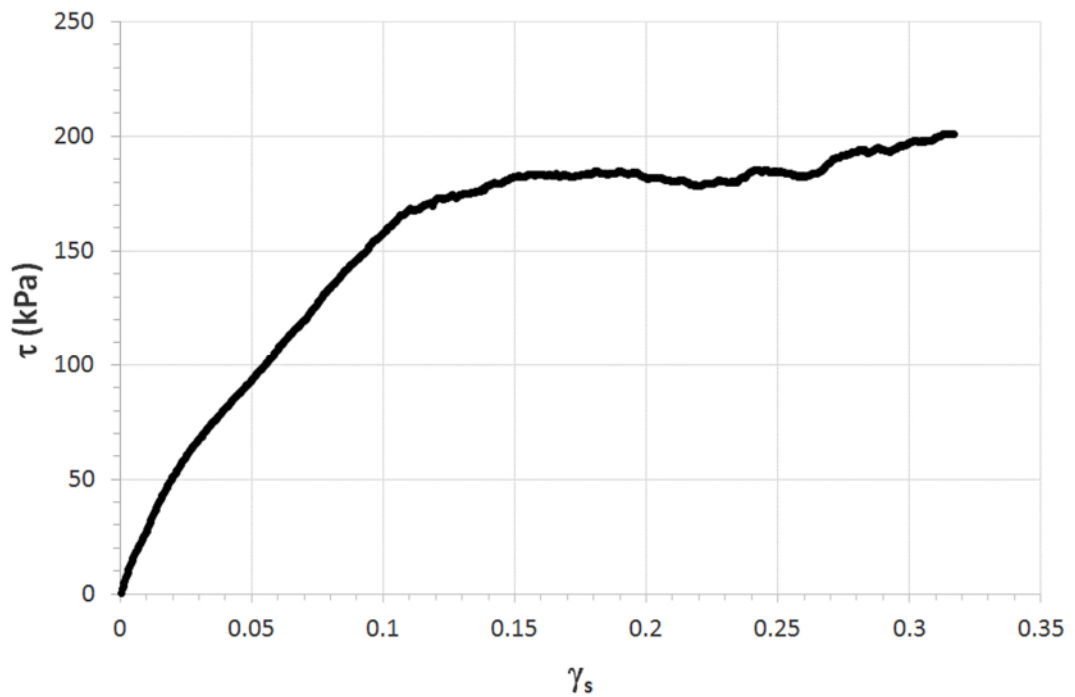


Figure 7. 35 Shear stress (τ) versus shear strain (γ_s) results derived from the third large shear box test ($\sigma'_v = 104$ kPa).

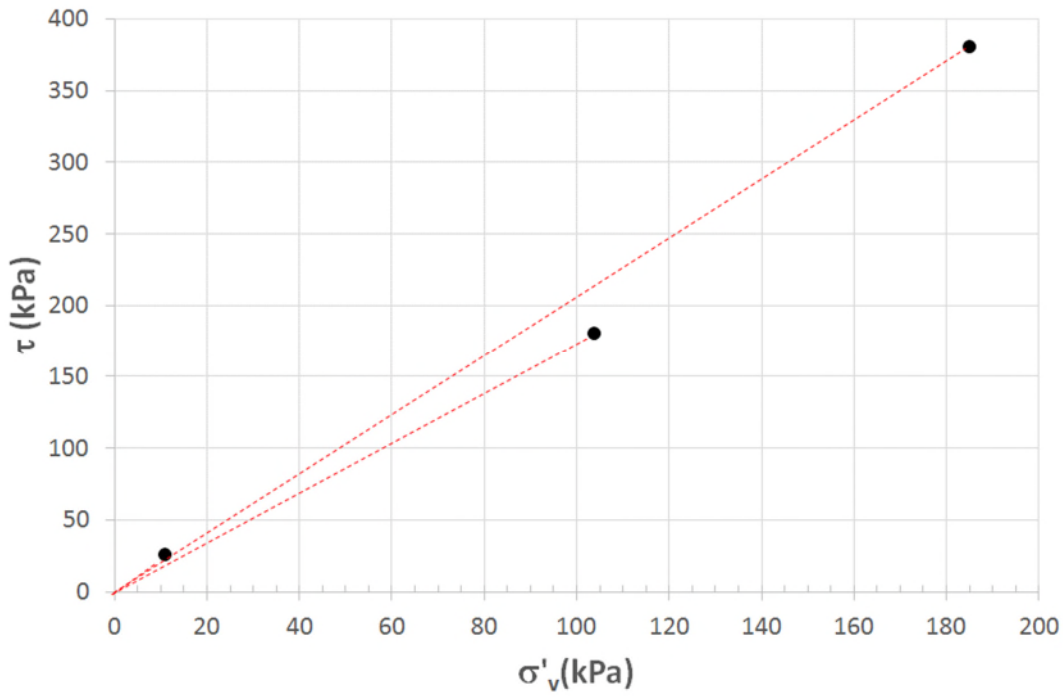


Figure 8. 1 Method for calculating the secant angle of friction for each test conducted using the large shear apparatus.

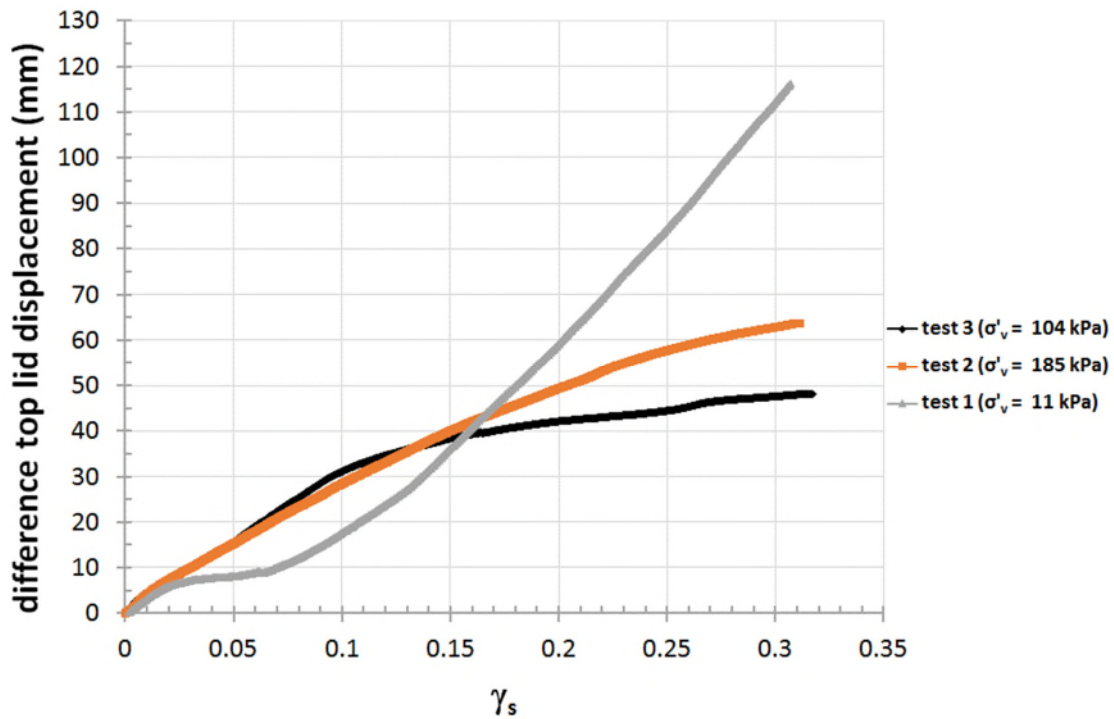


Figure 8. 2 Variation of the difference in vertical displacement between the two sides of the top plate during the three large shear box tests.

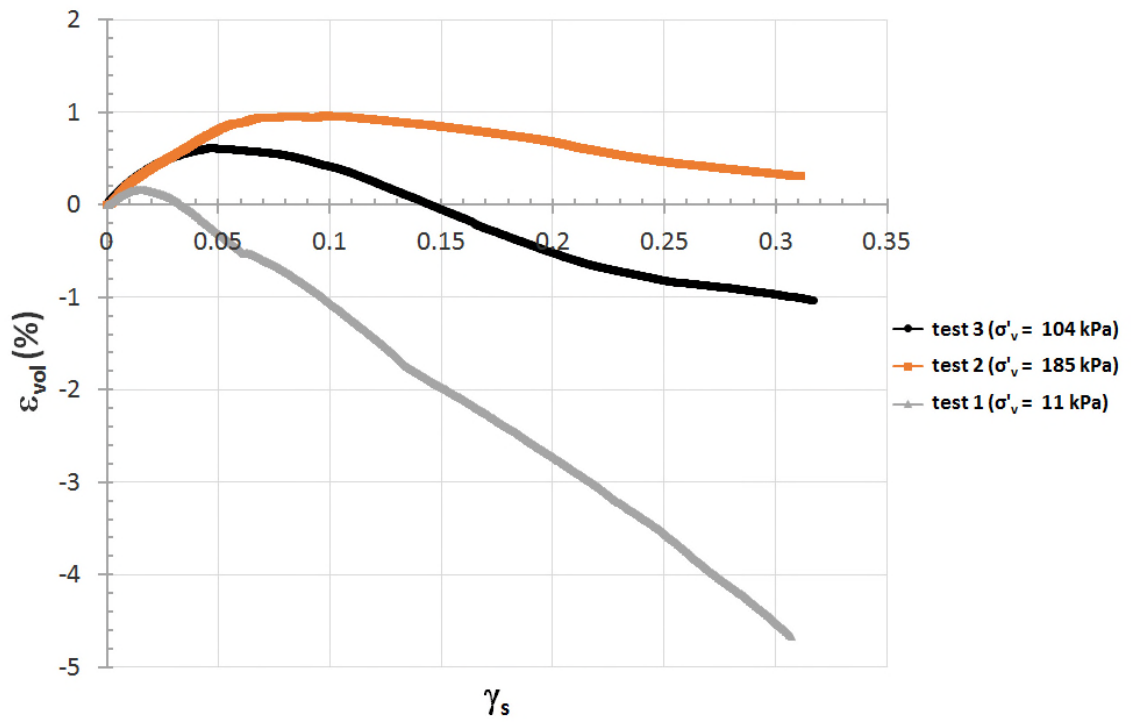


Figure 8.3 Volumetric strain (ϵ_{vol}) versus shear strain (γ_s) results derived from the three large shear box tests.

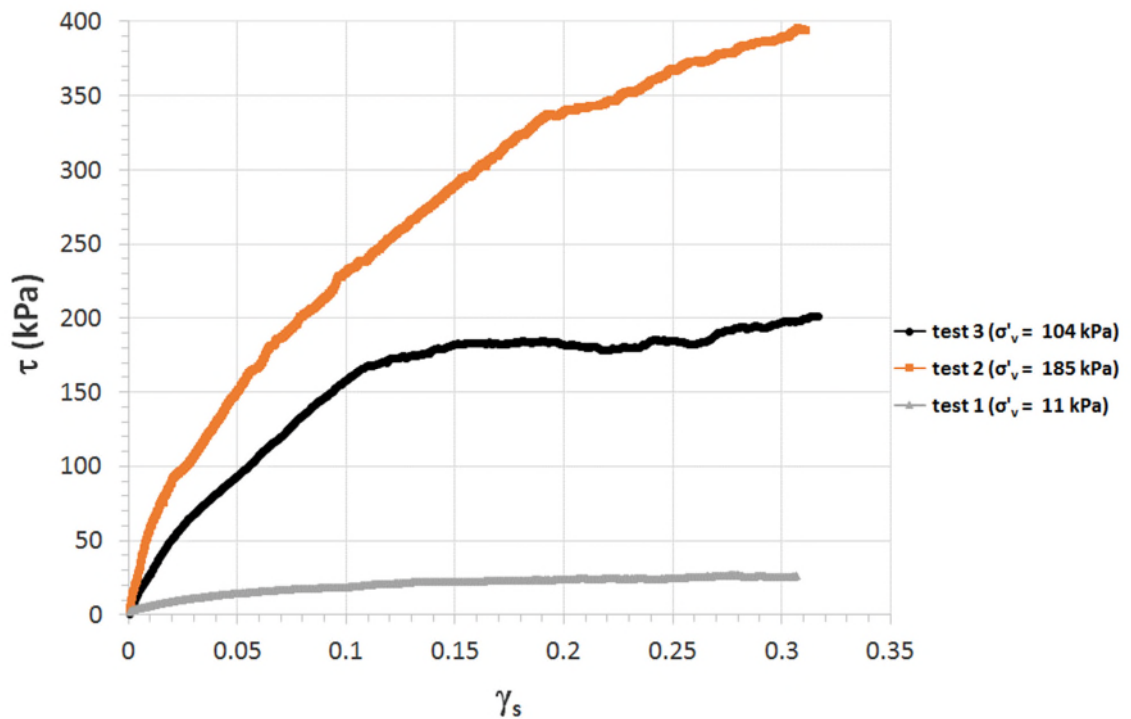


Figure 8.4 Shear stress (τ) versus shear strain (γ_s) results derived from the three large shear box tests.

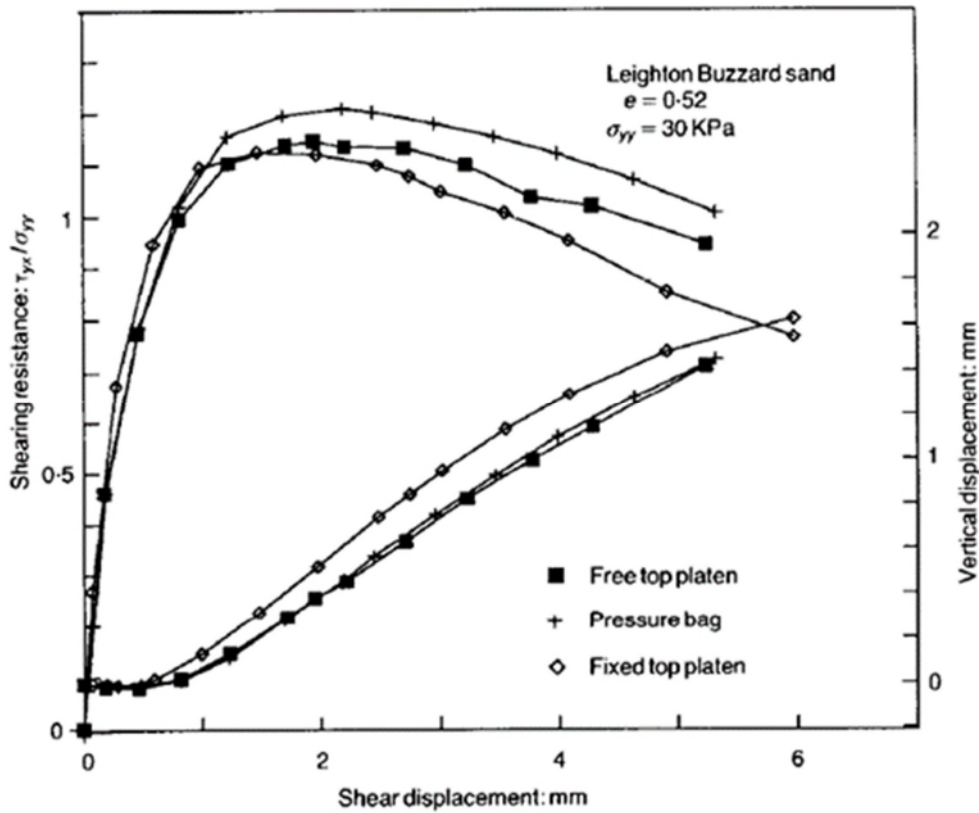


Figure 8.5 Increase of the measured peak shearing resistance and reduction of the peak rate of volume due to the rotation of the top lid (Palmeira 1987).

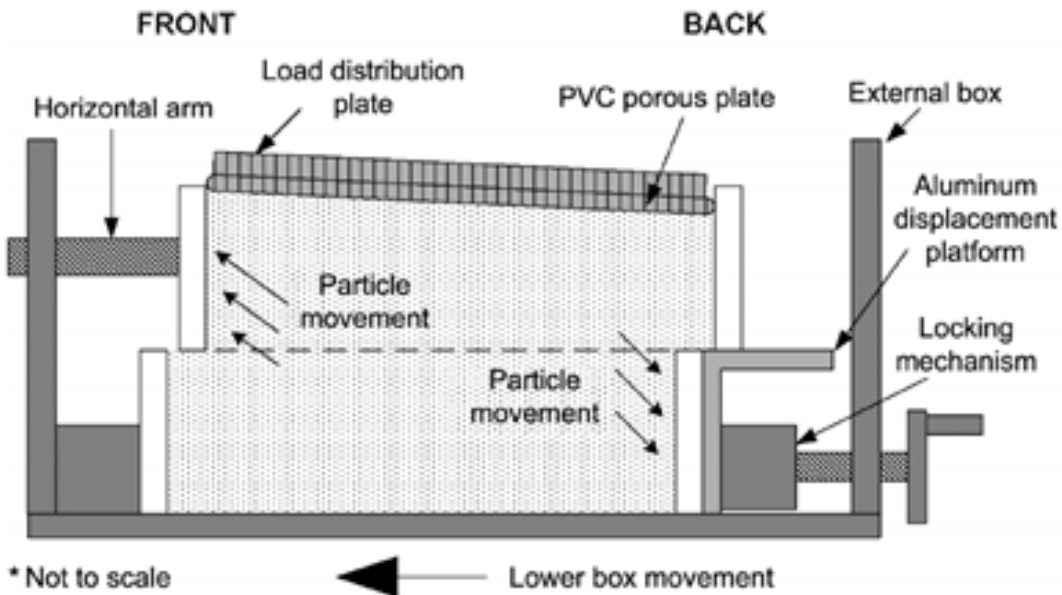


Figure 8.6 Schematic of particle movements during shearing in large scale direct shear (Bareither *et al.*, 2008).

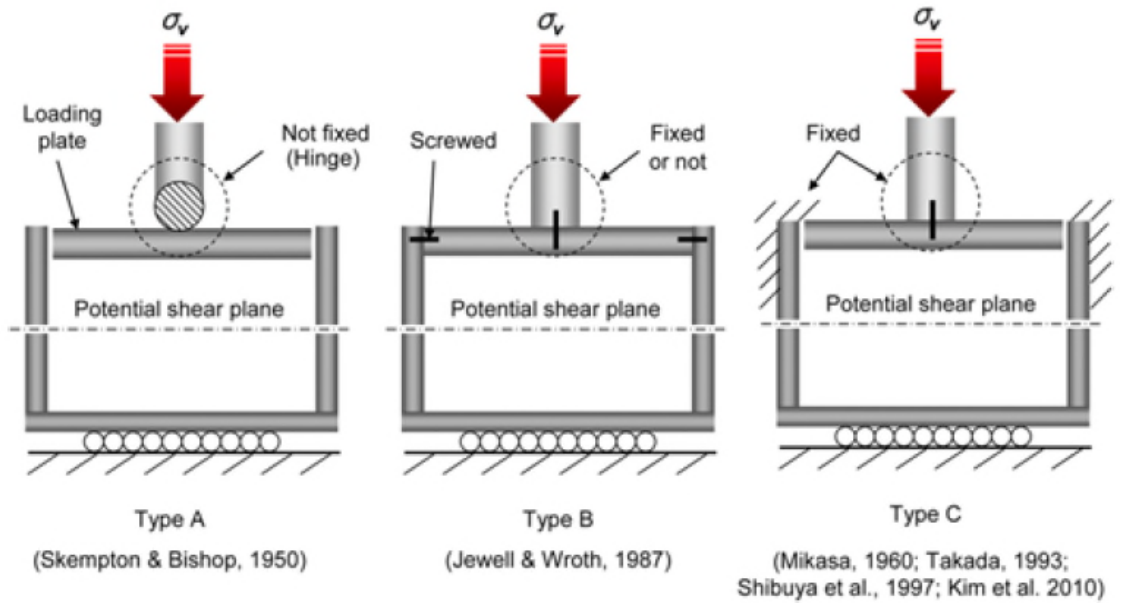


Figure 8.7 Direct shear box apparatus types considered by Kim *et al.* (2012).

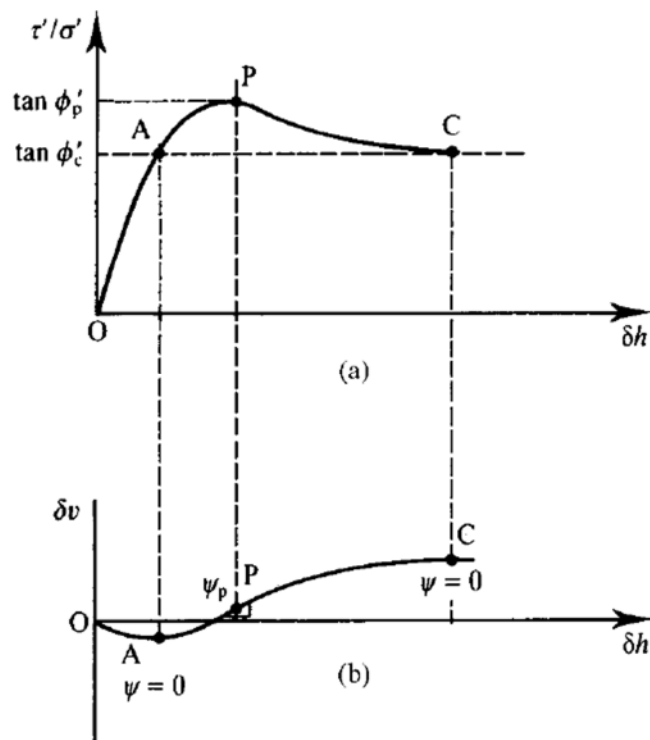
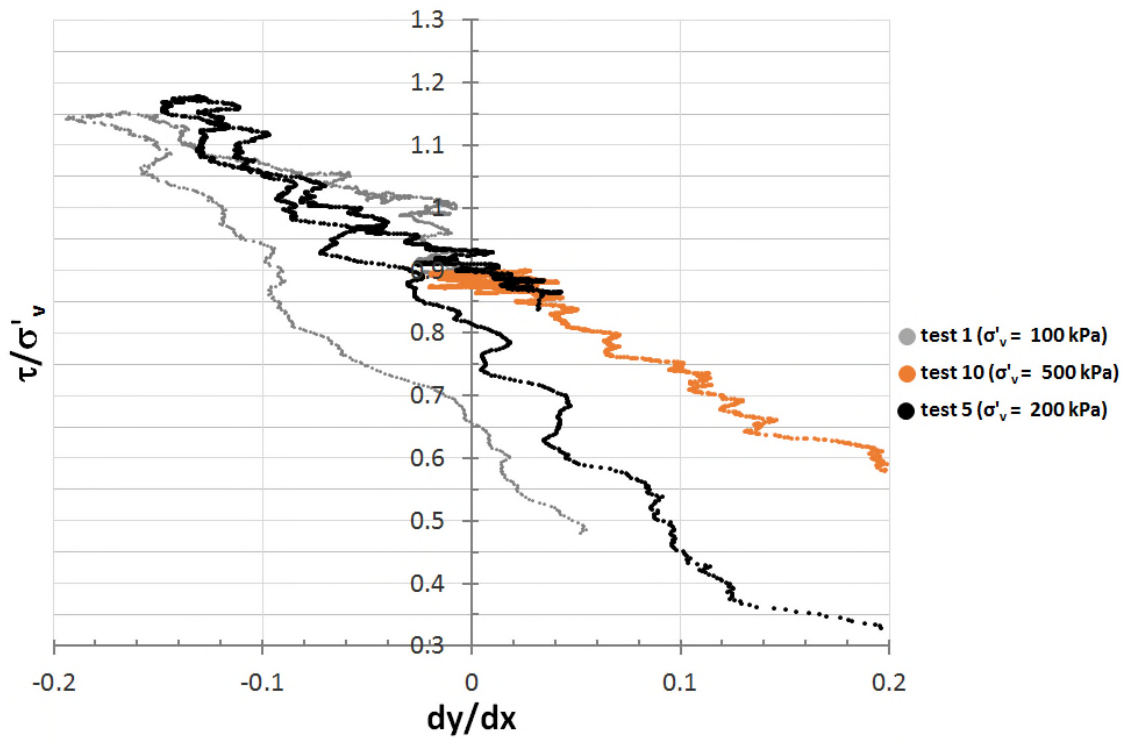
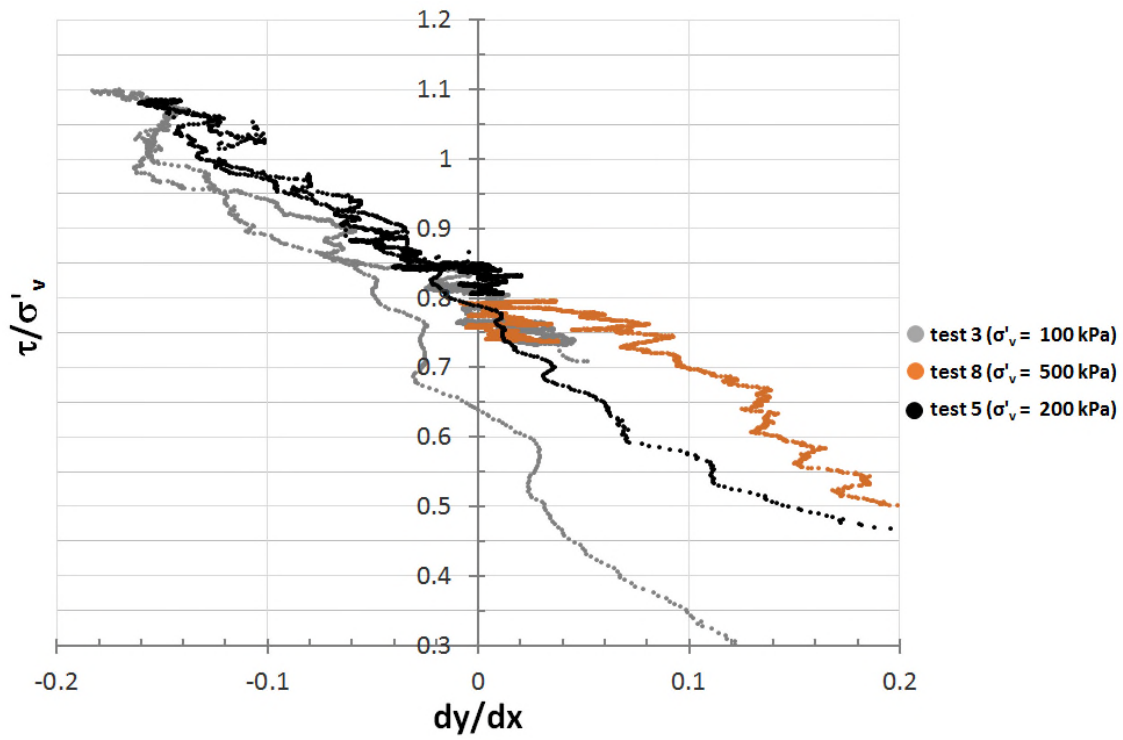


Figure 8.8 Points of zero change in volume of a dense sample: at maximum compressive strain (pre-peak strength phase, point A); at constant volume and constant shear stress (post-peak strength phase, point C) (Atkinson, 2007).



a)



b)

Figure 8.9 Variation of the stress ratio (τ/σ'_v) with dilatancy of the sample (dy/dx) for standard shear box tests conducted on (a) 3.35 mm and (b) 2 mm soil samples.

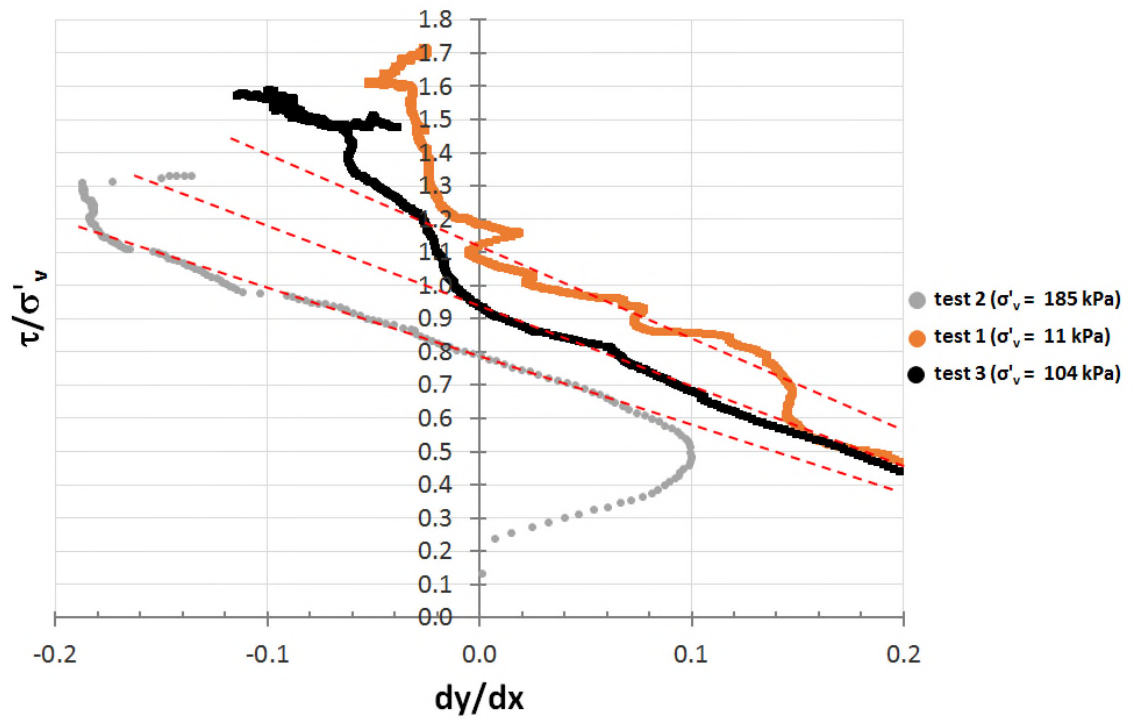


Figure 8. 10 Variation of the stress ratio (τ/σ'_v) with dilatancy of the sample (dy/dx) for the three large shear box tests.